



HAL
open science

Structure of cationic CNHC, Calkyl nickelacycles and their activity in the catalytic functionalization of the C–H bonds of azoles

Bernardo Rosa Lourenço de Pina Cardoso

► **To cite this version:**

Bernardo Rosa Lourenço de Pina Cardoso. Structure of cationic CNHC, Calkyl nickelacycles and their activity in the catalytic functionalization of the C–H bonds of azoles. Other. Université de Strasbourg, 2018. English. NNT : 2018STRAF033 . tel-02082624

HAL Id: tel-02082624

<https://theses.hal.science/tel-02082624>

Submitted on 28 Mar 2019

HAL is a multi-disciplinary open access archive for the deposit and dissemination of scientific research documents, whether they are published or not. The documents may come from teaching and research institutions in France or abroad, or from public or private research centers.

L'archive ouverte pluridisciplinaire **HAL**, est destinée au dépôt et à la diffusion de documents scientifiques de niveau recherche, publiés ou non, émanant des établissements d'enseignement et de recherche français ou étrangers, des laboratoires publics ou privés.

ÉCOLE DOCTORALE DES SCIENCES CHIMIQUES - ED222

Laboratoire d'innovation moléculaire et applications (LIMA) – UMR 7042

THÈSE présentée par :

Bernardo ROSA LOURENÇO DE PINA CARDOSO

soutenue le : 18 octobre 2018

pour obtenir le grade de : **Docteur de l'université de Strasbourg**

Discipline/ Spécialité : Sciences Chimiques

**Structure de nickelacycles cationiques
 C_{NHC} , C_{alkyle} et activité pour la fonctionnalisation
catalytique de liaisons C–H d'azoles**

THÈSE dirigée par :

M. RITLENG Vincent

M. CHETCUTI Michael J.

Professeur, Université de Strasbourg

Professeur, Université de Strasbourg

RAPPORTEURS :

M. POLI Rinaldo

Mme. AGBOSSOU-NIEDERCORN Francine

Professeur, Ecole Nationale Supérieure

des Ingénieurs en Arts Chimiques et Technologiques

Directeur de recherches, Ecole Nationale

Supérieure de Chimie de Lille

AUTRES MEMBRES DU JURY :

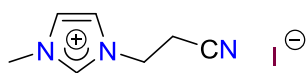
M. LE GENDRE Pierre

M. SÉMERIL David

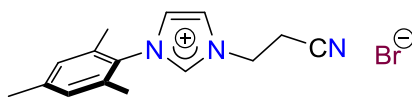
Professeur, Université de Bourgogne

Chargé de recherches, Université de Strasbourg

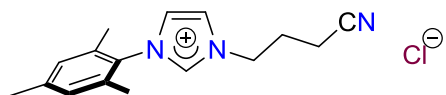
Chart 1. Structures of numbered compounds 1-16.



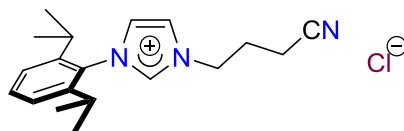
1



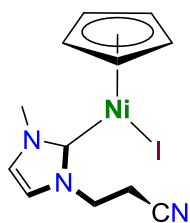
2



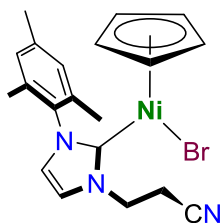
3



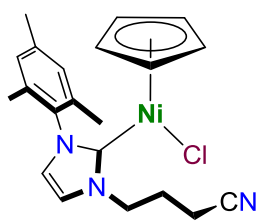
4



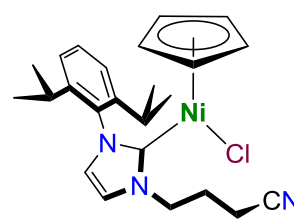
5



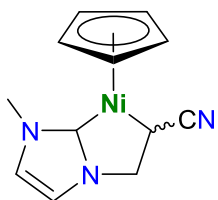
6



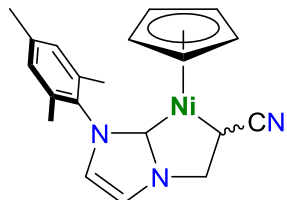
7



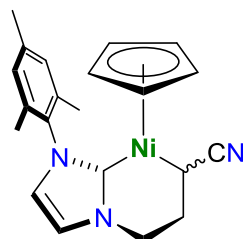
8



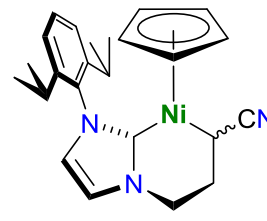
9



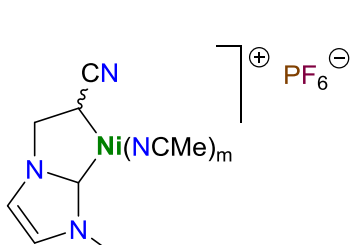
10



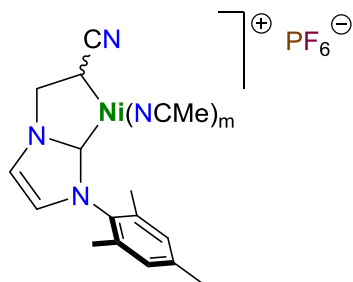
11



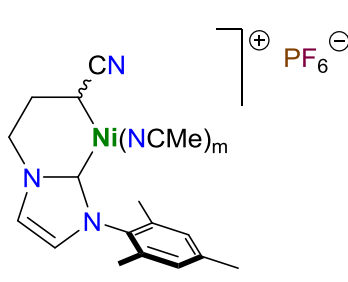
12



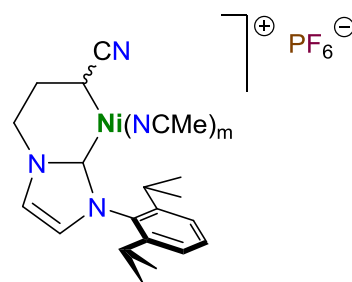
13



14



15



16

ÉCOLE DOCTORALE DES SCIENCES CHIMIQUES - ED222

Laboratoire d'innovation moléculaire et applications (LIMA) – UMR 7042

THÈSE présentée par :

Bernardo ROSA LOURENÇO DE PINA CARDOSO

soutenue le : 18 octobre 2018

pour obtenir le grade de : **Docteur de l'université de Strasbourg**

Discipline/ Spécialité : Sciences Chimiques

**Structure de nickelacycles cationiques
 C_{NHC} , C_{alkyle} et activité pour la fonctionnalisation
catalytique de liaisons C–H d'azoles**

THÈSE dirigée par :

M. RITLENG Vincent

M. CHETCUTI Michael J.

Professeur, Université de Strasbourg

Professeur, Université de Strasbourg

RAPPORTEURS :

M. POLI Rinaldo

Mme. AGBOSSOU-NIEDERCORN Francine

Professeur, Ecole Nationale Supérieure

des Ingénieurs en Arts Chimiques et Technologiques

Directeur de recherches, Ecole Nationale

Supérieure de Chimie de Lille

AUTRES MEMBRES DU JURY :

M. LE GENDRE Pierre

M. SÉMERIL David

Professeur, Université de Bourgogne

Chargé de recherches, Université de Strasbourg

“Time and time again the process of discovery in science reveals that what we thought was simple is really wondrously complicated.”

Roald Hoffmann
Vladimir I. Minkin
Barry K. Carpenter

1997

Acknowledgements

Acknowledgements

Was bleibt? Es bleibt die Muttersprache?

-Günther Gaus

Was ist geblieben? Geblieben ist die Muttersprache.

-Hanna Arendt

1964

Esta é a secção é sem dúvida a mais importante desta tese, que celebra todos que me acompanharam de uma forma ou outra nesta viagem que foi a tese, e por isso mesmo, não posso deixar de a escrever na língua do poeta, minha língua materna.

Assim gostaria de agradecer ao Michael e ao Vincent pelo acolhimento e a oportunidade. Em particular, ao Vincent pela paciência e optimismo mesmo quando a química não queria ajudar.

Quero também agradecer a toda a gente que contribuiu em toda a parte científica deste projecto, Luis Veiros, Mourad Elhabiri, Bruno Vincent, Emeric Wasielewski e Matthieu Chessé e todo o pessoal do LIMA. Às comunidades do r/chemistry e ao servidor de Discord da mesma, que foram uma fonte de conselhos e sugestões.

Agradeço também a todos os que passaram aqui pelo gabinete estes anos, em particular aos membros deste grupo, Franck, Ahmed, Alberto, Lobna, Rhama, Romain e Zélia.

À Mariana e ao Cão, que contiunam meus amigos de longa data. Aos meus amigos que, por acasos do destino, vieram Felix, Johboi, Manuel, Tom, RobotPuppy. Ao Stormofthefireflies. Ao “UnfunnyKitty” Tanner. Ao Joey.

Ao pessoal do 8.6.42 que viu o começo deste percurso a alguns anos. Em particular à Marta, ao Paulo e à Ana. Um obrigado muito especial à Sara, minha eterna colega de bancada.

Ao clã Mossman, em especial à Sue e ao Caine.

À minha família, que mais que tudo teve de suportar a distância destes últimos anos.

Ao Sérgio, que nestas minhas vadiagens leva sempre por tabela.

Aos meus pais, que talvez mais que todos os outros, suportaram os meus maus humores e a distância.

Ao Kolya.

Abbreviations

Abbreviations

% V_{bur} – percent buried volume

2,9-dmphen·H₂O – 2,9-dimethyl-1,10-phenanthroline hydrate

Ac – acetate

acac – acetylacetonate

Ad – 1-adamantyl

AIBN – azobisisobutyronitrile

Anal – analysis

aNHC – abnormal *N*-heterocyclic carbene

Ar – argon gas; aryl

ATR – attenuated total reflectance

b. p. – boiling point

bipy – 2,2'-bipyridine

BQ – 1,4-benzoquinone

br – broad

btz – 2-benzothiazolyl

ca. – circa

CAAC – cyclic (alkyl)aminocarbene

calcd. – calculated

C_{alkyl} – nickel-bound alkyl carbon

COD – 1,5-cyclooctadiene

Cp – cyclopentadienyl

Cp* – 1,2,3,4,5-pentamethylcyclopentadienyl

CP-MAS – cross-polarization magic angle spinning

CPME – cyclopentyl methyl ether

CV – cyclic voltammetry

Cy – cyclohexyl

Cys – cysteine

d – doublet

dba – dibenzylideneacetone

dcype – 1,2-bis(dicyclohexylphosphino)ethane

dcypt – 1,2-bis(dicyclohexylphosphino)thiophene

dd – doublet of doublets

dq – doublet of quartets

Abbreviations

ddd – doublet of doublet of doublets
DFT – density functional theory
DIPP – 2,6-di(*i*-propyl)phenyl
DMAc – *N,N*-dimethylacetamide
DME – dimethoxyethane
DMF – *N,N*-dimethylformamide
DMSO – dimethylsulfoxide
dppbz – 1,2-bis(diphenylphosphino)benzene
dppf – 1,1'-ferrocenediyl-bis(diphenylphosphine)
DoE – design of experiments
dtbpy – 4,4'-di(*t*-butyl)-2,2'-bipyridine
ECP – electron core potential
EDG – electron-donating group
ee – enantiomeric excess
EPR – electron paramagnetic resonance
equiv. – equivalent
esds – estimated standard deviations
ESI – electrospray ionization
Et – ethyl
EWG – electron-withdrawing group
Fc – ferrocene
Fc⁺ – ferrocenium
FMO – frontier molecular orbitals
GC – gas chromatography
GGA – generalized gradient approximation
GOF – goodness of fit
Het – hetero
HMQC – heteronuclear multiple-quantum correlation
HOMO – Highest Occupied Molecular Orbital
HRMS – high-resolution mass spectrometry
i – *iso*-
i-Pr – *iso*-propyl

Abbreviations

IR – infrared

KHMDS – potassium bis(trimethylsilyl)amide; The acronym HMDS comes from the older designation hexamethyldisilazane

KIE – kinetic isotope effect

LEP – Lever electronic parameter

LUMO – Lowest Unoccupied Molecular Orbital

m – medium; multiplet

m- – *meta-*

m/z – mass per charge

MAD – methylaluminum bis(2,6-di-*t*-butyl-4-methylphenoxide)

MALDI-TOF-MES – matrix-assisted laser desorption/ionization time-of-flight mass spectrometry

Me – methyl

Mes – mesityl or 2,4,6-trimethylphenyl

n. d. – not determined

n. r. – not reported

NHE – normal hydrogen electrode

NHC – *N*-heterocyclic carbene

NMR – nuclear magnetic resonance

NOESY – nuclear Overhauser effect spectroscopy

o- – *ortho-*

p- – *para-*

PBE – Perdew, Burke and Ernzerhof [functional]

PCA – Principal Component Analysis

PCM – Polarisable Continuum Model

Ph – phenyl

phen – 1,10-phenanthroline

Piv – pivalyl

ppm – parts per million

py-*d*₅ – pyridine-*d*₅

q – quartet

quint – quintuplet

Abbreviations

r. t. – room temperature

ref – refecence

refs – references

s – singlet; strong

SDD – Stuttgart/Dresden ECP basis set

sept – septuplet

SET – single-electron transfer

SHOP – Shell Higher Olefin Process

SMD – Solvation Model based on Density

STQN – Synchronous Transit-Guided Quasi-Newton

T – temperature

t – time; triplet

t – *tert*-

t-Bu – *tert*-butyl

td – triplet of doublets

TEMPO – (2,2,6,6-tetramethylpiperidin-1-yl)oxyl

TEP – Tolman electronic parameter

terpy – terpyridine

Tf – triflate

THF – tetrahydrofuran

TON – turnover number

TTR – transthyretin

w – weak

v. – very

vs – very strong

vs. – versus

Table of contents

Table of contents

Resumé.....	10
Chapter 1 – Introduction: from the periodic table to nickel-<i>N</i>-heterocyclic carbene catalysts	30
I. Emergence of nickel homogenous catalysis	30
II. Nickel-NHC complexes in homogeneous catalysis	34
II.1. <i>N</i> -Heterocyclic carbene (NHC) ligands.....	34
II.2. Metal- <i>N</i> -heterocyclic carbene (M-NHC) bond	36
III. Nickel- <i>N</i> -heterocyclic carbene (Ni-NHC) in homogeneous catalysis: C–H bond functionalization (2015-2018).....	41
III.1. C–H cross-coupling	42
III.1.1. C _{sp} and C _{sp2} functionalization	42
III.1.2. C _{sp3} –H functionalization	46
III.2. Formal 1,2-Additions to unsaturated C–C bonds.....	47
III.2.1. To alkynes (C≡C)	47
III.2.1.A. Hydroarylation.....	47
III.2.1.B. Three-component couplings.....	50
III.2.2. To alkenes (C=C)	52
III.2.2.A. Hydro(hetero)arylation reactions.....	52
III.2.2.B. Formal C–H addition of carbonyl substrates to olefins.....	57
IV. Overview.....	58
Chapter 2 – Synthesis and characterization of new κ^2-C_{NHC}, C_{alkyl}-nickelacycle	66
I. Context and objectives.....	66
II. Results and discussion	69
II.1. Synthesis and characterization of imidazolium salt pro-ligands.....	69
II.2. Synthesis and characterization of half-sandwich nickel(II)-NHC complexes.....	72
II.3. Synthesis and characterization of half-sandwich κ^2 -C _{NHC} , C _{alkyl} -nickelacycles	74
II.4. Synthesis and characterization of cationic κ^2 -C _{NHC} , C _{alkyl} -nickelacycles.....	79

II.4.1. Synthesis and formula determination of cationic κ^2 -C _{NHC} , C _{alkyl} -nickelacycles	79
II.4.2. Insights into the structure of cationic κ^2 -C _{NHC} , C _{alkyl} -nickelacycles	87
II.5. Reactivity of cationic κ^2 -C _{NHC} , C _{alkyl} nickelacycles	94
II.5.1. Ligand substitution	94
II.5.1.A. With phosphines.....	94
II.5.1.B. Other substitution reactions	102
II.5.2. With strong bases	103
II.5.3. Redox chemistry	106
III. Conclusions.....	109
Chapter 3 – Catalytic C–H functionalization of O,S-azoles	115
I. Introduction	115
I.1. C(2)–H/C _{sp} –X	115
I.1.1. Electrophilic coupling partners	115
I.1.1.A. X =Bromide (-Br)	115
I.1.2. Nucleophilic coupling partners	116
I.1.2.A. X = Hydrogen (-H).....	116
I.2. C(2)-H/C _{sp2} –X.....	117
I.2.1. Electrophilic coupling partners	117
I.2.1.A. X = Halogen (-F, -Cl, -Br, -I)	117
I.2.1.B. X = Oxygen electrophiles (-OR): Triflate (-OTf), Sulfonate (-OSO ₂ R), Ester (-OCOR), Carbamate (-OCONRR'),.....	121
I.2.1.C. X = Carbon electrophiles.....	123
I.2.1.C.1. X = Carbonyl (-COOR)	123
I.2.1.C.2. X = Nitrile (-CN).....	126
I.2.2. Nucleophilic coupling partners	127
I.2.2.A. X = Metalloid	127
I.2.2.A.1. X = Silanes (-Si(OR) ₃)	127
I.2.2.A.2. X = Boronic acids (-B(OH) ₂)	127
I.2.2.B. X = Hydrogen (-H).....	128
I.3. C(2)–H/C _{sp3} –X	129

I.3.1. Electrophilic coupling partners	129
I.3.1.A. X = Halogen (-Br, -I).....	129
I.3.1.B. X = Carbonyl (-COOR).....	131
I.3.2. Nucleophilic coupling partners	131
I.3.2.A. X = Hydrazone (=N-NHR)	131
I.3.2.B. X = Hydrogen (-H).....	132
I.4. Mechanistic considerations.....	132
I.4.1. Catalytic cycles	132
I.4.2. Breaking the C–H bond.....	136
I.4.3. Heterogeneous vs. homogeneous catalysis	137
I.5. Overview.....	138
II. Results and discussion	139
II.1. Benzothiazole C _{sp2} cross-coupling.....	139
II.2. Benzothiazole C _{sp3} cross-coupling.....	147
II.3. Conclusions	160
Experimental section.....	168
I. Generalities	168
I.1. Materials.....	168
I.2. Methods.....	169
II. Synthetic procedures	171
II.1. Imidazolium salts	171
II.1.2. Compound 2 : [Mes-NHC-(CH ₂)CH ₂ CN]·HBr.....	171
II.1.2. Compound 3 : [Mes-NHC-(CH ₂) ₂ CH ₂ CN]·HCl	172
II.1.3. Compound 4 : [DIPP-NHC-(CH ₂) ₂ CH ₂ CN]·HCl.....	172
II.2. Nickel(II) complexes	173
II.2.1. Compound 5 : [Ni ^{II} I(Cp)(Me-NHC-(CH ₂)CH ₂ CN)].....	173
II.2.2. Compound 6 : [Ni ^{II} Br(Cp)(Mes-NHC-(CH ₂)CH ₂ CN)]	173
II.2.3. Compound 8 : [Ni ^{II} Cl(Cp)(DIPP-NHC-(CH ₂) ₂ CH ₂ CN)].....	174
II.2.4. Compound 9 : [Ni ^{II} (Cp){Me-NHC-(CH ₂)CH(CN)}].....	174
II.2.5. Compound 10 : [Ni ^{II} (Cp){Mes-NHC-(CH ₂)CH(CN)}].....	175
II.2.5. Compound 11 : [Ni ^{II} (Cp){Mes-NHC-(CH ₂) ₂ CH(CN)}].....	175
II.2.6. Compound 12 : [Ni ^{II} (Cp){DIPP-NHC-(CH ₂) ₂ CH(CN)}].....	176

II.2.7. Compound 13 : [Ni ^{II} {Me-NHC-(CH ₂)CH(CN)}(MeCN)]PF ₆	176
II.2.8. Compound 14 : [Ni ^{II} {Mes-NHC-(CH ₂)CH(CN)}(MeCN)]PF ₆	177
II.2.9. Compound 15 : [Ni ^{II} {Mes-NHC-(CH ₂) ₂ CH(CN)}(MeCN)]PF ₆	178
II.2.10. Compound 16 : [Ni ^{II} {DIPP-NHC-(CH ₂) ₂ CH(CN)}(MeCN)]PF ₆	178
II.2.11. Compound 17 : [Ni ^{II} {Mes-NHC-(CH ₂) ₂ CH(CN)}(PPh ₃)]PF ₆	179
II.2.12. Compound 18 : [Ni ^{II} {Mes-NHC-(CH ₂) ₂ CH(CN)}(PMe ₃)]PF ₆	180
II.2.13. Compound 19 : [Ni ^{II} (μ ² -OH){Mes-NHC-(CH ₂) ₂ CH(CN)}]PF ₆	180
II.2.14. Compound 22 : [Ni ^{II} {Mes-NHC-(CH ₂) ₂ CH(CN)}(bipy)]PF ₆	180
II.2.15. Compound 27 : [Ni ^{II} (btz)(Cp)(NHC-Mes ₂)]	181
II.2.16. Compound 28 : [Ni ^{II} (btz)(Cp*)(NHC-Mes ₂)]	181
II.2.17. Compound 29 : [Ni ^{II} Cl(Cp*)(^{4,5} Me ₂ NHC-Mes ₂)]	182
III. Catalytic reactions	183
III.1. Benzothiazole arylation	183
III.2. Benzothiazole alkylation	183
III.3. NMR data of the azole coupling products	184
IV. Crystal data and refinement data	187
IV.1. Hexaacetone nickel(II) hexafluorophosphate [Ni ^{II} (NCMe) ₆](PF ₆) ₂	187
IV.2. Complexes 9 and 10	189
IV.3. Complexes 19 and 27	190
V. Computational methods	191
General conclusions	196
References	203
Annex	219

Résumé

Résumé

1) Introduction

Les sciences chimiques ont conduit à une amélioration de la qualité de vie grâce à la production de connaissances et aux avancées technologiques résultantes. Pour ce faire, il a fallu mettre à jour de nouvelles réactions, exploiter des matières premières peu réactives et adopter des procédés moins sévères. Ces exigences ont conduit à la mise en place de la catalyse à la fois comme domaine technologique principal et comme sujet universitaire. Ainsi, la catalyse est présente dans environ 90 % des processus chimiques développés dans le monde ainsi que dans la production de 60 % des produits chimiques, tout en étant au cœur de nombreuses attributions du prix Nobel de chimie.

Les catalyseurs homogènes (catalyseurs qui se trouvent dans la même phase que les substrats; généralement en solution) sont reconnus pour leurs hautes activités et sélectivités, et leurs conditions de réaction modérées. En particulier, les catalyseurs à base de métaux de transition des deuxième et troisième rangées du tableau périodique tels que le palladium, le rhodium, l'iridium ou le ruthénium sont devenus les enfants chéris de l'industrie chimique. Cependant, les préoccupations croissantes de la société quant à la toxicité de ces métaux, leur prix et leur disponibilité (Fig. 1) ont conduit à une renaissance de la chimie des métaux de transition de la couche 3d.

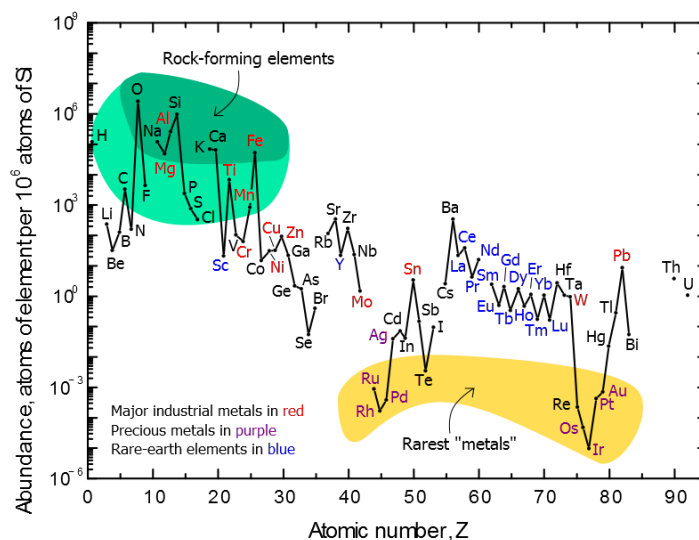


Figure 1. Abondance des éléments dans la croûte terrestre, normalisée par rapport à l'abondance du silicium (10^6 atomes). Les métaux rares les plus populaires utilisés en catalyse homogène (Ru, Rh, Pd, Ir) se trouvent tous dans le quartile inférieur du graphique, tandis que leurs homologues 3d se trouvent dans la moitié supérieure du graphique.

Résumé

Ainsi, il est attendu des catalyseurs à base de métal 3d qu'ils agissent comme des substitués abondants et bon marché de leurs congénères à base de métaux rares. En outre, des réactivités nouvelles sont attendues de l'exploitation de leur réactivité intrinsèque.

Ce récent intérêt pour l'utilisation de métaux de transition 3d en catalyse a engendré une ré-exploration de la réactivité du nickel. Parmi la variété d'applications désormais décrites avec ce dernier, l'essor de la fonctionnalisation catalytique de liaisons C–H est notable. En particulier, une des familles de molécules ayant le plus bénéficié de ce nouveau paradigme synthétique est celle des azoles qui se caractérise par des hétérocycles à 5 membres comportant un atome d'azote et au moins un autre hétéroatome (O, S), et qu'on trouve dans de nombreux produits naturels, molécules synthétiques biologiquement actives, et matériaux pour l'énergie. Ainsi, la catalyse au nickel a marqué de son empreinte ce sous-domaine avec des méthodologies originales pour la fonctionnalisation des liaisons C(2)–H de ces derniers avec une vaste gamme de substrats. De façon intéressante, au contraire de nombreuses autres transformations, les ligands carbènes N-hétérocycliques (NHC) sont rarement associés au nickel dans ces réactions, et les ligands les plus fréquemment utilisés sont des ligands chélates pnictogène de type κ^2 -N,N ou P,P. Les hautes performances observées avec ces derniers nous ont incité à évaluer l'influence de ligands NHC bidentates de type κ^2 -C,C pour la fonctionnalisation directe d'azoles.

En 2010, notre groupe a décrit la formation d'un complexe demi-sandwich nickel(II)-NHC cyanométhyle résultant de l'activation C–H assistée par une base d'un ligand acétonitrile (Schéma 1). A la suite de ce premier exemple, cette réactivité a été étendue à l'activation d'autres liaisons C_{sp^3} –H en α d'un groupe fonctionnel nitrile ou cétone. Ces activations C–H ont formé le berceau pour l'emploi de ces espèces comme pré-catalyseurs de réactions de couplage C_{sp^3} –H/ C_{sp^2} –X.

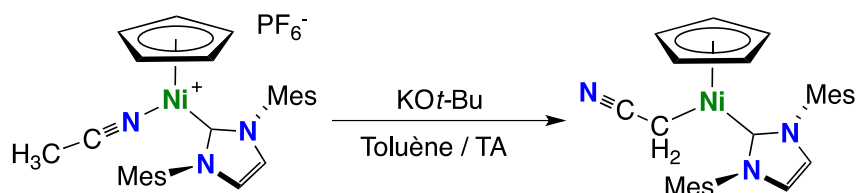


Schéma 1. Nickelation d'un ligand acétonitrile

Par ailleurs, cette capacité à activer des liaisons C_{sp^3} –H en α d'un groupe fonctionnel a également été utilisée pour la synthèse de nouveaux motifs organométalliques. Ainsi, des métallacycles, $[\text{Ni}(\eta^5\text{-C}_5\text{H}_5)\{\text{R-NHC}-(\text{CH}_2)_n\text{CH}(\text{CN})\}]$ ($\eta^5\text{-C}_5\text{H}_5 = \text{Cp} = \text{cyclopentadiényle}$), comportant un ligand chélate κ^2 - $C_{\text{NHC}}, C_{\text{alkyle}}$ ont été obtenus par activation d'une liaison C_{sp^3} –H en α du groupement nitrile de bras cyanoalkyles portés par le NHC (Schéma 2).

Résumé

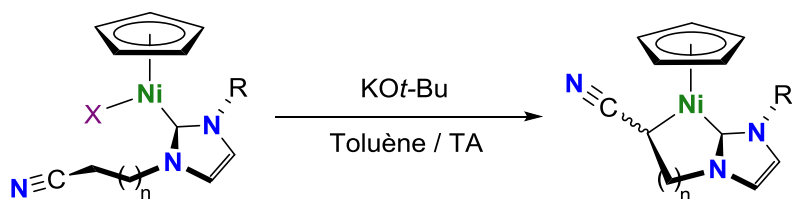


Schéma 2. Synthèse de nickelacycles par activation d'une liaison C–H en α d'un groupement nitrile.

Cette nouvelle génération de complexes s'est révélée peu réactive, mais la mise au point ultérieure d'une méthode d'acidolyse sans précédent du ligand Cp pour un complexe à 18 électrons de valence, permettant de dégager des sites de coordination sur le nickel sans toucher aux autres liaisons Ni–C (Ni–NHC et Ni–alkyle) (Schéma 3), ouvrait des perspectives intéressantes.

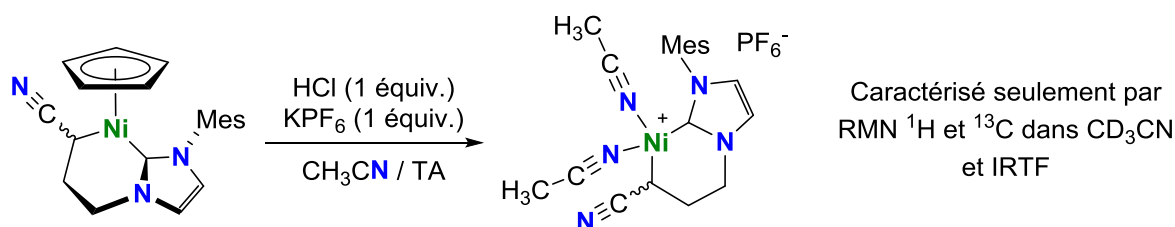


Schéma 3. Acidolyse du ligand Cp générant des complexes cationiques stabilisés par la coordination de molécules de solvant.

En effet, l'accès à ces chélates κ^2 - C_{NHC}, C_{alkyle} -nickel(II), vraisemblablement de structure carré-plan et à 16 électrons de valence, et comportant des ligands acétonitrile en lieu et place du Cp était potentiellement très intéressante au vu de la grande labilité de ces derniers. Cependant, ces espèces restaient mal caractérisées et des doutes subsistaient quant à leur véritable formulation et structure. Dans l'optique de l'étude de leur activité pour des réactions de fonctionnalisation C(2)–H d'azoles et de celle de l'effet d'un motif C,C comme ligand chélate dans ces réactions, le premier objectif de cette thèse a ainsi été d'optimiser la synthèse, de caractériser, et d'établir de façon définitive la structure de ces espèces

2) Résultats et discussions

1. Synthèse et caractérisation des nickelacycles

Une série de quatre complexes $[Ni\{R-NHC-(CH_2)_nCH(CN)\}(MeCN)_m]PF_6$ (**2a-d**) a été préparée via trois étapes optimisées. Ainsi, les complexes demi-sandwich parents **a-d** ont été préparés par réaction directe du nickelocène avec les sels d'imidazolium portant un bras cyanoalkyle à l'échelle de plusieurs grammes (Schéma 4). Lors de l'étape de cycloméallation par activation de la liaison C–H en position alpha du groupe nitrile, la substitution de la base originellement employée (KOt-Bu - cf. Schéma 2) par une solution de KHMDS a permis une

Résumé

augmentation significative des rendements des métallacycles à 6 membres, **1c** et **1d**. Les métallacycles à 5 membres **1a** et **1b** sont quant à eux obtenus avec des rendements plus faibles (25%), mais de façon parfaitement reproductible, mettant ainsi en évidence l'importance de la taille de la chaîne alkyle lors de la formation des métallacycles. Enfin lors de l'acidolyse du ligand Cp, le refroidissement du milieu réactionnel à 0 °C a permis d'améliorer la reproductibilité de la réaction. Dans ces conditions, la réaction est quasi-quantitative et peut être aisément réalisée à l'échelle de plusieurs centaines de milligrammes (Schéma 4).

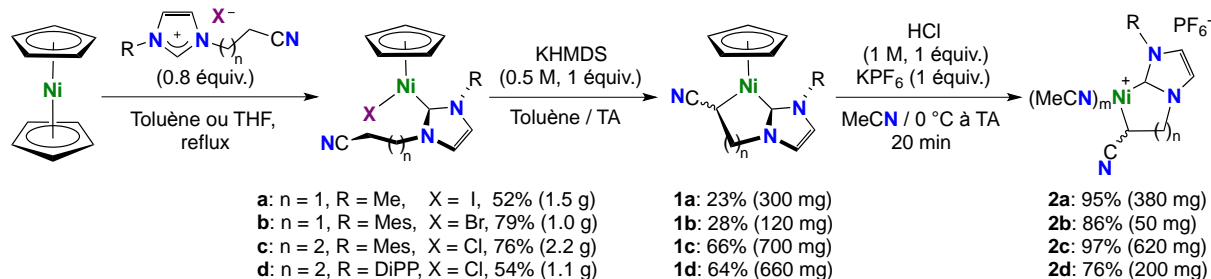


Schéma 4. Synthèse optimisée des complexes cationiques $[\text{Ni}\{\text{R-NHC}-(\text{CH}_2)_n\text{CH}(\text{CN})\}(\text{MeCN})_m]\text{PF}_6$ **2a-d**.

Disposant d'une solide méthodologie de synthèse, les nickelacycles **2a-d** ont ensuite été caractérisés par spectroscopie RMN ^1H et ^{13}C dans CD_3CN et la pyridine- d_5 , spectroscopie IR, spectrométrie de masse et microanalyses CHN. Malgré de nombreux essais de recristallisation, leur structure n'a pas pu être établie par diffraction des rayons X. Les résultats de spectroscopie RMN ^1H montrent la présence d'un seul ligand acétonitrile par nickelacycle à l'état solide. En accord avec ces données, les spectres de masse à haute résolution de **2a-d** montrent tous un ion $[\text{nickelacycle-NCMe}]^+$ comme pic de base, et les analyses élémentaires confirment toutes une formulation avec un seul ligand acétonitrile par atome de nickel, excluant donc la possibilité de complexes à carré-plan à 16 électrons de valence à l'état solide.

En absence d'un quatrième ligand pour compléter la sphère de coordination du nickel, la question de la structure des nickelacycles **2a-d** à l'état solide était légitime. Une étude structurale par calculs DFT, conduite sur les métallacycles à 5 et 6 membres **2a** et **2c**, a révélé un faible coût énergétique pour la perte d'un ligand acétonitrile des espèces carré-plan existant probablement en solution ($\Delta G = 7\text{-}12$ kcal/mol), qui devrait être facilement accessible par séchage sous vide ($\Delta G^\ddagger = 14$ kcal/mol dans le cas de **2c**). Deux structures avec un ligand acétonitrile ont pu être optimisées dans chaque cas : (i) une espèce de structure T à 14 électrons, et (ii) une espèce stabilisée par la coordination de côté du groupe nitrile de la chaîne alkyle, cette dernière étant favorisée de 2,4 kcal/mol dans le cas du métallacycle à 6 membres **2c** (Fig. 2).

Résumé

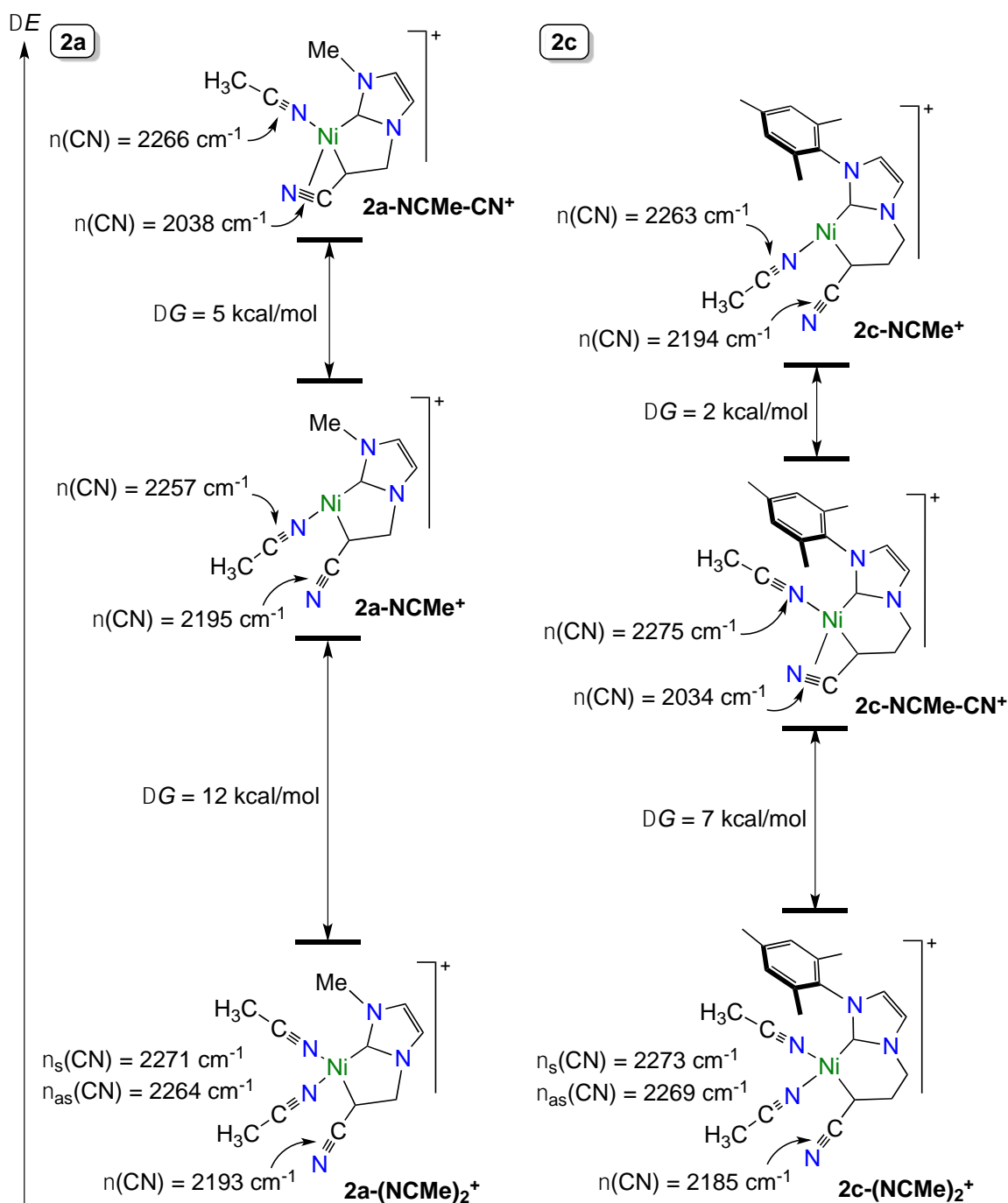


Figure 2. Energies libres des cations de **2a** et **2c** avec un ou deux ligands acétonitrile, et fréquences vibrationnelles calculées des liaisons C≡N.

La comparaison des fréquences vibrationnelles calculées pour ces structures avec les spectres IR expérimentaux a permis d'exclure la coordination π du groupement C≡N de la chaîne alkyle du fait de l'absence de bande $\nu(C\equiv N)$ entre 2030 et 2040 cm^{-1} (Fig. 3). Ainsi, les complexes **2a-d** existent très probablement sous forme de *rare espèces de nickel(II) tri-coordinées à 14 électrons de structure T*.

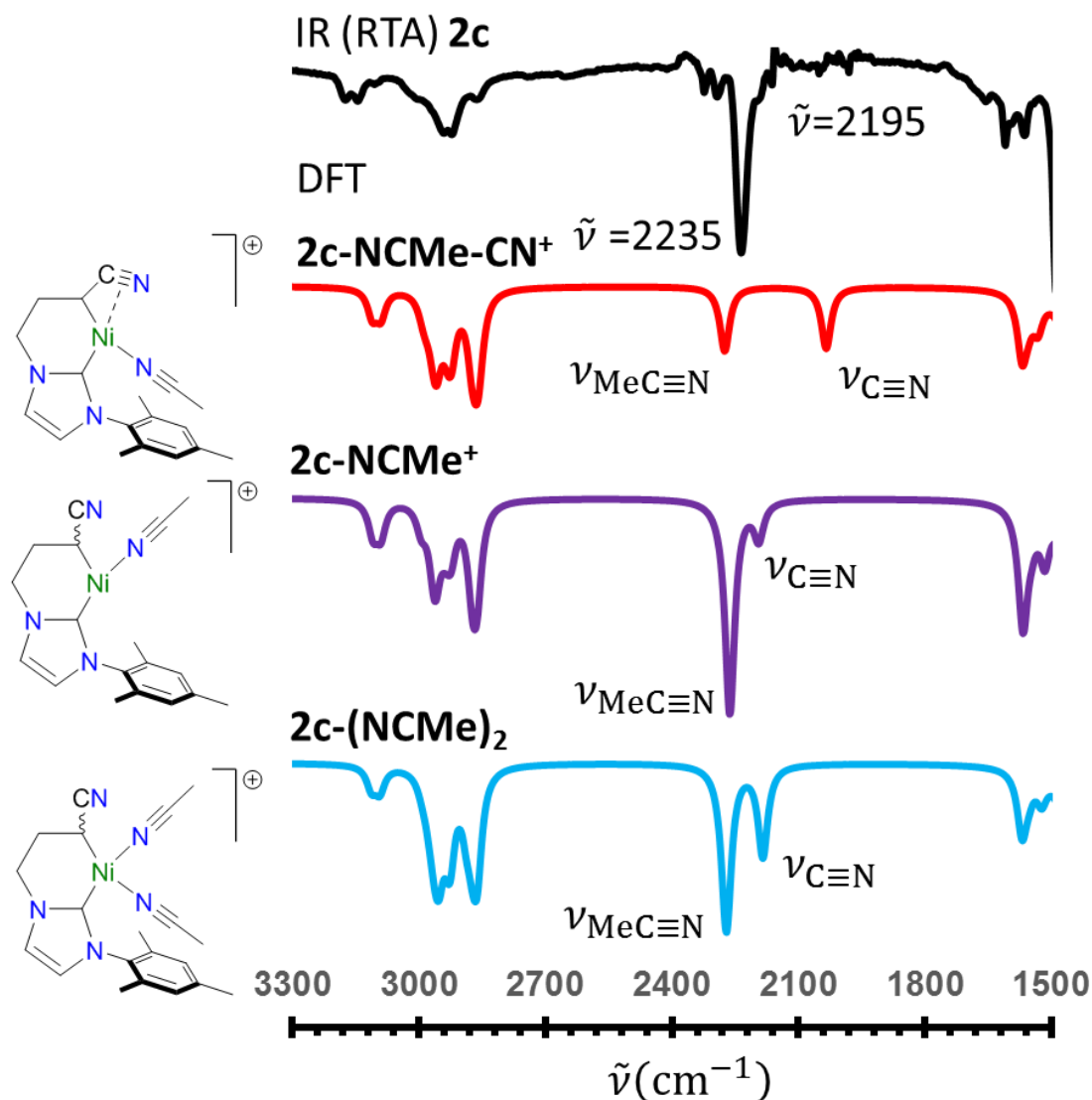


Figure 3. Détail des spectres expérimentales IR de **2c** (noir), et des fréquences vibrationnelles calculées par DFT de **2c-NCMe-CN⁺** (rouge), **2c-NCMe⁺** (violet) et **2c-(NCMe)₂⁺** (bleu).

2. Réactivité des nickelacycles **2** en conditions stoechiométriques

Le comportement des nickelacycles **2 a**, dans un premier temps, été étudié dans des réactions de substitution du ligand NCMe par des ligands phosphines, souvent utilisés dans des réactions catalytiques. Pour ce faire, le nickelacycle **2c** a été traité avec PPh_3 , un ligand volumineux et avec une liaison M–P relativement faible, et PMe_3 , un ligand avec une plus forte liaison M–P et une empreinte stérique plus faible (Schéma 5). Dans les deux cas, les complexes attendus dans lesquels le ligand acétonitrile a été substitué par la phosphine utilisée ont été obtenus avec d'excellents rendements (**3c** - PPh_3 , 85%; **4c** - PMe_3 , 97%).

Résumé

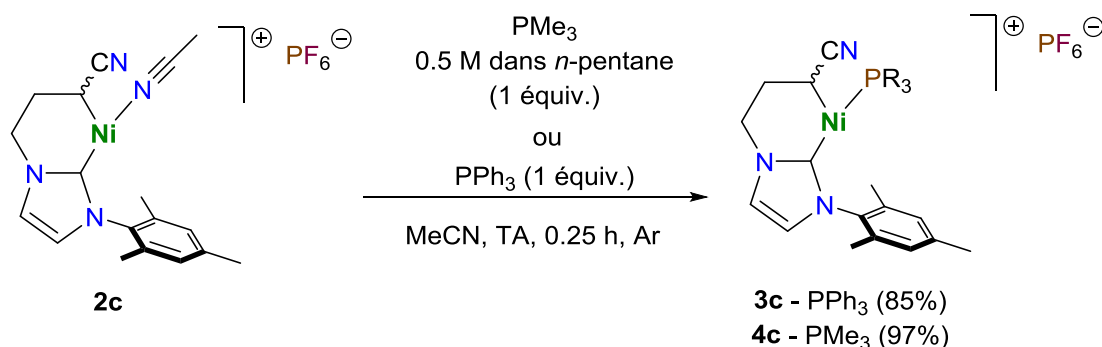


Schéma 5. Synthèse des complexes avec des ligands phosphine **3c** et **4c**.

De façon surprenante, alors que les spectres RMN ^1H (CD_3CN) de **3c** et **4c** à température ambiante (TA) montrent clairement la présence des ligands phosphines sous forme des signaux larges, les spectres RMN ^{31}P ne révèlent que des signaux très faibles. L'étude par RMN ^{31}P d'une solution de **3c** dans CD_3CN à laquelle on a progressivement ajouté de la PPh_3 a montré l'augmentation de l'intensité du signal de **3c** et son déplacement progressif vers le déplacement chimique de PPh_3 libre, ce qui suggère un échange rapide à l'échelle de temps de la RMN du ligand PPh_3 de **3c** avec le solvant. Par ailleurs, des études RMN ^1H et ^{31}P $\{^1\text{H}\}$ à température variable du complexe **4c** ont révélé distinctement la présence de deux espèces phosphorées à basse température (-40°C). En outre, des expériences de corrélation de RMN ^1H - ^{31}P hétéronucléaires ont permis de montrer que ces deux espèces étaient reliées, suggérant ainsi qu'elles étaient deux formes d'un même complexe. Dans les deux cas (**3c** et **4c**), des équilibres semblent donc être en jeu. Ainsi, dans le cas de **3c**, le ligand PPh_3 , plus volumineux et avec une liaison M-P plus faible, serait soumis à un échange avec le solvant MeCN pour donner le complexe **2c** (Schéma 6, **A** et **2c**). Dans le cas de **4c**, en plus de ce phénomène, le ligand PMe_3 , plus petit et plus fortement lié au métal, subirait une isomérisation *cis/trans* pour donner deux isomères carré-plan mixtes N,P (Schéma 6, **A** et **D**) via des intermédiaires insaturés (Schéma 6, **B** et **C**).

Résumé

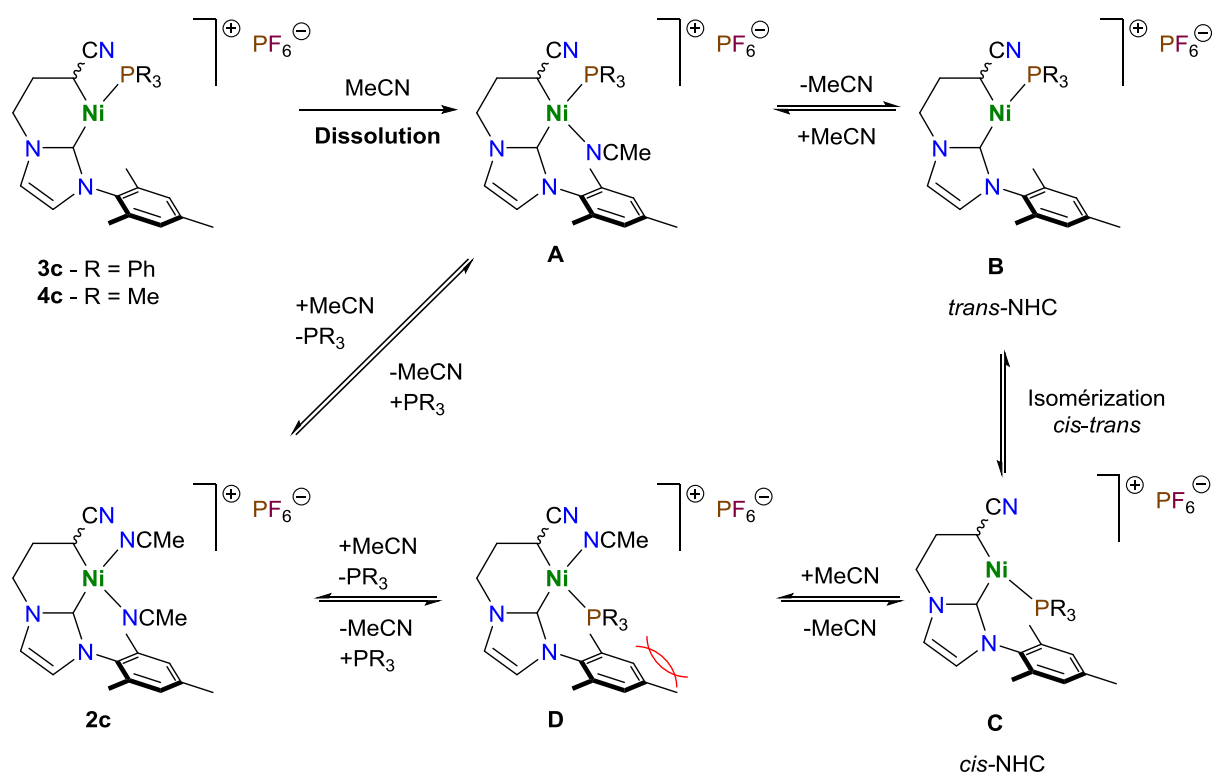


Schéma 6. Équilibre chimique en solution (MeCN) déplace le ligand phosphine de **3c** et **4c**.

En parallèle à ces travaux, voyant l'opportunité de réaliser un second exemple de nickelation d'un ligand acétonitrile par activation C–H (voir Schéma 1), avec à la clef la génération potentielle d'une espèce C,C,C-Ni, le complexe **2c** a été traité avec KO*t*-Bu. L'analyse du spectre RMN ¹H (CDCl₃) du produit a révélé la formation de deux nouveaux nickelacycles avec l'apparition concomitante de deux nouveaux signaux à –5.34 et –5.60 ppm dont les déplacements chimiques étaient cohérents avec la présence possible de ligands cyanométhyle. Cependant, l'intégration relative de ces signaux était de un au lieu de deux attendus pour des unités méthylènes. Une étude de diffraction des rayons X sur monocristal a permis d'établir l'identité du complexe synthétisé (Fig. 4), comme étant celle d'un dimère de nickel(II) avec deux ligands hydroxyles pontants, [Ni(μ-OH){Mes-NHC-(CH₂)₂CH(CN)}]₂ (**5**), et existant sous la forme de deux paires d'énantiomères *RR*- et *SS*-**5**, et *RS*- et *SR*-**5** (seule la paire d'énantiomères *RR*- et *SS*-**5** est présente dans le cristal). La présence d'un ligand hydroxyle pontant a été confirmée par l'observation d'une bande νO–H à 3628 cm⁻¹ par spectroscopie IR.

Résumé

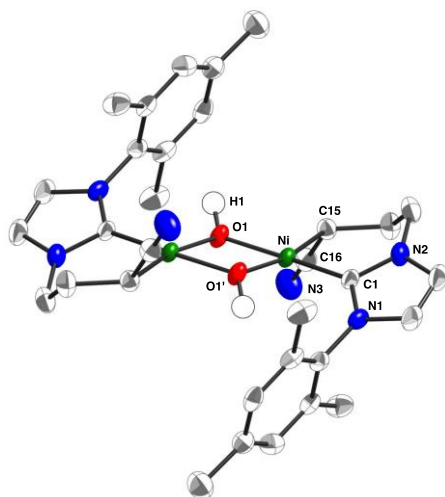


Figure 4. Structure de l'énantiomère *RS* du dimère **5** comportant des groupes hydroxyles pontants.

3. Etudes catalytiques

L'activité catalytique des nickelacycles insaturés **2a-d** a été étudiée pour l'arylation directe d'azoles, et comparée à celle de leurs précurseurs demi-sandwich **1** et dérivés carré-plan **6c**. De façon satisfaisante, un premier screening pour l'arylation du benzothiazole avec l'iodobenzène dans des conditions analogues à celles établies avec des sels de nickel et des ligands bidentates classiques a montré que les nickelacycles **2a-d** à 14 électrons étaient bien plus actifs que leur précurseurs à 18 électrons et leur dérivés à 16 électrons (Schéma 7).

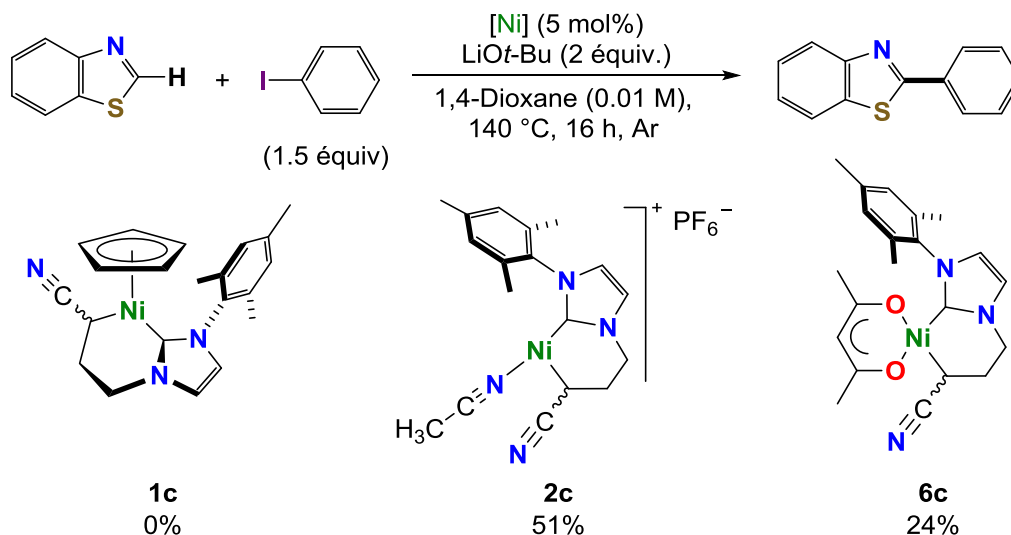


Schéma 7. Couplage du benzothiazole avec l'iodobenzène catalysé par **1c**, **2c** et **6c**; les valeurs en pourcentage correspondent à la conversion du benzothiazole mesurée par chromatographie gazeuse.

Résumé

L'étendue du champ réactionnel a ensuite été étudiée (Tableau 1), et **2c** s'est montré actif pour le couplage de quelques thiazoles et oxazoles avec des iodures d'aryles. Les rendements demeurent cependant modérés voire faibles.

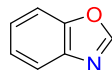
Tableau 1. Etude du champ réactionnel avec différents azoles et halogénures d'aryle

Y = O, S

Entrée	Azole	Haloarène	X	Conversion (%) ^{a,b}	Rendement (%) ^{a,b}
1			I	78	43
2			Cl	0	-
3			I	56	47
4			Br	0	-
5 ^d			Br	0	-
6			I	35	25
7			I	68	58
8			I	49	45
9			I	-	14
10			I	-	13
11			I	-	0
12			I	-	n. d. ^e
13				-	n. d. ^e
14				-	17
15				-	11

Résumé

Tableau 1. (suite)

Entrée	Azole	Haloarène	X	Conversion (%) ^{a,b}	Rendement (%) ^{a,b}
16				-	0

^a Valeur moyenne de 2 réaction minimum. ^b Conversion CG du benzothiazole. ^c Rendement isolé. ^d Réactions réalisées en présence de NaI ou KI (1 équiv.) ^e n.d. – Non déterminé.

De façon intéressante, des études mécanistiques suggèrent une réduction initiale du pré-catalyseur de nickel(II), vraisemblablement en une espèce de nickel(0), par dimérisation d'une quantité sacrificielle d'azole. Par ailleurs, l'empoisonnement de la réaction par addition de mercure(0) suggère que cette espèce de nickel(0) n'existerait pas sous la forme d'une espèce moléculaire discrète mais sous la forme de particules hétérogènes. En outre, des expériences de piégeage radicalaire réalisées avec le radical libre, TEMPO, présent en faible quantité (5 mol%) dans le milieu réactionnel, suggèrent la présence d'espèces radicalaires comme d'importants intermédiaires de la réaction (Schéma 8).

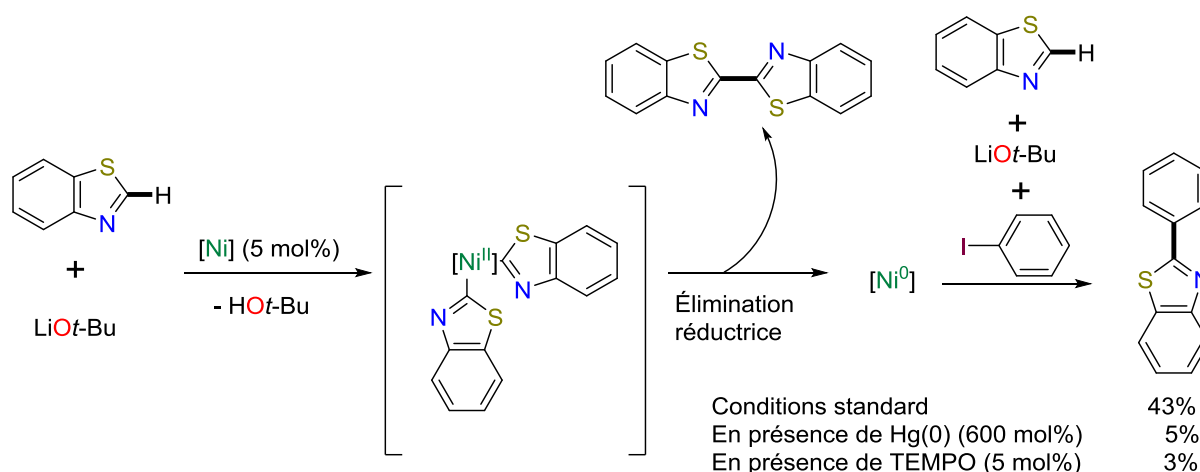


Schéma 8. Réduction du Ni(II) en Ni(0) par dimérisation sacrificielle du substrat et tests d'empoisonnement.

L'absence ou quasi-absence de réactivité de **1c** et **3c** pour ce couplage direct d'azoles avec des iodures d'aryle semblait suggérer la nécessité de ligands labiles ou d'un centre de nickel insaturé. Nous avons donc testé une série de complexes $[\text{Ni}^{\text{II}}\text{Cp}^{\dagger}\text{L}(\text{NHC})]^{(\dagger)}$ ($\text{Cp}^{\dagger} = \text{Cp}$, Cp^* ($\eta^5\text{-C}_5\text{Me}_5$); $\text{NHC} = \text{NHC-Mes}_2$, NHC-DIPP), qui se sont déjà montré actifs pour d'autres couplages C-H/C-X, dans des conditions analogues à celles utilisées avec **2c**. A l'exception du complexe $[\text{Ni}^{\text{II}}\text{Cl}(\text{Cp}^*)(\text{NHC-Mes}_2)]$ **6** qui montre une activité résiduelle pour le couplage de la benzothiazole avec l'iodobenzène, tous les autres complexes se sont révélés totalement inactifs. Le suivi de la réaction par RMN ^1H avec $[\text{Ni}^{\text{II}}\text{Cl}(\text{Cp})(\text{NHC-Mes}_2)]$ **7** montre la formation

Résumé

d'un complexe C(2)-benzothiazolyle **8** qui semble constituer un puits de potentiel dans ces conditions (Schéma 9).

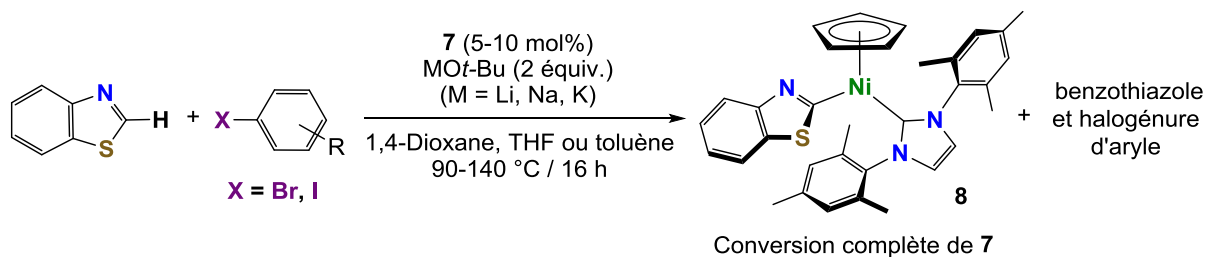


Schéma 9. Formation de **8** dans des conditions de couplage entre le benzothiazole et des haloarènes.

Bien que des complexes C(2)-benzoxazolyle ou C(2)-benzothiazolyle soient souvent proposés comme intermédiaires réactionnels de couplages de type C–H/C–X entre des hétéroarènes et des électrophiles aryliques, alcényliques ou alkyliques, les exemples décrits dans la littérature sont très rares. A notre connaissance, le seul ayant été décrit avec le nickel avant **8** est un complexe pince de type *N,N,N*-Ni(II) qui s'est révélé effectivement être un intermédiaire pour l'alkylation d'azoles. Ces réactions d'alkylations étant potentiellement plus intéressantes que les réactions d'arylation – étant données (i) la corrélation positive entre la pourcentage de C_{sp^3} dans une molécule pharmaceutique et sa performance thérapeutique et (ii) le nombre plus limité d'exemples de formation de liaisons C_{sp^2} – C_{sp^3} que de liaisons C_{sp^2} – C_{sp^2} – nous avons donc testé **6**, **7** et **8** pour l'alkylation du benzothiazole avec l'iododécane dans des conditions similaires à celles décrites avec ce complexe pince. De façon très satisfaisante, **6**, **7** et **8** se sont tous les trois révélés actifs dans cette réaction (Schéma 9).

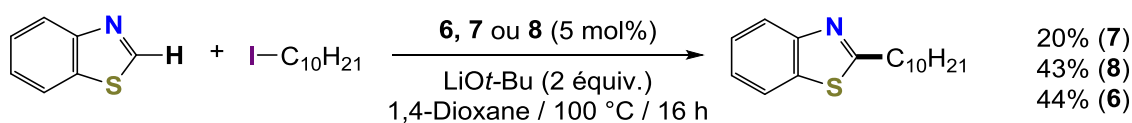


Schéma 9. Couplage du benzothiazole avec le 1-iododécane catalysé par **6**, **7** et **8**; les valeurs en pourcentage correspondent à des rendements isolés.

Ces résultats suggèrent que le complexe Ni(II)-benzothiazolyle **8** serait effectivement un intermédiaire de cette réaction d'alkylation du benzothiazole avec le 1-iododécane. En outre, la comparaison des performances des complexes Cp* **6** (44%) et Cp **7** (20%) suggérerait que le caractère plus électro-donneur du ligand Cp* serait bénéfique à la réaction. En conséquence, nous avons étudié le comportement électrochimique des complexes Cp et Cp* par voltampérométrie cyclique. Pour ce faire, la forme Ni(II)-benzothiazolyle étant supposée être

Résumé

plus avancée dans le chemin réactionnel, le complexe $[\text{Ni}^{\text{II}}(\text{benzothiazolyl})(\text{Cp}^*)(\text{NHC-Mes}_2)]$ (**9**) a été synthétisé afin de pouvoir être comparé avec **8**.

Les potentiels d'oxydation mesurés par rapport au couple Fc/Fc^+ pour **8** et **9**, et attribués à un couple $\text{Ni}(\text{II})/\text{Ni}(\text{III})$, sont de $E_{\text{p,a}} = 0.06 \text{ V}$ pour **8** et de $E_{\text{p,a}} = -0.44 \text{ V}$ pour **9** (Fig. 5). La corrélation de ces résultats avec l'activité catalytique des complexes parents **6** et **7** suggère que les espèces $\text{Ni}(\text{II})$ -benzothiazolyle **8** et **9** constituent un important intermédiaire avant la génération probable d'une espèce active de $\text{Ni}(\text{III})$, et que la génération de cette espèce est limitante pour la réaction.

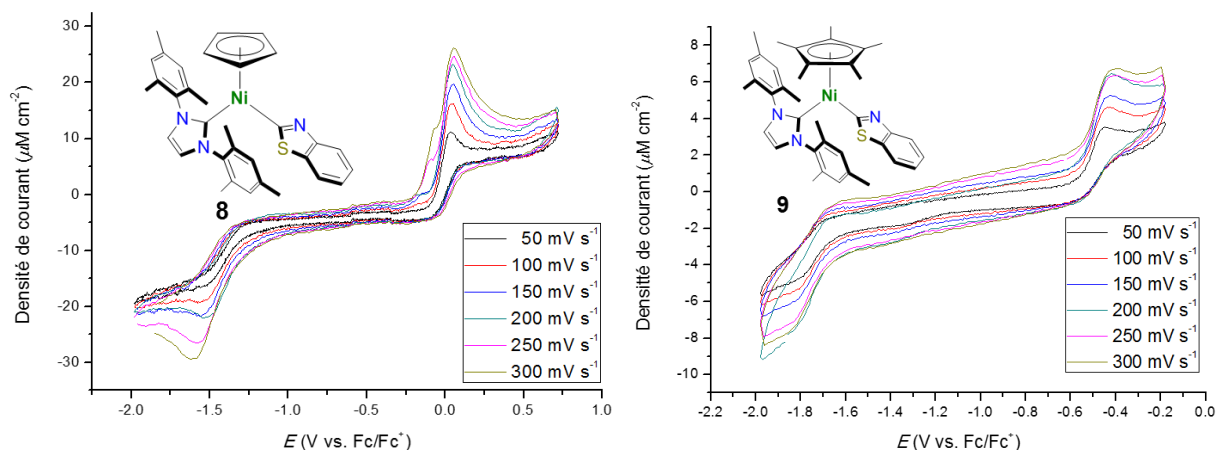


Figure 5. Voltampérogrammes cycliques des complexes **8** et **9**: 1 mM dans une solution à 0.1 M de $n\text{-BuNPF}_6$ dans MeCN, avec une électrode de travail en carbone vitreux, une contre-électrode à fil de platine, et une électrode de référence Ag/AgCl , KCl 3 M. Vitesses de scan de 50, 100, 150, 200, 250 et 300 mV s^{-1} . Voltampérogrammes référencés par rapport au couple Fc/Fc^+ (2 mM) ; $E = 0.48 \text{ vs. Ag}/\text{AgCl}$, KCl 3 M.

Dans l'optique de favoriser encore d'avantage l'oxydation de l'intermédiaire $\text{Ni}(\text{II})$ -benzothiazolyle, on a cherché à enrichir encore d'avantage le métal en électrons par une modification du ligand NHC. Pour ce faire, le complexe $[\text{Ni}^{\text{II}}(\text{Cl})(\text{Cp}^*)(^{4,5}\text{Me}_2\text{NHC-Mes}_2)]$ (**10**) comportant un NHC plus électro-donneur que NHC-Mes_2 a été synthétisé selon la méthode classique de préparation des complexes $\text{Cp}^*\text{Ni}(\text{II})\text{-NHC}$ et obtenu avec un rendement de 15% (Schéma 10).

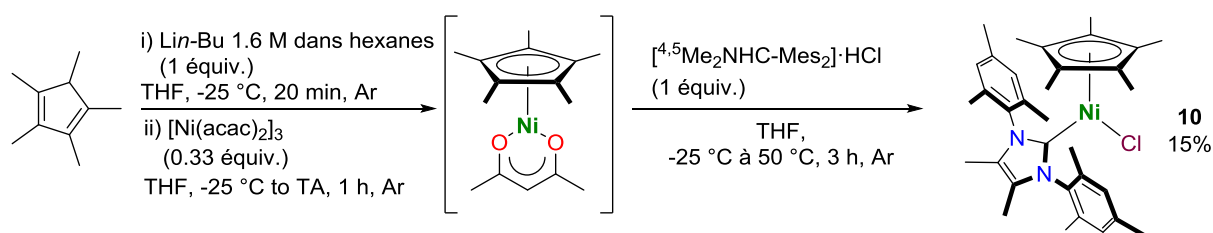


Schéma 10. Synthèse du complexe **10**.

Résumé

De façon décevante, l'activité catalytique du nouveau complexe **10** pour l'alkylation du benzothiazole avec le 1-iododecane (44% de rendement), s'est révélée être du même ordre que celle de **6**, le ligand $^{4,5}\text{Me}_2\text{NHC-Mes}_2$ n'apportant donc pas d'amélioration significative.

3) Conclusion générale

En conclusion, une série de quatre nickelacycles cationiques **2a-d** comportant un robuste chélate $\kappa^2\text{-C}_{\text{NHC}}, \text{C}_{\text{alkyle}}$ anionique a été synthétisée avec de très bons rendements via des procédures optimisées. La caractérisation complète de ces composés, couplée à une analyse structurale par calculs DFT, nous a permis d'établir qu'ils ne comportent qu'un seul ligand acétonitrile à l'état solide, et suggère qu'ils existent sous forme de rares espèces de nickel(II) tri-coordinées à 14 électrons de valence de structure T.

L'exploration de la réactivité de **2c** avec des ligands phosphine (PPh_3 et PMe_3) a montré la tendance des nickelacycles $\text{C}_{\text{NHC}}, \text{C}_{\text{alkyle}}$ à générer des systèmes dynamiques en solution. Ainsi, les ligands phosphines seraient soumis à un échange avec le solvant MeCN et, dans le cas de phosphines à faible encombrement stérique et fort pouvoir électro-donneur (PMe_3) à isomérisation *cis/trans* via un équilibre dynamique de coordination/décoordination des molécules de solvant.

L'application de ces complexes coordinativement et électroniquement insaturés dans des réactions de couplage direct entre des azoles et des halogénures d'aryle et la comparaison de leur activité à celles de leurs analogues saturés a montré l'importance de la combinaison de la chélation $\text{C}_{\text{NHC}}, \text{C}_{\text{alkyle}}$ et de l'insaturation du centre métallique pour réaliser ces couplages. Toutefois, leur performance reste loin de celles de sels de nickel associés à des chélates pnictogènes neutres *N,N* et *P,P* ou à des NHC décrits précédemment, que ce soit en terme d'activité ou d'étendu du champ réactionnel.

Par ailleurs, l'absence de réactivité dans ces couplages $\text{C}_{\text{sp}^2}\text{-H}/\text{C}_{\text{sp}^2}\text{-X}$ de complexes demi-sandwich de type $[\text{NiCp}^+\text{L}(\text{NHC})]^{(+)}$ a mené à l'isolement d'un rare intermédiaire Ni-benzothiazolyle actif dans des réactions d'alkylation directe d'azole (couplage $\text{C}_{\text{sp}^2}\text{-H}/\text{C}_{\text{sp}^3}\text{-X}$). Ce résultat a ouvert la voie à une nouvelle fonctionnalisation de liaisons C-H catalysée par des espèces nickel(II)-NHC pour laquelle des études électrochimiques suggèrent un mécanisme passant par une espèce de Ni(III).

Chapter 1

Introduction: from the periodic table to nickel-*N*-heterocyclic carbene catalysts

Chapter 1

Introduction: from the periodic table to nickel-*N*-heterocyclic carbene catalysts

I. Emergence of nickel homogenous catalysis	30
II. Nickel-NHC complexes in homogeneous catalysis	34
II.1. <i>N</i> -Heterocyclic carbene (NHC) ligands.....	34
II.2. Metal- <i>N</i> -heterocyclic carbene (M-NHC) bond.....	36
III. Nickel- <i>N</i> -heterocyclic carbene (Ni-NHC) in homogeneous catalysis: C–H bond functionalization (2015-2018).....	41
III.1. C–H cross-coupling	42
III.1.1 C_{sp} and C_{sp^2} functionalization	42
III.1.2. C_{sp^3} –H functionalization	46
III.2. Formal 1,2-Additions to unsaturated C–C bonds.....	47
III.2.1. To alkynes ($C\equiv C$)	47
III.2.1.A. Hydroarylation	47
III.2.1.B. Three-component couplings.....	50
III.2.2. To alkenes ($C=C$)	52
III.2.2.A. Hydro(hetero)arylation reactions.....	52
III.2.2.B. Formal C–H addition of carbonyl substrates to olefins.....	57
IV. Overview.....	58

Chapter 1 – Introduction: from the periodic table to nickel-*N*-heterocyclic carbene catalysts

I. Emergence of nickel homogenous catalysis

« Better Living Through Chemistry » entered pop culture as an offshoot of a DuPont advertising campaign (Figure 1). Apart from a slogan that permeated culture, it reflects the improvement in quality of life by the knowledge production and technological outputs of the chemical sciences. To accomplish this, novel reactions had to be unlocked, less reactive chemical feedstocks had to be tapped into, and milder processes had to be adopted. These demands led to the establishment of catalysis as both a main technological domain and an academic subject. Indeed, catalysis accounts for 90% of the world's chemical processes and the production of 60% of chemical products,¹ at the same time being at the core of numerous attributions of the Nobel Prize in Chemistry – from Ostwald in 1909 to, more recently Knowles, Noyori and Sharpless in 2001, Chauvin, Grubbs and Schrock in 2005 or Heck, Negishi and Suzuki in 2010.²



Figure 1. Original version of the DuPont company slogan. Image taken from - Mechanical Engineering at DuPont circa 1950 E. I. du Pont de Nemours and Company.³

More precisely, catalysis is the process by which a reaction's rate is increased without modifying the overall standard Gibbs energy, by action of an exogenous substance termed 'catalyst' that is both reagent and product of the reaction (Figure 2).⁴ As a corollary by choosing the appropriate catalyst, key steps can be controlled and the selectivity of the reaction dictated.

Homogenous catalysts (catalysts that react with the substrates in the same phase, usually in solution) have gained fame for performing with high activities, selectivity's and mild reaction conditions.⁵ In particular, catalysts based on rare second and third row transition metals such as palladium, rhodium, iridium or ruthenium have emerged as darlings of the

chemical industry.⁶ However, growing societal concerns over the toxicity of these metals,⁷ their price and availability (Figure 3)⁸ and researchers' need to find new hot topics to secure financing has led to a renaissance of first row transition metal chemistry. By acting as surrogates to their heavier congeners' reactivity, 3*d* metal based catalysts were expected to overcome these problems. Moreover, these are important trace elements in biological systems and they offer their own unique intrinsic reactivity to be exploited as novel homogeneous catalysts.⁹

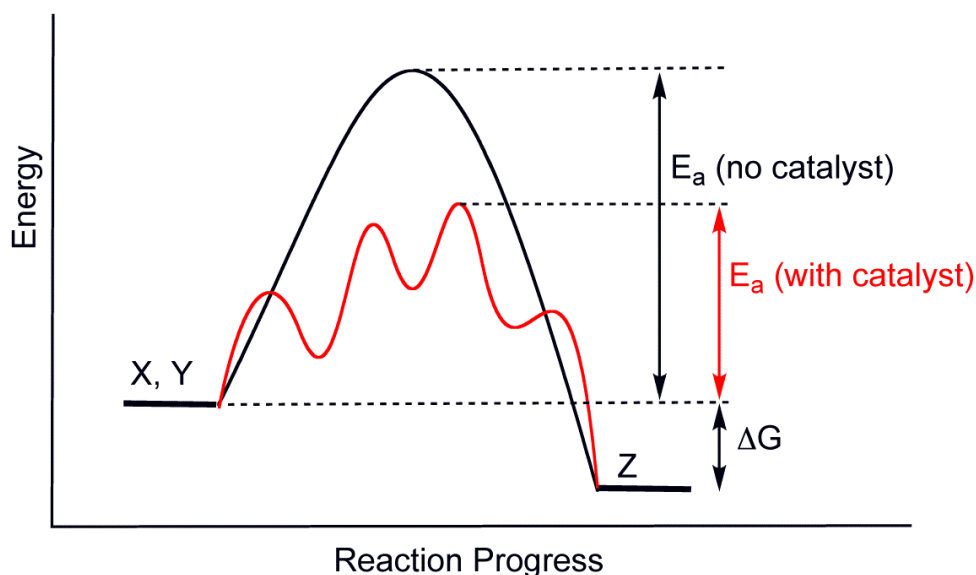


Figure 2. Energy diagram for a model exothermic reaction: X plus Y to give Z (black). Addition of a catalyst leads the reaction to take an alternate pathway (red). The overall activation energy (E_a) is thus lowered by the action of the catalyst with no change the overall Gibbs energy (ΔG) or product of the reaction.⁴

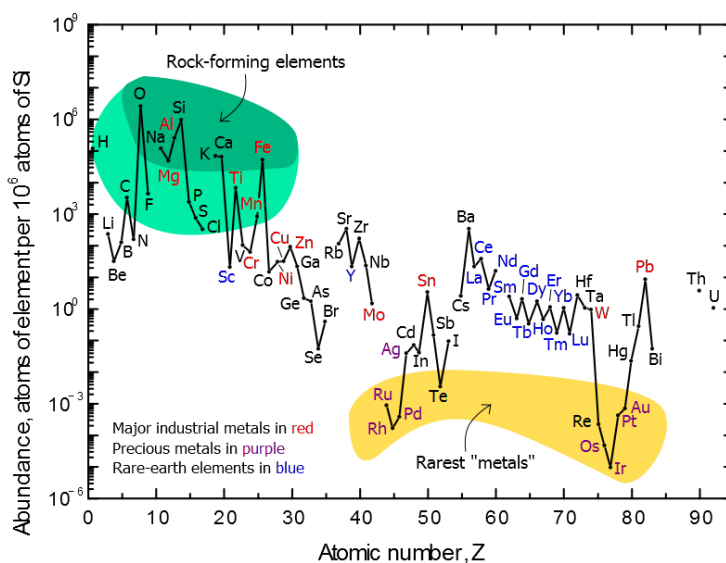
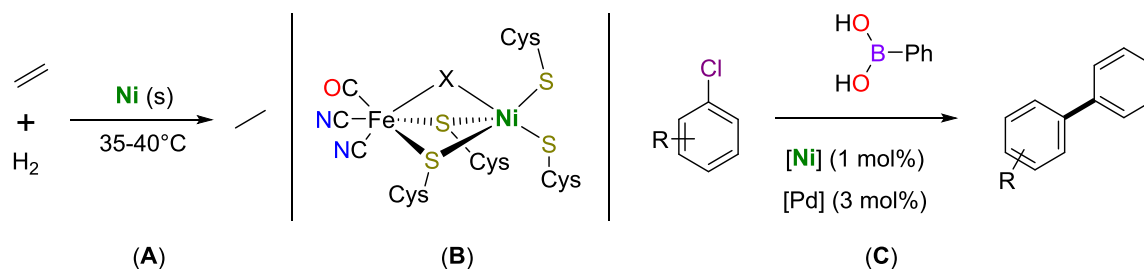


Figure 3. Elemental abundance in the Earth's crust, normalized to silicon abundance (10^6 atoms). The most popular rare metals used in homogeneous catalysis (Ru, Rh, Pd, Ir) are all found on the bottom quartile of the graph, while their lighter counterparts are found in the top half of the graph.⁸

The late transition metal subgroup for first row metals – iron, cobalt, nickel and copper – makes up a privileged choice as prospective homogeneous catalysts; having already found use at the industrial level.⁶ As the lighter counterpart of palladium – “the metal of the 21st century”¹⁰ – nickel has drawn interest in several domains due to its particular reactivity.^{11,12} Works by Paul Sabatier using it as an heterogeneous catalyst for the hydrogenation of olefins awarded him the co-attribution of the Nobel Prize in Chemistry in 1912 (Scheme 1, **A**).^{13,14} More recently, its role in enzymes has begun to be unveiled (Scheme 1, **B**).^{15,16} Notable applications as a homogeneous catalyst include the production of acetic and propionic acids, the production of adiponitrile, or the Shell higher olefin process (SHOP).¹⁷ There are also successes mimicking palladium catalyzed cross-coupling reactions (**C**), that have since given way to innovative coupling reactions.^{12,18}



Scheme 1. Notable examples of nickel catalyst systems: heterogeneous – ethylene hydrogenation (**A**);^{13,14} enzymatic – [NiFe] hydrogenase active site of *Desulfovibrio vulgaris* (**B**);¹⁹ homogeneous – cross-coupling reaction using aryl chlorides (**C**).^{20,21}

This last point has received considerable attention, bestowing upon nickel a reputation as a “poor man’s palladium” given its high availability, low cost¹² and higher toxicity limit* (2-3 times higher than for palladium).^{22,23} However, nickel shines brightest not as a stand-in for palladium but as a partner with complementary reactivity.^{11,12}

Nickel’s less electronegative character was found to facilitate oxidative addition, making traditionally less reactive phenol based coupling partners (i. e.: triflates, carbamates, tosylates, esters, ethers) exploitable. Its smaller size and harder nature²⁴ disfavor β -H elimination – which has historically limited the use of coupling partners in Pd-catalyzed cross-coupling reactions. Further, its ability to adopt many oxidation states (0, +1, +2, +3, +4) including odd electron ones, allows for radical type reactivity and single-electron transfer (SET) reactions. These have

* The reader should be aware that beyond regulatory limits, the determination of the toxicity of metals remains a complex unresolved problem. Despite the often invoked link between the biological role of transition metals and toxicity, no clear trend has been established ranking transition metal row and toxicity.^{353,354}

in more recent years been highlighted in photo-catalyzed cross-coupling systems (Figure 4).^{25,26}

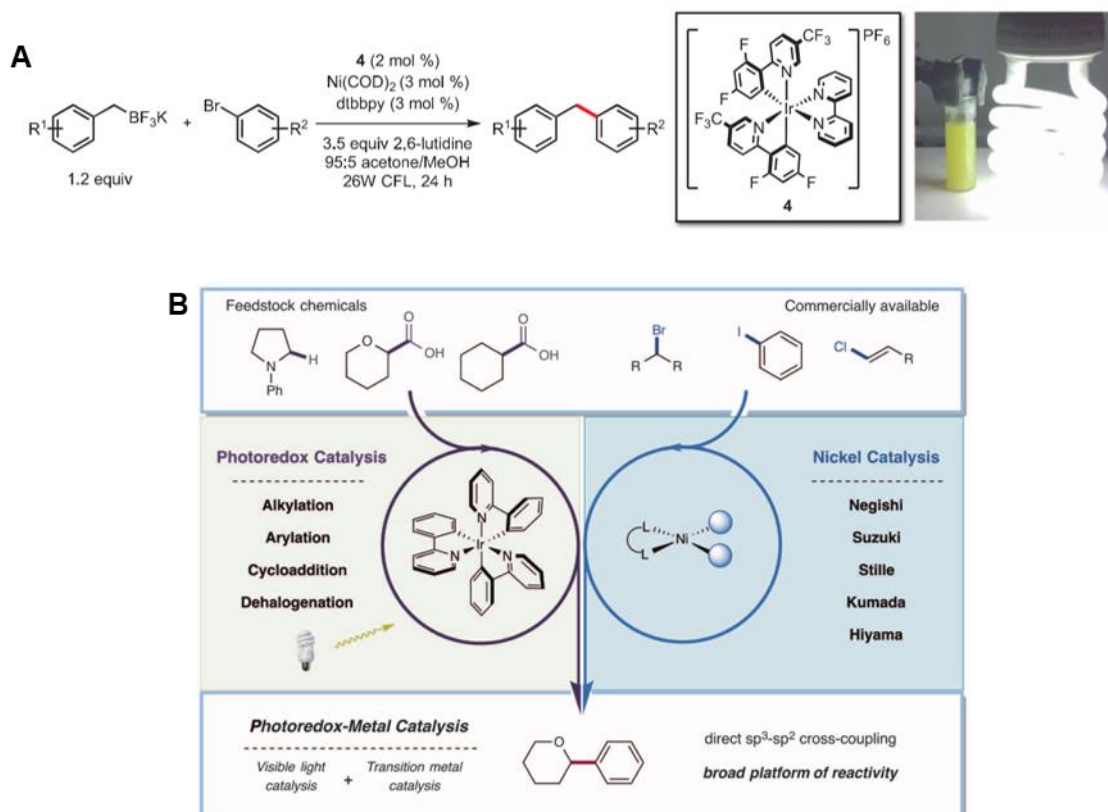


Figure 4. Simultaneous reports of photocatalytic nickel cross-coupling from the groups of Molander (A) and MacMillan (B). Images adapted from refs^{25,26}.

A downside to this less explored reactivity is that the mechanisms by which many nickel-catalyzed transformations are carried out are not altogether clear at this point (Table 1).¹² In part due to the relative infancy of the field, and to the expedient spillover of palladium's well-established mechanisms. Nickel's high reactivity often leads to the formation of many intermediates²⁷ and off-cycle species²⁸ that can be difficult to observe, identify and isolate. Two aggravating factors are the high catalytic charges often used (5-20 mol%) and the ferro- (for metallic nickel) or paramagnetic nature of the nickel species present. The first suggests inefficient catalyst generation and therefore a low concentration of the active catalyst and a high concentration of off-cycle products, hindering the identification of the active species. Also, spectroscopic analysis is made more complex by the possibility of both paramagnetic and diamagnetic species silent to NMR or EPR spectroscopic analysis, respectively. These open questions are a bottleneck to the rational and efficient design of nickel homogeneous catalysts that merit more dedicated study.

Table 1. Difficulties in studying mechanisms of nickel-catalyzed reactions, features and consequences.

Feature	Consequence
Infancy of the field	Few detailed studies in the literature False comparisons with Pd reactivity
High reactivity	Generation of many active or inactive nickel species in the mixture
High catalytic charges	Inefficient catalyst generation More off-cycle species formed Low concentration of the active species
Easy access to multiple oxidation states	Both diamagnetic and paramagnetic species can form that are either NMR or EPR silent

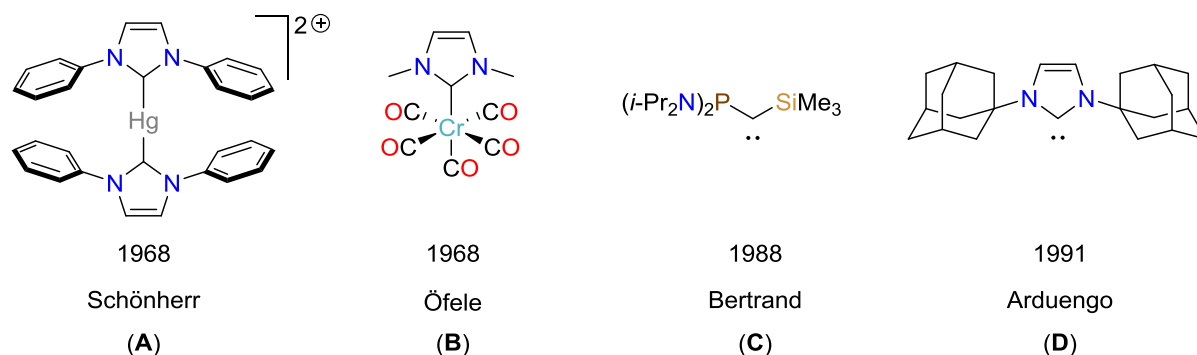
II. Nickel-NHC complexes in homogeneous catalysis

II.1. *N*-Heterocyclic carbene (NHC) ligands

Control of a metal's reactivity is exerted by the effect its ligands play in modulating the stereoelectronic environment of the coordination sphere. This has caused the development of powerful theoretical models such as the crystal field theory^{29,30} and its subsequent incorporation of molecular orbital theory to develop ligand field theory^{30,31} as powerful tools to the design and understanding of this dance. With these models and empirical observations, ligand design became an established practice in the field of homogeneous catalysis as the manner by which high activity, durability, recyclability and selectivity are controlled. Thus, ligand design and synthesis can be a critical and high resource consuming task with the ligands being at times the most expensive part of the catalyst.^{32,33} Among these, *N*-heterocyclic carbenes (NHCs) make up a highly impactful group.

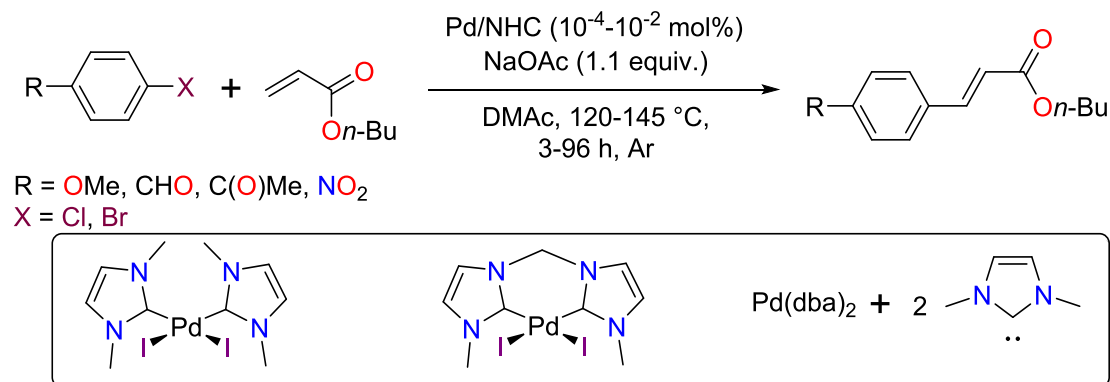
First observed as ligands in organometallic compounds in the late 1960's (Scheme 2, **A** and **B**),^{34,35} the isolation of the first free NHC had to wait until the early 1990's³⁶ (Scheme 2, **D**) shortly after the first isolation of a free carbene³⁷ (Scheme 2, **C**). The first carbene to be isolated was an acyclic phosphinocarbene (*i*-Pr₂N)₂P-C-SiMe₃ (Scheme 2, **C**) that found little subsequent application.³⁷ In contrast, α -heteroatom stabilized carbenes found widespread use with the successful isolation of the first 'bottleable' carbene

bis-1,1'-adamantyl-imidazol-2-ylidene [NHC-Ad₂][†] (Scheme 2, **D**), spearheading the imidazol-2-ylidene family and NHC chemistry as a whole. This discovery led to an explosion of research based on these carbenes (with the seminal report by Arduengo³⁶ counting 2 630 citations on the Web of Science database, www.webofknowledge.com accessed on 2018-07-09).



Scheme 2. Structures of the first complexes bearing NHC ligands (**A** and **B**), the first isolated free carbene (**C**) and the first isolated free NHC (**D**).

Key to the popularity of this research topic was the number of exciting applications of metal bound NHC systems, most notably in catalysis. The first reported use of this pair was for the cross-coupling of haloarenes and *n*-butylacrylate,³⁸ where palladium-NHC complexes were used instead of the usual palladium-phosphine systems³⁹ (Scheme 3).



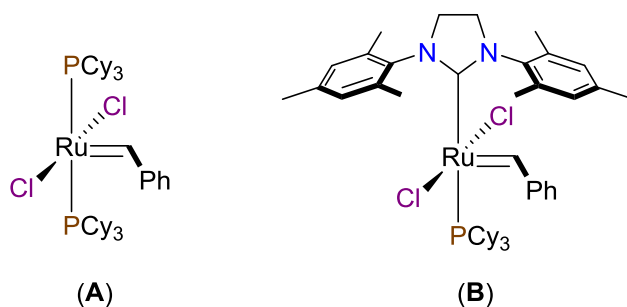
Scheme 3. First application of transition metal-NHC catalytic systems.³⁸

[†] In the literature bis-1,1'-adamantyl-imidazol-2-ylidene is noted as IAd. This formulation is most widespread with popular bis-1,1'-mesitylimidazol-2-ylidene (IMes) and bis-1,1'-(2,6-di-*i*-propylphenyl)-imidazol-2-ylidene (IPr) or the backbone saturated bis-1,1'-mesitylimidazoline-2-ylidene (SIMes) and bis-1,1'-(2,6-di-*i*-propylphenyl)-imidazol-2-ylidene (SIPr), however, in this document the formulation NHC-Ad₂, NHC-Mes₂, NHC-DIPP₂, ^{4,5}H₂NHC-Mes₂, ^{4,5}H₂NHC-DIPP₂ was preferred for allowing a clearer description of the motif especially with different *N*-substituents (e. g.: R¹-NHC-R²).

Amongst the highlighted results, high turnover numbers (TON) at very low catalyst loadings could be achieved by the direct addition of the free NHC and a source of palladium(0) to the reaction mixture.³⁸ The authors strongly emphasized the benefits of the new ligand; the stoichiometric ligand charge (vs. metal), and the high thermal stability of the resulting catalytic species, even at high temperatures for prolonged reaction times.³⁸

This first example was called by the authors “*a new structural principle for catalysts in homogeneous catalysis*”, a bold declaration that would be confirmed over the following decades.³⁸ Thus, for instance, the most well-known success story of metal-NHC (M-NHC) catalyst systems is that of the Grubbs 2nd generation olefin metathesis catalyst (Scheme 4, **B**),⁴⁰ now commercially available.³²

From the first ruthenium systems [Ru(PR₃)₂Cl₂(=CHPh)] (Scheme 4, **A**), a phosphine ligand was replaced with a NHC ligand to give complexes not only with higher activities but more air and moisture stable than the state-of-the-art at the time.^{40,41} The development of such high performing and stable catalysts was an integral part of the co-attribution of the Nobel Prize in Chemistry in 2005 to Robert H. Grubbs.⁴²



Scheme 4. 1st (**A**) and 2nd (**B**) generation Grubbs' catalysts.

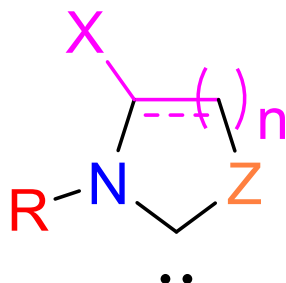
These examples are only the seminal and most successful cases of M-NHC catalyst systems out of a large number described as attested by the reviews, book chapters and books compiled on this topic.^{43–47}

II.2. Metal-*N*-heterocyclic carbene (M-NHC) bond

In order to be able to predict the effect of NHC ligands in chemical reactions, theoretical models had to be developed that could explain the M-NHC bond. For this, a description of the electronic structure of the NHC will be first exposed. *N*-Heterocyclic carbenes considered here are largely derived from the imidazol-2-ylidene family (Figure 5) and can be defined as:

*Heterocyclic species containing a carbene carbon (C_{NHC}) and at least one vicinal nitrogen atom within the ring structure.*⁴⁸

 α -Nitrogen (N)*Electronic stabilization*

Backbone (X)*Electronic stabilization by:*
aromaticity of the heterocycle,
substituent effect (X)*Steric influence from:*
Substituent (X) bulk & bite angle
by controlling cycle size (n)

N-Substituent (R)*Steric hindrance**Kinetic stabilization**Electronic stabilization (minor)*

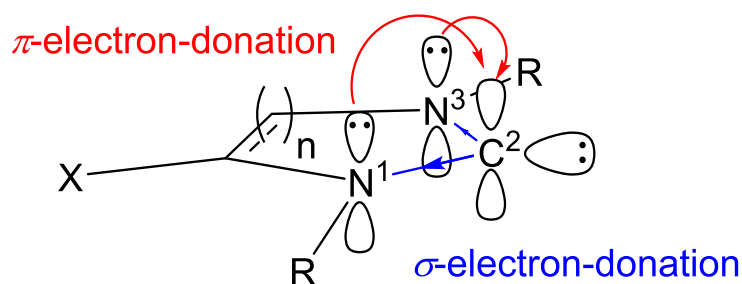
 α' -(Hetero)atom (Z)*Similar to α -nitrogen*

but can be B, C, N, O, Si, P, S

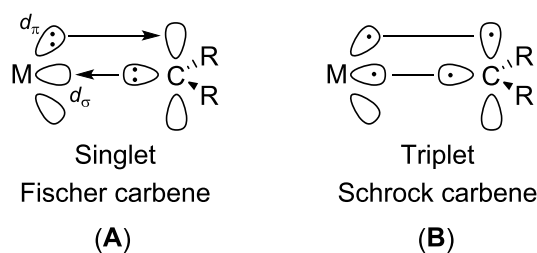
Varying number of substituents

Figure 5. General structure of a NHC with different modules and their influence highlighted. α -Nitrogen (blue), *N*-substituent (red), backbone (pink), α' -(hetero)atom (orange).

In these scaffolds, the carbene carbon atom is found in a trigonal geometry with its lone-pair filling one of the coordination positions, which is imposed by the rigidity of the ring. In view of this geometry the frontier molecular orbitals (FMO)⁴⁹ can be described as being a Highest Occupied Molecular Orbital (HOMO) in the form of a non-bonding sp^2 hybridized orbital hosting the C_{NHC}'s lone pair and a Lowest Unoccupied Molecular Orbital (LUMO) in the form of the corresponding vacant p orbital (Figure 6). This arrangement gives a large HOMO-LUMO gap that favors a singlet spin state, which is experimentally observed in NMR spectroscopy measurements. The adjacent nitrogen atoms provide further electronic stabilization by inductively draining electronic density away from the carbon via the σ -bonds. At the same time, they participate in mesomeric π -donation from the nitrogen lone pairs to the unoccupied p orbital of the carbon atom. As a consequence of the latter, a curved bond over the resonating atoms is often drawn in the literature to indicate the partial double bond character of these bonds. Electronic effects can be further tuned by the choice of substituents on the heterocycle's backbone and by the substituents at the nitrogen atoms. This last module plays a large role in stabilizing the carbene by imposing a kinetic barrier to access the divalent atom and, most notably disfavoring dimerization to the corresponding olefin (also known as Wanzlick dimer).^{50,51}

Figure 6. Electronic environment of the C_{NHC} .

Combining the above description with a metal fragment, M–NHC bonding can be interpreted in light of the models established for well-known singlet (Fischer)⁵² and triplet (Schrock)⁵³ modes of metal-carbene bonding (Figure 7).⁵⁴ Fischer type carbenes bear π -donor substituents, carry a δ^+ charge on the C_{NHC} , have an electrophilic character and act as neutral 2-electron donors (**A**). Opposite, in Schrock type carbenes, the C_{NHC} bears non- π -donating substituents, carry a δ^- charge and shows a nucleophilic character (**B**). These traits can be used to reference two extremes of singlet (Fischer type) and triplet (Schrock) carbene-metal bonding.

Figure 7. Representation of metal-carbene bonding for singlet (Fischer, **A**) and triplet (Schrock, **B**) carbenes.

From the above, the M–NHC bond is best described as a type of singlet (Fischer) carbene. It should then be noted that like phosphines they are not pure σ -electron donors and the π -acceptor character of the NHC can influence the M–NHC bond. Indeed, quantum chemical calculations employing methods from density functional theory (DFT)⁵⁵ have quantified a non-negligible π -orbital component of the bonding in some cases.⁵⁶ As such, depending on the metal/NHC combination, more or less of this bonding can be added or removed.

In light of these theoretical descriptions of NHCs and M–NHC bonding, tools have been developed to rank NHC's electronic and steric ligand properties. These descriptors have recently been extensively reviewed and are summarily mentioned here to give the reader an overview of the methods used to rank NHC ligand properties.^{57–60} Methods based on reactivity or spectroscopic studies have been used to rank NHCs. Reactivity methods have measured pK_a values⁶¹ and nucleophilicity parameters (N) on NHCs.^{62,63} Electrochemical studies on the

redox potential of M-NHC complexes⁶⁴ have been utilized to measure the Lever electronic parameter (LEP)^{65,66}. Spectroscopic measurements include: IR – Tolman electronic parameter (TEP)⁶⁷ values based on M-NHC complexes;^{68,69} NMR – ¹³C shifts of the C_{NHC} of Pd and Au complexes,^{70,71} *p*-block element (³¹P, ⁷⁷Se) shifts for carbene-phosphinidene adducts⁷² and selenoureas⁷³ and coupling constants of the latter (¹J_{Se-C_{NHC}}),⁷⁴ X-ray diffraction studies on selenoureas were also used to develop an electrostatic map.⁷⁵ Good correlations amongst some of these scales (¹³C-³¹P-⁷⁷Se) and complementary information from others (³¹P scale offers a measure of π -acceptor strength that explains some unexpected observations on the TEP scale) can thus be used to rank the electronic properties of NHCs.

With the importance of the *N*-substituent groups in stabilizing the NHC, they also make up a key aspect of the M–NHC bond and their subsequent reactivity. The *N*-substituents point towards the metal center (Figure 8, **A**) and not away from it as they do with phosphines, (Figure 8, **B**), which imposes a larger steric footprint and can increase stability of certain intermediate species or enact selectivity on the conformations they adopt.



Figure 8. Models of NHC (**A**) and phosphine (**B**) ligands' steric impact. The *N*-substituents are spatially close to the metal center taking a cavity shape. Phosphine substituents point away from the metal center in a cone shape.

Two major tools exist to quantify the NHC steric footprint: the percent buried volume (% V_{bur}) and the steric map (Figure 9). The percent buried volume⁷⁶ indicates how much of a sphere centered at the metal nuclei will be occupied by the ligand (**A**), and can be complemented by a steric map⁷⁷ that defines the calculated space occupied by the ligand, which will actually cause more steric interactions (**B**). However both these methods start from atomic coordinates obtained by X-ray diffraction structures or computational modeling and are 'limited' to one conformation. It presents therefore a concern in the case the initial coordinates are incorrect, but more so that a rigidified structure is used that does not accurately represent reality. This because – in particular with flexible ligands – the solid state structure might be imposed by interactions present in the packing and in the case of calculated structures a lowest energy structure found might not be as important as another accessible conformation.

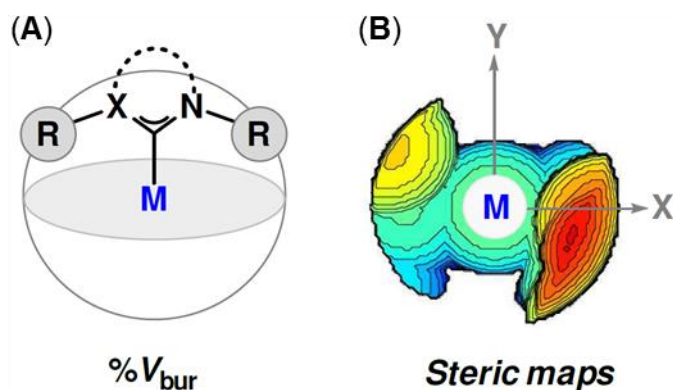


Figure 9. Tools for NHC steric evaluation: percent buried volume ($\%V_{bur}$, **A**) and steric maps (**B**). Image adapted from ref⁵⁸.

With tools to rank NHC stereo-electronic parameters giving complementary information, it is desirable that in the future more systematic approaches in line with the design of experiment (DoE)⁷⁸ principles should be followed. The use of these descriptors in the principle component analysis (PCA)⁷⁹ can be a big-data farming strategy to obtain information on how NHCs modulate chemical reactivity.

A final note on the M–NHC bond pertains to its fame as a strong metal-ligand bond. These bonds have been considered strong due to the inherent lower stability of a free divalent carbon and the thermal robustness observed in M–NHC complexes. However, recent studies have disproven the universality of this claim. For instance, platinum group complexes bearing NHC ligands were found to undergo decomposition under basic conditions typically found in catalytic reactions, most acutely with Pd and Pt (Figure 10).^{80,81} However, decomposition products and the mechanisms it undertook depended on the metal and conditions employed. In particular, homoleptic bis-NHC nickel(II) complexes were found to decompose in common solvents in the presence of water.⁸²

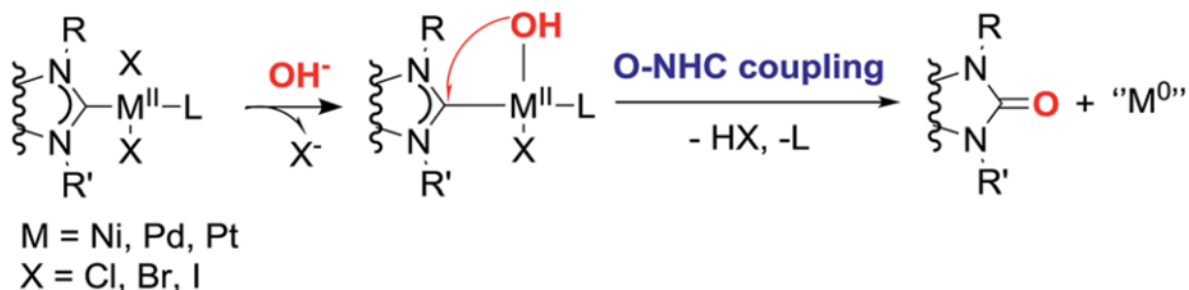


Figure 10. M–NHC bond breaking in basic media. Despite the proclaimed stability of the M–NHC bond the reaction conditions are determinant. Adapted from ref⁸¹.

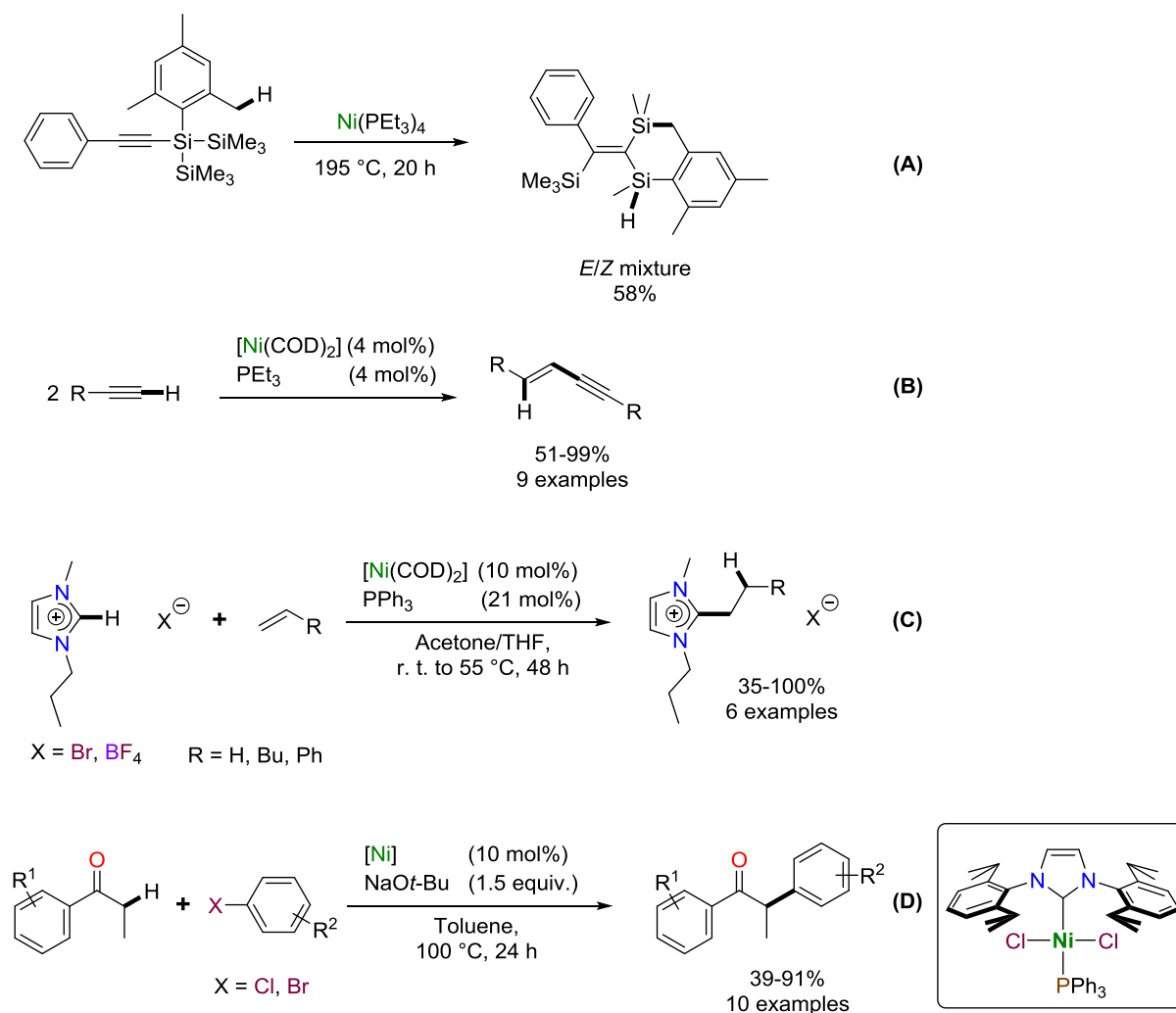
III. Nickel-*N*-heterocyclic carbene (Ni-NHC) in homogeneous catalysis: C–H bond functionalization (2015-2018)

The conjunction of this attractive metal/ligand pair has made Ni-NHC catalytic systems an increasingly popular strategy for organic synthesis. Recent reviews have extensively covered nickel-NHC chemistry and its catalytic applications^{83–85} in reactions such as C–B, C–C, C–N, C–O, C–S, C–Se bond formation, hydrosilylation, oxidation, reduction, cycloaddition, oligomerization and polymerization.

As such a review of the most recent literature (2015-2018) focusing on C–C bond formation by Ni-NHC catalyzed C–H functionalization follows to place the reader with the most recent developments in this field. In addition, in Chapter 3, a literature review of Ni-catalyzed chalcogen-azole C–H bond functionalization will be presented to further contextualize the topic within that specific problem. Overlapping examples will be presented both chapters.

The inherent advantages of using a high universal chemical function and, at the same time producing minimal waste are unquestionable; however such elegant synthetic processes must overcome limitations in reactivity and selectivity. This is a challenge our group has decided to accept in the latter years^{86,87} and the founding framework for this study.

The first example of Ni-catalyzed C–H bond functionalization goes back to Ichikawa's accidental construction of a new C–Si bond as a side product of a desired SiMe₃/Ph terminal alkyne isomerization (Scheme 5, **A**).⁸⁸ Ni-catalyzed C–C bond construction via C–H activation (C–H → C–C) came only in the 2000's with Ogoshi and Kurosawa's report on alkyne dimerization to (*E*)-enynes; using [Ni⁰(COD)₂]/P*t*-Bu₃ (Scheme 5, **B**).⁸⁹ Arguably the first C–C coupling reaction via C–H bond activation to involve an Ni-NHC system was the one reported by Cavell with the addition of imidazolium salts over olefins to give the corresponding alkylated imidazolium salts in the presence of [Ni⁰(COD)₂]/PPh₃ (Scheme 2, **C**).⁹⁰ But the first unequivocal Ni-NHC catalytic system for C–C cross-coupling via C–H bond activation was Matsubara's 2007 report on the α -arylation of acyclic ketones with a heteroleptic nickel-phosphine-NHC complex (Scheme 2, **D**).⁹¹

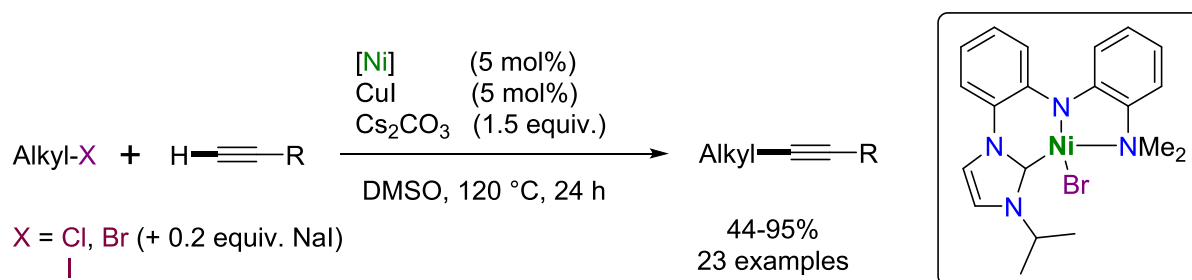


Scheme 5. Seminal reports of Ni mediated C–H bond activation (A), Ni-catalyzed C–H bond activation (B), Ni/NHC C–H bond activation (C) and Ni-NHC catalyzed C–H cross-coupling (D).

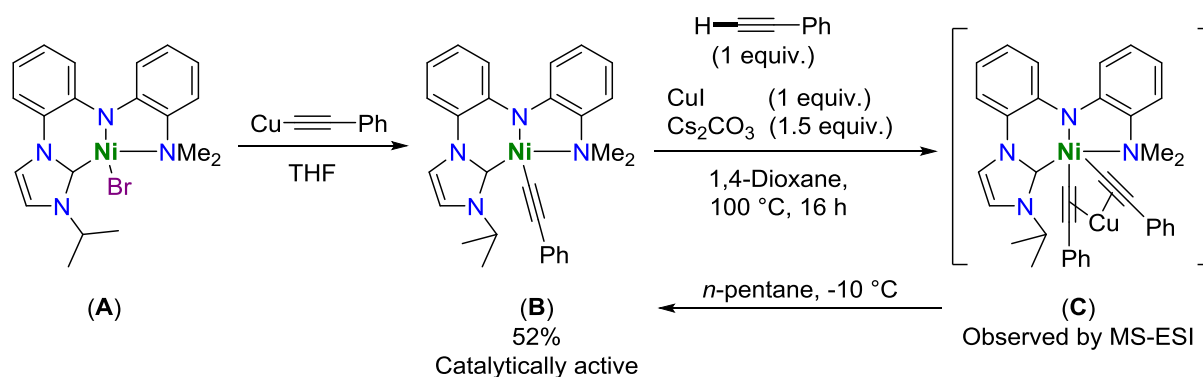
III.1. C–H cross-coupling

III.1.1. C_{sp} and C_{sp^2} functionalization

Li and co-workers reported the C_{sp} -H bond functionalization of alkynes by a Sonogashira⁹² alkylation, using a well-defined C_{NHC}, N, N -Ni(II) complex with a pincer ligand (Scheme 6).⁹³ Using this Ni(II) complex (5 mol%), CuI (5 mol%) and Cs_2CO_3 , a number of alkynes were successfully alkylated using iodides, bromides or chlorides (the latter two in the presence of NaI) (23 examples, 44-95% yield). The authors noted by a control experiment that CuI alone did not produce the coupling products.

Scheme 6. Sonogashira-type alkylation by a C_{NHC},N,N -Ni(II) pincer complex.

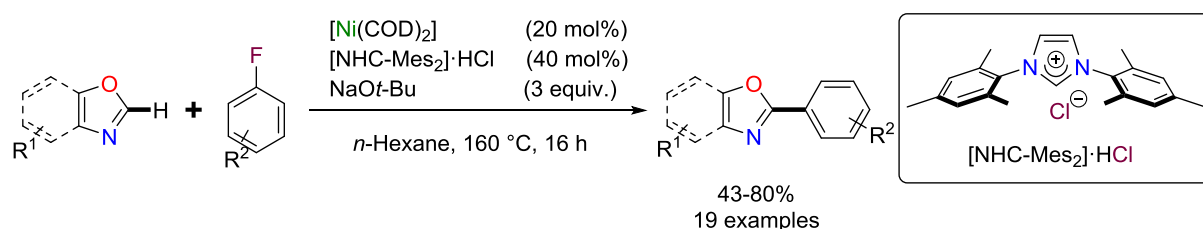
In efforts to understand the reaction mechanism, the authors synthesized a catalytically competent (5 mol%, 93% yield) Ni(II)-phenylacetylide complex (Scheme 7, **B**). They studied this complex by cyclic voltammetry in which it displayed a reversible redox behavior with an oxidation wave at $E_{1/2} = 0.21 \text{ V}$ vs. Fc/Fc^+ assigned to $[\text{Ni}(\text{C}\equiv\text{C}-\text{Ph})]^{+2/+3}$. This allowed the authors to rule out the intermediacy of a Ni(IV) species in this reaction. In addition, a control experiment using a free radical as a trapping agent (TEMPO, 5 mol%) did not show any meaningful loss of yield (95%). Finally, the authors reacted the complex with phenylacetylene, CuI and Cs_2CO_3 (1:1:1.5 equiv.) (Scheme 7, **B** \rightarrow **C**) to give a solid that was characterized by MS-ESI being a bis-phenylacetylide-Ni-Cu complex (Scheme 7, **C**), unfortunately they could not confirm this by NMR as it appeared to decompose back to the Ni-phenylacetylide complex in solution (Scheme 7, **C** \rightarrow **B**).



Scheme 7. Search for catalytic intermediates.

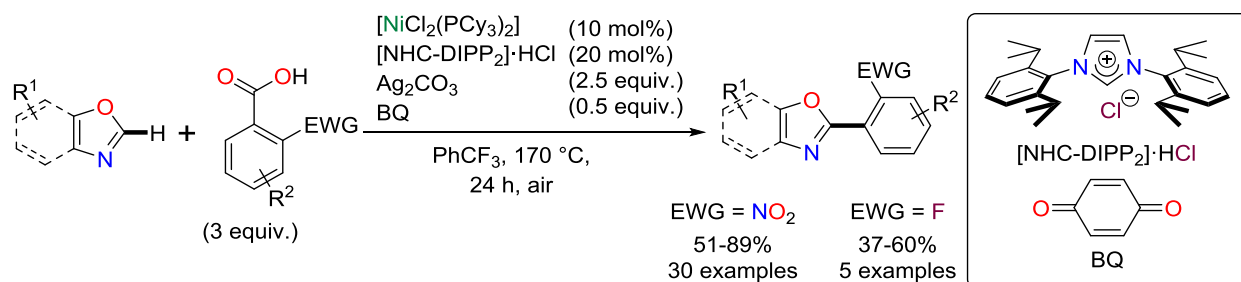
In one of the few examples of Ni-NHC C–H functionalization of azoles, Bai, Lan, Zhang and collaborators reported the use of aryl fluorides as electrophilic coupling partners.⁹⁴ Using $[\text{Ni}^0(\text{COD})_2]/[\text{NHC-Mes}_2]\cdot\text{HCl}$ (1:2 ratio, 20 mol%) and $\text{NaO}t\text{-Bu}$ as a base in *n*-hexane at 160 °C, benzoxazole and a series of fluoroarenes could be coupled in moderate to good yields (13 examples, 43-80% yield, Scheme 8). Substituted benzoxazoles (4 examples, 44-53% yield) and 5-aryloxazoles (2 examples, 54-55% yield) could also be successfully coupled.

Other azoles did not react in this reaction and a marked effect of the nature of the alkoxide's cation was observed, with KO*t*-Bu being much less efficient than NaO*t*-Bu.



Scheme 8. Aryl fluorides as benzoxazole coupling partners catalyzed by Ni-NHC.

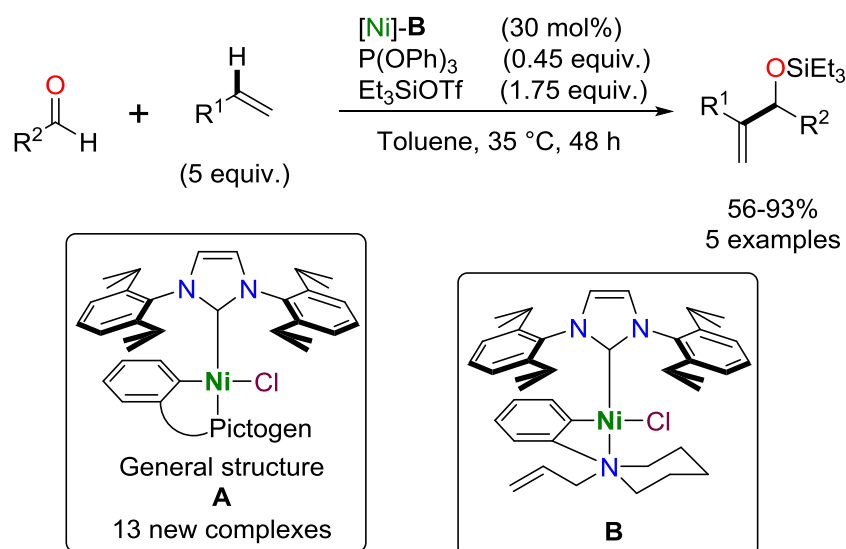
However, the first example of Ni-NHC catalyst system in for azole C–H bond functionalization made use of carbon electrophiles, by decarbonylative cross-coupling. Carboxylic acids were also reported as useful reagents undergoing decarboxylative arylation catalyzed by nickel (Scheme 9).⁹⁵ Using $[\text{Ni}^{\text{II}}\text{Cl}_2(\text{PCy}_3)_2]$ and $[\text{NHC-DIPP}_2]\cdot\text{HCl}$ (1:2 ratio, 10 mol%) mixed with Ag_2CO_3 as both base and oxidant and 1,4-benzoquinone (BQ) as a co-oxidant, substituted benzoxazoles (21 examples, 51-81% yield) and oxazoles (9 examples, 52-89% yield) could be coupled with either *o*-nitrobenzoic acids (30 examples, 51-89% yields, Scheme 9) or *o*-fluorobenzoic acids (5 examples, 37-60% yields) when heated to 170 °C in (trifluoromethyl)benzene. Of note, benzothiazole could also successfully be used as a substrate to couple with *o*-nitrobenzoic acid (75% yield).



Scheme 9. *o*-Nitrobenzoic acids as reagents for decarboxylative cross-coupling via nickel-NHC catalysis.

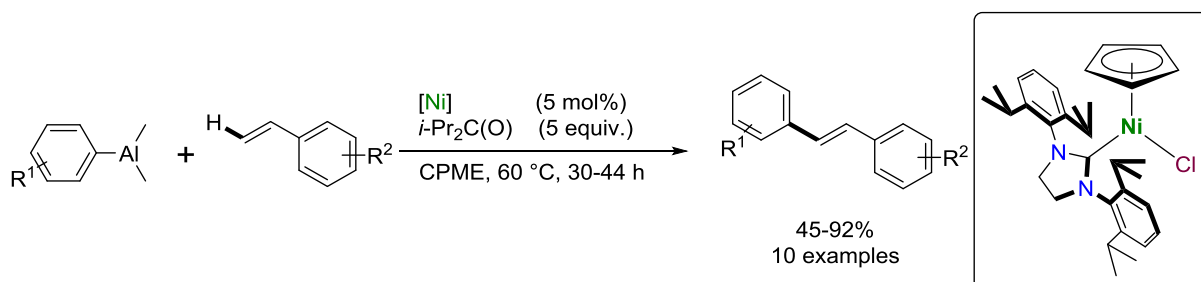
Jamison and co-workers used an aldehyde, olefin, silane three-component coupling reaction, that undergoes a formal C–H cross-coupling, to benchmark the effectiveness of new Ni(II)-NHC pre-catalysts (Scheme 10).⁹⁶ The authors envisioned their new cyclometallated κ^2 -carbon,pnictogen Ni(II) complexes (**A**) would be air-stable but easily activated in reaction conditions, by facile reductive elimination of the chelating ligand and generation of an active Ni(0)-NHC catalyst, a strategy previously used in Pd precatalysts.⁹⁷ Screening the new complexes (30 mol%) in the presence of $\text{P}(\text{OPh})_3$ (0.45 equiv.) and NEt_3 (6 equiv.) in toluene

at 35 °C, 2-octene (5 equiv.), benzaldehyde and Et₃SiOTf (1.75 equiv.) were coupled to give the corresponding α,β -unsaturated silyl ether, with the *C,N*-cyclometallated complex (**B**) as a distant top performer (93% yield). The reaction could then be expanded to couple other olefins (4 examples) and aldehydes (4 examples) to Et₃SiOTf in poor to excellent yields (6 examples, 5-93% yield). Most notably, when the same reaction was run using the popular [Ni⁰(COD)₂] and NHC-DIPP₂ (1:1 ratio, 30 mol%) the reactions showed a noticeably lower performance (4-73% yield). A control experiment where 2-octene, benzaldehyde and Et₃SiOTf were coupled by **B** (30 mol%) in the presence of COD (0.6 equiv.) demonstrated the detrimental effect of this diene to this three-component coupling a poor 23% yield.



Scheme 10. Moving towards easily activated Ni(II)-NHC pre-catalysts.

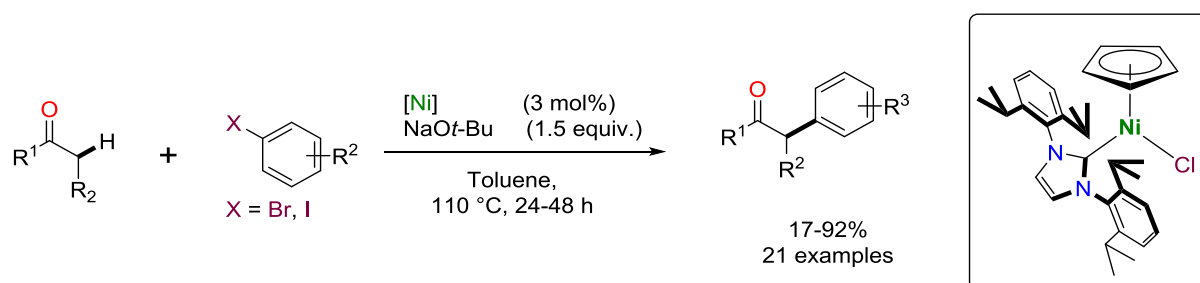
Mori and collaborators reported the use of half-sandwich Ni-NHC complexes in the Heck-type reaction⁹⁸ of styrenes with organoaluminum reagents (Scheme 11).⁹⁹ Using [Ni^{II}Cl(Cp)(^{4,5}H₂NHC-DIPP₂)] in the presence of di-*i*-propylketone as an additive in cyclopentyl methyl ether (CPME) at 60°C, a series of new *E*-styrenes could be constructed (10 examples, 37-92% yield), with minor *bis*-arylethanes as side-products (11:1 to 75:1 selectivity).



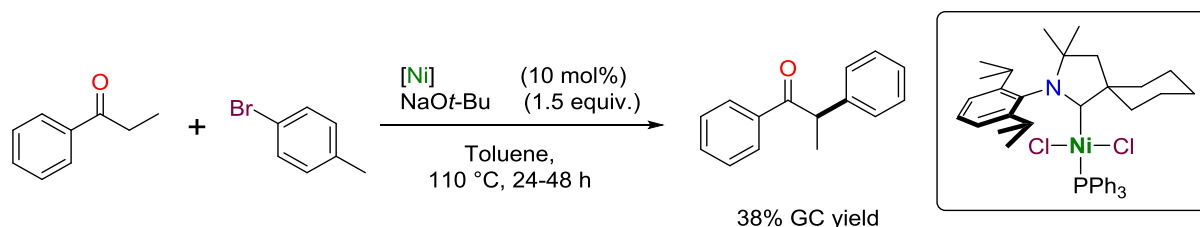
Scheme 11. Ni-NHC catalyzed Heck reaction with organoaluminum reagents.

III.1.2. C_{sp³}-H functionalization

Building on our group's earlier report that half-sandwich nickel-NHC complexes could trap acetyl and oxallyl moieties¹⁰⁰ a second communication went on to test these systems as ketone α -arylation catalysts.⁸⁶ After screening different [Ni(Cp⁺)L(NHC)]⁽⁺⁾ complexes, the [Ni^{II}Cl(Cp)(NHC-DIPP₂)] platform revealed itself the most active, arriving at near quantitative yields (97%) at only 1 mol% catalytic charge. From then a number of acyclic ketones and bromo- and iodo-arenes were successfully coupled in the presence of the precatalyst (3 mol%) and NaOt-Bu in toluene at 110 °C (Scheme 12). Mechanistic tests carried out with isolated ketonyl complexes however gave poor coupling yields suggesting the originally trapped complex is not an intermediate in the reaction.

Scheme 12. Ketone α -arylation with half-sandwich Ni-NHC complexes.

Trying to improve on this reaction, our group developed a new heteroleptic *trans*-[Ni^{II}Cl₂(CAAC)(PPh₃)] complex⁸⁷ (Scheme 13), bearing a highly σ -electron donating cyclic (alkyl)(amino)carbene (CAAC)¹⁰¹ that had been successfully used in Pd systems to give the best known results in this reaction.¹⁰¹ Disappointingly a moderate yield (38% GC yield) was obtained for this transformation using propiophenone, bromotoluene and the precatalyst (10 mol%) in otherwise similar conditions (Scheme 13).



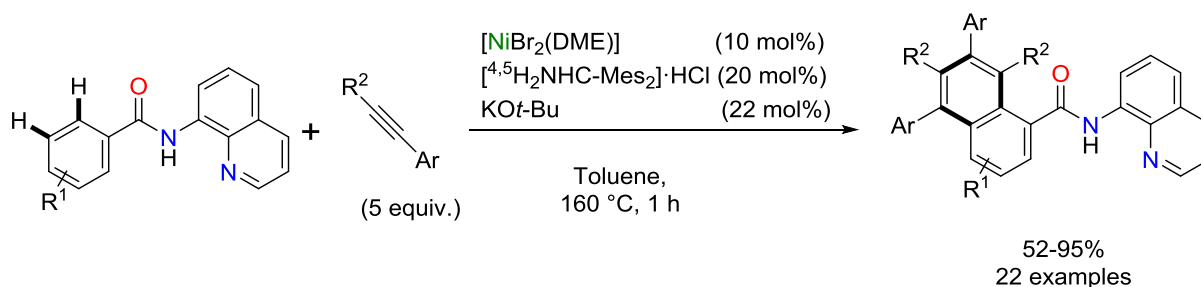
Scheme 13. First example of a Ni-CAAC catalyzed C-H functionalization reaction.

III.2. Formal 1,2-additions to unsaturated C–C bonds

III.2.1. To alkynes (C≡C)

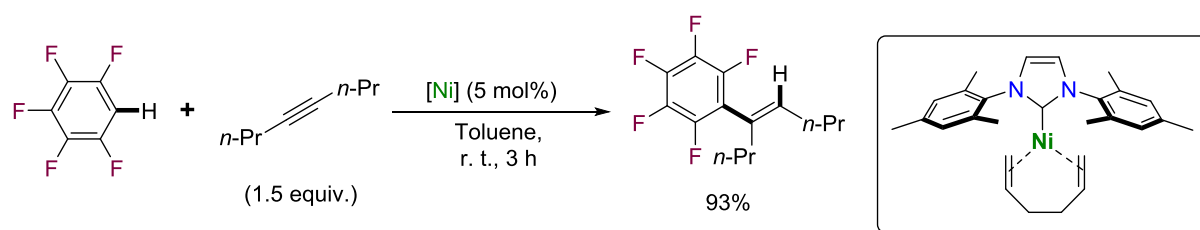
III.2.1.A. Hydroarylation

A widely successful strategy for nickel catalyzed C–H bond functionalization has involved the use of a 8-aminoquinoline directing group.^{102,103} Further developing on the applications of this directing group, Chatani and collaborators reported a double C–H functionalization/alkyne insertion using an NHC ligand.¹⁰⁴ A catalyst mixture of $[\text{Ni}^{\text{II}}\text{Br}_2(\text{DME})]/[\text{4}^{\text{,5}}\text{H}_2\text{NHC-Mes}_2]\cdot\text{HCl}$ (1:2 ratio, 10 mol%) and a sub-stoichiometric amount of KO t -Bu in toluene at 160 °C efficiently constructed a wide scope of new naphthamides from the corresponding benzamides and alkynes (22 examples, 52-95% yield, Scheme 14).



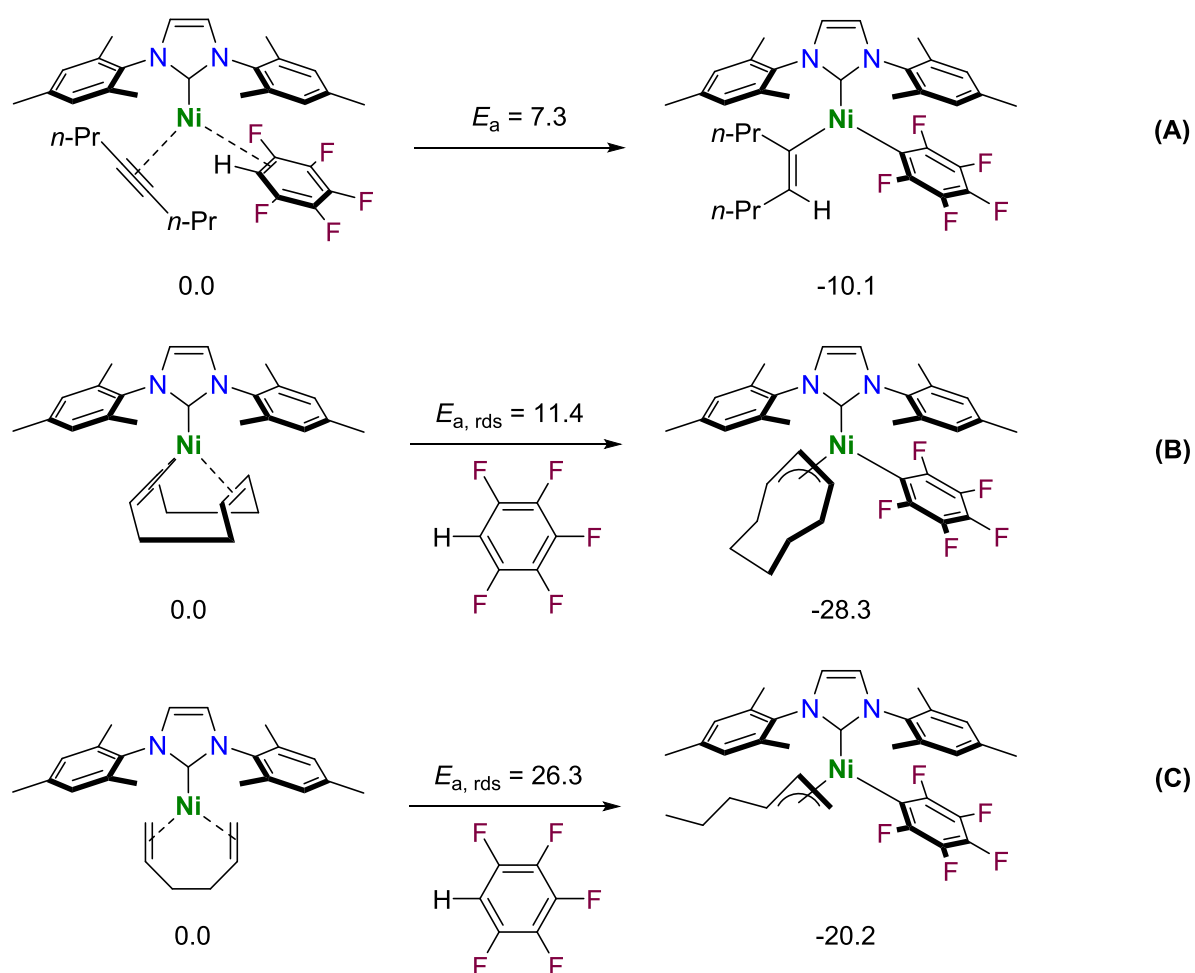
Scheme 14. Nickel-NHC catalyzed tandem C–H functionalization/alkyne insertion.

Guided initially by a DFT calculated (ω B97X-D/cc-pVTZ) mechanism for the hydroarylation of 4-octyne with $\text{C}_6\text{F}_5\text{H}$ catalyzed by $[\text{Ni}^0(\text{COD})_2]/\text{NHC-Mes}_2$, Montgomery and Zimmerman improved the Ni(0)-catalyzed hydroarylations of alkynes using $\text{C}_6\text{F}_5\text{H}$ or heterocycles.¹⁰⁵ In this mechanism an off-cycle intermediate that resulted from a series of β -hydride elimination/migratory insertion events (chain walking) was identified. The authors then reasoned that a similar structure that would be unable to generate such a stable unproductive species would be a better catalyst. As such, they tested a $[\text{Ni}^0(\text{NHC-Mes}_2)(1,5\text{-hexadiene})]$ complex¹⁰⁶ in the reaction above that afforded an excellent yield (93%) at r. t. (Scheme 15), whereas the original catalyst system was essentially unreactive (8% yield). Beyond $\text{C}_6\text{F}_5\text{H}$ a series of heterocycles were found to be accessible substrates (6 examples, 51-99% yield).



Scheme 15. Hydroarylation of 4-octyne with $\text{C}_6\text{F}_5\text{H}$ catalyzed by a well-defined $\text{Ni}(0)$ complex.

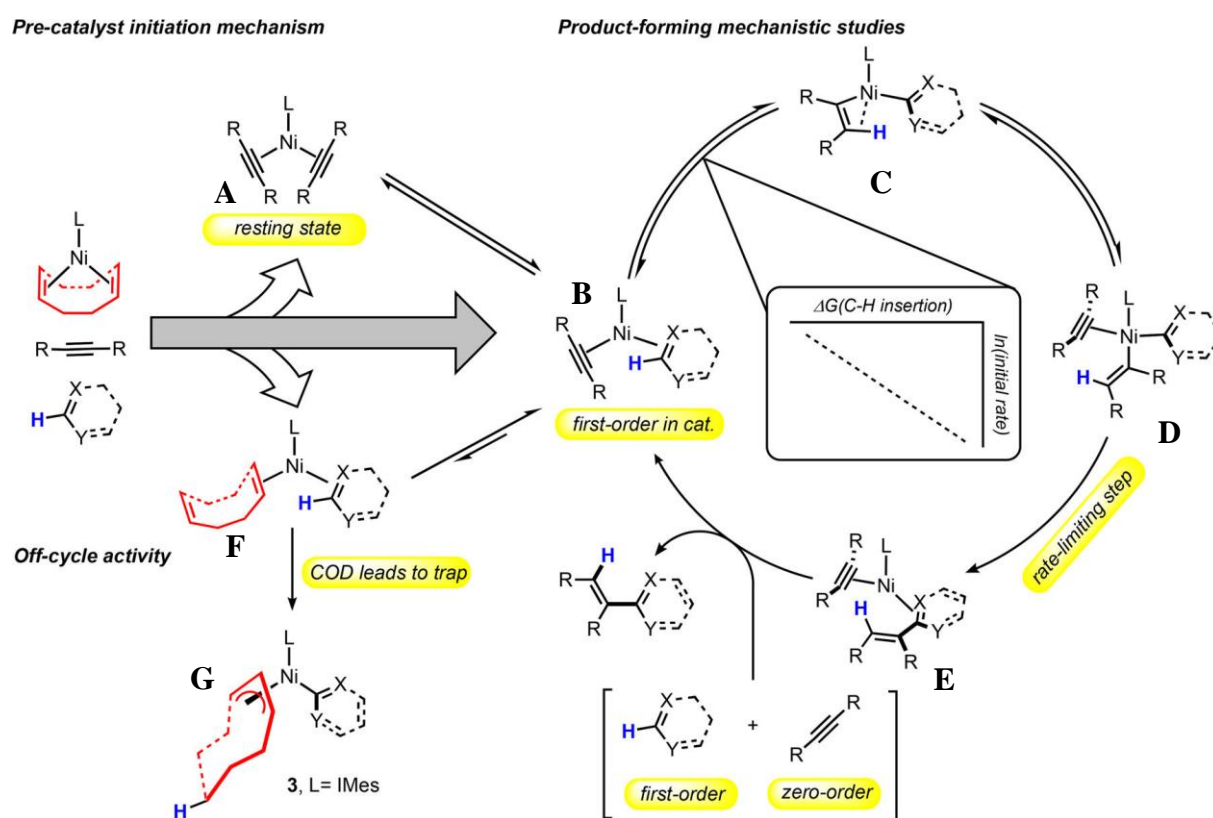
DFT calculations on the reaction between a $[\text{Ni}^0(\text{NHC-Mes}_2)(\text{olefin})]$ species and $\text{C}_6\text{F}_5\text{H}$ give an exothermic $\text{Ni}(\text{II})$ reaction product (Scheme 16). When the substrate 4-octyne is present a small barrier ($7.3 \text{ kcal mol}^{-1}$) is found for the generation of the productive $\text{Ni}(\text{II})$ vinyl species (**A**). On the other hand, when COD is present, a very stable ($-28.3 \text{ kcal mol}^{-1}$) π -allyl $\text{Ni}(\text{II})$ species is easily accessible ($11.4 \text{ kcal mol}^{-1}$) (**B**).



Scheme 16. DFT computed products from the reaction of $[\text{Ni}^0(\text{NHC-Mes}_2)(\text{L})]$ ($\text{L} = 4\text{-octyne}$ (**A**), $1,5\text{-cyclooctadiene}$ (**B**), $1,5\text{-hexadiene}$ (**C**)) complexes and $\text{C}_6\text{F}_5\text{H}$. Values correspond to Gibbs free energy, E_a corresponds to the Gibbs energy connecting transition state, $E_{a, \text{ rds}}$ corresponds to the Gibbs energy of the rate-determining step, all energies presented in kcal mol^{-1} .

The small difference in the activation energy (4.1 kcal mol⁻¹) required for both productive (**A**) and off-cycle (**B**) reaction pathways suggested that employing [Ni⁰(NHC-Mes₂)(COD)] the reaction while thermodynamically feasible, would quickly deactivate at r. t. (Scheme 16). This is corroborated by the low yield of (8%) of the hydroarylation reaction and the detection of the π -allyl Ni(II) product (**B**) with [Ni⁰(NHC-Mes₂)(COD)]. When 1,5-hexadiene is used however, the reaction with C₆F₅H must overcome a much higher barrier (26.3 kcal mol⁻¹) (**C**). This high energy cost to generate the Ni π -allyl species would impede this reaction to take place at r. t. and therefore allow the catalyst to remain in the catalytic cycle.

Subsequent detailed mechanistic studies gave further insight into the elemental steps of the reaction, allowing for a consistent picture of the mechanism to be drawn (Scheme 17).¹⁰⁷ Key addition was the establishment that the catalyst resting state is a [Ni⁰(NHC-Mes₂)(alkyne)₂] species (**A**) that upon ligand exchange with the substrate, gives an heterolytic Ni(0) complex (**B**) able to undergo reversible C–H activation to generate a Ni(II) vinyl intermediate (**C**). The latter (**C**) is stabilized by an agostic interaction of the new C–H bond of the vinyl fragment with the Ni center and requires coordination of an additional alkyne molecule to give an intermediate (**D**) with the proper geometry to undergo reductive elimination.

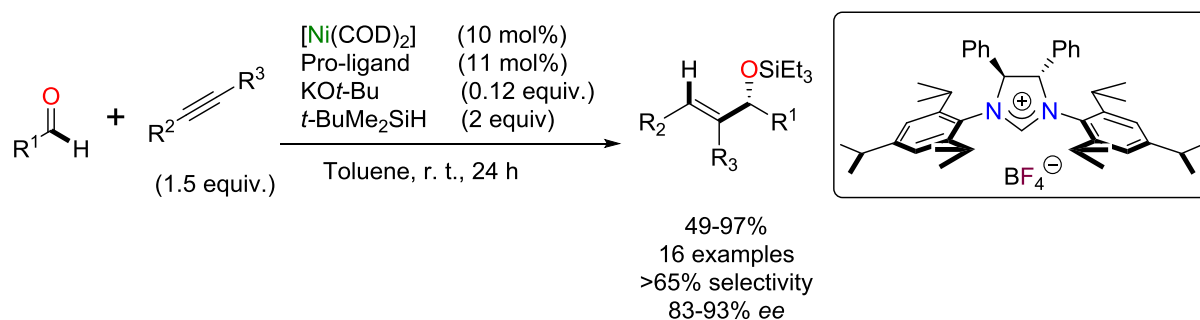


Scheme 17. Proposed reaction mechanism for the Ni(0) catalyzed heteroarylation of alkynes. Adapted from ref¹⁰⁷.

Reductive elimination (Scheme 17, **D** → **E**) to construct the vinyl-arene C–C bond is irreversible and the rate-limiting step of the reaction. Ligand substitution of the product by either the substrate (**E** → **B**) or the alkyne (**E** → **A**) close the catalytic cycle. It was again observed that COD acted as a trap creating an energetic well that reduces catalytic performance (**F** → **G**).

III.2.1.B. Three-component couplings

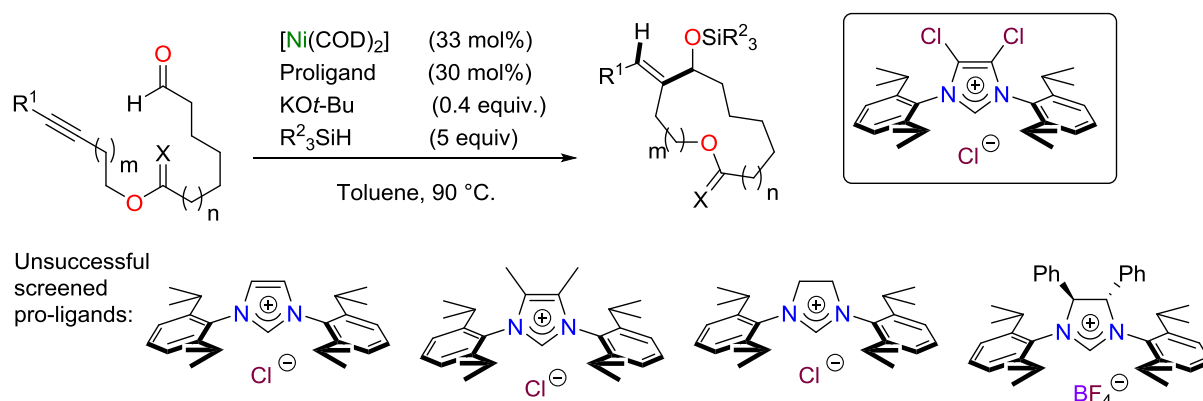
Multi-component reactions, which construct a series of new bonds all in one pot, minimize time and the energy cost of a synthesis and ally atom economy with less synthetic steps. Montgomery's group has in the last few years reported a few examples of Ni-NHC C–H bond functionalization in three-component couplings.^{108–110} In one such report, they discussed the asymmetric three-component coupling of aldehydes, alkynes and silanes to yield chiral α,β -unsaturated silyl ethers.¹⁰⁸ Using a chiral NHC ligand and $[\text{Ni}^0(\text{COD})_2]$ (1:1.1 ratio, 10 mol%) in the presence of $\text{KO}t\text{-Bu}$ and $t\text{-BuMe}_2\text{SiH}$, a series of aldehydes (10 examples) and alkynes (7 examples) could be coupled in moderate to excellent yields and in good to excellent ee's (Scheme 18). The key to this transformation was the choice of bulky *N*-aryl saturated NHC, which has a chiral 4,5-diphenylated backbone. The authors noted however that the use of a methyl function on the alkyne provided insufficient steric congestion and an ethyl group had to be used to give significant chiral induction.



Scheme 18. Asymmetric synthesis of α,β -unsaturated silyl ethers by three-component coupling of aldehydes, alkynes and silanes by a chiral Ni-NHC catalyst.

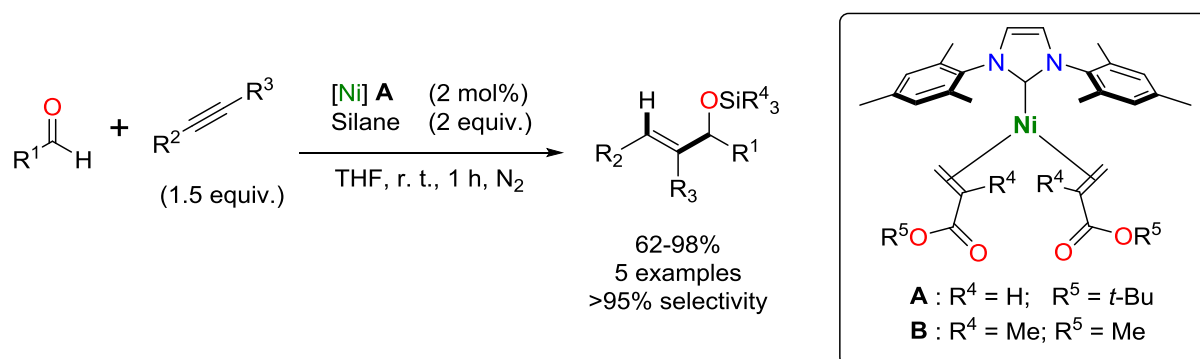
Applying this strategy to ynals,¹¹⁰ three-component coupling to ynals, they could construct a series of macrocyclic α,β -unsaturated silyl ethers by *exo*-selective macrocyclization. Using a catalyst mixture comprised of $[\text{Ni}^0(\text{COD})_2]$ and $[\text{4,5-Cl}_2\text{NHC-DIPP}_2]\cdot\text{HCl}$ (1.1:1 ratio, 30 mol%) in the presence of $\text{KO}t\text{-Bu}$ and excess silane, the desired macrocycles were obtained in moderate yields and excellent selectivity's

(12 examples, 45-74% yield, selectivity's >95%, Scheme 19). It is noteworthy that the $^{4,5}\text{Cl}_2\text{NHC-DIPP}_2$ ligand was crucial, as opposed to more strongly donating ligands screened.



Scheme 19. Ynal *exo*-selective macrocyclization by Ni-NHC catalysis.

Another contribution from this group tackled the issue of using high catalyst loadings of the $[\text{Ni}^0(\text{COD})_2]$ mixtures.¹⁰⁹ By developing a number of Ni(0) catalysts of the type $[\text{Ni}^0(\text{NHC})(\text{acrylate}/\text{fumarate})_2]$ complexes, a very active precatalyst in aldehyde-alkyne-silane three-component coupling $[\text{Ni}^0(\text{NHC-Mes}_2)(\text{methyl,methylacrylate})_2]$ was uncovered (Scheme 20, **B**). However the high activity compromised the catalyst's stability upon exposure to air. So as a compromise, they elected the air-stable, but reactive, $[\text{Ni}^0(\text{NHC-Mes}_2)(t\text{-Bu acrylate})_2]$ (Scheme 20, **A**). Choosing either precatalyst, the catalyst loadings could be reduced to 2 mol% without loss of activity in sharp contrast with the high charges (10-33 mol%) usually used for this type of reaction (see Scheme 18 and Scheme 19). The multi-component reaction could combine aldehydes and alkynes and trap them with a silane to give the corresponding products in moderate to excellent yields and excellent selectivity's (5 examples, 62-98% yield, >98% selectivity, Scheme 20).

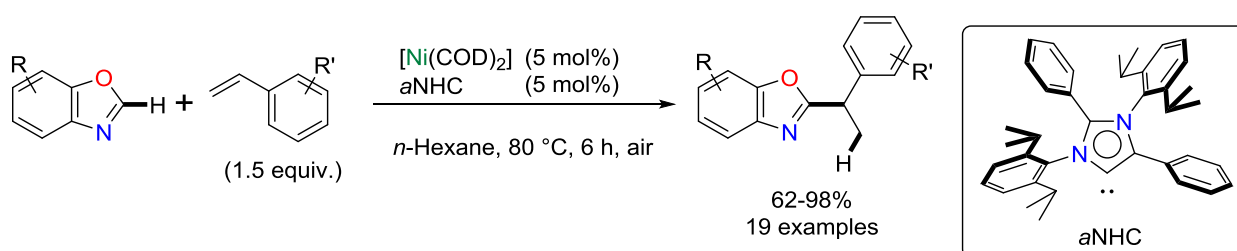


Scheme 20. Multicomponent synthesis of α,β -unsaturated silyl ethers by aldehyde insertion into alkynes. Gaining activity with well-defined designer precatalysts.

III.2.2. To alkenes (C=C)

III.2.2.A. Hydro(hetero)arylation reactions

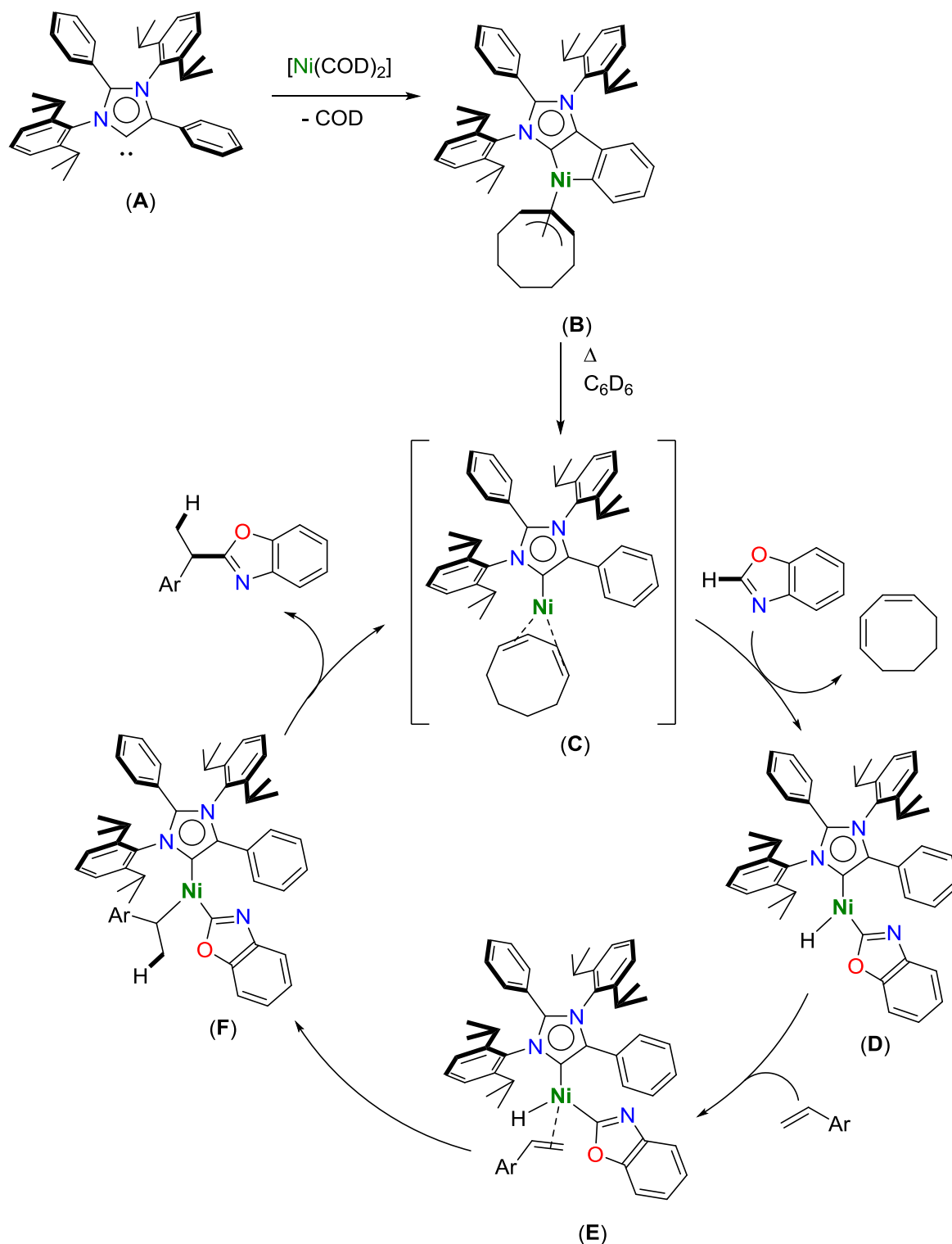
Mandal and co-workers reported the selective addition of benzoxazoles to styrenes, with 1,3-bis(2,6-di-*i*-propylphenyl)-2,4-diphenylimidazol-5-ylidene¹¹¹ an abnormal-NHC (aNHC).¹¹² The reaction took place in the presence of $[\text{Ni}^0(\text{COD})_2]/\text{aNHC}$ (1:1 ratio, 5 mol%), in *n*-hexane at 80 °C, to give selectively the branched product in moderate to excellent yields (19 examples, 62-98% yield, Scheme 21).



Scheme 21. Nickel-catalyzed hydroheteroarylation of styrenes with benzoxazoles. Nickel catalysis using abnormal NHCs.

In an effort to probe the reaction mechanism, the authors attempted to synthesize a putative $\text{Ni}(0)\text{-aNHC}$ complex but instead isolated a cyclonickelated $\text{Ni}(\text{II})\text{-}(\eta^3\text{-cyclooctyl})\text{-aNHC}$ complex (Scheme 22, **A** \rightarrow **B**). The latter was generated via an isomerization of 1,5-cyclooctadiene to 1,3-cyclooctadiene, and, presumably addition of a phenyl C–H bond onto it. This $\text{Ni}(\text{II})$ complex (**B**) proved to be a competent precatalyst (92% yield) and was proposed to be the resting state of the catalyst that would generate the active species, $\text{Ni}(0)\text{-}(1,3\text{-cyclooctadiene})\text{-aNHC}$, upon heating (Scheme 22, **B** \rightarrow **C**). Oxidative addition of benzoxazole would then generate an intermediate $\text{Ni}(\text{II})\text{-hydride-benzoxazolyl}$ complex (Scheme 22, **C** \rightarrow **D**) that would coordinate the olefin and finish the catalytic cycle via usual migratory insertion and reductive elimination steps (Scheme 22, **D** \rightarrow **E** \rightarrow **F** \rightarrow **C**).

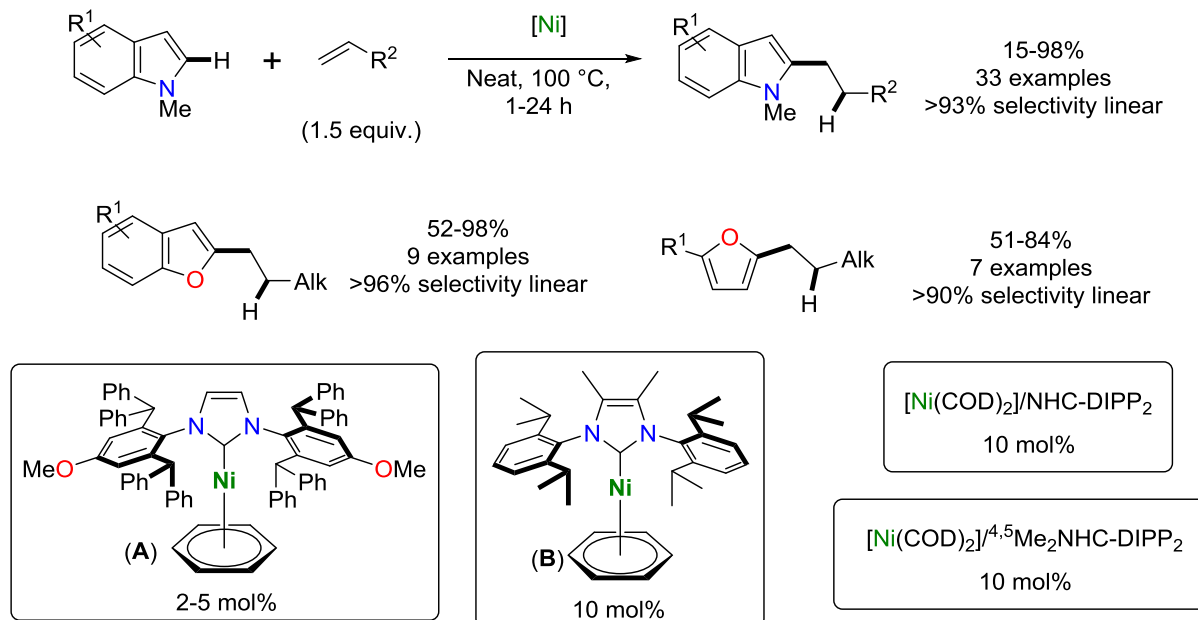
In a stoichiometric NMR experiment between complex (**B**) and benzoxazole, the authors did make several major observations, consistent with their formulation of an intermediate $\text{Ni}(\text{II})\text{-hydride}$: free COD, the appearance of a sharp singlet at -11.33 ppm (^1H , Ni-H) and the disappearance of the Ni- C_{Ph} signal (^{13}C).



Scheme 22. Proposed reaction mechanism.

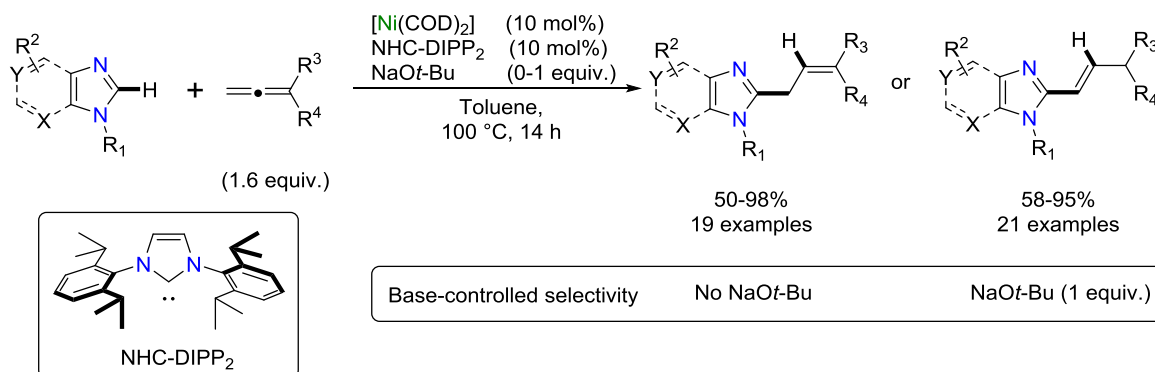
Hartwig et al. reported a versatile methodology to add heterocycles to olefins that selectively gives the linear products under neat conditions.¹¹³ Thus indoles (33 examples, 15-98% yield, selectivity >93%), benzofurans (9 examples, 52-98% yield, selectivity >96%), *N*-methylpyrrole (69% yield, selectivity 96%) and furans (7 examples, 51-80% yield,

selectivity >90%) were efficiently added to a number of different olefins (20 examples) (Scheme 23) in the presence of well-defined $[\text{Ni}^0(\eta^6\text{-C}_6\text{H}_6)(\text{NHC})]$ complexes bearing bulky NHC-DIPP₂ derivatives (Scheme 23, **A** and **B**). It is noteworthy that the reactions also proceed when using a 1:1 mixture of $[\text{Ni}^0(\text{COD})_2]$ and the aforementioned bulky NHC ligands.



Scheme 23. Selective nickel-catalyzed linear olefin hydroheteroarylation.

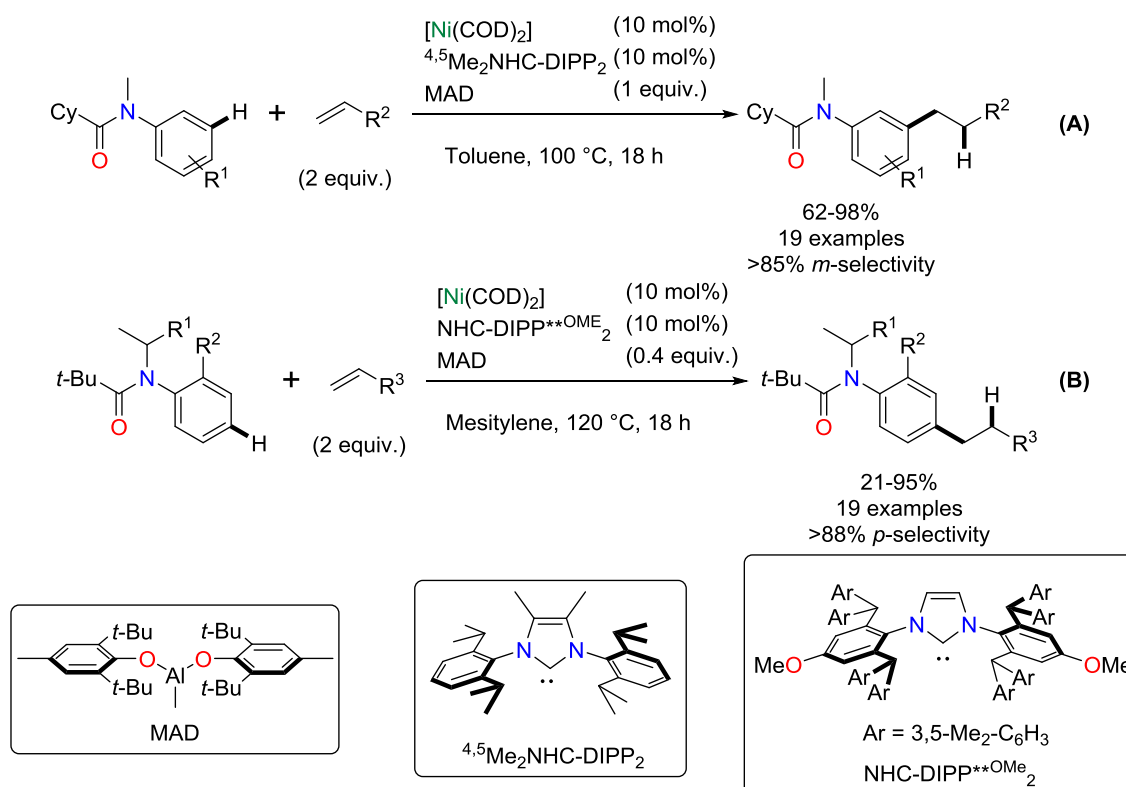
In one of the rare examples of nickel-catalyzed C–H functionalization of allenes, Ackermann and coworkers, developed a methodology for the selective hydroarylation of these substrates with imidazoles and purines to give the corresponding allylated or alkenylated products (Scheme 24).¹¹⁴ Using a catalyst system comprised of $[\text{Ni}^0(\text{COD})_2]/\text{NHC-DIPP}_2$ (1:1 ratio, 10 mol%), in the presence or absence of NaOt-Bu , diverse allenes and imidazoles or purines were reacted in toluene at 100 °C to give selectively the corresponding allylated (19 examples, 50-98% yield, no NaOt-Bu used) or alkenylated (21 examples, 58-95% yield, using 1 equiv. of NaOt-Bu) addition products.



Scheme 24. Base-controlled chemoselective hydroheteroarylation of allenes with imidazoles and purines.

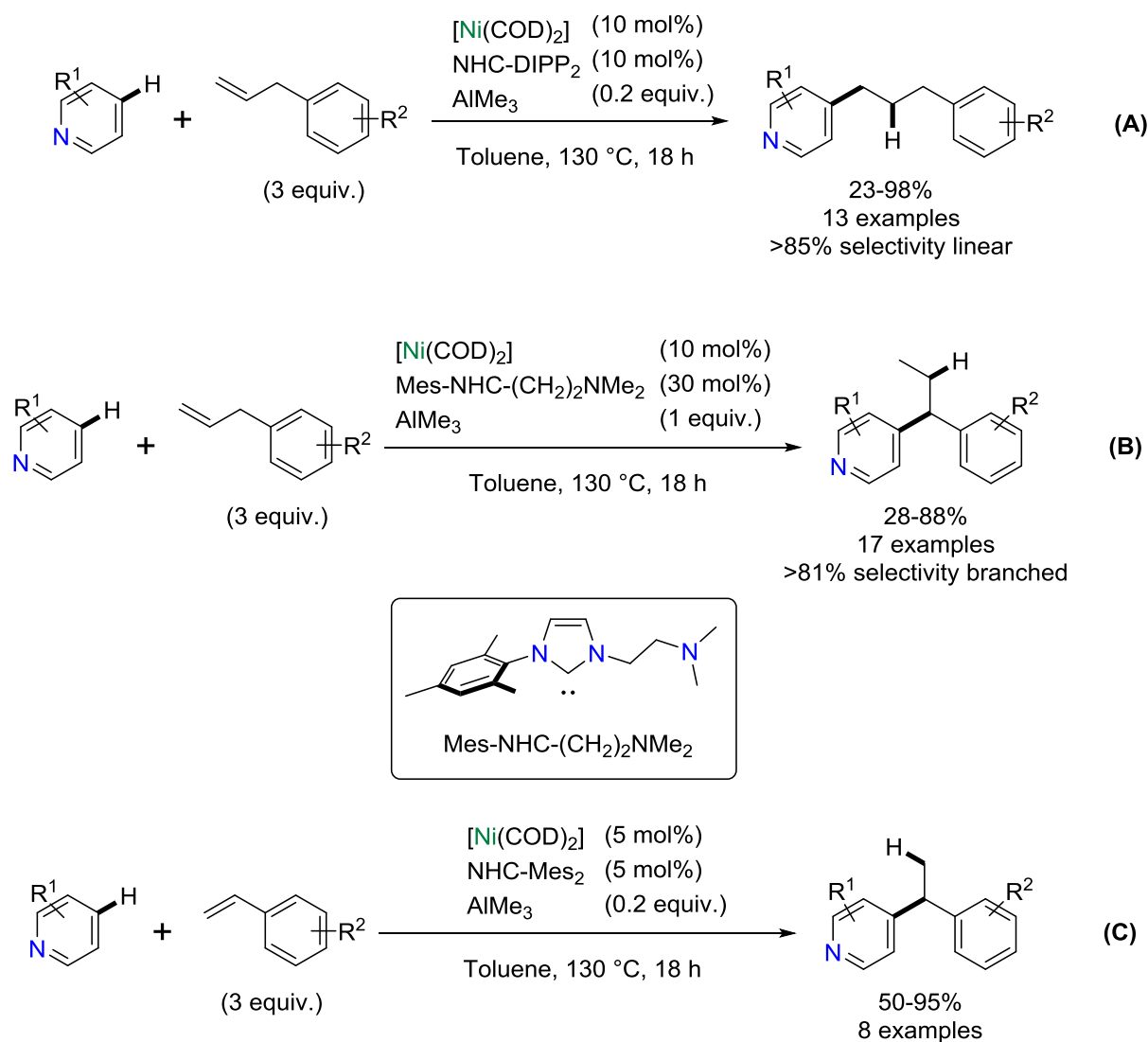
The authors utilized C(2)-D labelled *N*-heterocycles in their catalytic reaction, to seek to explain the role of the base in controlling the selectivity of the end product. When the reaction was run in the absence of base, the allylated products were obtained, with deuterium incorporation (78-89%) at the olefinic position. However, when base was added to the reaction mixture (NaO*t*-Bu, 1 equiv.) the alkenylated product was obtained with a lower deuterium content (56%) and distributed unselectively (1:1 ratio) across the double bond of the olefin. A subsequent isomerization study showed that, in the absence of the catalyst system, but in the presence of 1 equiv. of NaO*t*-Bu, when heated in toluene at 100 °C the allylated product would isomerize to the more stable alkene, whereas the alkene product would not react. As such they proposed the base's role would be to isomerize the allylated product, after the nickel-catalyzed transformation, to the more stable alkene.

Nakao and collaborators made use of cooperative nickel/aluminum catalysis to functionalize anilides (Scheme 25).¹¹⁵ By using a mixture of [Ni(COD)₂]/^{4,5}Me₂NHC-DIPP₂ (1:1 ratio, 10 mol%) in the presence of 1 equiv. of an aluminum Lewis acid (MAD),^{116,117} in toluene at 100 °C, selected anilides and olefins were selectively coupled in the *meta*-position in low to moderate yields (5 examples, 26-67% yield, 83-95% selectivity, Scheme 25, **A**). Selectivity in the arene position could be modulated by using *ortho*-substituted anilides in the presence of the bulkier (NHC-DIPP**OMe₂) and substoichiometric amount of MAD, in mesitylene at 120 °C (Scheme 25, **B**).



Scheme 25. Anilide selective C–H functionalization by cooperative Ni–Al catalysis.

Cooperative Ni/Al catalysis was also reported to catalyze the formal 1,2-addition of the *p*-C–H bond of pyridines to allylbenzenes and styrenes (Scheme 26).¹¹⁸ Using a mixture of $[\text{Ni}^0(\text{COD})_2]/\text{DIPP}$ (1:1 ratio, 10 mol%) and a substoichiometric amount of AlMe_3 (0.2 equiv.) in toluene at 130 °C, the coupling would proceed selectively to give the linear products in low to excellent yields (13 examples, 23-98% yield, >85% selectivity, **A**). The branched product could be selectively obtained when the NHC ligand was bearing an *N*-bound pendant aliphatic amine ($-(\text{CH}_2)_2\text{NMe}_2$) arm (**B**). By increasing the ligand content to 30 mol% and using stoichiometric AlMe_3 , the coupling could now be directed to the branched product in moderate to good yields (17 examples, 28-88% yield, >81% selectivity, **B**). Finally, styrenes could also be used to afford the branched products with lower catalyst loadings of $[\text{Ni}^0(\text{COD})_2]/\text{NHC-Mes}_2$ (1:1 ratio, 5 mol%) and a substoichiometric amount of AlMe_3 (8 examples, 50-95% yield, **C**).

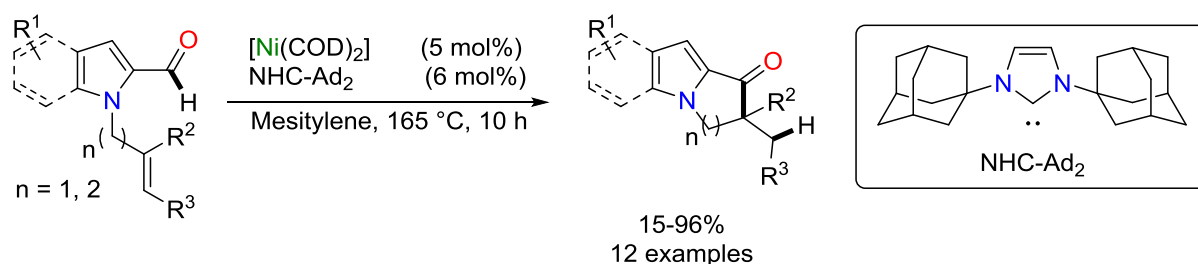


Scheme 26. Selective *p*-pyridine insertion into allylbenzenes and styrenes. Selectivity controlled by the tailored NHC ligand.

The authors went on to run a series of mechanistic tests to explain the insertion of pyridine at a remote position from the double-bond (Scheme 26, **B**). When allylbenzene was subject to catalytic reaction conditions in the absence of pyridine, *trans*- β -methylstyrene was quantitatively formed (GC yield) in only 30 min. The addition of pyridine to this reaction mixture affords, in 60 min, the desired product in good yield (89%). This indicated that a first rapid isomerization step converts allylbenzene to *trans*- β -methylstyrene that then reacts with pyridine. Curiously, the authors make no remark on the short reaction time (1.5 h total) the reaction took to complete in this mechanistic study, in contrast with the long reaction times in their standard catalytic procedure (18 h). Further studies using isotope labeling using pyridine- d_5 showed a great extent of hydrogen/deuterium scrambling (22-64% deuterium remaining on the pyridine moiety, 3-32% deuterium incorporation into the allylbenzene moiety) making it difficult to obtain further insight from these results.

III.2.2.B. Formal C–H addition of carbonyl substrates to olefins

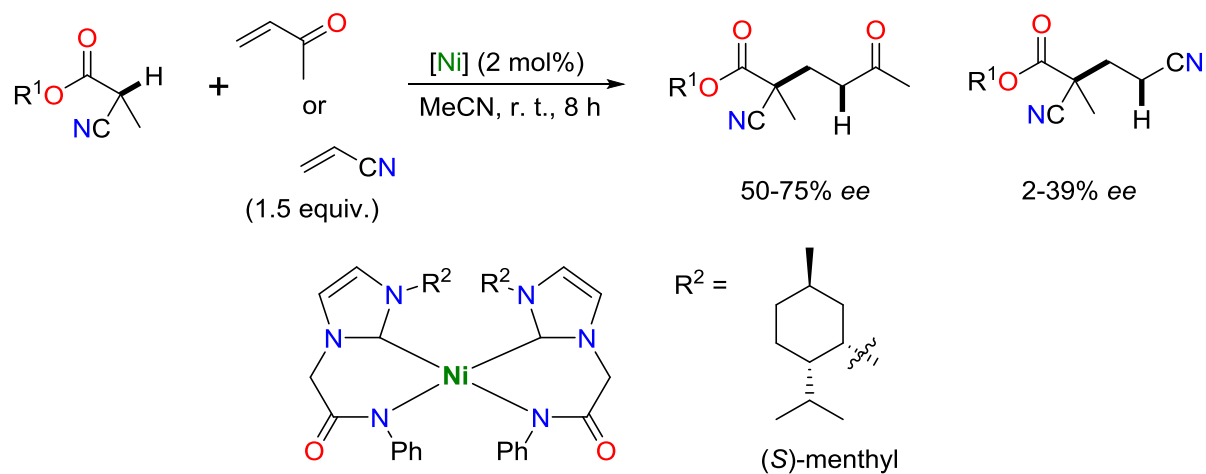
Stanley's group reported a Ni-NHC catalyzed branched-selective intramolecular cyclization of indoles (Scheme 27).¹¹⁹ Using a combination of $[\text{Ni}^0(\text{COD})_2]/\text{NHC-Ad}_2$ (1:1.2 ratio, 5 mol%) in mesitylene heated to 165 °C, *N*-alkeneindole-2-carboxaldehydes could be selectively cyclized to give the corresponding five- and six-membered cyclized indoles (12 examples, 15-96% yield).



Scheme 27. Selective intramolecular indole cyclization by Ni-NHC catalysis.

Ghosh and coworkers reported a 'base-free asymmetric Michael addition'^{120,121} of α -methyl cyano esters to electron poor olefins (Scheme 28).¹²² The authors designed well-defined neutral *cis*-bisNHC-Ni(II) complexes of the type *cis*- $[\text{Ni}^{\text{II}}(\text{R}^1\text{-NHC-CH}_2\text{C}(\text{O})\text{NR}^2)_2]$ bearing chiral *N*-substituents, that would adopt structures with chiral pockets near the metal center, enabling the catalyst to perform asymmetric catalysis. This strategy proved partially successful with a menthol derived complex inducing enantiomeric excesses of up to 75% when

using methyl vinyl ketone (3 examples, 50-75% ee), but would not not go beyond 39% ee when using vinyl nitrile (3 examples, 2-39% ee).



Scheme 28. Construction of chiral quaternary carbons using chiral Ni-NHC pre-catalysts.

IV. Overview

Some trends can be inferred from this review of the literature. C–H cross-coupling reactions with Ni-NHC systems remain underdeveloped, likely due to Ni(0)'s affinity for unsaturated carbon-carbon bonds, that make up many of the investigated substrates. There is also a growing concern with the development of new well-defined (pre)catalysts of either Ni(II) or Ni(0) that can replace $[\text{Ni}^0(\text{COD})_2]$, due not only to its high sensitivity to air but, perhaps more problematic, 1,5-cyclooctadiene's hard-to-predict non-innocence in many reactions. It remains crucial to continue developing easily activated Ni(II) complexes and synthetic methodologies to access alternative Ni(0) sources.

This divide in *modus operandi* – $[\text{Ni}^0(\text{COD})_2]/\text{L}$ mixture vs. well-defined (pre)catalyst – seems to be a strategic one in fact, with both methodologies having a set of advantages and drawbacks (Table 2). The use of $[\text{Ni}^0(\text{COD})_2]/\text{L}$ mixtures allows for the rapid screening of reaction conditions and ligands libraries. However, this scenario requires the use of pyrophoric $[\text{Ni}^0(\text{COD})_2]$ that must be handled in an inert atmosphere. The inefficient in situ generation of the active species pollutes the reaction medium with chemicals that do not take part in the reaction: this can lead to competing reactivity pathways or lead to catalyst deactivation, at the same time making mechanistic understanding much more of a guessing game. On the other hand, the precise structural control built into well-defined (pre)catalysts allows for a better mapping of the structure-reactivity relationships. At the same time, well-defined (pre)catalysts have a preorganized structure that can better resemble the active catalyst and allow for a more efficient activation of the catalyst, leading to lower catalyst loadings. The larger downside to

this scenario remains the time consuming task of synthesizing and purifying batches of complexes at each structural change that might be wasted if the particular structural niche is unreactive for the reaction at play.

Table 2. Comparative advantages and disadvantages in using well-defined (pre)catalysts or metal precursor/(pro)ligand mixtures.

Well-defined (pre-)catalyst	
Advantages <ul style="list-style-type: none"> • Lower catalyst charge • More complex structural motifs • Better structure-activity relationship • Clearer outline of possible elemental steps and mechanistic studies 	Disadvantages <ul style="list-style-type: none"> • Resource consuming synthesis and purification with each structural change • Lack of synthetic methodologies and alternative sources to access Ni(0) complexes
Metal/ligand mixture	
Advantages <ul style="list-style-type: none"> • Fast screening of large ligand libraries • Easy access to reactive Ni(0) 	Disadvantages <ul style="list-style-type: none"> • High metal+(pro)ligand charge • More likely to have side-reactions, catalyst poisoning from the abundance of non-productive chemicals • Difficult to establish structure-activity relationships • Difficult to probe mechanisms

The philosophy of this work is decidedly more geared towards an understanding of the reactivity of organometallic species in the context of given catalytic challenges. As such, Chapter 2 discusses the synthesis and characterization of cationic C_{NHC} , C_{alkyl} -nickel(II) chelate cationic complexes; Chapter 3 focusses on their study as azole C–H bond functionalization catalysts; an Experimental section describes the procedures and the thesis ends with a General Conclusion.

Chapter 2

Synthesis and characterization of new κ^2 -C_{NHC}, C_{alkyl}-nickelacycles

Chapter 2

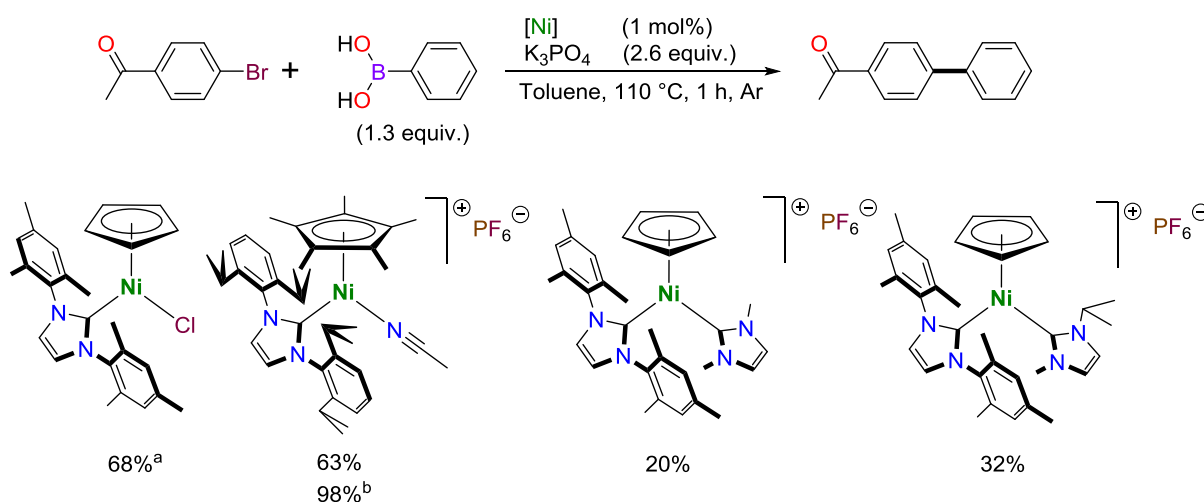
Synthesis and characterization of new κ^2 -C_{NHC}, C_{alkyl}-nickelacycles

I. Context and objectives.....	66
II. Results and discussion	69
II.1. Synthesis and characterization of imidazolium salt pro-ligands.....	69
II.2. Synthesis and characterization of half-sandwich nickel(II)-NHC complexes.....	72
II.3. Synthesis and characterization of half-sandwich κ^2 -C _{NHC} , C _{alkyl} -nickelacycles	74
II.4. Synthesis and characterization of cationic κ^2 -C _{NHC} , C _{alkyl} -nickelacycles.....	79
II.4.1. Synthesis and formula determination of cationic κ^2 -C _{NHC} , C _{alkyl} -nickelacycles	79
II.4.2. Insights into the structure of cationic κ^2 -C _{NHC} , C _{alkyl} -nickelacycles	87
II.5. Reactivity of cationic κ^2 -C _{NHC} , C _{alkyl} nickelacycles	94
II.5.1. Ligand substitution	94
II.5.1.A. With phosphines	94
II.5.1.B. Other substitution reactions	102
II.5.2. With strong bases	103
II.5.3. Redox chemistry	106
III. Conclusions	109

Chapter 2 – Synthesis and characterization of new κ^2 -C_{NHC}, C_{alkyl}-nickelacycles

I. Context and objectives

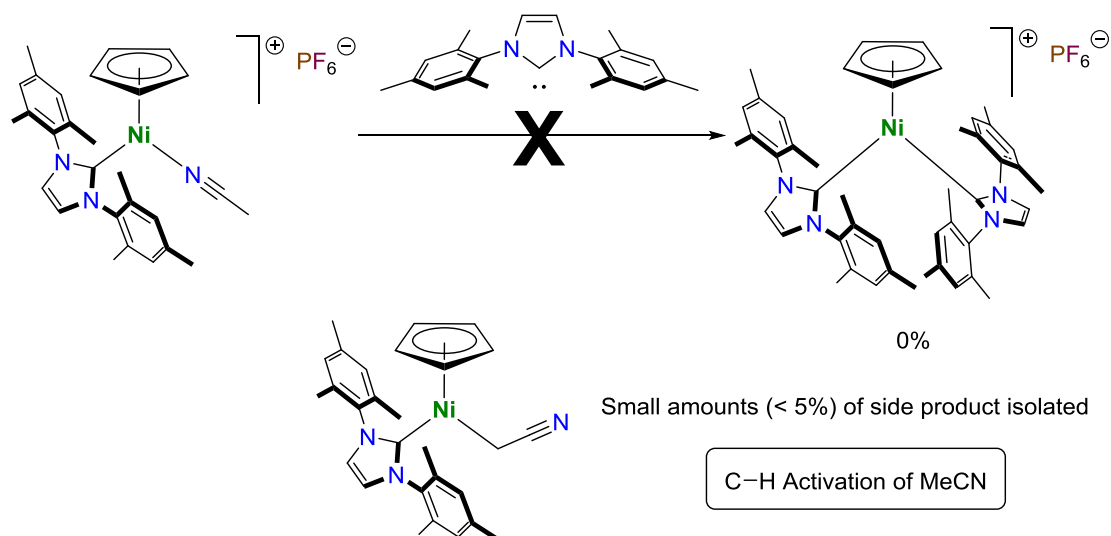
Our group has for some years now developed a research axis focusing on Ni-NHC systems for catalytic applications.^{123,124} In this axis, two main branches cover: the synthesis of [Ni^{II}X(Cp)(NHC)] complexes^{87,125–133} and their applications as catalysts in cross-coupling reactions (Suzuki-Miyaura coupling^{87,124,125,130} and C–H bond functionalization^{86,87,133})⁸⁴ and reduction reactions (hydrosilylation of C–heteroatom multiple bonds and hydroboration of C=C double bonds).^{132,134,135} During these studies we reported that half-sandwich nickel(II)-NHC complexes could be used as efficient precatalysts for the Suzuki-Miyaura cross-coupling reaction of haloarenes and phenylboronic acid.¹²⁴ In that report, it was divulged that the catalyst was initially very active in the first minutes of the reaction but quickly became deactivated. As a strategy to prolong catalyst lifetime, a second NHC ligand was incorporated, giving complexes of the type [Ni^{II}(Cp)(NHC-R¹)₂(Me-NHC-R²)]⁺X⁻ that were prepared by reaction of a cationic [Ni^{II}(Cp)(MeCN)(NHC-R¹)₂]⁺PF₆⁻ complex with the corresponding free carbene. However, these proved disappointingly inert in this reaction (Scheme 29).¹²⁵



Scheme 29. Suzuki-Miyaura cross-coupling of 4-bromoacetophenone and phenylboronic acid catalyzed by half-sandwich Ni(II)-NHC complexes.^{124,130} a 3 mol%, 90 °C, 30 min.¹²⁴ b 3 mol%, 15 min.¹²⁴

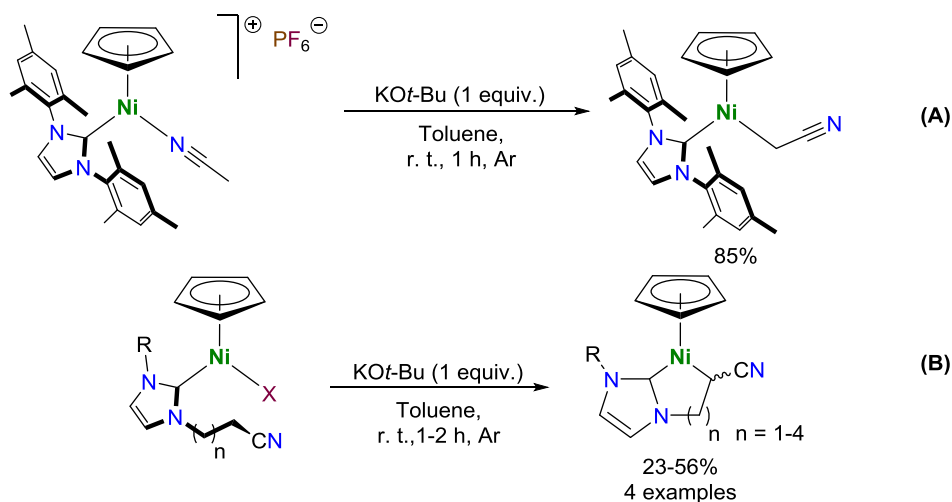
The synthesis of these bis-NHC complexes was however limited by the steric bulk of the NHCs. Indeed the reaction between [Ni^{II}(Cp)(NCMe)(NHC-Mes₂)]⁺PF₆⁻ and the free carbene

NHC-Mes₂ systematically failed to yield the desired intended target [Ni^{II}(Cp)(NHC-Mes₂)₂]⁺PF₆⁻, but small amounts of the cyanomethyl complex, [Ni^{II}(CH₂CN)(Cp)(NHC-Mes₂)], could be isolated instead (Scheme 30).¹³⁰



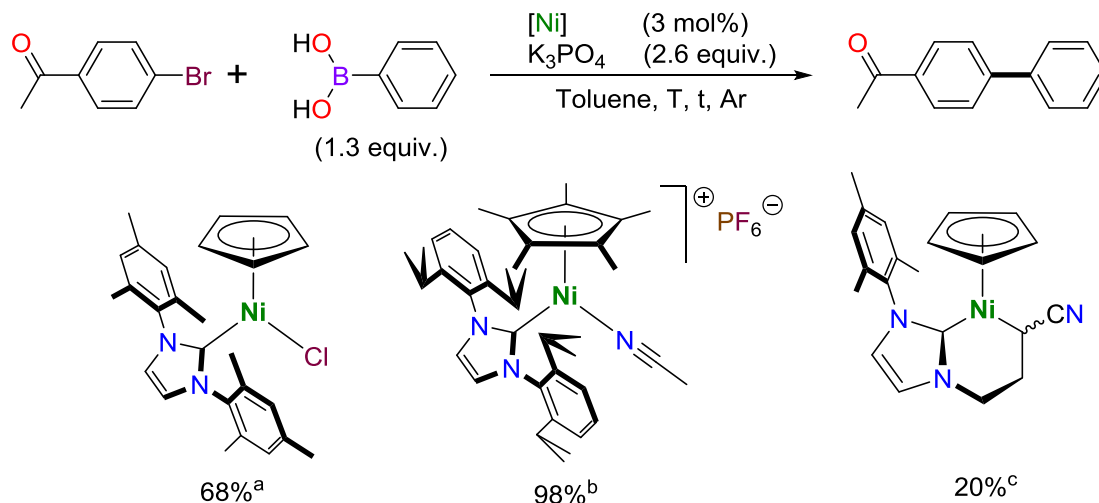
Scheme 30. Unsuccessful synthesis of bis-NHC Ni(II) complexes and unexpected C–H activation of acetonitrile coordinated to a nickel(II) center to form a new nickel–carbon bond.¹³⁰

The unexpected basicity of the free carbene species ($pK_a = 19.4$, DMSO at 25 °C; for the conjugate acid)¹³⁶ abstracting a proton from surprisingly acidic C–H bonds on acetonitrile ($pK_a = 31.3$, DMSO at 25 °C)¹³⁷ led instead to a route for complex derivatization via C–H bond activation with KO^t-Bu (Scheme 31, **A**).¹²⁷ This reaction was then established as a robust methodology for the preparation of half-sandwich κ^2 -C_{NHC}, C_{alkyl}-nickelacycles by intramolecular C–H bond activation (Scheme 31, **B**).¹²⁸



Scheme 31. Base-assisted intramolecular C–H bond activation for the construction of Ni-CH₂CN complexes (**A**) and κ^2 -C,C-nickelacycles (**B**).^{127,128}

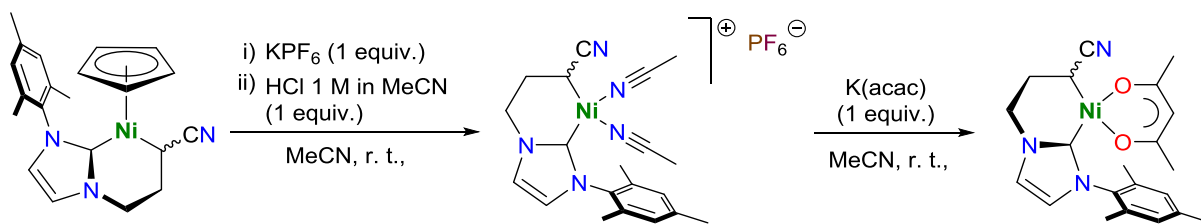
These nickelacycles were a serendipitous opportunity to overcome catalyst deactivation of [Ni^{II}X(Cp)(NHC)] species in Suzuki-Miyaura cross-coupling reactions, by taking advantage of the heightened stability conferred by a bidentate ligand. A study of their performance showed however the same decreased activity (Scheme 32) as the bis-NHC complexes (Scheme 29).¹³⁸



Scheme 32. Comparison between halogen and C,C-chelated half-sandwich complexes in the Suzuki-Miyaura cross-coupling reaction. Percentage values correspond to conversion as measured by ¹H NMR. ^a t = 0.5 h, T = 90 °C.¹²⁴ ^b t = 0.25 h T = 90 °C.¹²⁴ ^c t = 1 h, T = 110 °C.¹³⁸

These negative results revealed nonetheless an important link between structural features and reactivity in these complexes. The labile ligands (halogen, MeCN) present in the original complexes¹²⁴ were of the utmost importance for an active catalyst, likely for allowing an easy access to the metal center. On the basis of this hypothesis, the Ni–C bonds could be too strong to dissociate and not allow reagents to approach the metal's coordination sphere. To tiptoe this balancing act of chemical design – robust species for practicality, yet highly reactive for performance – our group devised a deceptively simplistic solution; the opening of coordination positions via acidolysis of the cyclopentadienyl ligand.¹³¹ Despite the apparent simplicity of the reaction, its surprising selectivity must be stressed – in a molecule where all metal-carbon bonds were constructed by deprotonation of the corresponding organic moieties (C_{Cp}, C_{NHC}, C_{alkyl}), only the M–C_{Cp} bond was cleaved (Scheme 33). It also constituted the first known example of Cp removal in an 18 valence electron complex.

Cyclopentadienyl ligand removal afforded a cationic solvent adduct that could be successfully trapped with an anionic acetylacetonate (acac) ligand (Scheme 33). And whereas this neutral derivative was fully characterized, the acetonitrile adduct, in contrast, remained ill-characterized (with only ¹H, ¹³C NMR and IR spectroscopic characterization reported).¹³¹



Scheme 33. Synthesis of new square planar 16 valence electron C,C complexes by displacement of the η^5 -cyclopentadienyl ligand using hydrochloric acid.¹³¹

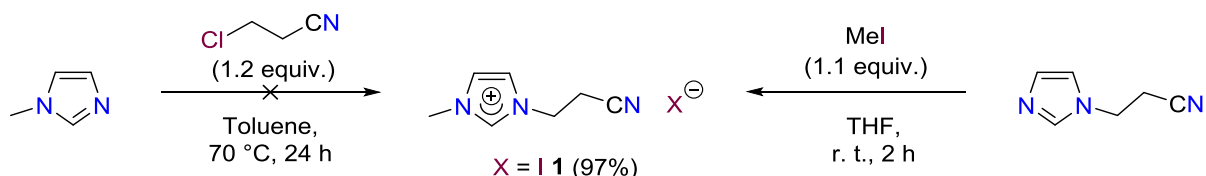
As it so happens, this cationic complex was the most attractive of the two as a potential (pre)catalyst. The labile acetonitrile ligands could easily be displaced to allow reagents access to the metal center. However, despite the elegant synthetic strategy, the cationic complexes were poorly amenable to crystallization deterring detailed structural characterization and purification. The questions, opportunities and challenges that arose with the full characterization of these cationic chelated complexes form the project that propelled the work developed in this chapter.

II. Results and discussion

II.1. Synthesis and characterization of imidazolium salt proligands

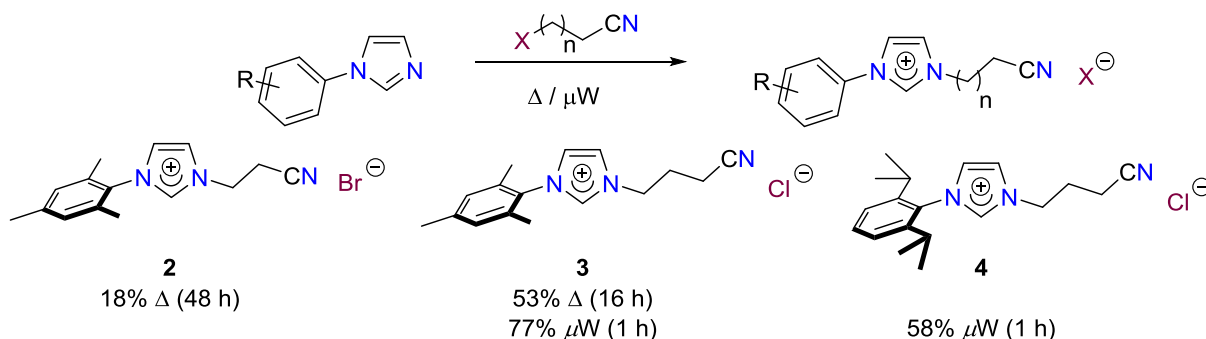
Imidazolium salts make up the most utilized precursors to access *N*-heterocyclic carbenes. Depending on the module being tailored many routes have been devised.¹³⁹ A number of asymmetric imidazolium salts of the type [R-NHC-(CH₂)_nCH₂CN]·HX (**1**: R = Me, n = 1, X = I; **2**: R = Mes, n = 1, X = Br; **3**: R = Mes, n = 2, X = Cl; **4**: R = DIPP, n = 2, X = Cl) bearing an alkylnitrile side-arm were synthesized.

The initially targeted compound [Me-NHC-(CH₂)CH₂CN]·HCl could not be prepared by *N*-quaternarization of *N*-methyl imidazole with chloropropionitrile. Although being known in the literature,^{140,141} this route could not be reproduced despite numerous attempts with chemicals from different suppliers (TCI, Sigma-Aldrich, Acros Organics, Alfa Aesar) and by different chemists (Scheme 34, left). Hence, the alternative iodide salt [Me-NHC-(CH₂)CH₂CN]·HI (**1**), was prepared instead by the reaction of *N*-propionitrile imidazole with methyl iodide in THF at room temperature in excellent yields (Scheme 34, right).¹²⁸



Scheme 34. Synthesis of [Me-NHC-(CH₂)CH₂CN]·HI **1**. Reported route was irreproducible (left) but methylation of *N*-propionitrileimidazole was successful (right).

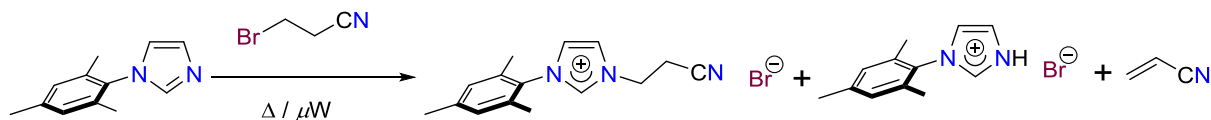
For the construction of the *N*-aryl imidazolium salts, *N*-quaternarization of the appropriate aryl imidazole precursors gave the desired organic salts (Scheme 35). Under either thermal heating or microwave irradiation in THF, the desired imidazolium salts [Mes-NHC-(CH₂)CH₂CN]·HBr (**2**), [Mes-NHC-(CH₂)₂CH₂CN]·HCl (**3**) and [DIPP-NHC-(CH₂)₂CH₂CN]·HCl (**4**) were obtained in low (**2** - 18%) to good (**3** - 53-77%, **4** - 58%) yields. Microwave irradiation has recently appeared as a powerful alternative to conventional heating, that is able to drastically reduce reaction times.¹⁴²⁻¹⁴⁴ This technique allowed for the time efficient reaction of less reactive but more available chloroalkylnitriles in the case of **3** and **4**. The yield was significantly increased when compared to the synthesis by thermal heating for **2** (+20%) and the reaction was carried out in a much shorter reaction time (heating: microwave irradiation - 1 h, thermal - 16 h).



Scheme 35. Synthesis of *N*-aryl, *N'*-alkylnitrile-imidazolium salts (**2-4**) by *N*-alkylation, using either thermal heating (Δ) or heating by microwave irradiation (μW).

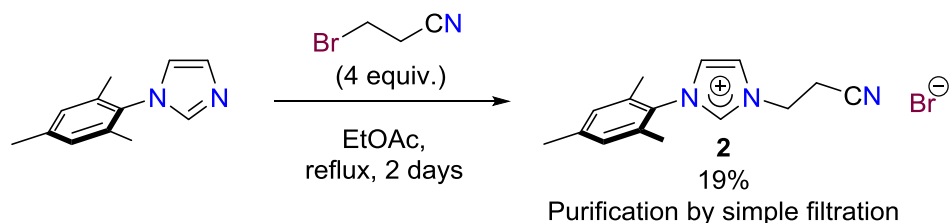
Compound **2** had been previously described¹⁴⁵ and the authors remarked that lower yields were obtained for this, as well as for other imidazolium salts with an *N*-bound ethyl chain

bearing an electron-withdrawing group (nitrile, ester). This is due to a Hofmann-type elimination¹⁴⁶ as a side reaction (Scheme 36).[‡]



Scheme 36. Reaction between *N*-mesitylimidazole and 3-bromopropionitrile. Competitive Hofmann-type elimination reaction produces both acrylonitrile and the *N*-protonated mesityl imidazolium salt.

Disappointingly however, this methodology still gave low yields (19%), showed poor scalability, and required a tight control of both reaction time and concentration to avoid the competing elimination reaction (Scheme 37).



Scheme 37. Column-free synthesis of [Mes-NHC-(CH₂)₂CH₂CN]·HBr (**2**).

These imidazolium salts showed varying hygroscopicity, depending on their substituents and synthesis route. The modified synthesis of **2** and the use of microwave irradiation in synthesizing **3** and **4** led to non-hygroscopic powders/solids. However, when **3** is obtained by thermal heating, it is highly hygroscopic. The bis-alkyl salt **1** is also highly hygroscopic, quickly turning into a paste or oil if exposed to air.

Characterization of **1-4** by ¹H NMR spectroscopy (see Figure 11, for a representative spectrum of **3**) confirms the *N*-quaternization of the imidazole by the appearance of the characteristic C(2)-H signal at an acidic downfield shift (10.70-8.90 ppm). Furthermore, incorporation of the nitrile function was confirmed by its characteristic $\nu(\text{C}\equiv\text{N})$ band in the corresponding IR (ATR) spectra, observed as a weak band at 2243-2250 cm⁻¹.

[‡] The Hofmann-type elimination of *N*-propionitrile imidazolium salts is known and has been purposefully exploited to construct *N*-alkylated imidazoles in basic³⁵⁵ or neutral^{145,356} conditions.

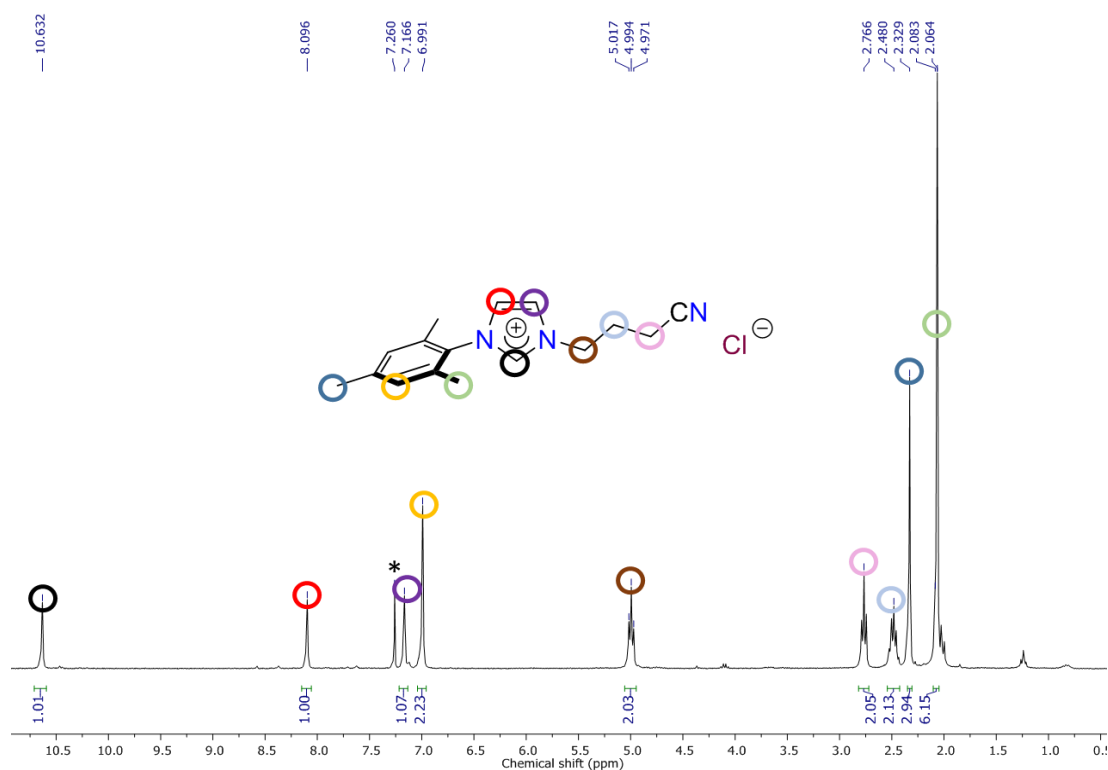


Figure 11. ¹H (300.13 MHz) NMR of **3** in CDCl₃. Residual CHCl₃ noted by an asterisk (*).

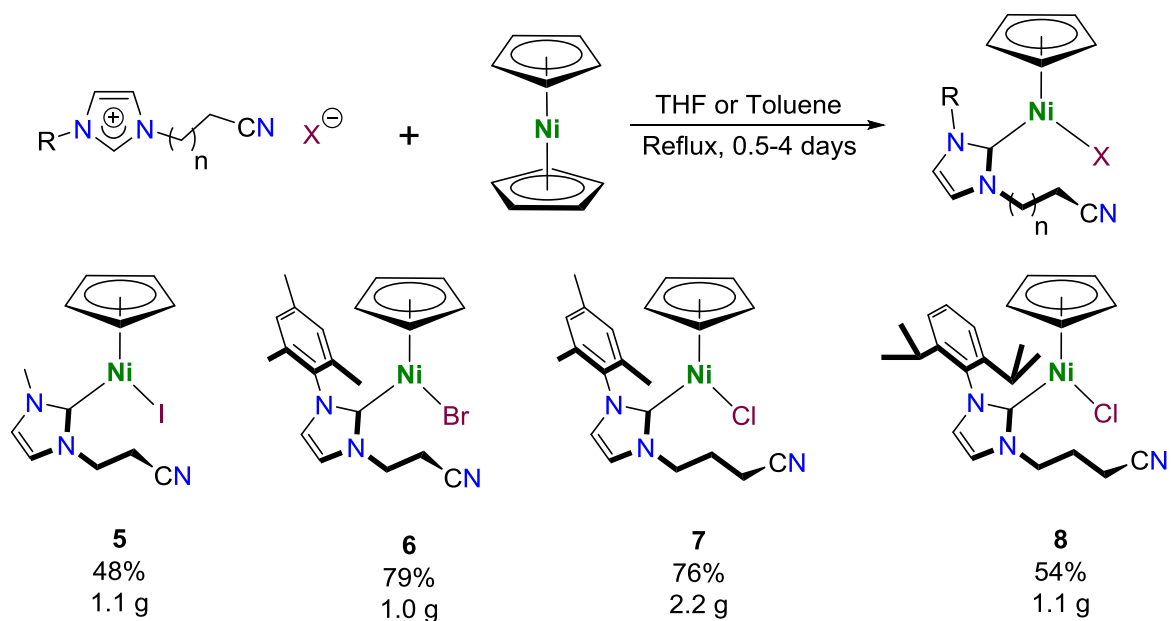
II.2. Synthesis and characterization of half-sandwich nickel(II)-NHC complexes

With the desired proligands in hand, *N*-alkylnitrile chain half-sandwich nickel(II)-NHC complexes of the type [Ni^{II}X(Cp)(R-NHC-(CH₂)_nCH₂CN)] could be readily obtained by direct reaction with nickelocene.¹⁴⁷ Refluxing in THF or toluene yielded the desired complexes [Ni^{II}I(Cp)(Me-NHC-(CH₂)CH₂CN)] (**5**), [Ni^{II}Br(Cp)(Mes-NHC-(CH₂)CH₂CN)] (**6**), [Ni^{II}Cl(Cp)(Mes-NHC-(CH₂)₂CH₂CN)] (**7**) and [Ni^{II}Cl(Cp)(DIPP-NHC-(CH₂)₂CH₂CN)] (**8**) in good to excellent yields, up to multigram scales (Scheme 38).

The reported procedure for the iodo complex **5** gave much lower yields than originally described (reported 64%,¹²⁸ obtained 20%), but could be improved by running the reaction in refluxing toluene for two days instead of DME to give **5** in 48% yield after purification.

Characteristic changes to the ¹H NMR spectra (see Figure 12, for a representative spectrum of **7**) when compared to the corresponding imidazolium salt are the disappearance of the imidazolium acidic proton signal concurrent with the appearance of a singlet corresponding to the Cp group (5.5-4.5 ppm, 5H). It is noteworthy that integration of this signal is at times deficient in protons (4.6-4.8 protons observed), possibly due to slower relaxation of the H_{Cp} nuclei. When larger halogens (bromide, iodide) were present (**5**, **6**) their size hindered the rotation of the *N*-substituent groups near the metal atom. This caused a broadening of *o*-Me peaks in **6**, as previously observed for related compounds.^{123,148} In **5**, iodide interacts

with the *N*-methylene protons in such a way as to induce diastereotopy and a much more complex coupling of the affected signals.¹⁴⁸



Scheme 38. Synthesis of $[\text{Ni}^{\text{II}}\text{X}(\text{Cp})(\text{R-NHC}-(\text{CH}_2)_n\text{CH}_2\text{CN})]$ complexes **5-8** bearing an alkylnitrile function. General synthesis route (top) and yields and scale obtained (bottom).

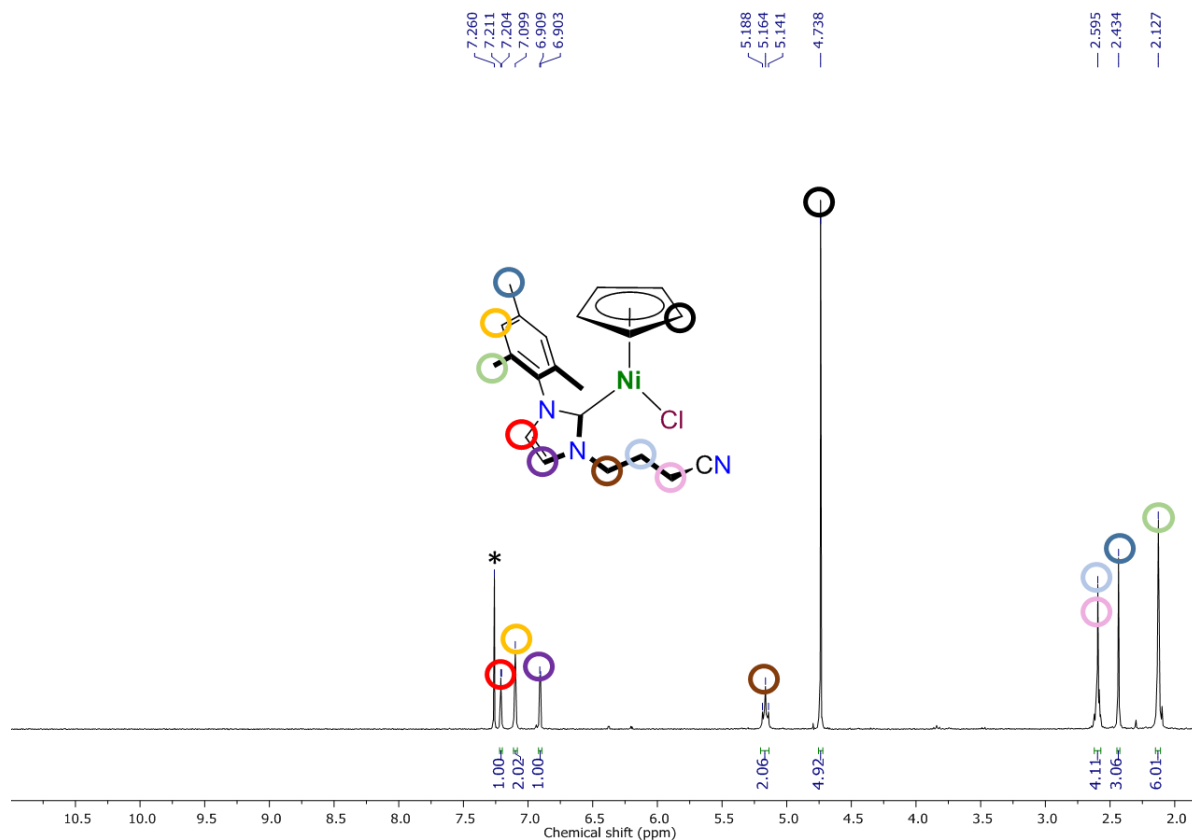


Figure 12. ^1H (300.13 MHz) NMR of **7** in CDCl_3 . Residual CHCl_3 noted by an asterisk (*).

In the ^{13}C { ^1H } NMR spectrum, the nickelated carbene carbon (C_{NHC}) is seen as a weak signal at 164-167 ppm, and the Cp carbons as a strong signal at ca. 90 ppm. Of note, the nitrile signal in the IR (ATR) spectra of **5-8** is much less intense than in the proligands **1-4**, but is found in the same region at 2245-2253 cm⁻¹.

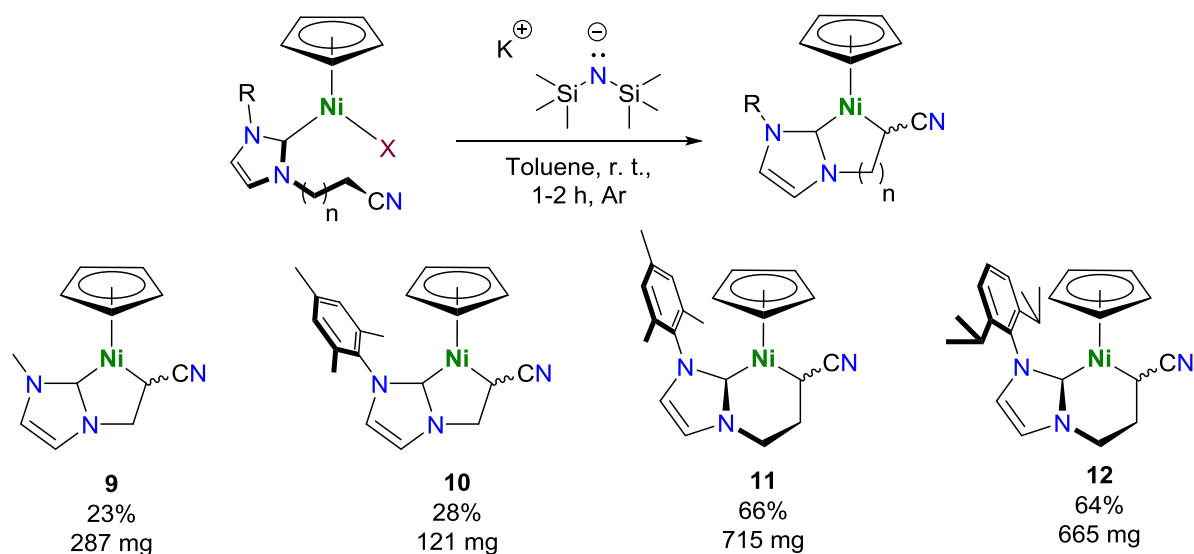
II.3. Synthesis and characterization of half-sandwich κ^2 -C_{NHC}, C_{alkyl}-nickelacycles

From the serendipitous discovery of [Ni^{II}(CH₂CN)(Cp)(NHC-Mes₂)] by basic intramolecular C–H activation of an acetonitrile ligand (Scheme 31, **A**),¹²⁷ our group went on to solidly establish the reaction by using KO^{*t*}Bu (pK_a = 32.2, DMSO at 25 °C, conjugate acid).¹⁴⁹ This reaction was further exploited to synthesize a number of racemic nickelacycles in low to moderate yields by C–H activation of *N*-bound alkylnitrile side arms of NHC ligands (Scheme 31, **B**).¹²⁸

To efficiently source these intermediates, their syntheses were revisited and the nickelacycle family [Ni^{II}(Cp){R-NHC-(CH₂)_nCH(CN)}] further expanded to include complexes **9-12** (Scheme 39). Replacement of the poorly toluene-soluble base, KO^{*t*}Bu, by a solution of potassium bis(trimethylsilyl)amide (KHMDs; pK_a = 25.8, THF at 25°C, conjugate acid)¹⁵⁰ in toluene afforded cleaner reactions and a yield increase of 10% for the synthesis of [Ni^{II}(Cp){Mes-NHC-(CH₂)₂CH(CN)}] (**11**). Likewise [Ni^{II}(Cp){Mes-NHC-(CH₂)CH(CN)}] (**10**), [Ni^{II}(Cp){Me-NHC-(CH₂)CH(CN)}] (**9**) and [Ni^{II}(Cp){DIPP-NHC-(CH₂)₂CH(CN)}] (**12**) were obtained as green powders in low (five-membered nickelacycles) to good (six-membered nickelacycles) yields (Scheme 39).

Spectroscopic characterization of these complexes by ^1H NMR spectroscopy (see Figure 13, for a representative spectrum of complex **11**) showed both the disappearance of one methylene proton, and a loss of symmetry for the new complexes. Indeed, the protons of the nickelated alkyl chain are diastereotopic as a consequence of the formation of the asymmetric center in the nickel bound α -nitrile carbon (C_{alkyl}). Thus the previously equivalent signals are now non-equivalent due to their position *syn*- or *anti*-CN. In addition, the substituents of the *N*-aryl groups (*o*-Me, *m*-H of Mes in **10** and **11**; *m*-H, *o*-(*i*-Pr) of DIPP in **12**) also become non-equivalent at r. t., this time due to restricted rotation about the *N*-aryl bond on the NMR time scale. The ^{13}C { ^1H } NMR spectra of **9-12** all showed a slight (~5 ppm) downfield shift of the C_{NHC} peak when compared with the spectra of their acyclic precursors **5-8**, as well as a large (30-50 ppm) upfield shift of the peak of the nickel-bound C_{alkyl} (Table 3). Curiously, the chemical shift of C_{alkyl} varies with the size of the metallacycle. The most upfield signal is observed for six-membered nickelacycles (**11**: -25.3 ppm, **12**: -25.1 ppm) and the least for the five-membered nickelacycles (**9**: -11.6 ppm, **10**: -11.0 ppm) whereas the previously

reported eight-membered nickelacycle $[\text{Ni}^{\text{II}}(\text{Cp})\{\text{Mes-NHC}-(\text{CH}_2)_4\text{CH}(\text{CN})\}]$ shows an intermediate upfield shift (-18.7 ppm)¹²⁸ (Table 3).



Scheme 39. Half-sandwich C_{NHC}, C_{alkyl}-nickelacycle complex **9-12** synthesis by base-assisted intramolecular C–H activation.

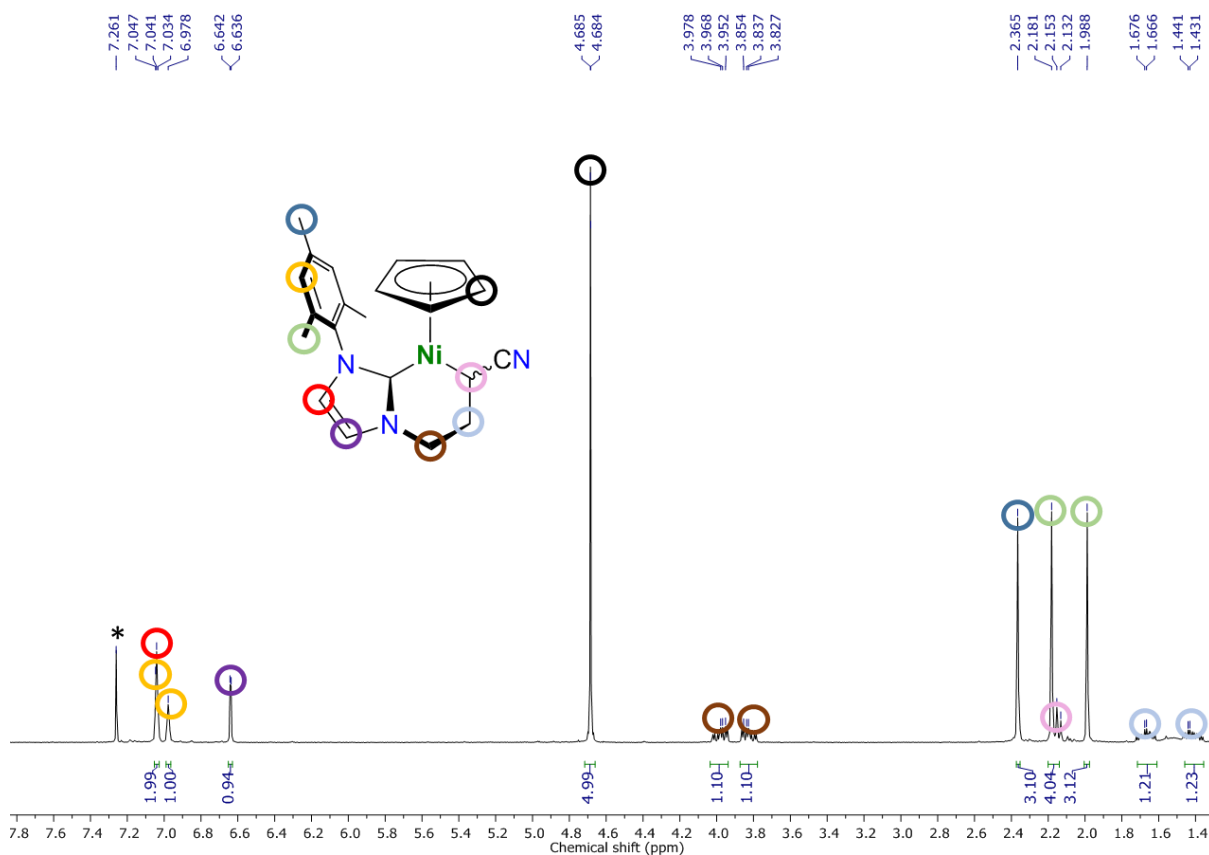


Figure 13. ¹H (300.13 MHz) NMR of **11** in CDCl₃. Residual CHCl₃ noted by an asterisk (*).

Table 3. ¹³C {¹H} NMR (CDCl₃) chemical shifts (δ) of the nickel-bound carbons (C_{NHC}, C_{alkyl}) in the metallacycles and of the corresponding carbons in their acyclic precursors (C_{NHC}, C α -CN) and metallacyclic bite angle (C_{NHC}-Ni-C_{alkyl}) determined by X-ray diffraction studies.

Complex	δ (ppm)		Complex	δ (ppm)		Bite angle (°)
	C _{NHC}	C α -CN		C _{NHC}	C _{alkyl}	
5	167.3	19.6	9	173.5	-11.6	85
6	166.8	20.4	10	175.9	-11.0	84
7	164.2	14.8	11	171.3	-25.3	94
8	165.7	15.1	12	172.6	-25.1	-
A	164.1	17.3	B	177.3	-18.7	90

A: [Ni^{II}Br(Cp)(Mes-NHC-(CH₂)₄CH₂CN)]; **B**: [Ni^{II}(Cp){Mes-NHC-(CH₂)₄CH(CN)}].¹²⁸

Crystals suitable for X-ray diffraction studies were grown for **9** and **10**. The two structures with selected bond lengths and angles are shown in Figure 14 and Figure 15. A summary of crystal data, data collection parameters and structure refinements can be found in the Experimental section. For both structures, most parameters were found to be invariant when compared with the related nickelacycles of different size, **11** and [Ni^{II}(Cp){Mes-NHC-(CH₂)₄CH(CN)}] (see Table 3, complex **B**).¹²⁸ Apart from the bite angle (vide supra), the most remarkable geometrical feature in the structures of these five-membered nickelacycles is these structures' is the coplanarity found between the atoms in both the nickelacycle and the imidazole core.

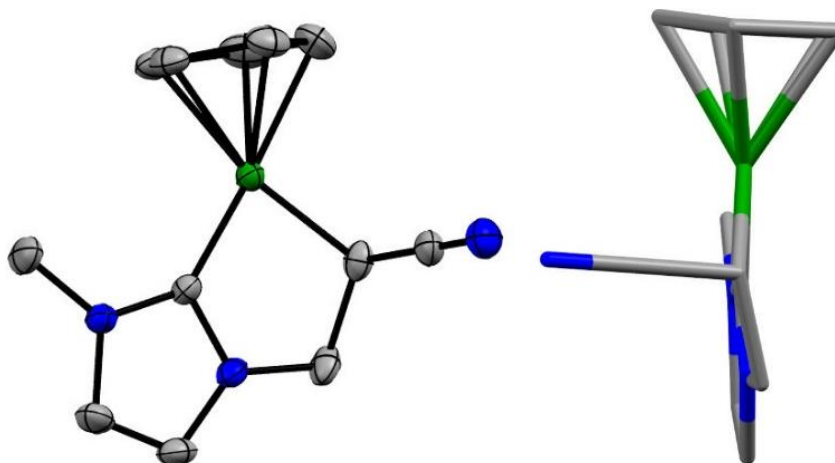


Figure 14. Left - Molecular structure of **9** showing all non-H atoms. Carbon atoms in grey; nitrogen atoms in blue and nickel atom in green. The centro-symmetric space group $P2_1/c$ contains both enantiomers; only the (*S*) enantiomer is shown. Selected distances (Å) and angles (°) with esds in parenthesis: Ni-C_{NHC}, 1.8475(11); Ni-C_{alkyl}, 1.9697(11); C_{alkyl}-C_{CN}, 1.4491(17); C_{CN}-N_{CN}, 1.1491(17); Ni-Cp_{centroid}, 1.756; C_{alkyl}-C_{CN}-N_{CN}, 178.84(14). Ellipsoids are shown at the 50% probability level. Right – Capped stick representation showing the coplanarity of the atoms in the imidazole core and the nickelacycle.

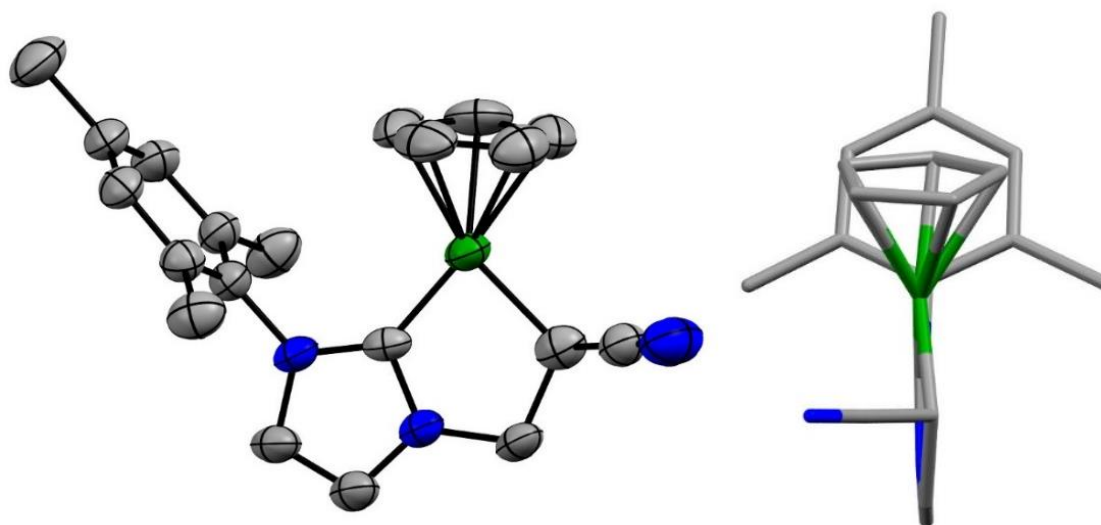


Figure 15. Left - Molecular structure of **10** showing all non-H atoms. Carbon atoms in grey; nitrogen atoms in blue and nickel atom in green. Ellipsoids are shown at the 50% probability level. Two independent but very similar molecules (A and B) are present in the asymmetric unit. The centrosymmetric space group $P\bar{1}$ contains both enantiomers of each molecule and only the (S) enantiomer of molecule A is shown. Selected distances (Å) and angles (°) with esds in parenthesis of the two independent molecules are given here: C_{alkyl}–C_{CN}, 1.432(9), 1.444(9); C_{CN}–N_{CN}, 1.135(8), 1.142(8); Ni–Cp_{centroid}, 1.748, 1.754; C_{alkyl}–C_{CN}–N_{CN}, 177.8(8), 179.0(7). Right – Capped stick representation showing the coplanarity of the atoms in the imidazole core and the nickelacycle.

A correlation can be found between the chemical shift of the C_{alkyl} and the nickelacycle's bite angle (C_{NHC}–Ni–C_{alkyl}, °) (Table 3). This suggests that metallacycle exerts a particularly great influence on the electron density of the C_{alkyl}, but it is worth noting that the acyclic complex [Ni^{II}(CH₂CN)(Cp)(NHC-Mes₂)]¹²⁷ does not follow this trend. Despite this difference in electron density observed by NMR spectroscopy, the corresponding Ni–C_{alkyl} bond lengths (1.970-1.980 Å) show no appreciable difference.

The C≡N stretch in the IR (ATR) spectra of **9-12** is very different to that of the acyclic complexes **5-8** and of the imidazolium salts **1-4** (Table 4). This vibration that had become very weak and difficult to observe for **5-8** is the dominant feature of the spectra of **9-12**, appearing as a strong band at 2151-2185 cm⁻¹, considerably red-shifted (~ -80 cm⁻¹) when compared to its precursors **1-8**. This shift to a lower wavenumber is consistent with an increased electron density at the triple bond populating an antibonding orbital of the nitrile fragment, while the increased intensity of this band, might be caused by an increase in this bonds polarization. When comparing the distances d(C≡N) of the structurally characterized pairs **5/9** and **7/11**, the former shows no statistically significant change while the latter suffers a small elongation

(+0.045 Å) consistent with a weaker bond. No correlation between the wavenumber or intensity of $\nu(\text{C}\equiv\text{N})$ and with the size of the metallacycle was observed.

Table 4. Average wavenumbers ($\tilde{\nu}$) and relative intensity of $\nu(\text{C}\equiv\text{N})$ (cm^{-1}) for the imidazolium salts **1-4**, the half-sandwich Ni(II)-NHC complexes **5-8** and the nickelacycles **9-12**.

Compound family		Average $\nu(\text{C}\equiv\text{N})$ (cm^{-1})
[R-NHC-(CH ₂) _n CH ₂ CN]·HX	1-4	2247 (m)
[Ni ^{II} X(Cp)(R-NHC-(CH ₂) _n CH ₂ CN)]	5-8	2249 (w)
[Ni ^{II} (Cp){R-NHC-(CH ₂) _n CH(CN)}]	9-12	2168 (s)

m = medium; s = strong; w = weak

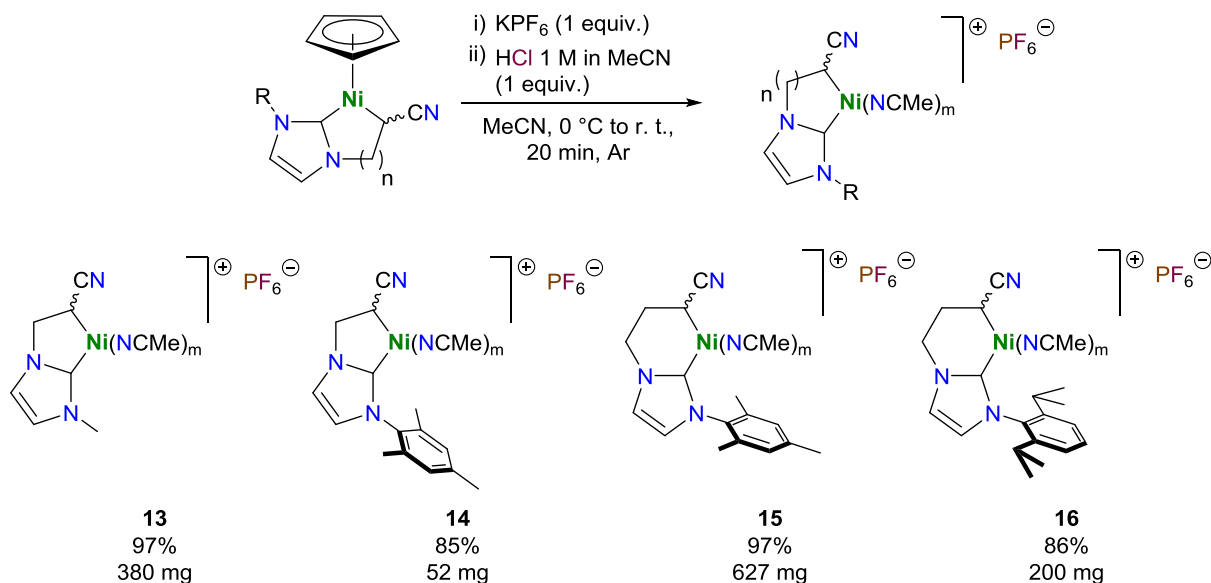
II.4. Synthesis and characterization of cationic κ^2 -C_{NHC}, C_{alkyl}-nickelacycles

II.4.1. Synthesis and formula determination of cationic κ^2 -C_{NHC}, C_{alkyl}-nickelacycles

As previously discussed, our group showed that acidolysis could cleave the nickel-cyclopentadienyl bonds (Scheme 33) opening up coordination positions necessary for reactive complexes. At the time an intermediate acetonitrile adduct was briefly characterized (¹H, ¹³C NMR and IR (ATR) spectroscopies),¹³¹ leaving open its full characterization before testing its activity as a (pre)catalyst.

Carrying out the reaction following the reported protocol showed however a marked problem in reproducibility i. e., following the same protocol, one experiment would yield the pure target compound and a second experiment led to heavy decomposition; note that visually both the successful and unsuccessful reactions look akin as dark yellow/ocher powders but can be easily distinguished by ¹H NMR analysis. While in most chemical syntheses this would just result in a loss in yield after further purification steps, complexes **13-16** studied here were not amenable to purification by standard techniques: e. g., extraction, precipitation and column chromatography over silica or neutral alumina. Fortunately, carrying out the reaction at lower temperature (0 °C) led to a marked increase in the reproducibility of the reaction (Scheme 40, top). With this improvement, a family of cationic complexes could be synthesized, counting [Ni^{II}{Me-NHC-(CH₂)CH(CN)}(MeCN)_m]PF₆ **13**, [Ni^{II}{Mes-NHC-(CH₂)CH(CN)}(MeCN)_m]PF₆ **14**, [Ni^{II}{Mes-NHC-(CH₂)₂CH(CN)}(MeCN)_m]PF₆ **15** and [Ni^{II}{DIPP-NHC-(CH₂)₂CH(CN)}(MeCN)_m]PF₆ **16**. It is noteworthy that the syntheses can now be performed at multi-hundred milligram scales (Scheme 40, bottom).

Characterization of these complexes by ¹H NMR in MeCN-*d*₃ distinctly showed the disappearance of the singlet peak corresponding to the cyclopentadienyl ligand (see Figure 16 for a representative spectrum of **15**). The integrity of the nickelacycle was also demonstrated by the persistent non-equivalence of the methylenic protons. In addition, the persistent non-equivalence of the substituent groups of the *N*-aryl NHCs still indicates restricted rotation about the *N*-aryl bond on the NMR time scale. Coordinating acetonitrile appeared at the same chemical shift as free acetonitrile (in MeCN-*d*₃) indicative of chemical exchange with the deuterated solvent and thus of its high lability.



Scheme 40. Cyclopentadienyl acidolysis by dilute hydrochloric acid at 0 °C and formation of κ^2 -C_{NHC}, C_{alkyl}-nickel(II) cationic complexes **13-16**.

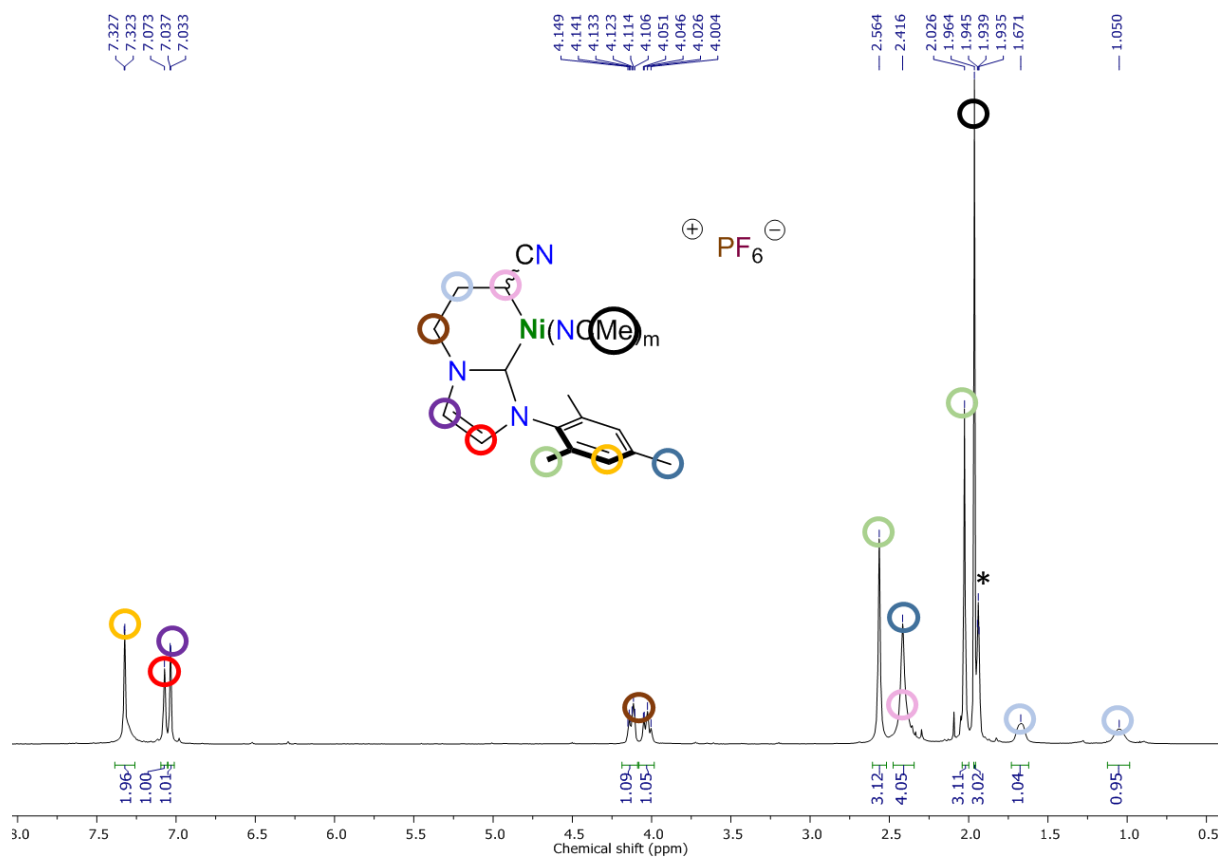


Figure 16. ¹H (500.14 MHz) NMR of **15** in MeCN-*d*₃. Residual CHD₂CN noted by an asterisk (*).

The ^{13}C $\{^1\text{H}\}$ NMR spectra of **13-16** confirmed the departure of the cyclopentadienyl ligand and showed a considerable broadening (Figure 17) and significant shifts for the C_{NHC} and C_{alkyl} peaks (Table 5). Comparison between the ^{13}C $\{^1\text{H}\}$ NMR spectra of the parent half-sandwich nickelacycles **9-12** and the acetonitrile adducts **13-16** bore striking differences.[§] The C_{NHC} peak of **13-16** becomes less intense and is upfield shifted by ~17 ppm (average $\delta(\text{C}_{\text{NHC}}) = 156$ ppm in **13-16** vs. average $\delta(\text{C}_{\text{NHC}}) = 173$ ppm in **9-12**). A reverse phenomenon is observed for the C_{alkyl} peak, which undergoes a large downfield shift (>15 ppm) along with a broadening of the signal. As was the case for the half-sandwich nickelacycles **9-12**, the signal for C_{alkyl} is very sensitive to the size of the metallacycle (five-membered $\delta(\text{C}_{\text{NHC}}) = \mathbf{13}$: 7.1 ppm; **14**: 7.8 ppm; six-membered $\delta(\text{C}_{\text{NHC}}) = \mathbf{15}$: -2.0 ppm; **16**: -2.7 ppm).

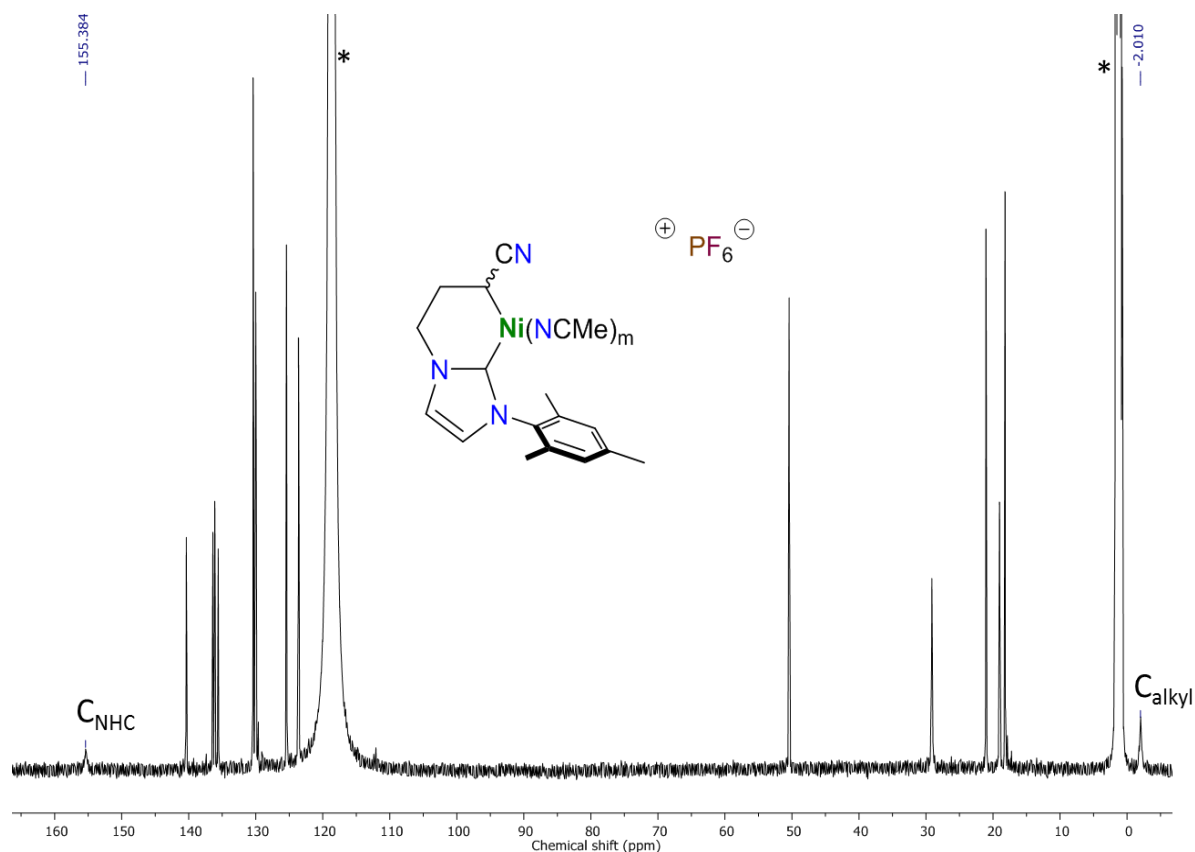


Figure 17. ^{13}C $\{^1\text{H}\}$ (125.77 MHz) NMR of **15** in MeCN- d_3 . Peaks of MeCN- d_3 noted by an asterisk (*).

[§]The comparison between NMR spectra in different solvents (CDCl₃; MeCN- d_3) should be taken judiciously due to possible interference by solvation effects.

Table 5. ¹³C {¹H} NMR chemical shifts (δ) for nickel-bound C_{NHC} and C_{alkyl} for half-sandwich nickelacycles **9-12** (CDCl₃) and cationic complexes **13-16** (MeCN-*d*₃).

Complex	δ C _{NHC} (ppm)	δ C _{alkyl} (ppm)	Complex	δ C _{NHC} (ppm)	δ C _{alkyl} (ppm)
9	173.5	-11.6	13	155.4	7.1
10	175.9	-11.0	14	153.8	7.8
11	171.3	-25.3	15	158.6	-2.0
12	172.6	-25.1	16	156.6	-2.7

The IR (ATR) spectrum of each complex **13-16** shows a broad intense band at 823-834 cm⁻¹ and a sharp intense peak at 555-557 cm⁻¹ assignable to the P–F stretching modes of the PF₆⁻ counteranion.¹⁵¹ Despite the intensity and width of these peaks dwarfing most of the spectrum, a characteristic ν (C≡N) is still observable (Table 6). This broad band appears at 2233-2243 cm⁻¹, and has suffered a blue shift of ~70 cm⁻¹ compared to the ν (C≡N) of **9-12**. This band can be attributed to: the new acetonitrile ligand(s), the nickelacyclic nitrile group or a combination of both. If this band does contain a significant contribution from the nickelacyclic nitrile, the higher wavenumber and lower intensity are consistent with the removal of the electron-rich Cp ligand, leading to an electron-impooverished metal center and less available electron density for the empty antibonding orbitals of the nitrile.

Table 6. Average wavenumbers ($\bar{\nu}$) and relative intensity of for ν (C≡N) (cm⁻¹) for the imidazolium salts **1-4**, the half-sandwich Ni(II)-NHC complexes **5-8**, the nickelacycles **9-12** and cationic complexes **13-16**.

Compound family		Average ν (C≡N) (cm ⁻¹)
[R-NHC-(CH ₂) _n CH ₂ CN]·HX	1-4	2247 (m)
[Ni ^{II} X(Cp)(R-NHC-(CH ₂) _n CH ₂ CN)]	5-8	2249 (w)
[Ni ^{II} (Cp){R-NHC-(CH ₂) _n CH(CN)}]	9-12	2168 (s)
[Ni ^{II} {R-NHC-(CH ₂) _n CH(CN)}(MeCN) _m]	13-16	2238 (m)

m = medium; s = strong; w = weak; $\bar{\nu}$ (C≡N_{MeCN}) = 2253 cm⁻¹

Characterization of **15** by electrospray high-resolution mass spectrometry (HRMS-ESI) found a main molecular ion peak at a m/z = 351.1126, which was attributed to [Ni^{II}{Mes-NHC-(CH₂)₂CH(CN)}(MeCN)]⁺ (calculated m/z = 351.1120) indicating the loss of an acetonitrile ligand (Figure 18). The HRMS spectrum showed no other significant peaks as was the case for **16**. However, in the case of **13** and **14**, the two-acetonitrile-ligand species was observed as a minor peak.

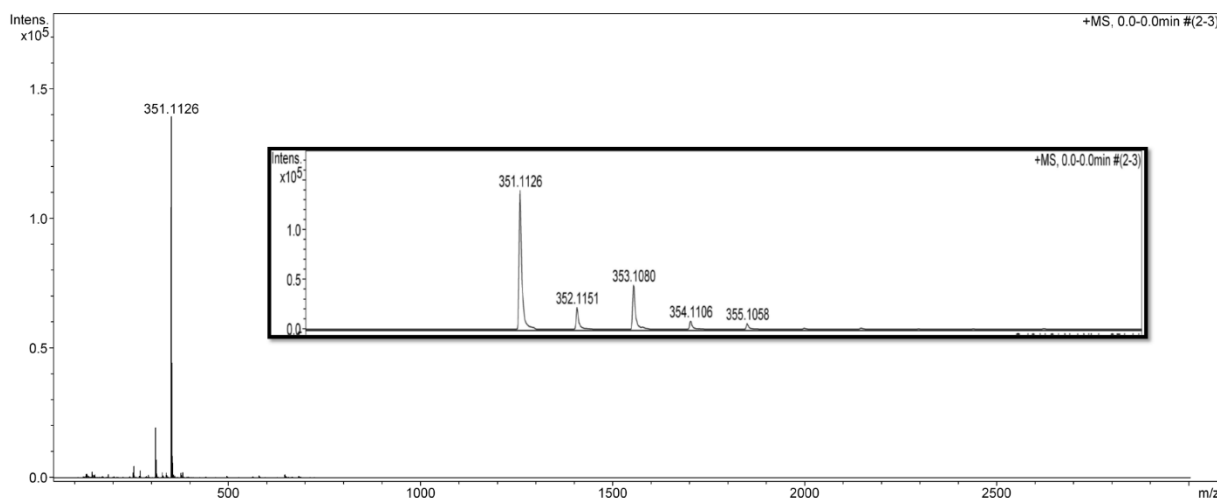


Figure 18. HRMS-ESI analysis of **15**. One dominant molecular ion peak and detail highlighting the exact mass and confirming the presence of nickel by its isotope pattern.

This led to a more careful re-reading of the ^1H NMR spectra of these complexes that showed varying amounts of free acetonitrile, underscoring the difficulty in obtaining consistent and meaningful values for the integration of the acetonitrile peak. Thus, thorough drying for 1 to 2 days in a warm bath at 40 °C under high vacuum was required for stable and coherent integration for all complexes that would account for 3 protons, that is - *one acetonitrile per molecule*.

Nevertheless conclusions made on the basis of these analyses (NMR, HRMS) must be cautious. In HRMS-ESI the high energy state of the molecule can induce fragmentation of one acetonitrile ligand and make the resulting fragment the dominant ion. Likewise, in ^1H NMR spectra, in a regime of chemical exchange with the solvent, kinetics on the NMR timescale could mask the amount of natural acetonitrile originating from the analyte.

To solve these ambiguities a first approach was to quantify the ligated solvent by ^1H NMR spectroscopy by means of eliminating the chemical exchange. However, hydrocarbons (toluene, benzene) failed to dissolve the complex, even when boiled. Low polarity halogenated solvents were also inadequate (1,2-dichlorobenzene, chloroform) or led to immediate decomposition (dichloromethane, 1,2-dichloroethane) even at low temperatures (-40 to 0 °C). Slightly polar organic ether solvents (THF, 1,4-dioxane) were also found to be inadequate. Polar, coordinating organic solvents (acetone, DMSO, DMF, MeOH, MeNO₂) readily dissolved the samples, but degraded it as quickly. Water was also ineffective at dissolving the compound. Only two solvents were found to be fit for analysis: the nitrogen Lewis bases, acetonitrile and pyridine.

NMR analysis of a sample of **15** in pyridine-*d*₅ gave a ^1H spectrum with small changes of the chemical shifts when compared to the spectra in MeCN-*d*₃ (Figure 19). A singlet peak at

1.86 ppm integrating for 3 protons corresponding to free acetonitrile is observed.** Given that the only source of acetonitrile possible was the analyte, it provided further evidence for the hypothesis of a single acetonitrile ligand. The fact that the ligand appears at chemical shift of free acetonitrile further corroborated that chemical exchange happens with nitrogen bases, thus confirming that the metal's coordination sphere is now accessible, in contrast with complexes **9-12**.

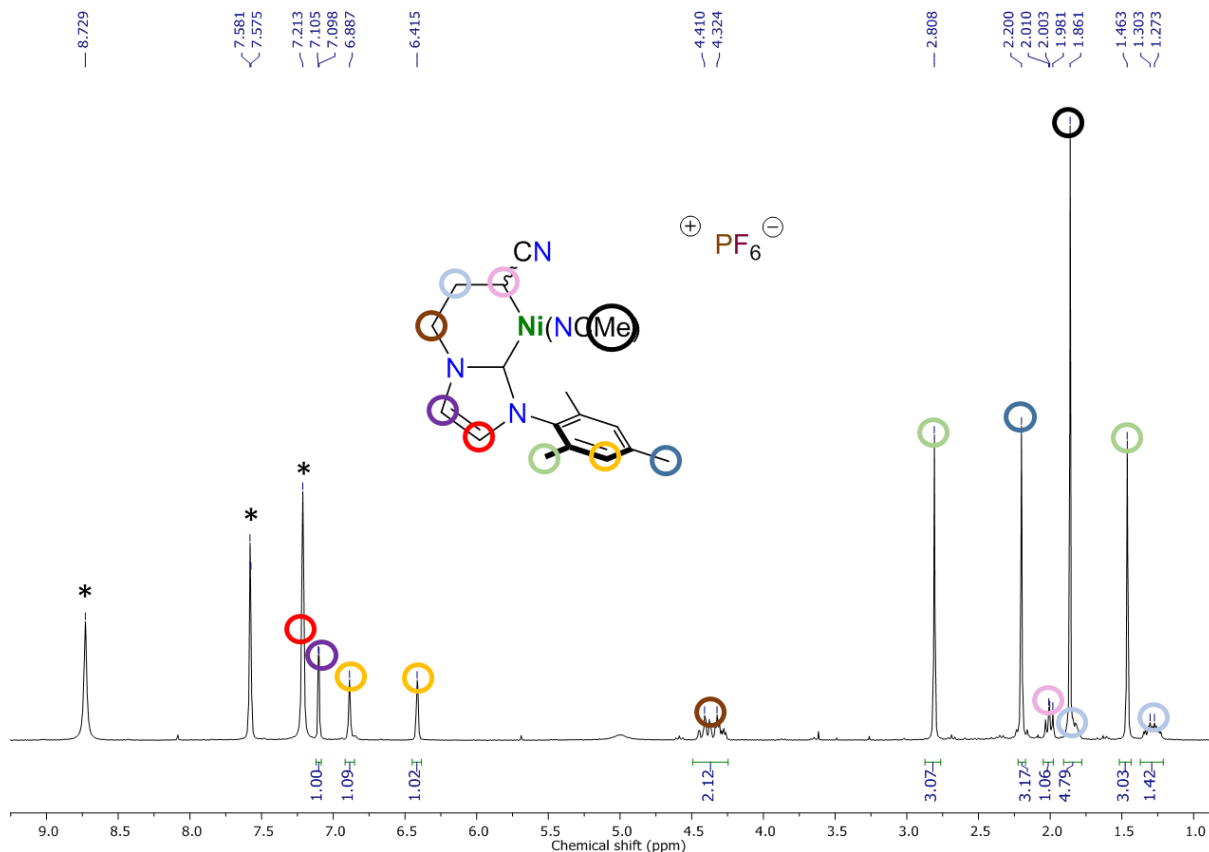


Figure 19. ^1H (300.13 MHz) NMR of **15** in pyridine- d_5 . Peaks of pyridine- d_4 noted by an asterisk (*).

An analogous situation was observed for both **14** and **16**, but not for **13**. For this complex, no peaks attributable to free acetonitrile were observed. Instead, peaks attributed to acetonitrile were identified at slightly shifted chemical shifts in ^1H and ^{13}C $\{^1\text{H}\}$ spectra (compared to those of free MeCN), indicating that the least hindered cation does not release MeCN in these conditions (Figure 20). This observation was surprising as one would expect the least hindered complex to be able to accommodate multiple solvent (py- d_5) molecules. One possible explanation may lie with the stronger electron-donating character of *N,N'*-bis-alkyl

** Pyridine- d_5 is an uncommon NMR solvent, as such, we independently registered the ^1H and ^{13}C NMR spectra of acetonitrile in pyridine- d_5 , calibrated the spectra to the residual $\text{C}_5\text{HD}_4\text{N}$ signal and used these as reference, see Figures S1 and S2, Annex.

NHC ligands exerting a difference on the acetonitrile ligand positioned *trans*-NHC (vide infra), as to disfavor decoordination. However, no other NMR or IR measurements comparing **13** with **14-16** show a different behavior of the *N,N'*-bis-alkyl NHC ligands of **13** apart from the one now discussed. A solvent molecule is nonetheless expected to coordinate to the nickel center to give a square planar species in solution (Scheme 41).

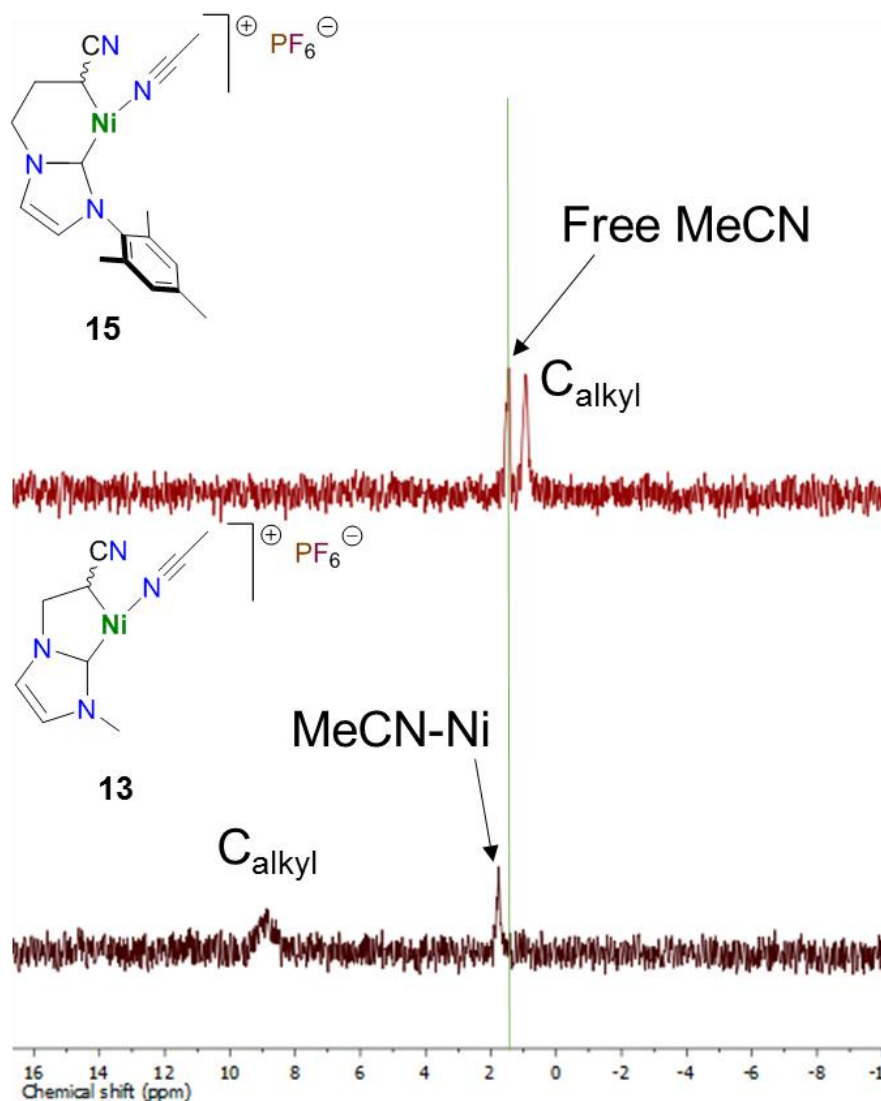
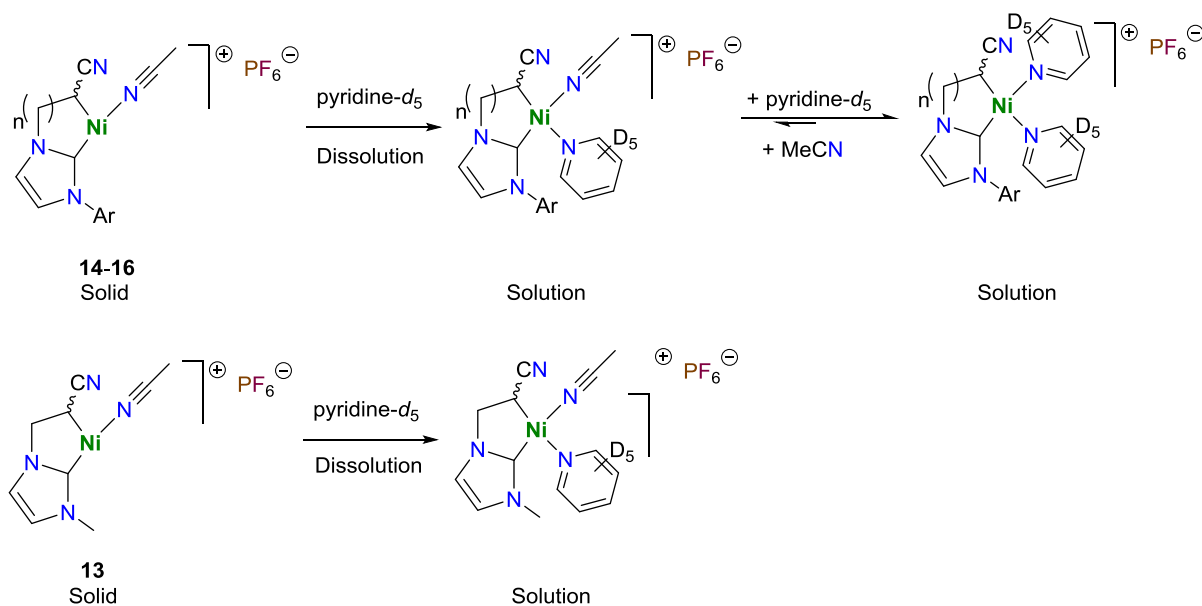


Figure 20. $^{13}\text{C}\{^1\text{H}\}$ (125.77 MHz) NMR spectra of **13** and **15** in pyridine- d_5 . Green line marks the chemical shift of free MeCN.

Analysis of the $^{13}\text{C}\{^1\text{H}\}$ NMR spectra of **13-16** in pyridine- d_5 shows a significant increase in the intensity and sharpness of the critical C_{NHC} and C_{alkyl} peaks for **14-16** when compared with the spectra in MeCN- d_3 (see Figure 21 for a representative example of **15**). This increased sharpness of these signals suggests that the solvent exchange is slower (or absent) in pyridine. The sole exception is **13** for which the C_{alkyl} signal remains broad (Figure 20).



Scheme 41. Possible chemical equilibrium with pyridine-*d*₅ leading to release of acetonitrile in *N*-aryl substituted complexes **14-16**. No free acetonitrile is released with the dissolution of **13**.

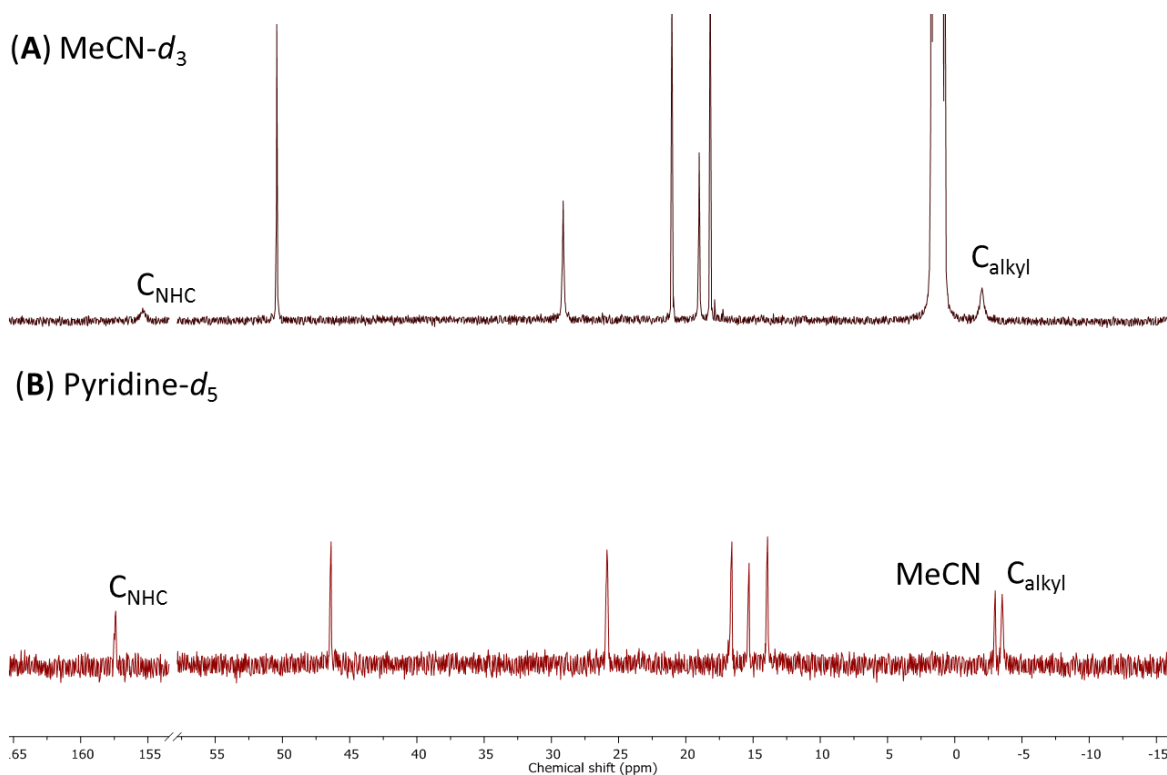


Figure 21. Detail of the ¹³C {¹H} (125.77 MHz) NMR spectra of **15** in MeCN-*d*₃ (A) and pyridine-*d*₅ (B). Free acetonitrile is observed in the pyridine-*d*₅ solution.

Finally, elemental analyses of **13-16** confirmed the formulation with only one acetonitrile ligand in the solid state.

II.4.2. Insights into the structure of cationic κ^2 -C_{NHC}, C_{alkyl}-nickelacycles

With the molecular formula definitively established, the next question to tackle was the solid-state structure of these complexes. Several arrangements were a priori plausible: (i) dimers/oligomers with bridging acetonitrile ligands, (ii) monomers with a four-electron donor side-on acetonitrile ligand, or (iii) with a two-electron donor end-on or side-on acetonitrile ligand resulting in a 14 valence electron Ni(II) species (Figure 22).

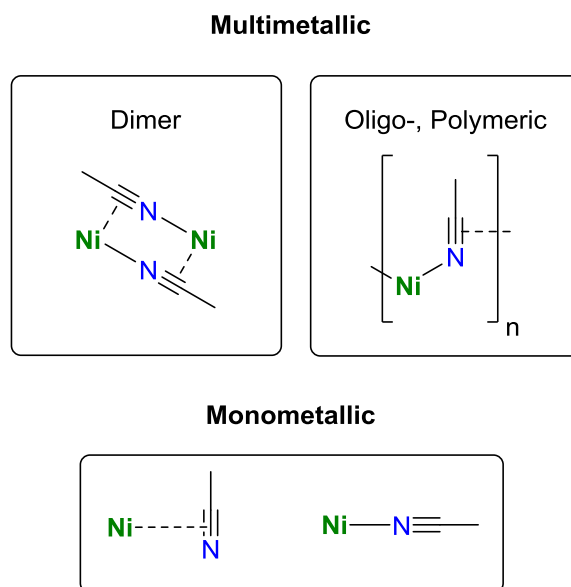


Figure 22. Possible binding modes for acetonitrile in either multimetallic or monometallic arrangements.

The most direct answer to this question would be characterization by single crystal X-ray diffraction studies. However, the complexes show very restricted solubility (*vide supra*), being only adequately soluble in nitriles and pyridine, in which they are extremely soluble. Thus attempts at crystallization by common techniques¹⁵² and using a series of solvent systems (acetonitrile, *n*-propionitrile, *n*-butyronitrile, benzonitrile, pyridine, Et₂O, THF, tetrahydropyrene, benzene, toluene, *n*-hexane) were all unsuccessful. The system would in general crash out as an oil or an amorphous solid. On occasion, if air entered the system, the mixture would turn to a pasty green with purple crystals over the course of weeks. The crystals could be collected and identified by X-ray diffraction studies as [Ni^{II}(NCMe)₆](PF₆)₂ (see Experimental section). Exchanging the counter-anion PF₆⁻ for other weakly-coordinating anions (BF₄⁻, BPh₄⁻) showed no noticeable change in the solubility of the cationic complexes nor did it allow the growth of suitable crystals.

The difficulty in obtaining crystals when acetonitrile acts both as a solvent and a ligand has been recently noted for a related C_{NHC}, C_{cycloheptatrienyl}-palladacycle acetonitrile adduct,¹⁵³ that was isolated as an oligomer bound by bridging bromide ligands.^{153,154} However, in our case,

the PF₆⁻ anion is weakly coordinating and unsuitable for this role. Furthermore, few well-characterized structures are known with MeCN acting as a bridging ligand.^{155–170} In fact, only three examples report crystal structures of nickel complexes with bridging MeCN ligands. In these species, μ^2, η^1, η^2 -acetonitrile ligands are side-on bonded to a nickel(0) atom and end-on bonded to a second one in multimetallic environments.^{171–173} Beyond these rare examples of side-on bound bridging MeCN, several examples are known of monomeric Ni(0) with a side-on bound nitrile ligand acting as a side-on 2 electron-donor (Figure 23).^{174–179} We are unaware of any example of 4 electron-donor side-on nitrile coordinated to a nickel species.

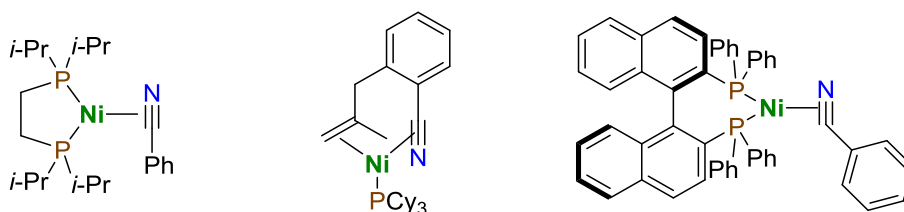


Figure 23. Examples of side-on bound Ni(0)-benzonitrile complexes.^{175,178,179}

Nitrile side-on bonding can be observed by IR spectroscopy where a characteristic lowering of the $\nu(\text{C}\equiv\text{N})$ band's wavenumber places it in the 1700 cm⁻¹ region,^{171,180–182} even if this band is at times weak^{159,168,180,181} so much so that it is at times unobservable.^{182–186} The IR (ATR) spectra of complexes **13-16** show no band in this region to support a side-on bound MeCN. Thus, the most common case of end-on coordination could be expected for the systems studied. In this case, the IR $\nu(\text{C}\equiv\text{N})$ is expected between 2200 and 2300 cm⁻¹.¹⁸⁷ This is in agreement with the medium intensity peaks observed between 2233 and 2243 cm⁻¹ in the spectra of **13-16**. This is however the same region where the equivalent signal for the pending nitrile arm of the metallacycle is expected. Interestingly, a shoulder that might originate from combinations of these bands is observed at 2195-2200 cm⁻¹, but no definitive affirmations could be made on this point.

Given the lack of success growing single crystals and the ambiguity of spectral data, we decided to run DFT calculations on model cations of the five-membered nickelacycle **13**, and of the six-membered nickelacycle **15**. Calculation of the Gibbs energy balance of the species with one and two end-on acetonitrile ligands allowed us to identify three stable structures in each case (**Erreur ! Source du renvoi introuvable.**): (i) a 16-electron square planar structure with two acetonitrile ligands (**13A** and **15A**), (ii) a T-shaped 14-electron structure (**13B** and **15B**) and (iii) a pseudo T-shaped structure stabilized by the dangling nitrile of the nickelacycle via side-on coordination (**13C** and **15C**).

The 16-electron two-acetonitrile cations **13A** and **15A** were calculated as being the most stable (and so the referenced as 0 kcal mol⁻¹), which is consistent with the expected

formulation of the compounds in solution. The energy balance in **13B-C** and **15B-C** differs by virtue of the size of the metallacycle. The five-membered model **13B** was found at +12 kcal mol⁻¹ adopting a T-shaped structure with the acetonitrile ligand arranged *trans* to the NHC, whereas the pseudo-square planar isomer **13C** with a side-on bound dangling nitrile was found at +17 kcal mol⁻¹. Analogous structures were found for **15B-C**, but here by virtue of the flexibility of the nickelacycle, the pseudo-square planar structure **15C** is slightly more stable (+7 kcal mol⁻¹) than the T-shaped isomer **15B** (+9 kcal mol⁻¹). Of note, no side-on bound acetonitrile isomer could be optimized, allowing us to rule out this hypothesis.

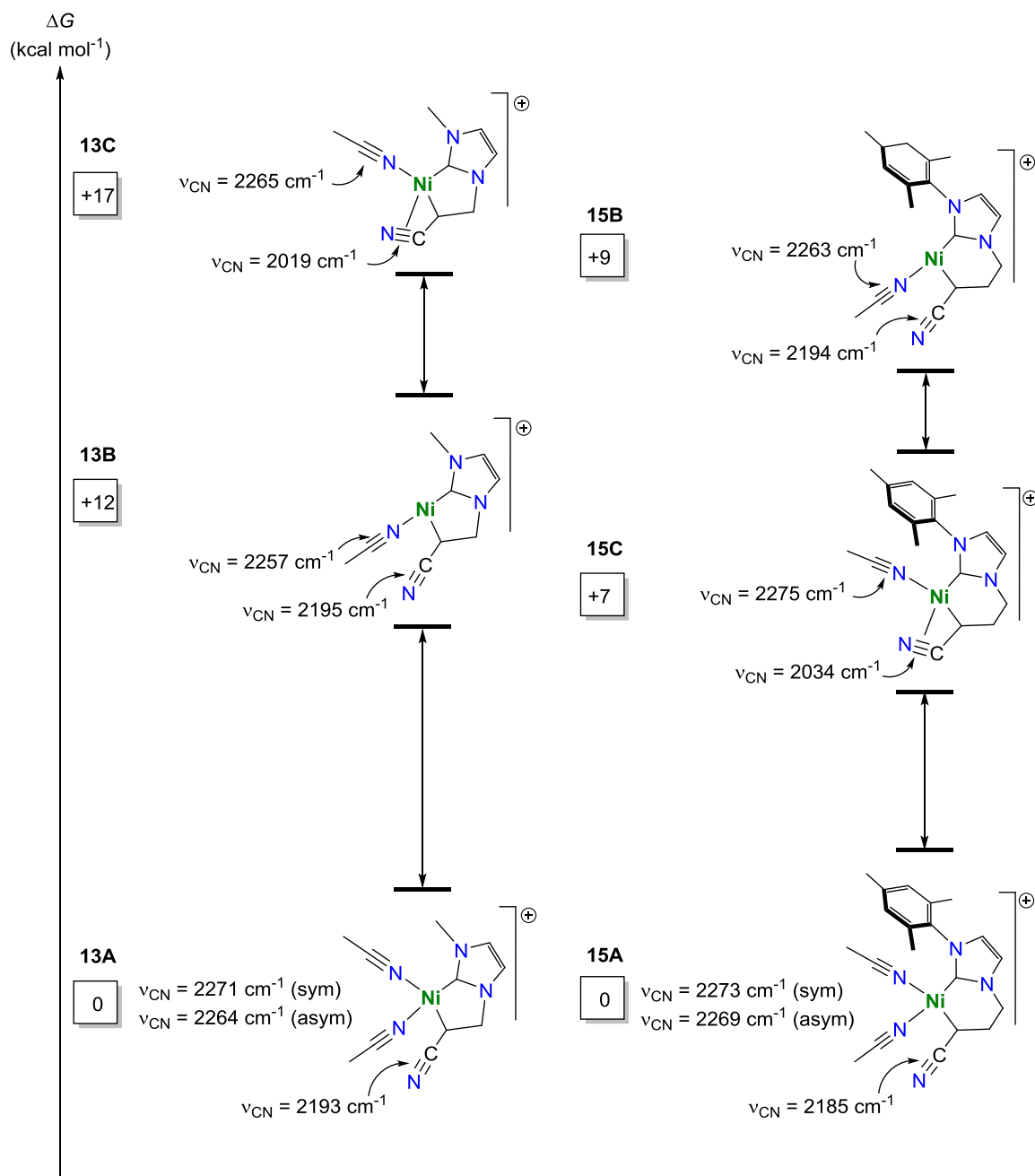


Figure 24. Gibbs energy balance calculated by DFT between the model cations **13A-C** and **15A-C** with one or two acetonitrile ligands and calculated vibrational frequencies of the C≡N bond.

Finally, no paramagnetic open shell systems or structures adopting a D_{3h} or Y-shape geometry could be optimized. This is consistent with our observations of diamagnetic samples (¹³C CP-MAS NMR and solution magnetic moment measurements by the Evans' method)¹⁸⁸ as such structures often give paramagnetic compounds (Figure 25).^{189–191}

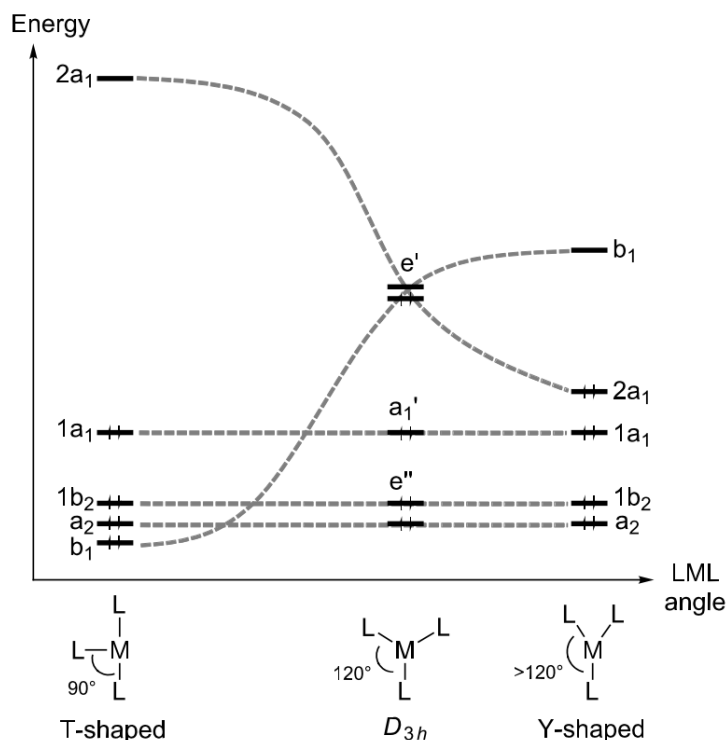
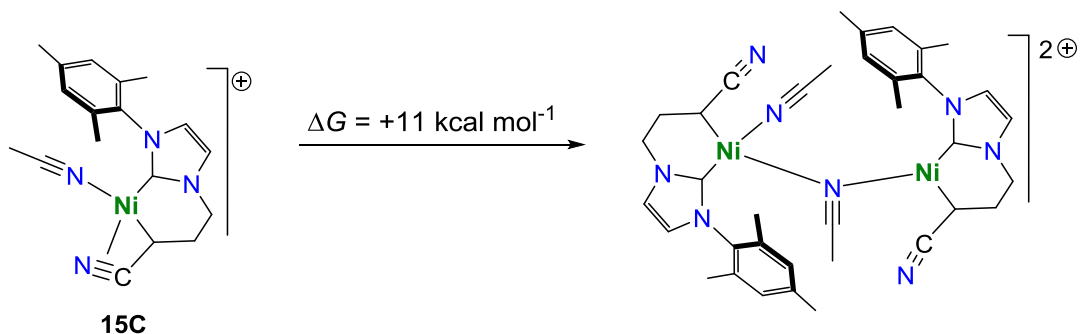


Figure 24. Walsh diagram for a d -block d^6 ML_3 complex upon bending of one L-M-L angle. Notice how the larger HOMO-LUMO gap is found for the T-shaped geometry. Adapted from ref¹⁹².

At this point we decided to probe the energetic feasibility of a multimetallic species by DFT calculations. The most stable dimeric structure optimized is that of a doubly charged cation with a “naked” nickelacycle and one nickelacycle bearing one end-on MeCN linked together by a bridging μ^2, η^1, η^1 -acetonitrile ligand bound exclusively at the nitrogen atom. However, the high energy cost vis-à-vis the monomeric cation **15C** (+11 kcal mol⁻¹) lead us to consider multimetallic arrangements very unlikely (Scheme 42).

These results show that the loss of an acetonitrile ligand is thermodynamically feasible, even if endothermic. The reaction profile from **15A** to **15C** was traced (Figure 26). From **15A** a transition state (**TS**) could be found at a cost of 14 kcal mol⁻¹ corresponding to the ejection of acetonitrile at a $d(\text{Ni-N}) = 3.80 \text{ \AA}$ by the dangling nitrile that now takes the fourth coordination position. An intermediate (**INT**) was found just 1 kcal mol⁻¹ lower in energy as acetonitrile distanced itself from the molecule; $d(\text{Ni-N}) = 4.676 \text{ \AA}$. The latter would eventually lead to the 6 kcal mol⁻¹ more stable **15C**. Hence these results show that the actual barrier for acetonitrile extrusion is double the enthalpic balance (Figure 26). It remains however feasible considering the conditions under which the product is isolated; heat and vacuum for 24-48 h.



Scheme 42. Gibbs energy balance of the dimerization of **15C**.

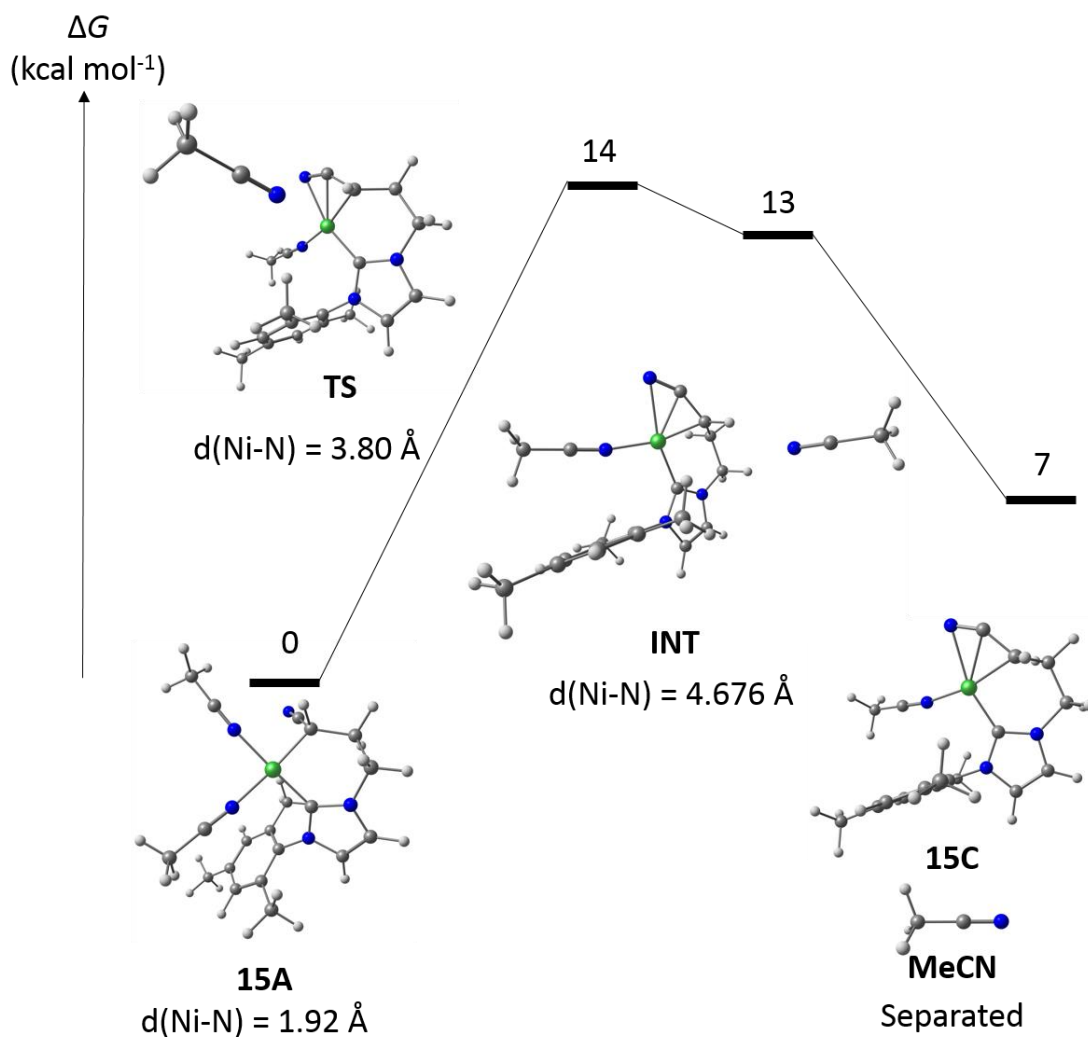


Figure 25. Gibbs energy profile and optimized structures of relevant species for acetonitrile extrusion. Distances given for the Ni-N of the leaving MeCN. Gibbs energy of **15C** and **MeCN** the sum of independent calculations. Color code: white – hydrogen, grey – carbon, blue – nitrogen, green – nickel.

These DFT results are thus consistent with the isolation of monomeric a T-shaped 14 valence electron complex in the case of **13** but an ambiguity exists for **15** for which this

structure is isoenergetic with the one side-on bound to the dangling nitrile. Looking to experimentally validate our analysis of the DFT calculations we decided to compare the IR (ATR) spectra of **13** and **15** with calculated vibrational frequencies (without anharmonic corrections) of **13A-C** and **15A-C**. In the case of **15** (Figure 26) there is a poor agreement between the IR spectra and the calculated spectra of **15C** (red), for which two distinct bands are calculated; the one corresponding to the side-on coordinated nitrile (at a lower frequency) being absent from the IR spectra. A very good agreement is found however with the calculated spectrum of **15B** (purple), with the small shoulder at the base of the peak (2195 cm⁻¹) being attributed to the nickelacyclic nitrile.

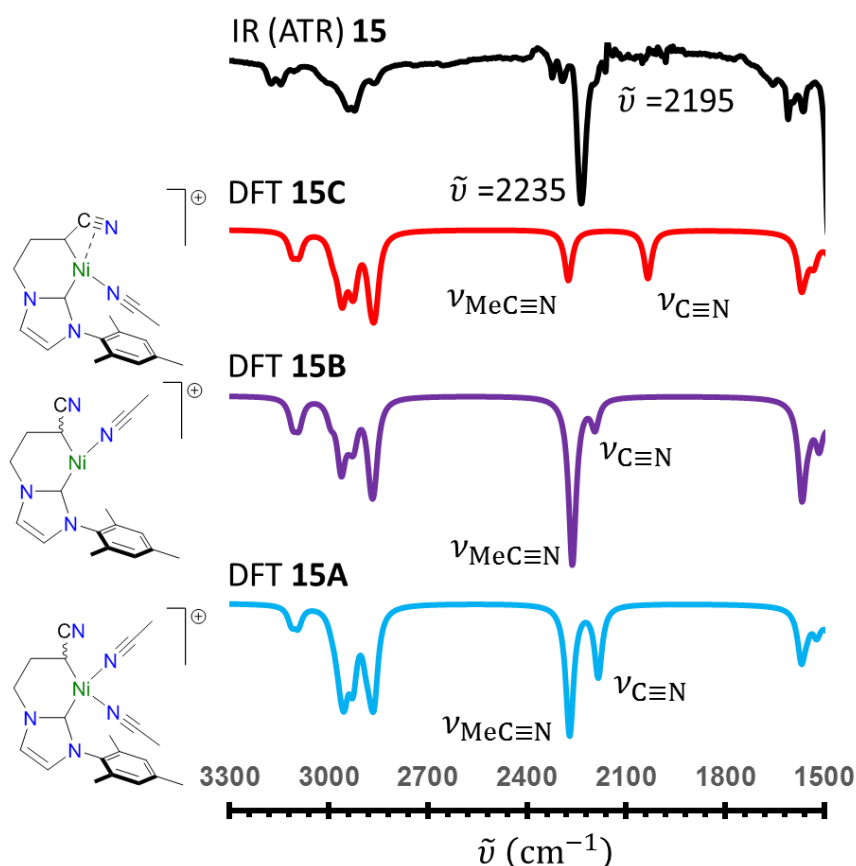


Figure 26. Detail of experimental IR (ATR) spectra of **15** (black), DFT calculated vibrational frequencies of **15A** (blue), **15B** (purple) and **15C** (red).

Comparing with the calculated spectrum for **15A** (blue) we would expect a strengthening of this shoulder, but although this is a better match than **15C** it has been experimentally verified not to be a correct description of these complexes in the solid state. Interestingly, these calculations afford an explanation of the broad profile of the $\nu(\text{C}\equiv\text{N})$ band in **13-16** as combination of vibrational modes pertaining to both nitrile functions of the complexes (coordinated acetonitrile and dangling nitrile) and suggested that the higher intensity band corresponded to the acetonitrile moiety, while the shoulder at circa 2200 cm⁻¹

originates from the dangling nitrile's $\nu(\text{C}\equiv\text{N})$. The same behavior was observed for the comparison between **13** and **13A-C** (Figure S3, Annex), and given that the IR (ATR) spectroscopic profile is similar for all complexes **13-16**, we can infer that the behavior is similar for all these complexes.

As a final consideration we re-analyzed the 400-800 cm^{-1} region of the IR (ATR) spectra of **13-16** for bands attributable to coordination of by the PF_6^- counter anion.^{193–196} However, no bands could be distinctively attributed to such an interaction.

This combined experimental and theoretical characterization approach allows us to assign the structure of these complexes as most probably adopting a T-shaped geometry. A consequence follows that these molecules count formally 14 valence electrons. Examples of such unsaturated Ni(II) are rare,^{197–204} and of this small pool, many have been found to be intermediates in organic transformations^{197,201–203} in which such species are theoretically predicted to intervene (Figure 28).²⁰⁵

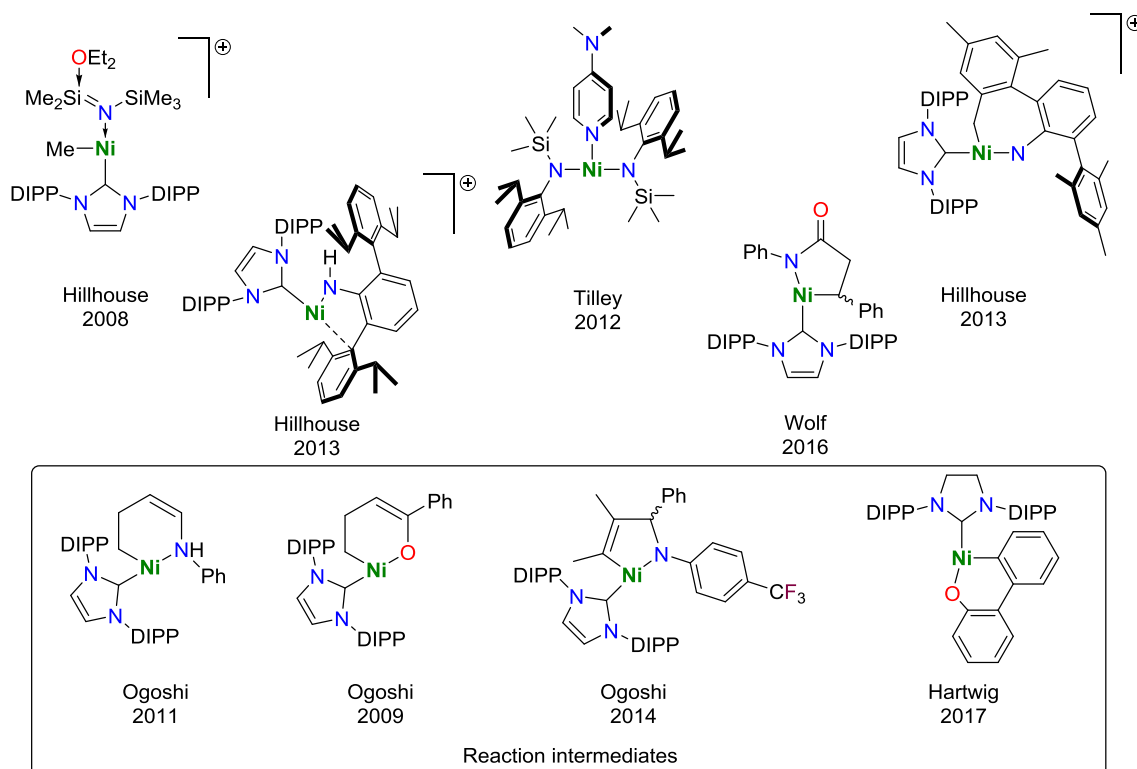


Figure 27. Structures depicting T-shaped nickel(II) complexes/cations characterized by X-ray diffraction studies. In the lower box are the complexes found as intermediates in Ni-NHC catalyzed reactions.

A few trends are apparent despite the small sample size: the near ubiquitous presence of a bulky NHC ligand (NHC-DIPP₂), of a second nickel–carbon bond, and the fact that the metal is most often in a nickelacyclic arrangement and is bound to one heteroatom (N or O) that is part of the metallacycle. Complexes **13-16** are as such even more exceptional as they allow

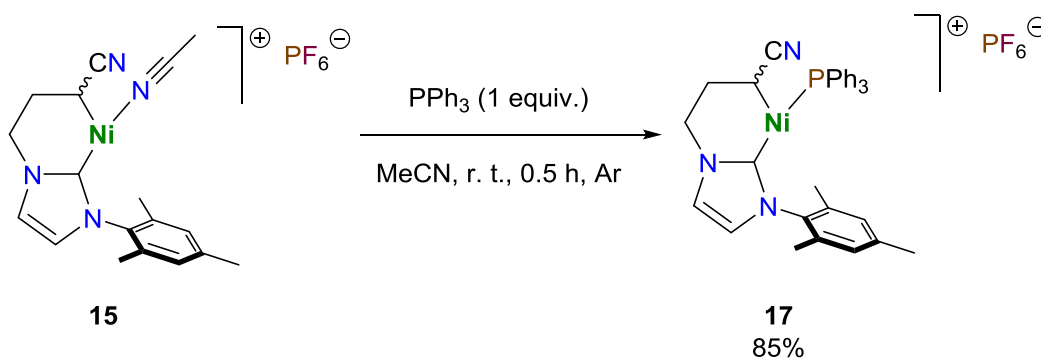
for much less sterically shielding NHCs, and the nickel atom is bound by two carbon atoms in the nickelacycle.

II.5. Reactivity of cationic $\kappa^2\text{-C}_{\text{NHC}}, \text{C}_{\text{alkyl}}$ nickelacycles

II.5.1. Ligand substitution

II.5.1.A. With phosphines

A first study of the reactivity of these complexes targeted their behavior towards substitution of the labile acetonitrile ligand. Phosphines are a well-known class of neutral two-electron donors, as mentioned in Chapter 1, that should easily displace acetonitrile. Mixing complex **15** and 1 equiv. of PPh_3 in acetonitrile gave an orange solution that yielded an orange powder (**17**) in 85% isolated yield after filtration and solvent removal (Scheme 43). Analysis by ^1H NMR in $\text{MeCN-}d_3$ confirmed the presence of PPh_3 by the appearance of signals integrating for circa 15 protons attributable to its aromatic protons. At the same time, restricted rotation of the *N*-aryl substituent is still observed but methylene signals remained non-equivalent. In samples containing residual MeCN solvent this was observed in the ^1H NMR spectra at the chemical shift characteristic of free MeCN. This allowed us to tentatively identify **17** as the expected substitution product.



Scheme 43. Proposed ligand substitution of MeCN for PPh_3 .

However, in the ^{31}P $\{^1\text{H}\}$ NMR spectrum of **17**, the ligated phosphorus nucleus could only be tentatively assigned to a very broad low intensity signal around 5 ppm (the signal for the PF_6^- anion being clearly visible, at -144.36 ppm). As a consequence, increasing amounts of PPh_3 were added to the NMR tube (Figure 28). The weak signal observed for **17** suffered an upfield shift nearing the chemical shift of free PPh_3 (**A-D**), along with an increase in

sharpness and intensity. This averaging of the signal with excess phosphine points to a regime of chemical equilibrium with the solvent in solution.

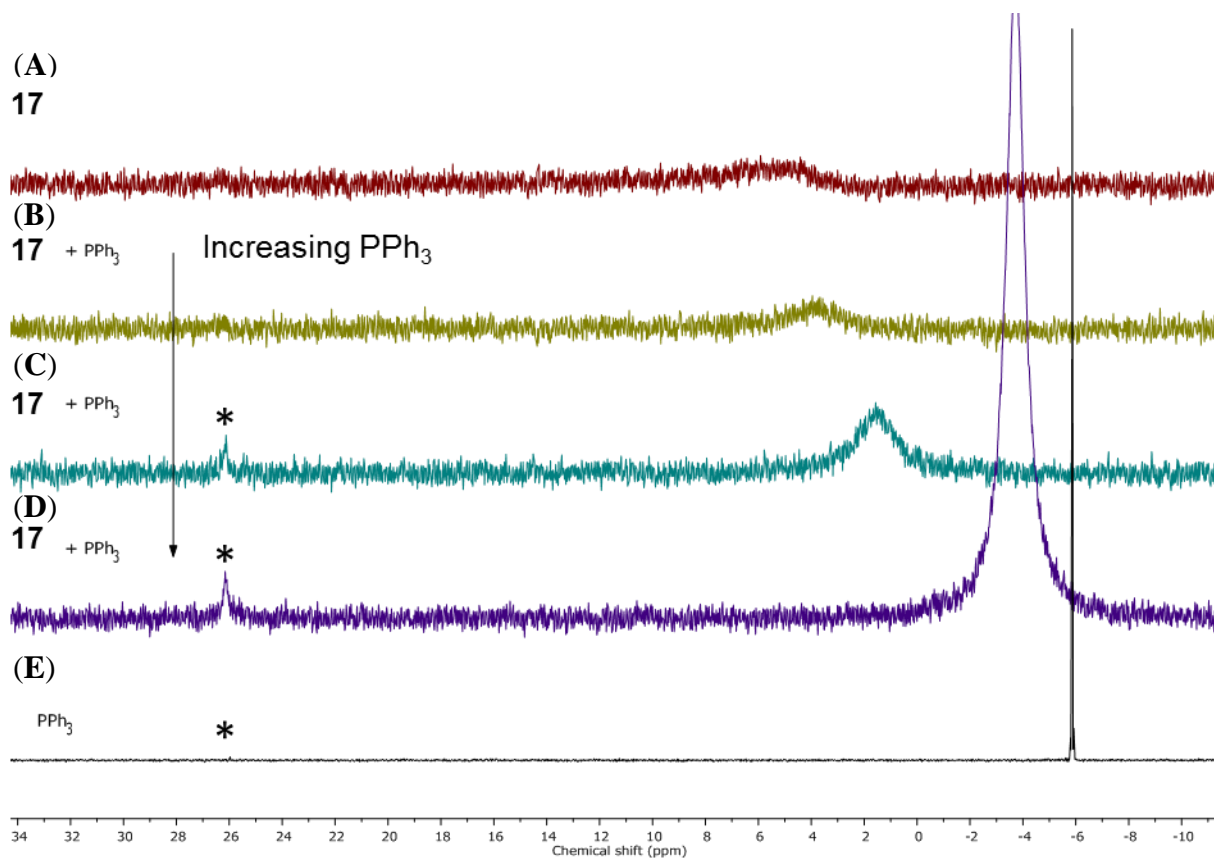


Figure 28. Effect of addition (**B** → **D**) of PPh₃ (**E**) to the ³¹P {¹H} (161.97 MHz) NMR spectrum of a solution of **17** (**A**) in MeCN-*d*₃. A peak (*) attributed to free (O)PPh₃ appears at circa 26 ppm.²⁰⁶

This came as a surprise as phosphine ligands are make stronger M–L bonds than acetonitrile and should thus substitute it easily. To attempt to rationalize these observations the following was put forward: PPh₃ does not form a strong enough M–P bond to sufficiently stabilize the metal center and its large steric bulk hinders the possibility of a mixed NCMe + PPh₃ species (similar to the proposed mixed pyridine/acetonitrile species for **13**, Scheme 41) in solution.

Assuming this equilibrium to be strongly influenced by the steric footprint of PPh₃ we envisioned a smaller alkyl phosphine would be less prone to exchange with MeCN in solution. Thus, PMe₃ was envisioned as a suitable replacement, with an additional advantage of being a stronger ligand that would be less prone to isomerization (Figure 29).^{207,208}

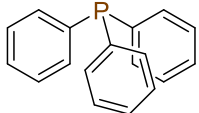
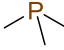
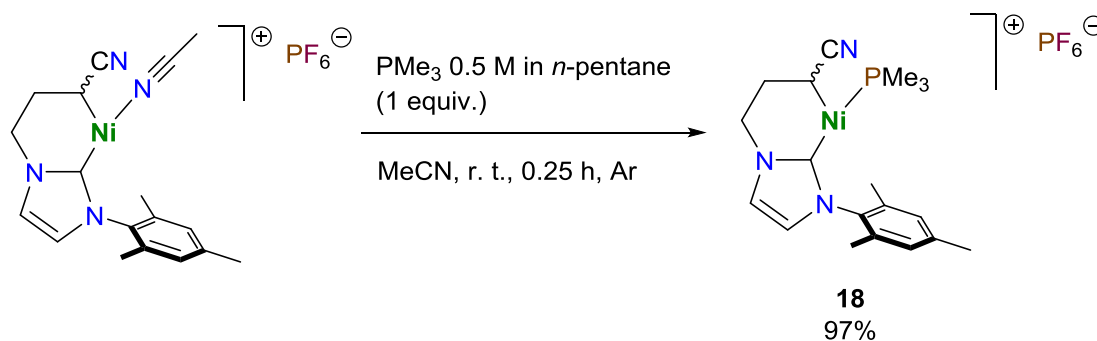
			
Tolman electronic parameter (cm ⁻¹)	2068.9	2064.1	◆ Stronger ligand
Minimum cone angle (°)	145	114	♣ Less steric hindrance

Figure 29. Electronic and steric factors between PPh₃ and PMe₃.

To an acetonitrile solution of **15**, a 0.5 M solution of PMe₃ in *n*-pentane (1 equiv.) was added dropwise to give an orange-red solution, that was then evaporated, washed with *n*-pentane and dried under vacuum to give an orange powder in near quantitative yield. Methyl substituents of the phosphine ligand were clearly identified as a broad singlet at 1.27 ppm integrating for 9 protons, in ¹H NMR spectrum (MeCN-*d*₃) therefore allowing us to tentatively identify the new compound as the expected substitution product **18** (Scheme 44).

Scheme 44. Ligand substitution of MeCN with PMe₃.

In agreement, in the ¹³C {¹H} NMR of this compound a small, broad peak can be attributed to the PMe₃ ligand (11.8 ppm). This contrasts however with the reported trend for nickel(II) ligated PMe₃ to appear as a sharp doublet instead.²⁰⁹ Furthermore, all three aliphatic carbon atoms of the metallacycle are unusually small and broad, and the Ni-bound C_{alkyl} peak in particular is almost unobservable (at -3.4 ppm). On the ³¹P {¹H} spectrum a small, broad but clearly observable peak was found at -11.9 ppm.

With all three nuclei analyzed showing broad peaks typical of dynamic systems we carried out a set of variable temperature NMR experiments. We began by analyzing the ¹H NMR spectra region associated with the PMe₃ ligand (Figure 30). At low temperatures (-40 to 0 °C) a large well-defined doublet is observed in the 1.15-1.25 ppm (¹H) region, with a phosphorus-hydrogen coupling constant of ²J_{P-H} = 9.6 Hz. However, integration of this signal is deficient of about two protons. Both neighboring signals in the downfield vicinity (1.57 and 1.39 ppm at -40 °C) correspond to the β-*N*-methylene position and are much sharper at low temperatures (< 0 °C). The most deshielded of these over-integrates by 2 protons, suggesting

overlap with the unaccounted *P*-methyl signals. Heating to temperatures above 0 °C leads to the collapse of the doublet into a singlet and a continuous broadening of all three signals that progressively converge together.

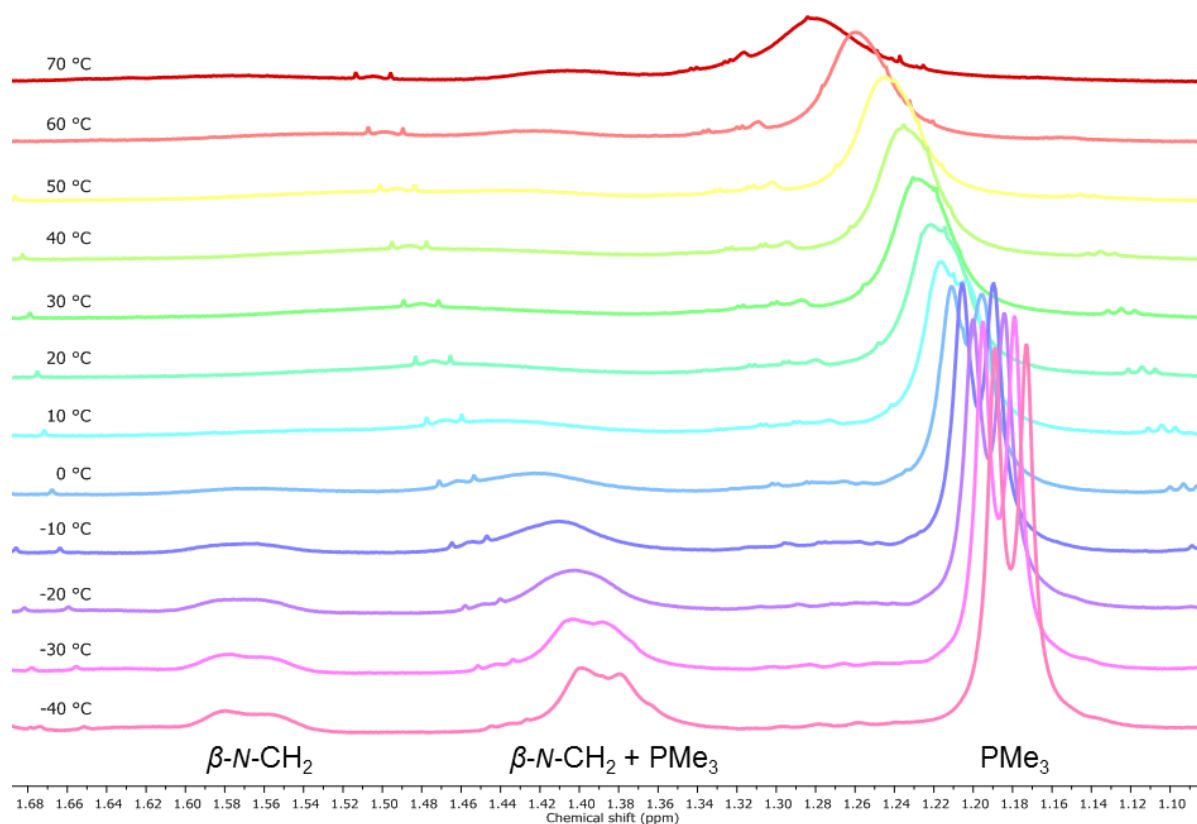


Figure 30. Variable temperature ^1H (600.13 MHz) NMR analysis of **18** in $\text{MeCN-}d_3$, detail 1.0 to 1.7 ppm region.

The analysis of the ^{31}P nucleus under the same conditions shows a mirror effect (Figure 32). At -40 °C two clear signals appear at -10.0 and -15.1 ppm, with the first being much more intense than the second one. Heating causes both peaks to move to lower chemical shifts together with the broadening of the major peak and the disappearance of the second. The minor peak disappears at -10 °C while the major peak is weak but still observable at 70 °C. Unlike with PPh_3 (Figure 28), the small peak does not correspond to the oxide $(\text{O})\text{PMe}_3$ (36 ppm).²⁰⁶

The analysis of both the ^1H and ^{31}P $\{^1\text{H}\}$ NMR spectra suggest a splitting of the PMe_3 signals. To test this hypothesis a ^1H - ^{31}P HMQC heteronuclear correlation experiment was carried out (Figure 32). The major and minor peaks correlate amongst themselves as was expected, allowing us to attribute the two unassigned protons that appear at the same chemical shift, at -40 °C, as one β -*N*-methylene proton and two protons of the PMe_3 moiety. A

complementary NOESY experiment (at -10 °C) confirmed the exchange between these peaks (Figure 33).

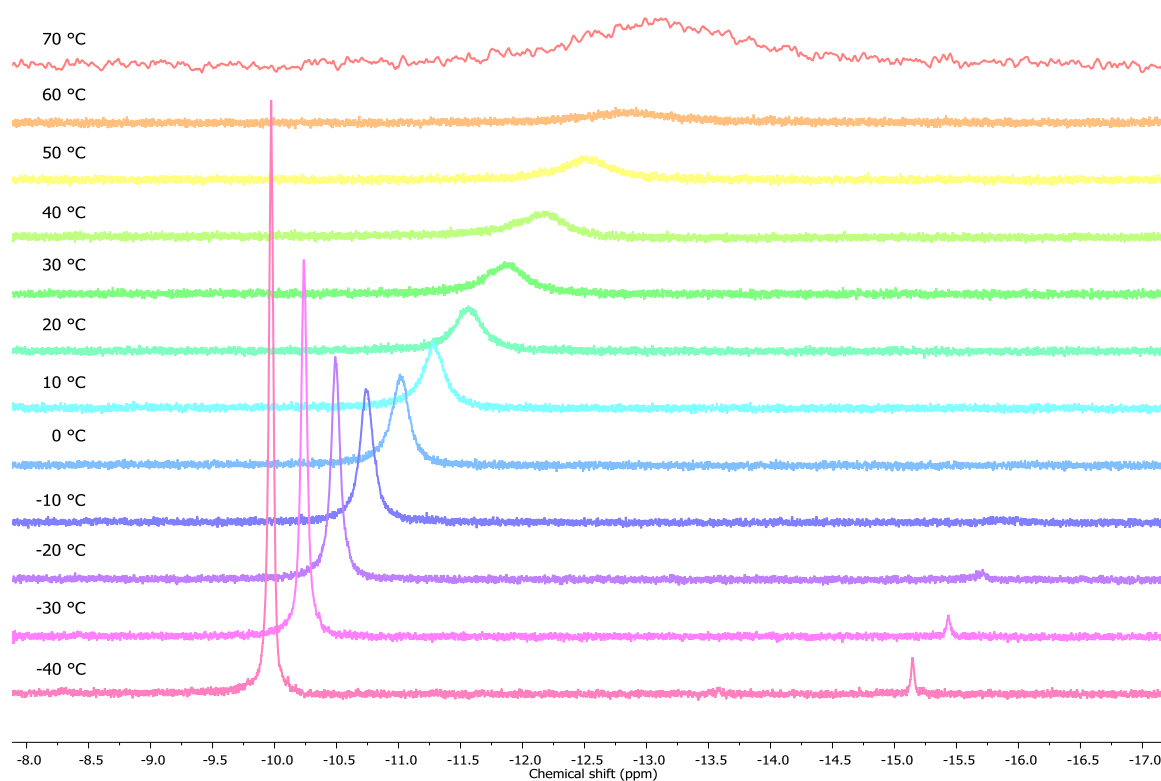


Figure 31. Variable temperature ³¹P {¹H} (242.92 MHz) NMR analysis of **18** in MeCN-*d*₃, detail -8.0 to -17.0 ppm region.

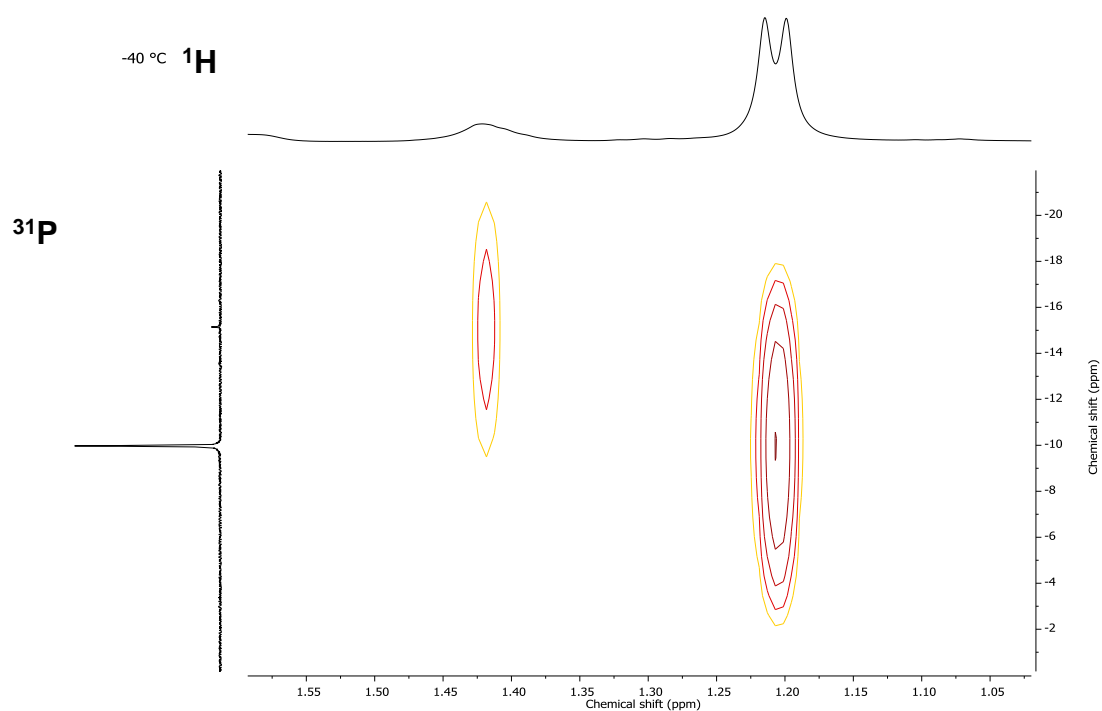


Figure 32. Heteronuclear NMR signal correlation – ¹H-³¹P HMQC of **18** in MeCN-*d*₃ at -40 °C.

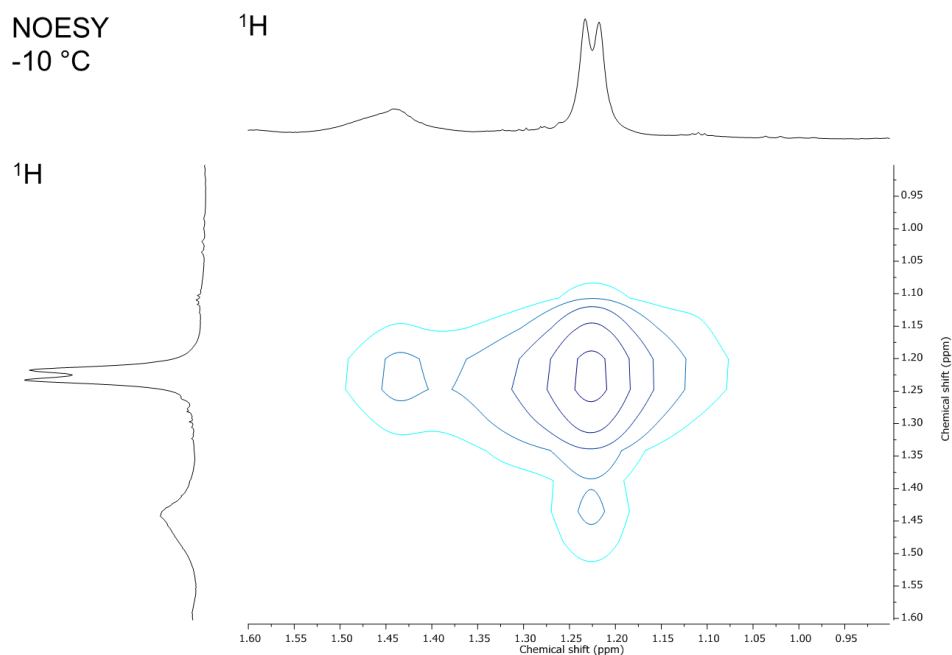


Figure 33. NOESY correlation in **18** in MeCN-*d*₃ at -10 °C.

Other temperature dependent effects were observed for the remaining signals. Aryl *m*-H signals at low temperatures are closer (Figure 34). Upon heating they move in opposite directions, overlapping as a single peak at 0 °C and splitting into independent peaks again at 10 °C. The α -*N*-methylene is well resolved as two diastereotopic signals at low temperatures, coalescing at 20 °C. The minor peaks nearby the *m*-H signals are attributed to conformers (vide infra).

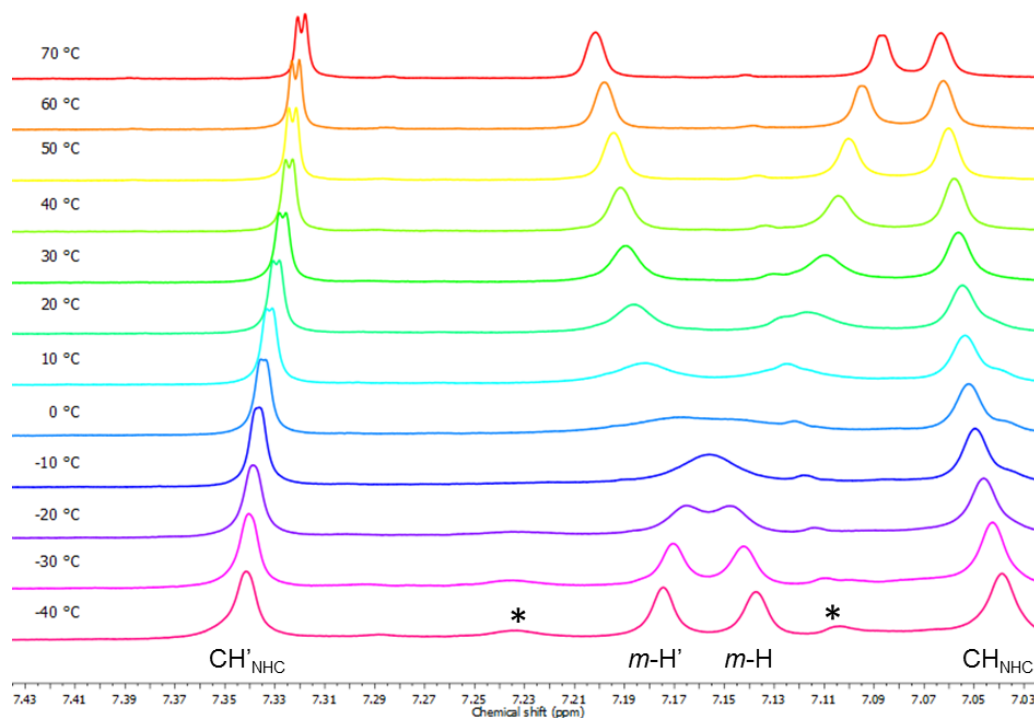
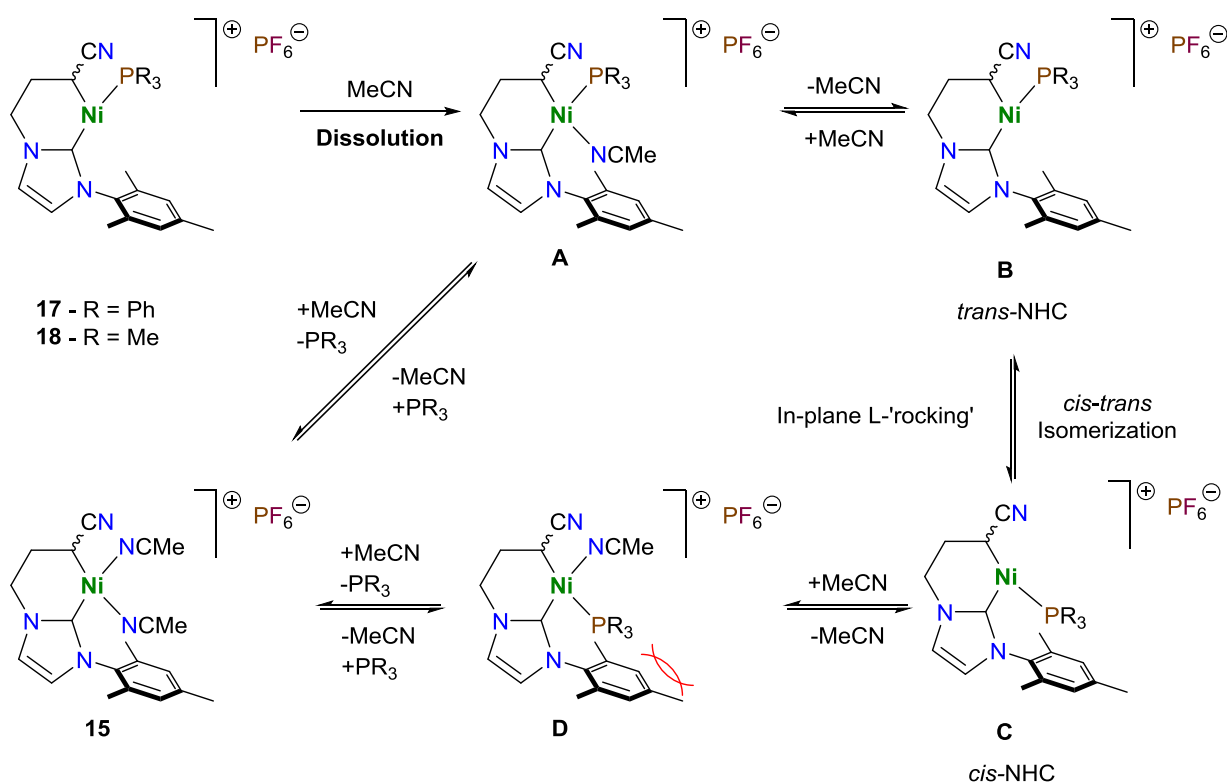


Figure 34. Variable temperature ¹H (600.13 MHz) NMR analysis of **18** in MeCN-*d*₃, detail 7.00 to 7.40 ppm region.

Considering the dynamic behavior in solution (MeCN) observed in both phosphine-substituted complexes **17** and **18** by NMR spectroscopy, we propose the existence of several isomers in equilibrium (Scheme 45). Upon dissolution of a sample of either phosphine complex **17** or **18** in MeCN a solvent molecule fills the cation's coordination sphere and a mixed N,P square planar 16 valence electron species **A** is formed. This species **A** exists then in equilibrium with the bis-acetonitrile complex **15** formed by substitution of the phosphine with a second solvent molecule. Alternatively, the labile MeCN ligand of **A** can dissociate to free the unsaturated T-shaped structure **B** in solution. Given the low steric demands of the T-shaped structure, the phosphine ligand positioned *trans*-NHC in **B**, can by an in-plane ligand-migration isomerize to a *cis*-NHC position, and give isomer **C**. Association of a solvent molecule to **C** gives another N,P mixed square planar species, **D**. In **D**, as in **C**, the phosphine ligand is both positioned *trans*- to the alkyl ligand, which is less capable of backdonation than the NHC ligand and *cis*- to the NHC ligand, making it and the *N*-Mes substituent spatially close. **D** can then either regenerate **C** or extrude the phosphine ligand to give **15**. Although not depicted in Scheme 44, the passages of **A** and **D** to **15** can take place by an intermediate mono-acetonitrile species, like that found for the solid state of complexes **13-16**.



Scheme 45. Chemical equilibrium in solution (MeCN) displaces the phosphine ligand.

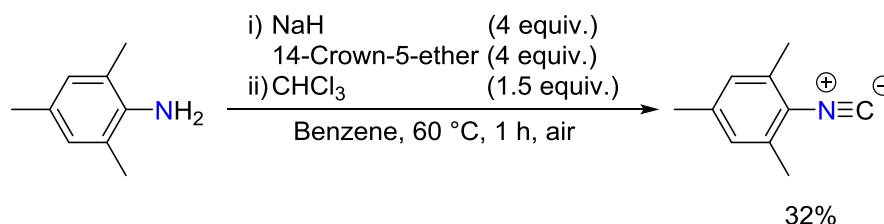
This series of chemical equilibria which place the metal bound atoms in different electronic environments can justify the weak and broad signals observed for these atoms in ¹³C and ³¹P NMR spectroscopy at r. t. This game of chemical equilibria outlined above is expected to be commanded by the phosphine ligands' electron-donor ability and steric footprint, with the stronger donor stabilizing the intermediate **A** and a smaller steric bulk stabilizing intermediate **D**. As such, when PPh₃ is used (complex **17**) the equilibrium is expected to be rapid as both key 16 valence electron intermediates **A** and **D** are destabilized. In the case of the former by the relative weakness of the M–PPh₃ bond and in the case of the latter by the steric bulk of its phenyl substituents. Indeed, this is consistent with the difficulty in observing the phosphorus nuclei's signal on ³¹P NMR and excess exogenous PPh₃ appearing as an average signal that tended to the chemical shift of free PPh₃ with increasing concentration of the latter. On the other hand, when PMe₃ is used, the reverse happens: intermediate **A** is stabilized by its strong M–P bond and intermediate **B** by the smaller steric impact of its Me groups. This allows us to propose that the two phosphorus-ligated species observed in the NMR spectroscopic analysis of **18** belong to the respective forms of intermediate **A** (major) and **D** (minor).

It is interesting to interpret the atypical ¹³C {¹H} NMR spectra of complex **13** in pyridine-*d*₅ in light of the equilibria proposed above for the phosphine bearing complexes **17** and **18**. The acetonitrile ligand that remains Ni-bound can take the same role as the phosphine ligands and undergo a rapid in-plane *cis-trans* isomerization to give the corresponding intermediate forms **A** and **D**. Although this can furnish an explanation for the low intensity and broadness of these carbon signals in the ¹³C {¹H} NMR spectra of complex **13**, it offers no insight on why the pyridine ligands fail to replace the acetonitrile ligand.

Unfortunately, phosphine ligated **17** and **18** showed the same limited solubility as **13-16** and an additional heightened sensitivity to oxygen and temperature. Thus, satisfactory elemental analyses of the complex were impossible to obtain. Moreover as noted before, thorough drying of complexes **13-18** requires drying for 1-2 days under high vacuum at 40 °C. However, when applied to **17** or **18** phosphine derivative, heating leads to the appearance of peaks both in ¹H and ³¹P NMR corresponding to the degradation of the complex. Adding to this, HRMS-ESI of a solution of **18** in MeCN reveals a molecular ionic peak *m/z* = 386.1293 matching the expected cation [Ni^{II}{Mes-NHC-(CH₂)₂CH(CN)}(PMe₃)]⁺ (*m/z* = 386.1296), but this peak is a third the intensity of the main molecular ion peak at *m/z* = 351.1109 which corresponds to [Ni^{II}{Mes-NHC-(CH₂)₂CH(CN)}(MeCN)]⁺ (*m/z* = 351.1120). Assuming that no PMe₃ is lost to the solvent, this result heightens the sensibility of these neutral ligands to dissociate in the conditions of the analysis.

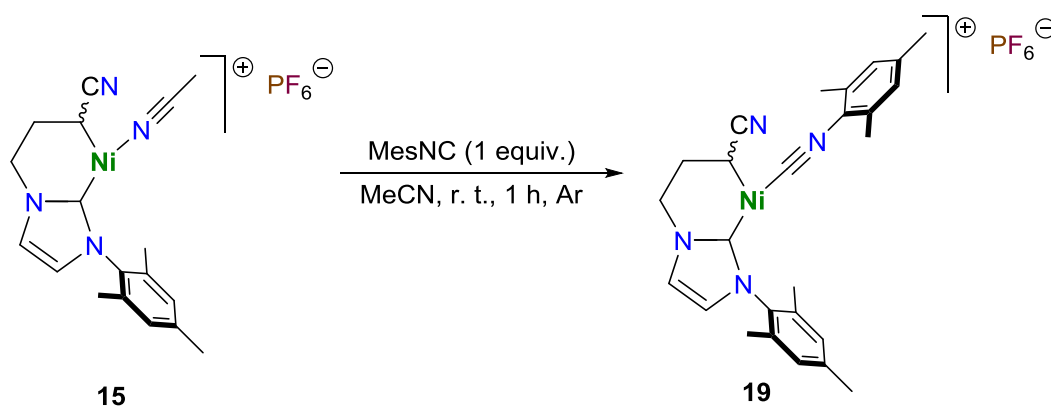
II.5.1.B. Other substitution reactions

This set back led us to consider using an isonitrile ligand. Being both σ - and π -electron-donating and π -accepting, they could help to stabilize an electron poor nickel cation. To this purpose, mesitylisonitrile was synthesized²¹⁰ in a low yield (Scheme 46).



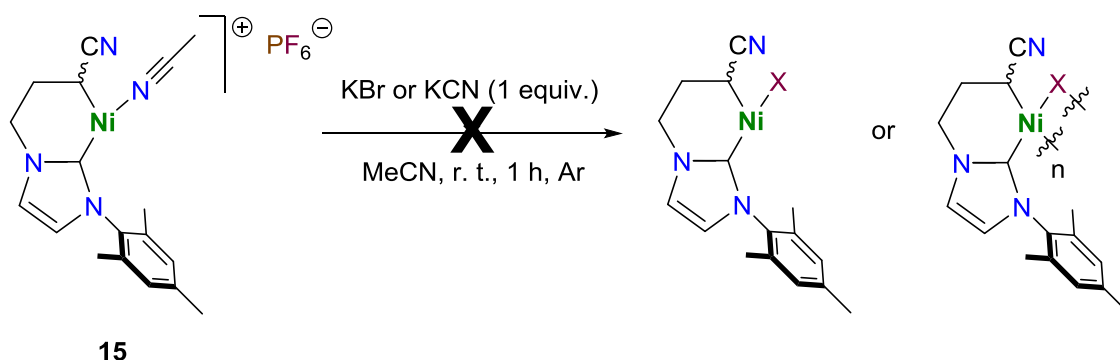
Scheme 46. Synthesis of mesitylisonitrile.

Substitution attempts with the isonitrile gave a brown solid (Scheme 47). IR (ATR) analysis showed both a band at 2230 cm^{-1} attributed a nitrile $\nu(\text{C}\equiv\text{N})$ and a stronger band at 2176 cm^{-1} attributed to the isonitrile $\nu\text{N}\equiv\text{C}$ stretch and blue shifted by 60 cm^{-1} with regards to the free isonitrile. While the observation of a shift in the $\nu\text{N}\equiv\text{C}$ stretch suggested coordination and formation of the expected product **19**, this could never be confirmed by ^1H NMR. Thus, ^1H NMR spectra never accounted for the new ligand and showed some degree of decomposition. Thus, signals clearly attributable to *m*-H signals of the isonitrile were missing and integration of the aromatic signals failed to account for these. The same case was observed for the *p*-Me and *o*-Me groups of the isonitrile ligand. Finally, the product showed the same solubility issues as the parent complex, but less stability in solution, hindering its purification.



Scheme 47. Proposed reaction for acetonitrile substitution by mesitylisonitrile.

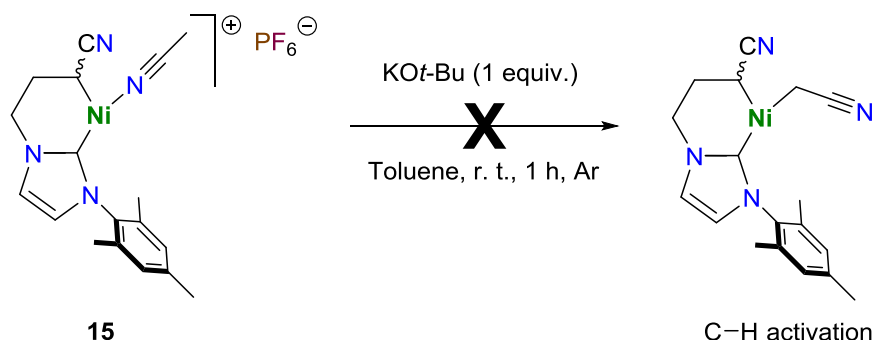
On a final note, inspired by the findings of oligomeric structures with complexes showing the same issues of exchange with solvent KCN and KBr were also tested this time as monodentate anionic trapping agents, but no reaction took place (Scheme 48).^{153,154}



Scheme 48. Failed reactions to synthesize oligo- polymeric bridging complexes.

II.5.2. With strong bases

Consistently frustrated by the crystallization issues presented by these cationic complexes, we envisioned that the MeCN ligands of these Ni(II)-NHC species again be available for C–H activation. As such **15** was treated with KO t -Bu in toluene to give a brown solid upon filtration and isolation (Scheme 49). Upon initial analysis of the ¹H NMR spectrum of the product it seemed possible that C–H activation had occurred, as marked by the appearance of two new nickelacycles concomitantly with two new signals at -5.34 and -5.60 ppm, whose chemical shifts could account for the formation of the expected cyanomethyl ligands ([Ni^{II}(CH₂CN)(Cp)(NHC-Mes₂)] (δ (H α -CN) = -0.02 ppm; CDCl₃).¹²⁷ The relative integration of these signals was however not consistent with the proposed formulation, as they integrated for 1 proton instead of the expected 2 of a methylene signal



Scheme 49. Supposed product of the reaction between **15** and KO t -Bu: post-functionalization by C–H activation product.

Fortunately, crystals suitable for X-ray diffraction of this solid could be grown by layering of a dichloromethane solution with *n*-hexane (1/3 ratio) and allowing it to sit overnight at -28 °C. Analysis of these crystals revealed the true nature of the reaction product as a dimer held by bridging hydroxo ligands in a [Ni(μ -OH)]₂ core **20** (Figure 35). The space group is chiral and two enantiomers (*RS* and *SR*) are present in the crystals. Hence, the observation of two metallacycles by ¹H NMR is explained by the existence of two pairs of enantiomers: *RR*- and *SS*-**20**, and *RS*- and *SR*-**20**. Full crystallographic details can be found in the Experimental section.

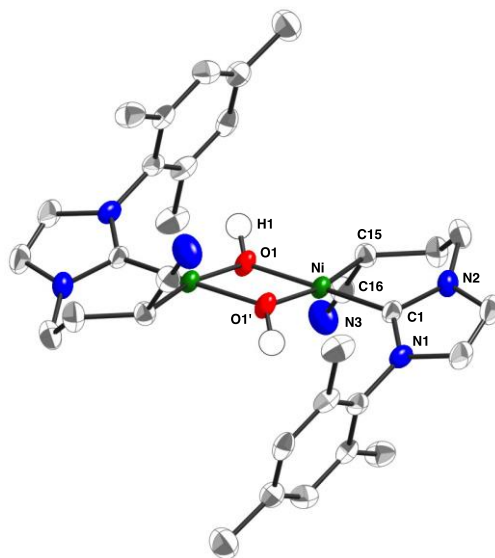
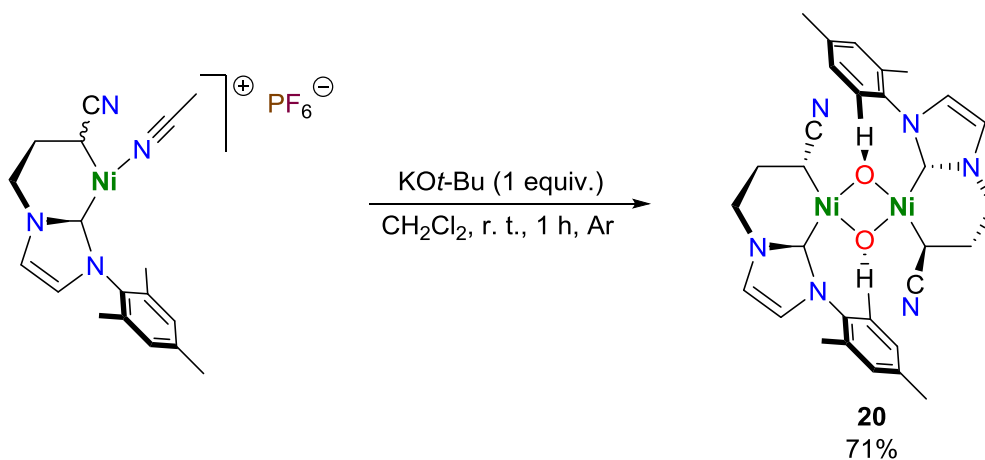


Figure 35. Molecular structure of **20**. The only hydrogen atoms shown are those of the hydroxyl groups (as white isotropic spheres). Ellipsoids are shown at the 50% probability level, and key atoms are labeled. The space group ($P2_1/c$) is centrosymmetric and contains both enantiomers; only one enantiomer (*RS*) is shown. Selected distances (Å) and angles (°) with esds's in parenthesis: Ni–C1, 1.855(4); Ni–C15, 1.936(4); Ni–O1, 1.906(3); Ni–O1', 1.898(3); C15–C16, 1.455(7); C16–N3, 1.143(6); C1–Ni–C15, 93.3(2); O1–Ni–C15, 90.16(16); O1–Ni–O1', 80.30(13); O1'–Ni–C1, 96.17(16); C15–C16–N3, 178.6(5); Ni–C15–C16, 105.0(3).

The complex belongs to the centrosymmetric $P2_1/c$ symmetry group and crystallized as two enantiomers. Analysis of the structural features show values well within those found in the literature for [Ni(μ -OH)]₂ complexes.^{211–225} Both nickel atoms are in slightly deformed square planar environments, owing to the bite angle of the [Ni(μ -OH)]₂ rhombus (O–Ni–O = 80 °). Both nickel planes are also co-planar. The distance between the two nickel atoms is 2.908 Å and considered too distant for metal-metal bonding. Overall the structural parameters of the metallacycle are essentially the same as in monometallic **13**¹²⁸ and [Ni^{II}(acac){Mes-NHC-(CH₂)₂CH(CN)}]¹³¹ showing the structure's insensitivity to the nature of its anionic ligands. Interestingly, the hydroxide ligands point towards the mesityl groups.

The values of -5.34 and -5.60 ppm for the hydroxyl protons in ¹H NMR fall in line with those observed for such complexes. Additionally, a distinct $\nu(\text{O-H})$ band at 3628 cm⁻¹ could be measured on the bulk solid, supporting the X-ray analysis. Notably, as for **15** and [Ni^{II}(acac){Mes-NHC-(CH₂)₂CH(CN)}]¹³¹ the $\nu(\text{C}\equiv\text{N})$ is now at 2180 cm⁻¹, and the bond is elongated to $d(\text{C}\equiv\text{N}) = 1.143 \text{ \AA}$. In all three cases, the capping of the molecule with an anionic ligand leads to a noticeable influence on the nitrile bond.

This reaction posed one big question however: what is the origin of oxygen in this reaction. Mass balance would point to the alkoxide as the unlikely source of oxygen. We decided to screen reaction solvents to assess if trace oxygen or water would originate from these and be the source of oxygen. Consistently, the only identifiable reaction product was **20**, with CH₂Cl₂ giving the cleanest reactions (Scheme 50). Furthermore, trying alternative *t*-butoxides (Li, Na, K) or KHMDS as a base showed no difference, discouraging the hypothesis of the alkoxide as the oxygen source. Interestingly, the reaction did not progress with pure KOH in CH₂Cl₂. Even after thorough degassing and drying of the solvents together with subliming the bases and carrying out the reaction in a glovebox the reaction successfully took place, despite there being no expected source of oxygen. At this point we cannot determine the source of oxygen in **20**.



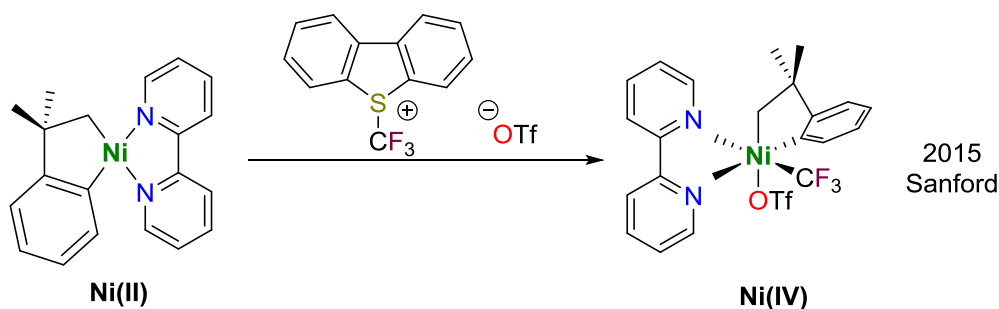
Scheme 50. Syntheses of the bis-bridging hydroxo nickel(II) dimer [Ni^{II}(μ -OH){Mes-NHC-(CH₂)₂CH(CN)}]₂ **20**. Only one enantiomer is shown.

Unfortunately, the complex proved difficult to isolate analytically pure and HRMS-ESI analysis of the complex was unsuccessful, with high fragmentation and no peak corresponding to the dimer being observable.

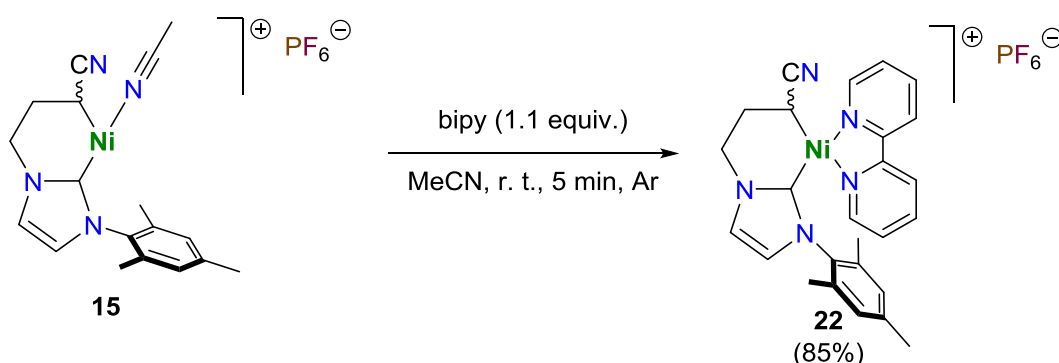
II.5.3. Redox chemistry

Upon reviewing the literature, we came across recent reports from Sanford's group where the exceedingly rare Ni(IV) oxidation state was accessed,²²⁶ in one instance by C–H activation,²²⁷ and utilized to construct new C–C and C–heteroatom bonds in organic fragments.^{228–230} Comparing the general structure of one of the Ni(II) precursors of these Ni(IV) complexes [Ni^{II}(CH₂CMe₂-*o*-C₆H₄)(bipy)],²³¹ with that of our C,C-chelates showed, that both are inserted in a metallacyclic scaffold and stabilized by neutral donors (Scheme 51).

This led us to consider that a new complex with a 2,2'-bipyridine (bipy) ligand, in lieu of the acetonitrile ligand or of the previously disclosed [Ni^{II}(acac){Mes-NHC-(CH₂)₂CH(CN)}] (**21**),¹³¹ could be a suitable platform to access high-valent Ni complexes. To this effect, we synthesized the bipy substituted complex [Ni^{II}{Mes-NHC-(CH₂)₂CH(CN)}(bipy)]PF₆ (**22**), by mixing **15** and bipy in MeCN, evaporating the residue and washing the resulting orange powder with Et₂O, to obtain the product in 85% yield (Scheme 52).



Scheme 51. Sanford's Ni(II) to Ni(IV) oxidation.

Scheme 52. Synthesis of the bipy-substituted cationic complex **22**.

Characterization of **22** the ¹H NMR (MeCN-*d*₃) shows a more complex aromatic region compared to the ¹H NMR spectrum of **15** due to the presence of the bipy ligand. The rest of the spectrum, shows no other interesting features. The IR (ATR) spectra of **22** shows a broad, weak (once again, the PF₆⁻ anion dominates the spectra) band at 2193 cm⁻¹, which we assign

as the $\nu(\text{C}\equiv\text{N})$ of the nitrile arm. Noticeably this band is red-shifted by 43 cm^{-1} , with regards to **15**, which likely accounts for the shoulder observed in the $\nu(\text{C}\equiv\text{N})$ band of the acetonitrile complexes **13-16**.

As such we decided to study **15**, **21** and **22** by cyclic voltammetry (CV), to evaluate the redox behavior of these complexes. In the CV of a solution of **15** (1 mM) in MeCN (Figure 36, **A**) a first oxidation can be seen at $E_{p,a} = 0.77\text{ V}$ vs. Fc/Fc⁺ (scan rate = 200 mV s^{-1}) that we assign to a Ni(II)/Ni(III) one-electron oxidation. A reduction, we ascribe to a Ni(II)/Ni(I) reduction can be observed at $E_{p,c} = -1.24\text{ V}$ vs. Fc/Fc⁺, (scan rate = 200 mV s^{-1}).

The voltammogram of neutral complex **21** shows a similar profile (Figure 37). A first oxidation is observed at $E_{p,a} = 0.72\text{ V}$ vs. Fc/Fc⁺ (scan rate = 200 mV s^{-1}), that we attribute to a Ni(II)/Ni(III) one-electron oxidation, suggesting that the anionic acac ligand does not significantly enrich the metal center. A second oxidation wave can then be seen at 1.04 V vs. Fc/Fc⁺ that we ascribe to oxidations centered on the acac ligand. A reduction can be faintly seen at -1.30 V vs. Fc/Fc⁺, that we attribute to a Ni(II)/Ni(I) reduction. Both proposed metal-centered electrochemical reactions are at potentials very close to those found for **15** and suggest indeed a weak effect of the acac ligand of **21** in the metal's electron-density. As for complex **21** none of the reverse half-reactions can be observed. When **21** is analyzed with varying scan rates, the same correlation between of increasing $E_{p,a}$ with increasing scan rate.

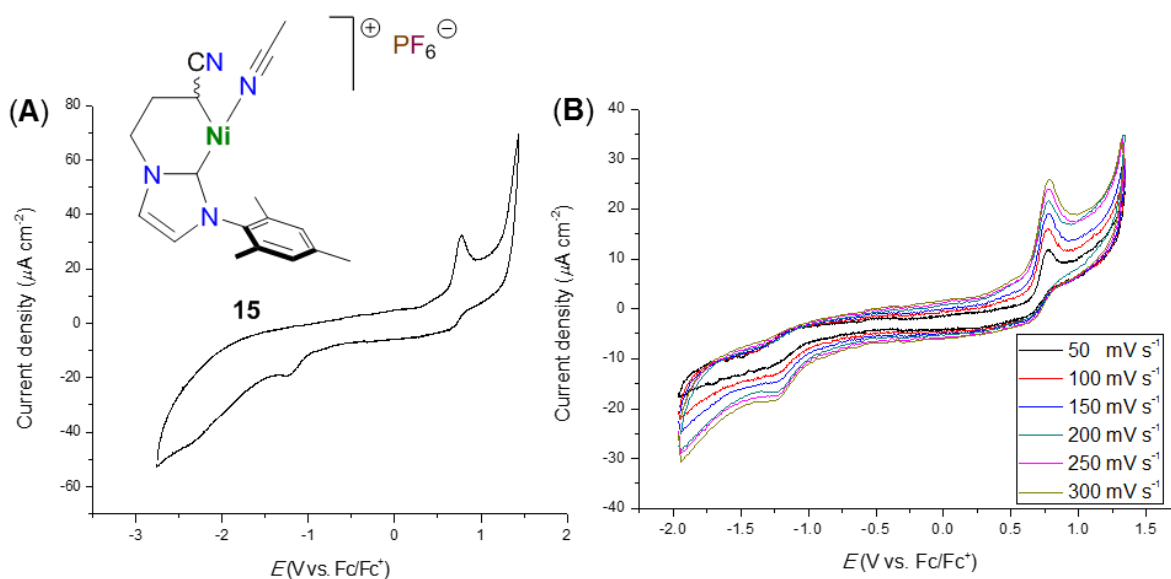


Figure 36. Cyclic voltammogram of complex **15**: 1 mM in a 0.1 M *n*-Bu₄NPF₆ solution in MeCN, using a glassy carbon working electrode, a platinum wire counter electrode and an Ag/AgCl, KCl 3 M reference electrode. **A**, scan rate = 200 mV s^{-1} ; **B**, varying scan rates of 50, 100, 150, 200, 250, 300 mV s^{-1} . Referenced to a Fc 2 mM internal standard $E = 0.46\text{ V}$ vs. Ag/AgCl, KCl 3 M.

Finally, analysis of the bipy complex **22** by CV showed a much richer electrochemical response (Figure 38). Unfortunately, this response relates to reduction reactions, and is likely

largely ligand centered. Ni(II)-bipy systems have been described exhibiting complex reductive electrochemical behavior.²³² Nonetheless, an oxidation can be seen at 0.78 V vs. Fc/Fc⁺, similarly to **15** and **21** and we attribute this oxidation to a Ni(II)/Ni(III) oxidation. This is however a much higher oxidation potential than those observed by Sanford et al., -0.61 V vs. Fc/Fc⁺ for Ni(II)/Ni(III) and 0.27 V vs. Fc/Fc⁺ for Ni(III)/Ni(IV),²²⁶ for us to expect easy access to high-valent Ni(III) or Ni(IV) with our bipy complex **22**.

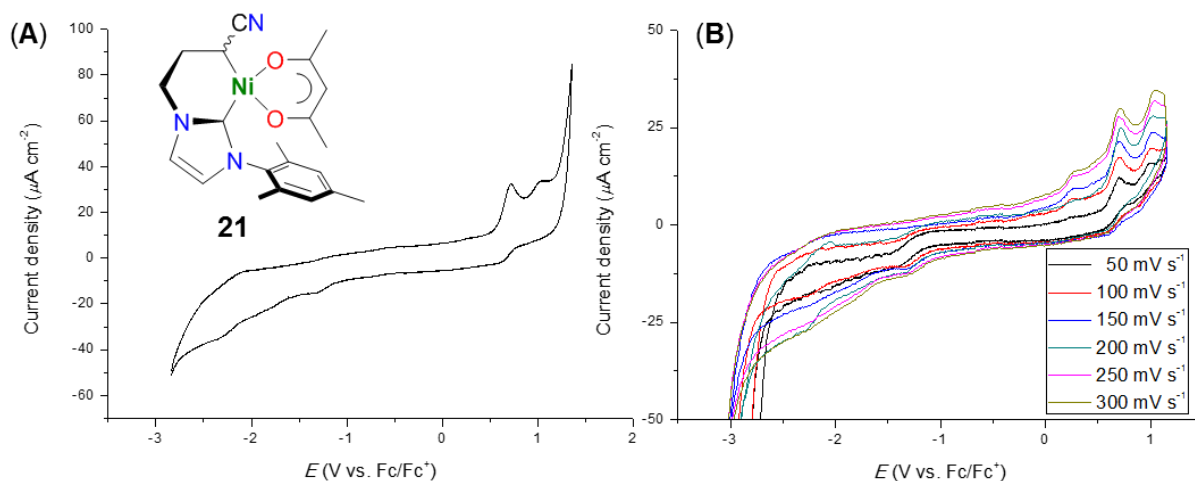


Figure 37. Cyclic voltammogram of complex **21**: 1 mM in a 0.1 M *n*-BuNPF₆ solution in MeCN, using a glassy carbon working electrode, a platinum wire counter electrode and an Ag/AgCl, KCl 3 M reference electrode. **A**, scan rate = 200 mV s⁻¹; **B**, varying scan rates of 50, 100, 150, 200, 250, 300 mV s⁻¹. Referenced to a Fc 2 mM internal standard $E = 0.46$ V vs. Ag/AgCl, KCl 3 M.

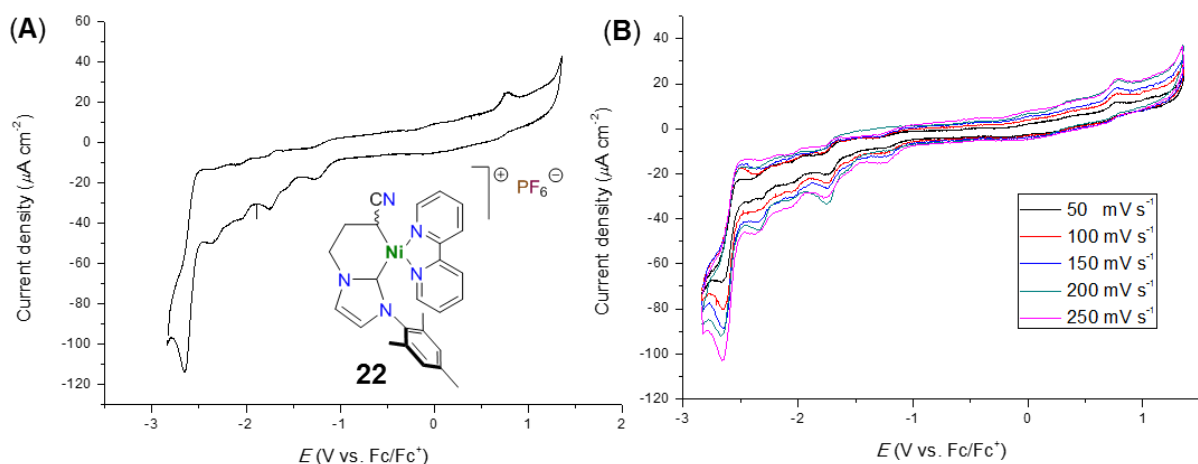


Figure 38. Cyclic voltammogram of complex **22**: 1 mM in a 0.1 M *n*-BuNPF₆ solution in MeCN, using a glassy carbon working electrode, a platinum wire counter electrode and an Ag/AgCl, KCl 3 M reference electrode. **A**, scan rate = 200 mV s⁻¹; **B**, varying scan rates of 50, 100, 150, 200, 250 mV s⁻¹. Referenced to a Fc 2 mM internal standard $E = 0.46$ V vs. Ag/AgCl, KCl 3 M.

III. Conclusions

In conclusion, four new $C_{\text{NHC}}, C_{\text{alkyl}}$ -nickel(II) cationic complexes were synthesized in a stepwise fashion: alkylnitrile imidazolium salt \rightarrow half-sandwich nickel(II)-NHC complex \rightarrow half-sandwich κ^2 - $C_{\text{NHC}}, C_{\text{alkyl}}$ -nickel(II) nickelacycle \rightarrow cationic κ^2 - $C_{\text{NHC}}, C_{\text{alkyl}}$ -nickel(II) acetonitrile adducts.

The original formula for the latter bearing two acetonitrile ligands in the solid state was corrected (^1H NMR, elemental analysis) to a formula with a single MeCN ligand. The complexes' limited solubility (nitriles, pyridine) and dynamic ligand exchange with the solvent made it impossible to grow crystals and resolve the structure by X-ray diffraction. As such a combined theoretical and spectroscopic study (DFT, IR) was carried out to reveal a T-shaped structure to be the most probable form adopted by these complexes in the solid state.

As a consequence of their structure, these are rare examples of Ni(II) 14 valence electron T-shaped complexes. In contrast with the few known complexes of this class, these complexes are stabilized in a C,C chelate and the NHC is not limited to NHC-DIPP₂.

A study of their reactivity in ligand substitution reactions showed that they retained their particular solubility and dynamic solution behavior. Detailed NMR studies of phosphine substituted derivatives in solution in MeCN allowed us to better understand the dynamic processes at play and to propose that it consists of a *cis/trans* isomerization of the monodentate ligand, via an in-plane migration, possibly combined to an exchange with the solvent.

Attempts at reacting these cationic $C_{\text{NHC}}, C_{\text{alkyl}}$ -nickel(II) with a base inadvertently led to the isolation of a binuclear hydroxide as revealed by X-ray diffraction studies.

Finally, we studied the redox behavior of a series of κ^2 - $C_{\text{NHC}}, C_{\text{alkyl}}$ -nickel(II) complexes, to test their capability to access high-valent Ni(IV) states, but our electrochemical studies showed them all too be too electron-poor and unable to undergo oxidation easily.

Chapter 3

Catalytic C–H functionalization of O,S-azoles

Chapter 3

Catalytic C–H functionalization of O,S azoles

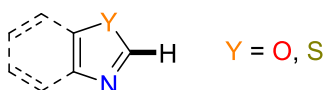
I. Introduction	115
I.1. C(2)–H/C _{sp} –X	115
I.1.1. Electrophilic coupling partners	115
I.1.1.A. X = Bromide (-Br)	115
I.1.2. Nucleophilic coupling partners	116
I.1.2.A. X = Hydrogen (-H)	116
I.2. C(2)–H/C _{sp2} –X	117
I.2.1. Electrophilic coupling partners	117
I.2.1.A. X = Halogen (-F, -Cl, -Br, -I)	117
I.2.1.B. X = Oxygen electrophiles (-OR): Triflate (-OTf), Sulfonate (-OSO ₂ R), Ester (-OCOR), Carbamate (-OCONRR'),	121
I.2.1.C. X = Carbon electrophiles	123
I.2.1.C.1. X = Carbonyl (-COOR)	123
I.2.1.C.2. X = Nitrile (-CN)	126
I.2.2. Nucleophilic coupling partners	127
I.2.2.A. X = Metalloid	127
I.2.2.A.1. X = Silanes (-Si(OR) ₃)	127
I.2.2.A.2. X = Boronic acids (-B(OH) ₂)	127
I.2.2.B. X = Hydrogen (-H)	128
I.3. C(2)–H/C _{sp3} –X	129
I.3.1. Electrophilic coupling partners	129
I.3.1.A. X = Halogen (-Br, -I)	129
I.3.1.B. X = Carbonyl (-COOR)	131
I.3.2. Nucleophilic coupling partners	131
I.3.2.A. X = Hydrazone (=N-NHR)	131
I.3.2.B. X = Hydrogen (-H)	132
I.4. Mechanistic considerations	132
I.4.1. Catalytic cycles	132
I.4.2. Breaking the C–H bond	136

I.4.3. Heterogeneous vs. homogeneous catalysis	137
I.5. Overview	138
II. Results and discussion	139
II.1. Benzothiazole C _{sp²} cross-coupling	139
II.2. Benzothiazole C _{sp³} cross-coupling	147
II.3. Conclusions	160

Chapter 3 – Catalytic C–H functionalization of O,S-azoles

I. Introduction

From the wide chemical landscape available for C–H bond functionalization, a particular class, azoles, which are five membered heterocyclic molecules bearing one nitrogen atom and at least one other heteroatom in the heterocycle,²³³ have been targeted by researchers in the last few years. This motif is broadly represented in natural products, bioactive molecules and materials chemistry. In particular, a lot of attention has been given to 1-chalcogen-3-(benzo)azoles. In this context the state of the art on nickel-catalyzed C–H cross-coupling of (benz)oxazoles and (benz)thiazoles (Scheme 53) is here presented and discussed, listed by the geometry of the coupled carbon atom (linear – C_{sp}, trigonal – C_{sp2}, tetrahedral – C_{sp3}).



Scheme 53. General structure of (benz)oxazoles (Y = O) and (benz)thiazoles (Y = S).

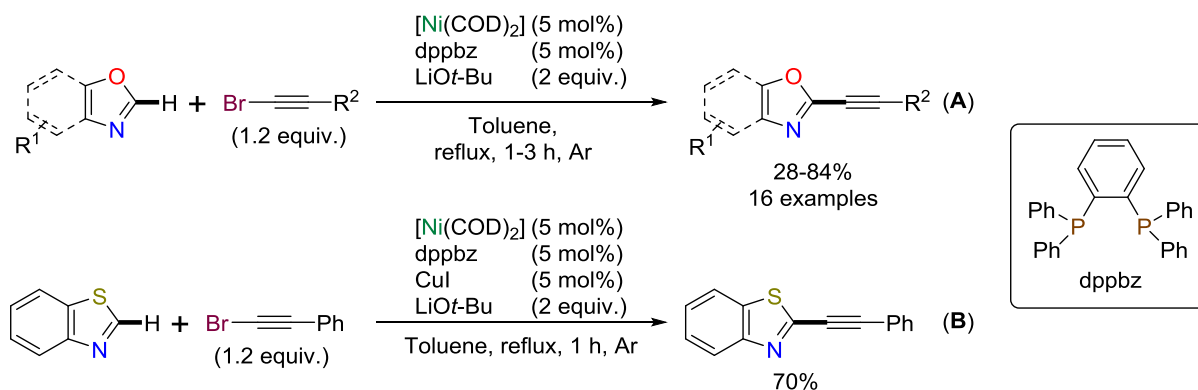
I.1. C(2)–H/C_{sp}–X

I.1.1. Electrophilic coupling partners

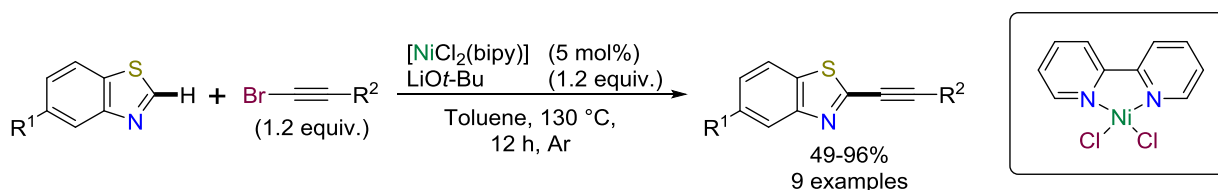
I.1.1.A. X = Bromide (-Br)

In 2009 Miura et al.²³⁴ reported the coupling of benzoxazole with bromoalkynes in refluxing toluene for 1 h, in good yields (8 examples, 56-84% yield). The reaction was catalyzed by a system comprised of [Ni⁰(COD)₂]/dppbz (1,2-bis(diphenylphosphino)benzene; 1:1 ratio, 5 mol%) and LiOt-Bu (Scheme 54, **A**). The reaction could be extended to 5-aryloxazoles (8 examples, 28-84% yield) if longer reaction times (3 h) were used. In the same report, the authors observed that benzothiazole (Scheme 54, **B**) and *N*-phenylbenzimidazole could also be transformed but, only if CuI was added as a cocatalyst. It is worth noting, however, that the authors reported no control experiment in the absence of [Ni⁰(COD)₂].

More recently, Punji's group reported that benzothiazoles can be converted in the absence of CuI using a different nickel precatalyst.²³⁵ By using $[\text{Ni}^{\text{II}}\text{Cl}_2(\text{bipy})]$ (5 mol%) in the presence of LiOt-Bu , benzothiazoles were coupled with bromoalkynes in moderate to excellent yields (9 examples, 49-96% yield, Scheme 55). The authors noted, however, that bromoalkynes bearing alkyl substituents could not be coupled using this methodology.



Scheme 54. Ni-catalyzed (benz)oxazole (A) and benzothiazole (B) C–H/C–X alkylation.

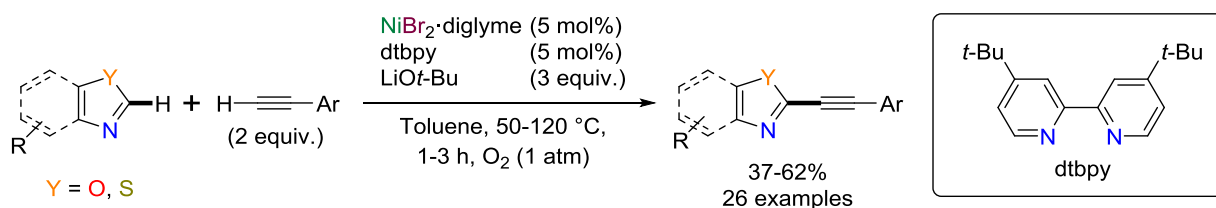


Scheme 55. Copper-free nickel-catalyzed benzothiazole alkylation.

I.1.2. Nucleophilic coupling partners

I.1.2.A. X = Hydrogen (-H)

In 2010, the Miura's group reported that the same coupling products could be formed by C–H/C–H oxidative cross-coupling using a Ni(II) system (Scheme 56).²³⁶ Employing a $\text{Ni}^{\text{II}}\text{Br}_2$ -diglyme/dtbbpy (4,4'-di(*t*-butyl)-2,2'-bipyridine, 1:1 ratio, 5 mol%) combination and LiOt-Bu , heated to 100 °C in toluene for 1 h under an oxygen atmosphere, benzoxazole was coupled with various arylalkynes in moderate yields (12 examples, 43–62% yield). Adjusting the reaction time (1–3 h) and temperature (50–120 °C), various benzoxazoles (6 examples, 40–61% yield), 5-aryloxazoles (7 examples, 40–56% yield), as well as benzothiazole (37% yield) could also be functionalized with a small variety of arylalkynes.



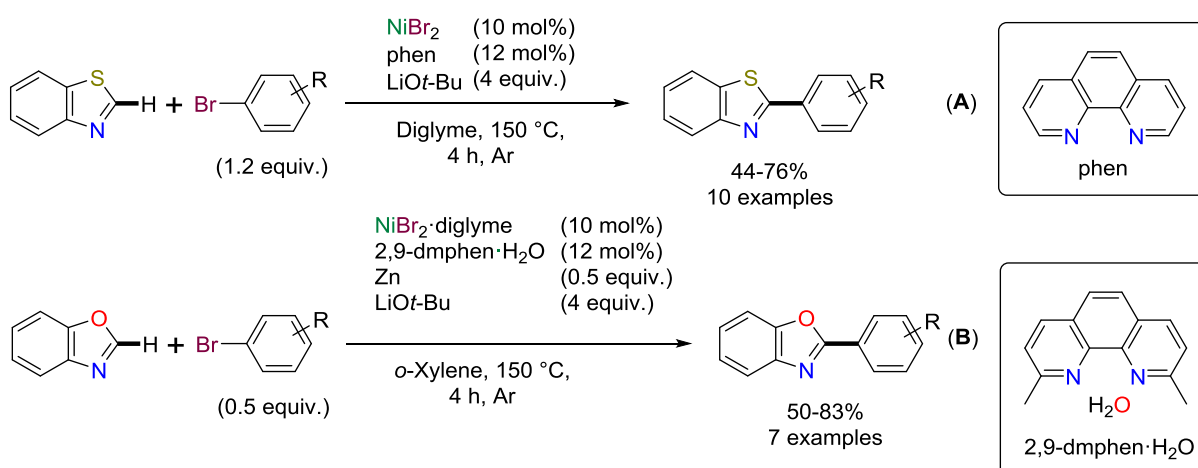
Scheme 56. Ni-catalyzed C–H/C–H oxidative coupling of benzoxazoles and terminal alkynes under an oxygen atmosphere.

I.2. C(2)-H/C_{sp2}-X

I.2.1. Electrophilic coupling partners

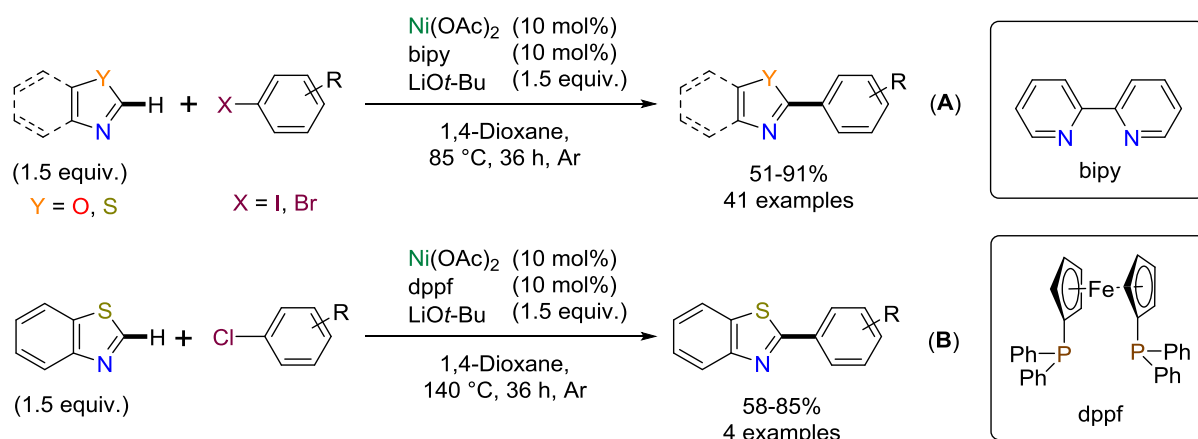
I.2.1.A. X = Halogen (-F, -Cl, -Br, -I)

The scarce examples of nickel-catalyzed azole alkylation contrast with the much larger body of work developed concerning biaryl construction. Concurrently, in 2009, the groups of Miura²³⁷ and Itami²³⁸ reported the first examples of this type of C–H/C–X cross-coupling catalyzed by nickel. The first employing $\text{Ni}^{\text{II}}\text{Br}_2/\text{phen}$ (1,10-phenanthroline, 1:1.2 ratio, 10 mol%) and LiOt-Bu in diglyme at 150 °C for 4 h, coupled benzothiazole with bromoaryls in moderate to good yields (10 examples, 44-76% yield; Scheme 57, **A**). To transpose the reaction to the transformation of benzoxazole, zinc dust was necessary along with a bulkier ligand in the form of 2,9-dimethyl-1,10-phenanthroline hydrate (2,9-dmphen·H₂O) in *o*-xylene at 150 °C (7 examples, 50-83% yield; Scheme 57, **B**).



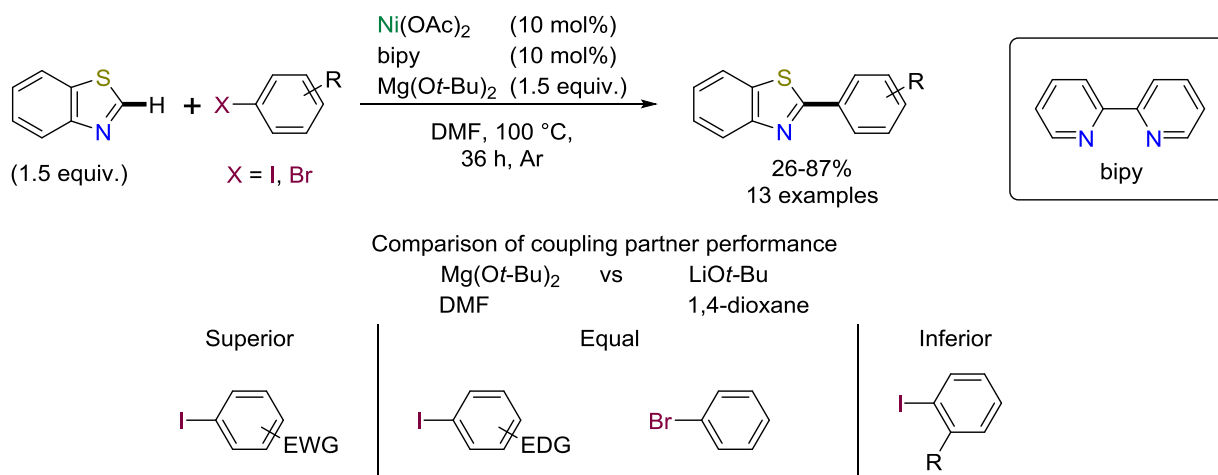
Scheme 57. Benzothiazole (**A**) and benzoxazole (**B**) coupling with aryl bromides catalyzed by nickel/phenanthrolines.

In a twin fashion, the latter report conveyed that using $\text{Ni}^{\text{II}}(\text{OAc})_2/\text{bipy}$ (2,2'-bipyridine, 1:1 ratio, 10 mol%) and LiOt-Bu in 1,4-dioxane at 85 °C for 36 h, benzothiazole and haloaryls (iodo, bromo) could be coupled in moderate to excellent yields (21 examples, 51-91% yield; Scheme 58, **A**). In addition, this methodology allowed benzoxazole, thiazole and oxazole to be coupled with iodobenzene in moderate to good yields (20 examples, 51-80% yield, Scheme 58, **A**). Finally, more challenging aryl chlorides could be coupled with benzothiazole in good yields (4 examples, 58-85% yield; Scheme 58, **B**) in the presence of 1,1'-ferrocenediyl-bis(diphenylphosphine) (dppf) as a ligand instead of bipy and at 140 °C instead of 85 °C.



Scheme 58. Azole coupling with haloarenes by nickel catalysis. The choice of ligand allows for both reactive (**A**) and challenging (**B**) electrophiles to be coupled.

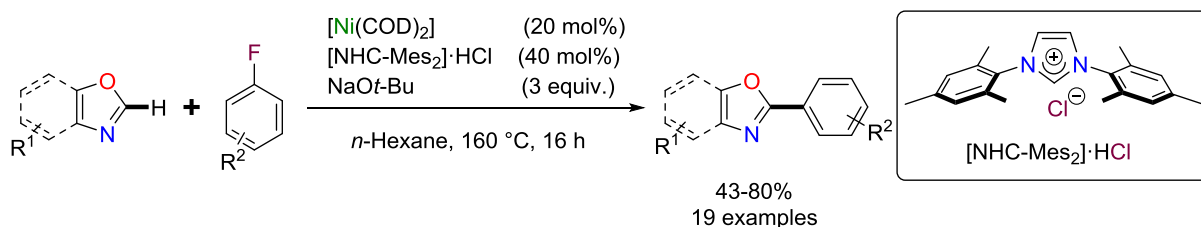
This reaction's scope was later further expanded to include a wide scope of iodo- and bromoarenes (32 examples, 48-96% yield, conditions as shown in Scheme 58, **A**) and less reactive chloroarenes (10 examples, 32-74% yield, conditions as shown in Scheme 58, **B**).²³⁹ Importantly, the authors recognized some of the limitations of their synthetic protocol: the need for LiOt-Bu as a base and 1,4-dioxane as a solvent. As a result, they found that the reaction of benzothiazole with aryl halides could take place in the polar solvent, DMF, in the presence of $\text{Mg}(\text{Ot-Bu})_2$. Comparison of the performance of the new reaction conditions with that of former conditions showed both reaction conditions to be complementary (Scheme 59).



Scheme 59. Benzothiazole coupling in polar DMF solvent using alternative base Mg(O*t*-Bu)₂. Complementary reactivity varying with electronic and steric properties of the haloarenes.

Polar, electron-deficient iodoarenes were better partners in the novel reaction conditions (5 examples, 29-87% yield, Scheme 59), while electron-rich or neutral iodo and bromoarenes were found to be equal (4 examples, 57-73% yield), and *o*-substituted iodoarenes were found to be inferior partners (4 examples, 26-63% yield).²³⁹

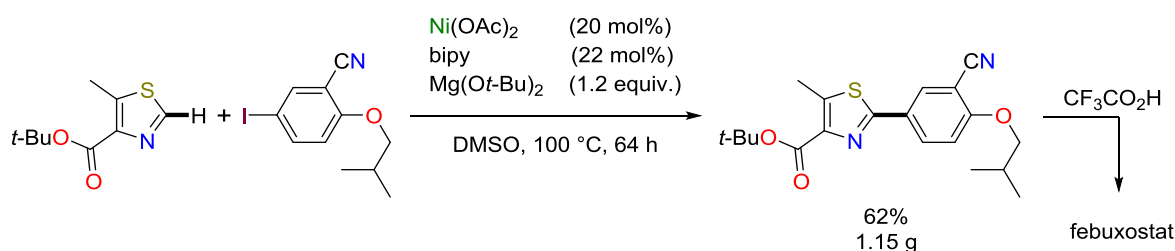
Impressively, Bai, Lan, Zhang and collaborators reported the use of aryl fluorides as electrophilic coupling partners catalyzed by a Ni-NHC pair.⁹⁴ Using [Ni⁰(COD)₂]/[NHC-Mes₂]₂·HCl (1:2 ratio, 20 mol%) and Na*Ot*-Bu as a base in *n*-hexane at 160 °C, benzoxazole and a series of fluoroarenes could be coupled in moderate to good yields (13 examples, 43-80% yield, Scheme 60). Substituted benzoxazoles (4 examples, 44-53% yield) and 5-aryloxazoles (2 examples, 54-55% yield) could also be successfully coupled. Other azoles did not react in this reaction and a marked effect of the nature of the alkoxide's cation was observed, with KO*t*-Bu being much less efficient than Na*Ot*-Bu. This is one of the rare examples of the successful application of Ni-NHC catalytic systems in azole C–H bond functionalization.



Scheme 60. Aryl fluorides as (benz)oxazole coupling partners catalyzed by Ni-NHC.

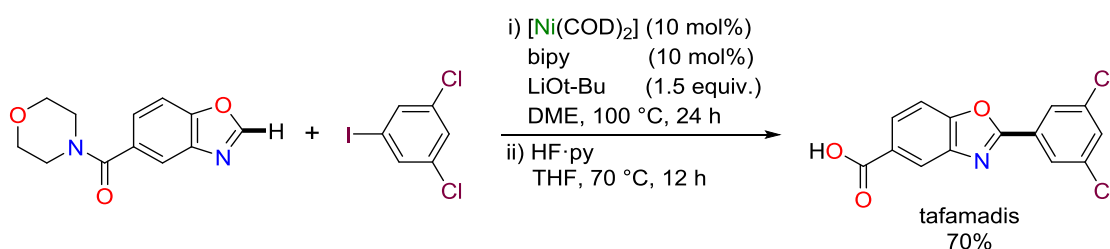
To exemplify the application of these C–H/C–halogen coupling protocols to molecules beyond model systems, Itami's group and others applied this methodology to the synthesis of a series of biologically active molecules (febuxostat,^{238,239} tafamadis,²³⁹ texaline^{239,240}).

Febuxostat is a selective inhibitor of xanthine oxidase, effective for the treatment of gout and hyperuricemia.^{241,242} This compound could be synthesized in 51% overall yield from the corresponding thiazole and iodoarene by employing Ni^{II}(OAc)₂/bipy (1:1 ratio, 10 mol%) and LiOt-Bu in 1,4-dioxane at 100 °C, followed by treatment with CF₃CO₂H.²³⁸ More impactful perhaps was their improvement of this methodology by using Mg(Ot-Bu)₂ and DMSO at 100 °C.²³⁹ This allowed the synthesis of protected febuxostat in a gram scale (Scheme 61) which yielded the target compound after quantitative deprotection by treatment with CF₃CO₂H.



Scheme 61. Gram scale Ni-catalyzed synthesis of *t*-Bu protected febuxostat ester.²³⁹

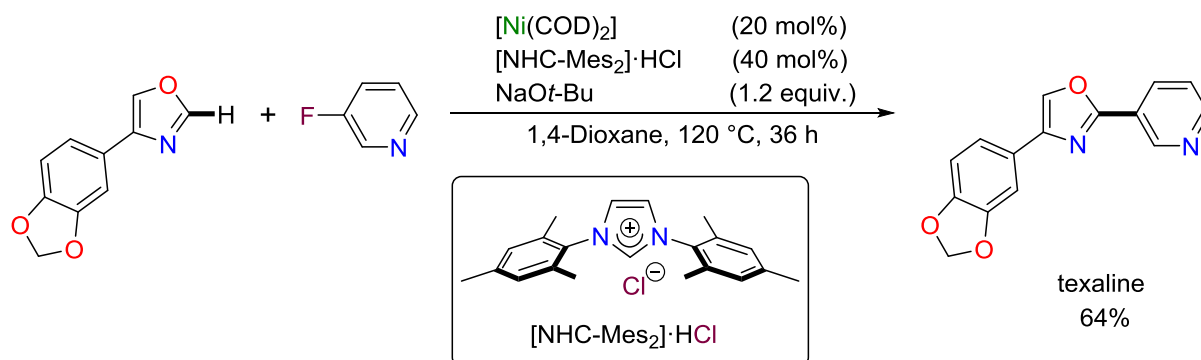
The prospective TTR amyloid polyneuropathy drug, tafamadis²⁴³ could be synthesized by using a [Ni⁰(COD)₂]/bipy catalyst system (Scheme 62). Coupling of an amidebenzoxazole with 4,5-dichloro-1-iodobenzene catalyzed by [Ni⁰(COD)₂]/bipy (1:1 ratio, 10 mol%) in the presence of LiOt-Bu in DME at 100 °C occurred in a good yield (74%), to afford the corresponding intermediate that could then be deprotected by HF·py to give tafamadis in a good overall yield (70%).²³⁹



Scheme 62. Nickel-catalyzed synthesis of tafamadis.²³⁹

As mentioned above, texaline, a natural product with antitubercular activity^{244–246} could also be synthesized by nickel catalysis following the methodology developed by Itami's group (see Scheme 58). Indeed from a 5-aryloxazole and 3-bromopyridine, Ni^{II}(OAc)₂/bipy (1:1 ratio, 5 mol%) and LiOt-Bu in 1,4-dioxane at 120 °C would give texaline in a good yield (84%)²³⁹ improving on the reported palladium cross-coupling synthesis (57%).²⁴⁴ More interestingly perhaps, this product could also be synthesized from 3-fluoropyridine by the

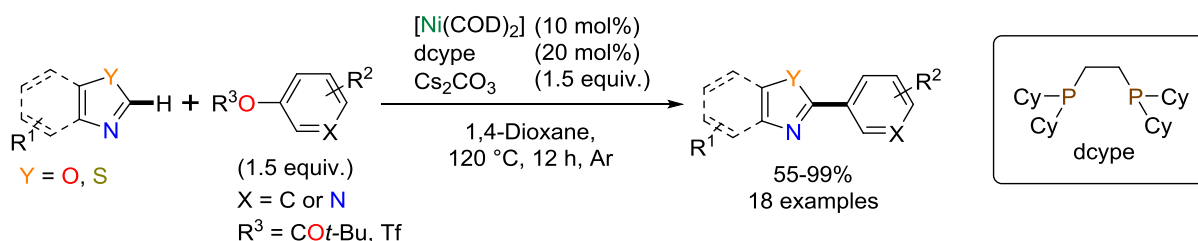
$[\text{Ni}^0(\text{COD})_2]/[\text{NHC-Mes}_2]\cdot\text{HCl}$ (1:2 ratio, 20 mol%) catalyst system studied by Bai, Lan, Zhang et al. in the presence of LiOt-Bu in 1,4-dioxane at 120 °C in a moderate yield (64%, Scheme 63).⁹⁴



Scheme 63. Ni-NHC-catalyzed synthesis of texaline.⁹⁴

1.2.1.B. X = Oxygen electrophiles (-OR): Triflate (-OTf), Sulfonate (-OSO₂R), Ester (-OCOR), Carbamate (-OCONRR')

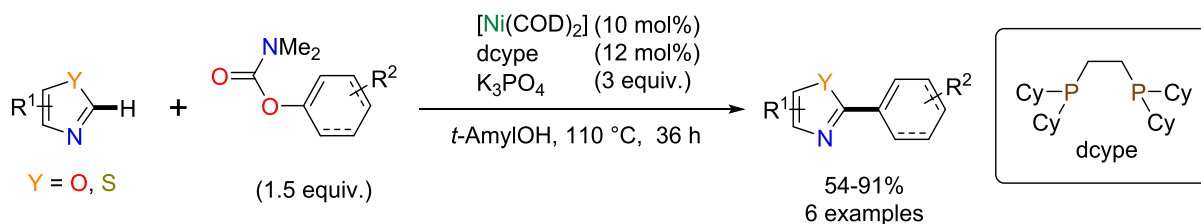
A couple of examples of oxygen bound electrophilic coupling partners had been reported earlier,^{238,239} but true synthetic methodologies for C–H/C–O cross-coupling were only reported in 2012 by Itami's group.^{247,248} From those early examples with a triflate coupling partner,^{238,239} a series of -OR electrophilic coupling partners, including pivalates, could now be used by scission the C_{Ar}–O bond (Scheme 64). The new reaction is catalyzed by a package of $[\text{Ni}^0(\text{COD})_2]/\text{dcype}$ (1,2-bis(dicyclohexylphosphino)ethane, 1:2 ratio, 10 mol%) and Cs_2CO_3 in 1,4-dioxane at 120 °C (Scheme 64). Benzoxazoles (12 examples, 52-99% yield), 4,5-substituted-oxazoles (5 examples, 62-73% yield) and benzothiazole (65% yield) could in the same manner be transformed in moderate to excellent yields.



Scheme 64. First example of esters as azole C–H/C–O cross-coupling partners, by nickel(0) catalysis.

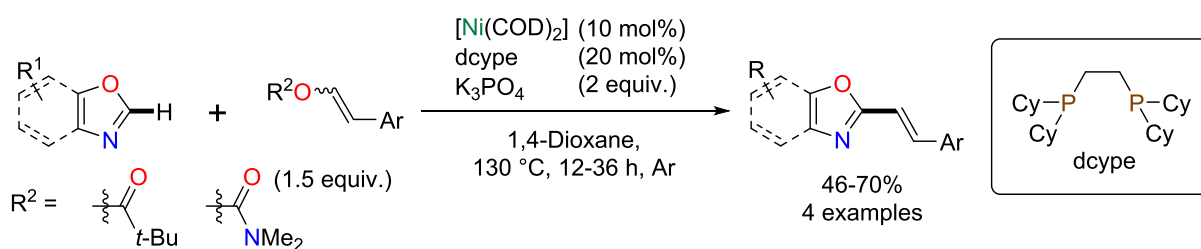
Later on, carbamates were also found to perform in this reaction, provided that reaction conditions were adapted.²⁴⁹ Electron-rich thiazoles and oxazoles could be transformed when

the base and solvent were switched for K_3PO_4 and *t*-AmylOH to give moderate to excellent yields of the desired cross-coupled product (6 examples, 54-91% yield, Scheme 65).



Scheme 65. Carbamates as suitable electrophiles for nickel-catalyzed direct functionalization of azoles.

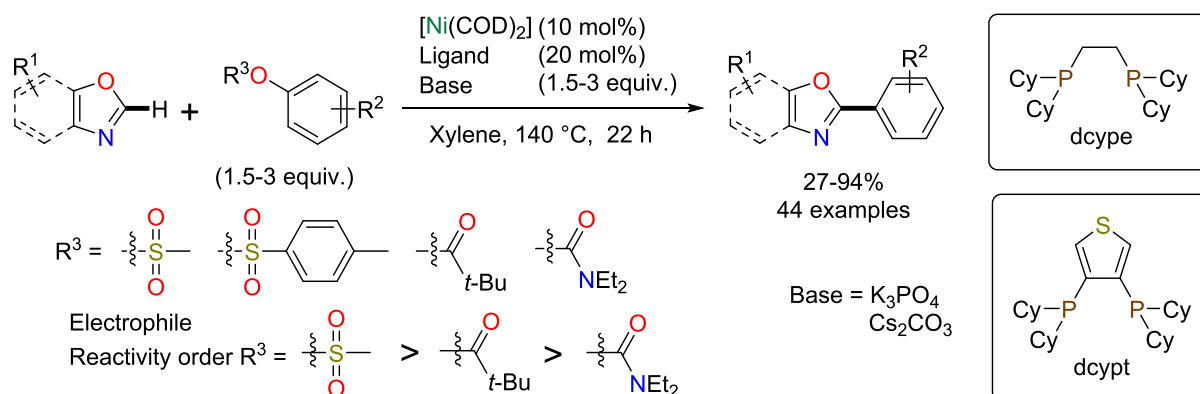
With the objective of extending the scope of alkenyl coupling partners Itami and collaborators divulged the use of α,β -unsaturated aryl esters and carbamates as reagents (Scheme 65).²⁵⁰ Keeping with a similar catalytic ensemble ($[Ni^0(COD)_2]/dcype$), a styrene function could be added to the C(2) position of substituted benzoxazoles and oxazoles in moderate to good yields (4 examples, 46-70% yield, Scheme 66). Benzothiazole was found to be unreactive in these conditions.



Scheme 66. Vinyl esters and carbamates as alkenylation reagents with $[Ni^0(COD)_2]/dcype$.

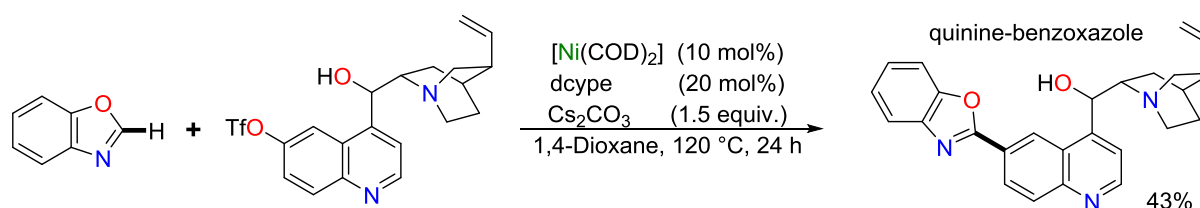
Building on these reports, Kalyani and co-workers undertook an exhaustive benchmarking study on nickel-catalyzed azole coupling with oxygen electrophiles.²⁵¹ Coupling of benzoxazole with different pivalates was more or less successful with the judicious choice of both ligand, dcype or 1,2-bis(dicyclohexylphosphino)thiophene (dcypt), and base, K_3PO_4 or Cs_2CO_3 (Scheme 67). Notably, using the standard $[Ni^0(COD)_2]/dcype$ (1:2 ratio, 10 mol%) and Cs_2CO_3 was optimal for electron rich pivalates, whereas electron poor pivalates preferred dcypt and those bearing an ester function were particularly sensitive to the choice of base (K_3PO_4) (10 examples, 44-94% yield). Varying the azole with substituted benzoxazoles, oxazoles and benzothiazole showed less sensitivity to the ligand/base pair (12 examples, 47-94% yield), but highlighted the correlation between azole acidity and yield. These observations were then transferred to the coupling of sulfonates (aryl mesylates and tosylates), albeit in lower yields (13 examples, 27-82% yield). Finally, they explored the use of carbamates as electrophiles, with the dcypt/ K_3PO_4 pair being optimal for the transformations of oxazoles (9 examples,

22-83% yield). In addition to the previous results, competition studies allowed to establish a reactivity order of mesylates > pivalates > carbamates in this reaction.



Scheme 67. Study on the effect of electronic parameters in oxygen bound electrophiles in nickel catalyzed C–H coupling.

Nickel-catalyzed C–H/C–O cross-coupling was also applied to the synthesis of complex molecules with biological activity, by Itami et al. Thus, triflates were also used to construct complex steroid and alkaloid scaffolds comprising reactive alcohol, olefin and ketone functions in moderate yields (43-52% yield, Scheme 68).²⁴⁷



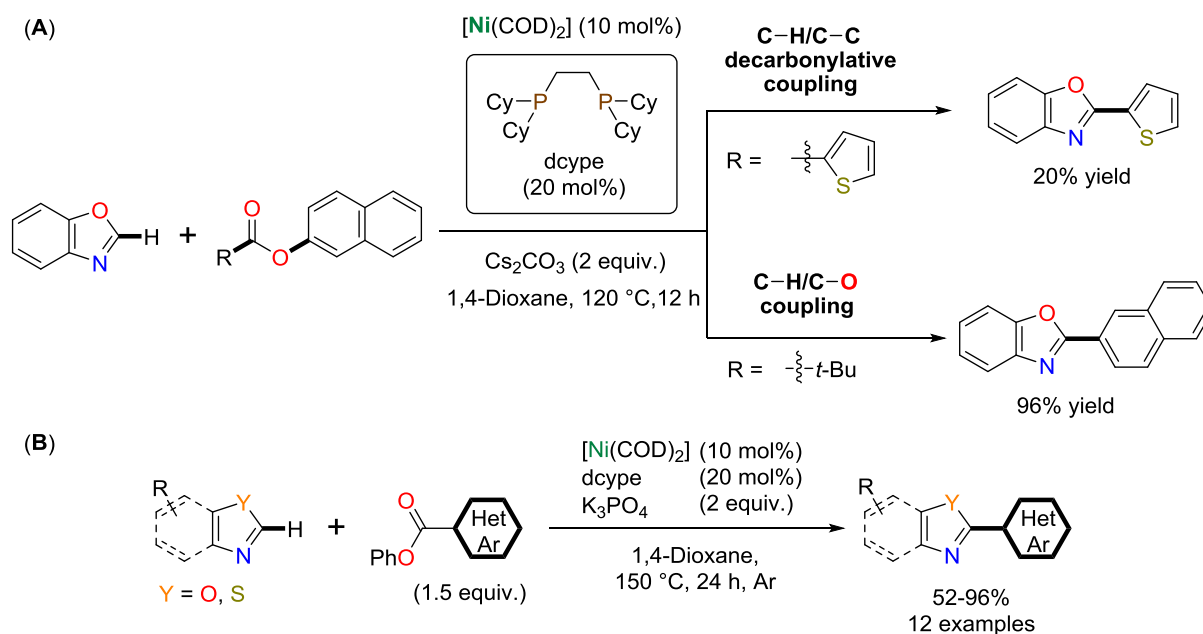
Scheme 68. Modification of alkaloid (quinine) scaffolds by C–H/C–O Ni-catalysis.

I.2.1.C. X = Carbon electrophiles

I.2.1.C.1. X = Carbonyl (-COOR)

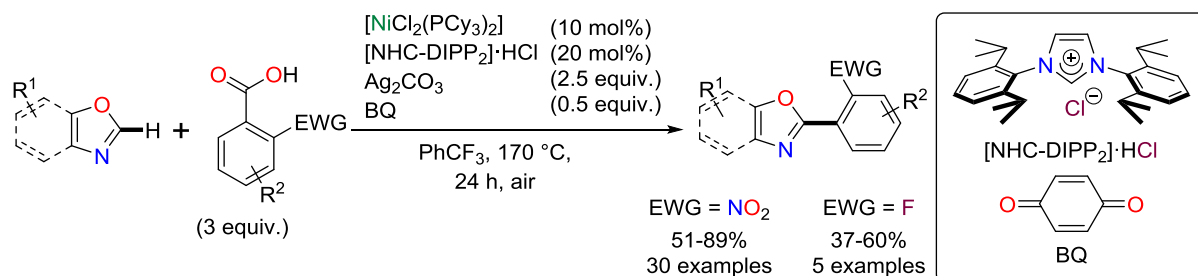
Another important development was the discovery that both the C–O and the C–C bond of esters could be used selectively, expanding the diversity of coupling partners available to nickel catalysis.²⁴⁸ Using the same catalytic package as for the couplings with pivalates (i. e.: $[\text{Ni}^0(\text{COD})_2]/\text{dcype}$ (1:2 ratio, 10 mol%), see Scheme 64), but switching the base from Cs_2CO_3 to K_3PO_4 , bis-aryl esters with a carbon bound heterocycle, underwent decarbonylative coupling with benzothiazole, this time incorporating the carbon bound heterocycle (Scheme 69, **A**).

Benzoxazole, 5-phenyloxazole and 5-phenylthiazole were coupled in this manner in good to excellent yields (12 examples, 52-96% yield, Scheme 69, **B**).



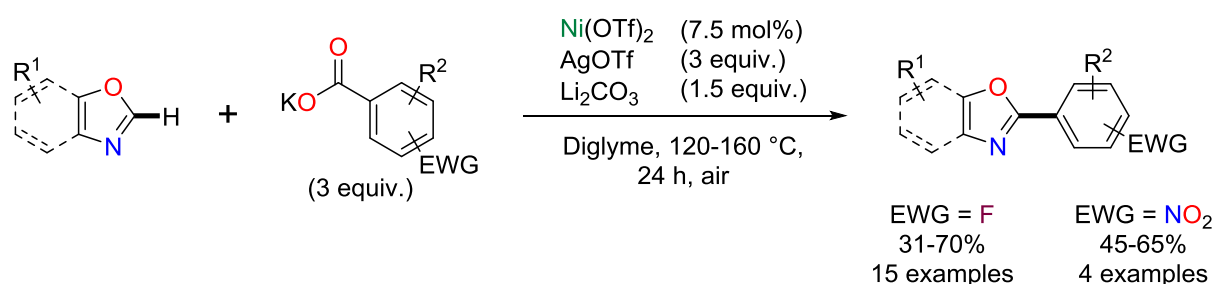
Scheme 69. Discovery of decarbonylative coupling in search of C–H/C–O coupling (**A**) and scope of decarbonylative cross-coupling of benzoxazole and phenyl heteroarylates (**B**).

Carboxylic acids were also reported as useful reagents undergoing decarboxylative arylation catalyzed by nickel (Scheme 70).⁹⁵ Using $[\text{Ni}^{\text{II}}\text{Cl}_2(\text{PCy}_3)_2]$ and $[\text{NHC-DIPP}_2]\cdot\text{HCl}$ (1:2 ratio, 10 mol%) mixed with Ag_2CO_3 as both base and oxidant and 1,4-benzoquinone (BQ) as a co-oxidant, substituted benzoxazoles (21 examples, 51-81% yield) and oxazoles (9 examples, 52-89% yield) could be coupled with either *o*-nitrobenzoic acids (30 examples, 51-89% yields, Scheme 70) or *o*-fluorobenzoic acids (5 examples, 37-60% yields) when heated to 170 °C in (trifluoromethyl)benzene. Of note, benzothiazole could also successfully be used as a substrate to couple with *o*-nitrobenzoic acid (75% yield). This was the first example of a Ni-NHC catalyst system in catalytic azole C–H bond functionalization.



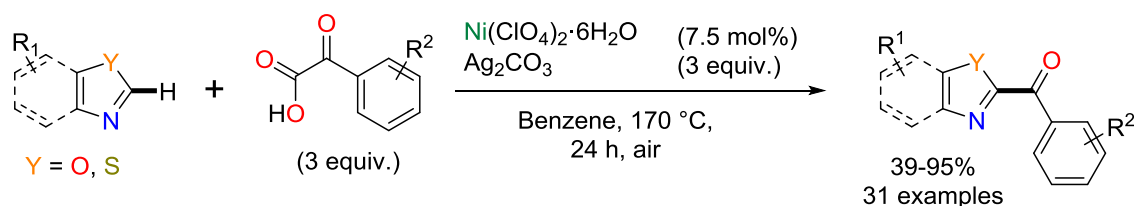
Scheme 70. *o*-Nitrobenzoic acids as reagents for decarboxylative cross-coupling via nickel-NHC catalysis.

More recently Kalyani and collaborators have explored the decarboxylative coupling using fluorinated benzoates.²⁵² The strategy was successful in assembling biaryl fluorinated azoles by ligand-free action of Ni^{II}(OTf)₂ (7.5 mol%) associated with AgOTf as an oxidant and Li₂CO₃ as a base in hot (120-160 °C) diglyme (Scheme 71). A range of fluorobenzoates could be coupled to benzoxazole in moderate to good yields (8 examples, 31-70% yield), and a range of substituted benzoxazoles and 5-(4-nitrobenzene)-oxazole could be coupled with potassium 2,3,6-trifluorobenzoate in moderate yields (7 examples, 53-59%). In addition, by analogy with Zhang, Lu et al.'s work⁹⁵ (see Scheme 70), changing the fluoroaryl motif for a 2-nitrophenyl motif proved also successful with this catalytic system for the coupling of substituted benzoxazoles (4 examples, 45-65% yields, Scheme 71).



Scheme 71. Decarboxylative coupling using activated benzoates. Electron-withdrawing groups (F, NO₂) make ligandless nickel catalysis effective.

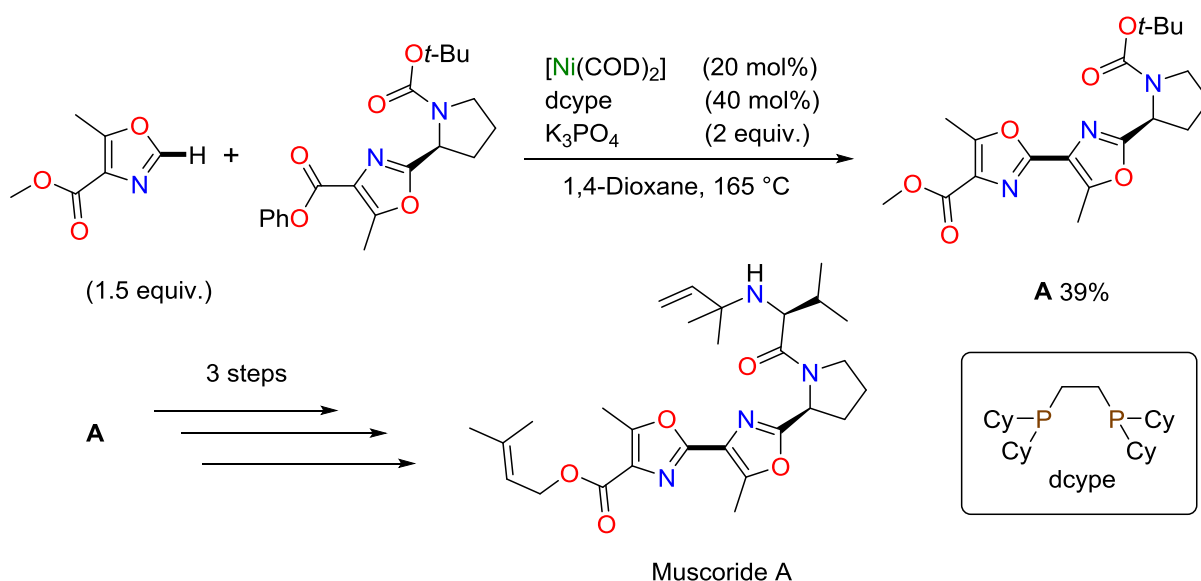
In a similar fashion, α -oxoglyoxylic acids could be used in ligand-free nickel catalysis (Scheme 72).²⁵³ The simple nickel salt, Ni^{II}(ClO₄)₂·6H₂O, allied with Ag₂CO₃ and heated to 170 °C in toluene constructed the desired biarylketones from substituted benzoxazoles (21 examples, 39-95% yields), substituted oxazoles (8 examples, 75-91% yields) and benzothiazole (60% yield) in moderate to excellent yields.



Scheme 72. Ligand free biaryl ketone construction by azole/ α -oxoglyoxylic acid decarbonylative coupling. Widening the scope of chemical functions constructed by nickel catalysis.

Decarbonylative cross-coupling was exploited by Itami and co-workers towards the synthesis of biomolecules. Using their methodology they prepared an important intermediate in the synthesis^{254–256} of muscoride A,²⁵⁷ a natural product with antibacterial activity.²⁴⁸ Thus,

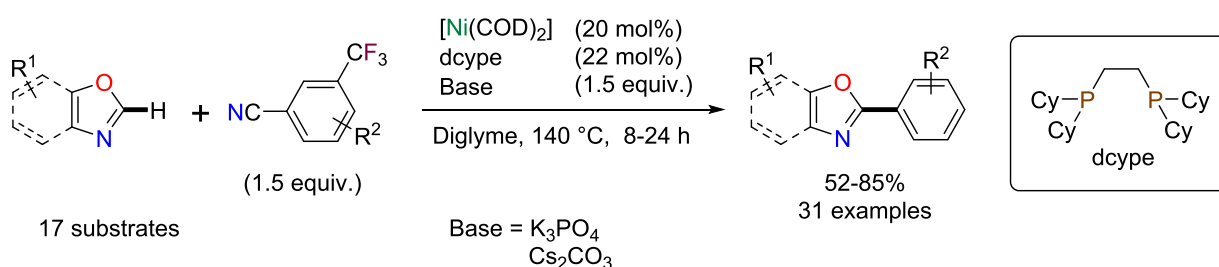
the appropriate oxazoles could be coupled using $[\text{Ni}^0(\text{COD})_2]/\text{dcype}$ (ratio 1:1, 20 mol%) in the presence of K_3PO_4 in 1,4-dioxane at 165 °C to give intermediate **A** in a moderate yield (39%, Scheme 73).²⁴⁸



Scheme 73. Decarbonylative cross-coupling in the synthesis of muscoride A.²⁴⁸

I.2.1.C.2. X = Nitrile (-CN)

The use of aromatic nitriles as electrophiles was also recently reported (Scheme 74).²⁵⁸ By employing $[\text{Ni}^0(\text{COD})_2]/\text{dcype}$ (1:1.1 ratio, 20 mol%) and K_3PO_4 in diglyme at 140 °C Kalyani et al. could constructively couple 5-aryl-oxazoles and 3-(trifluoromethyl)benzonitrile in good yields (8 examples 52-59% yield). Substituted benzoxazoles (7 examples, 70-85% yield) as well as benzothiazole (66% yield) could also participate in good yields, provided that the base was changed to Cs_2CO_3 .



Scheme 74. Aryl nitriles as electrophilic coupling partners for Ni-catalyzed cross-coupling.

The authors highlighted however that for these later substrates the reaction would proceed up to 68% yield, even in the absence of the metal/ligand pair! The scope of suitable nitriles (10 examples) was also studied and the reaction was shown to be compatible with both electron-donating and -withdrawing groups, with no clear reactivity trends emerging. Finally, it was noted that addition of BPH_3 (0.4 equiv.) to act as a Lewis acid allowed halving the metal/ligand charge and retaining similar reactivity (loss of 5-10% yield).

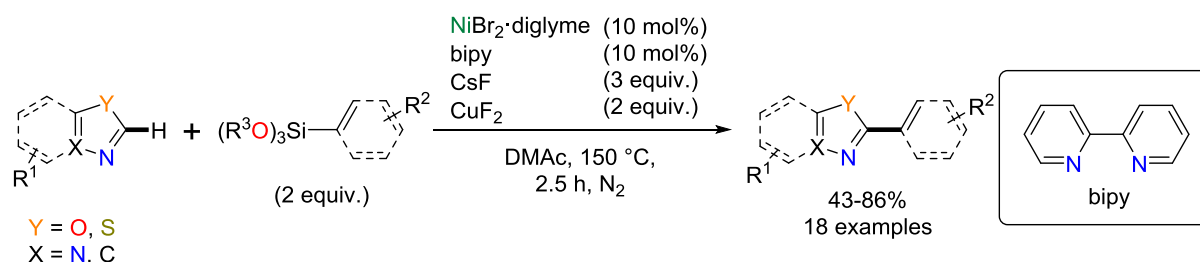
I.2.2. Nucleophilic coupling partners

I.2.2.A. X = Metalloid

An important expansion of the available coupling partner scope came from Miura and coworkers' reports that nucleophilic organometalloids – organosilanes²⁵⁹ and boronic acids²⁶⁰ – could replace electrophiles as coupling partners.

I.2.2.A.1. X = Silanes (-Si(OR)₃)

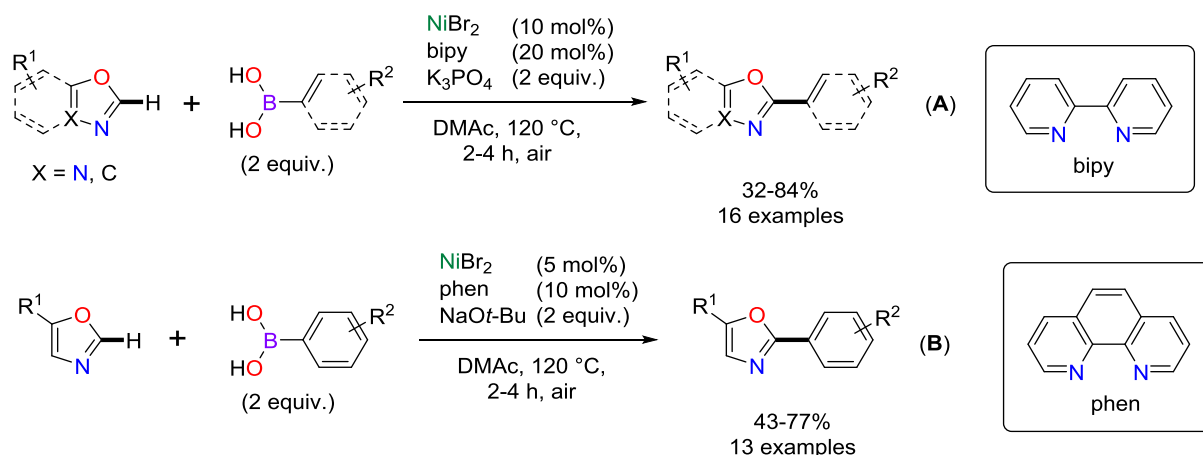
By a combination of Ni^{II}Br₂·diglyme/bipy (1:1 ratio, 10 mol%) with a mixture of CsF and CuF₂ in *N,N*-dimethylamide (DMAc) at 150 °C, aryl and alkenyl organosilanes could be coupled to benzoxazoles in moderate to good yields (7 examples, 52-80% yield; Scheme 75). The same reaction conditions could also be utilized for 5-aryloxazoles (5 examples, 45-86% yield), benzothiazole (3 examples, 43-64% yield) or 5-aryl-1,3,4-oxadiazoles (3 examples, 54-61% yield; Scheme 75).



Scheme 75. Benzoxazole C–H arylation with aryl/alkene organosilanes catalyzed by nickel in the presence of fluoride salts.

I.2.2.A.2. X = Boronic acids (-B(OH)₂)

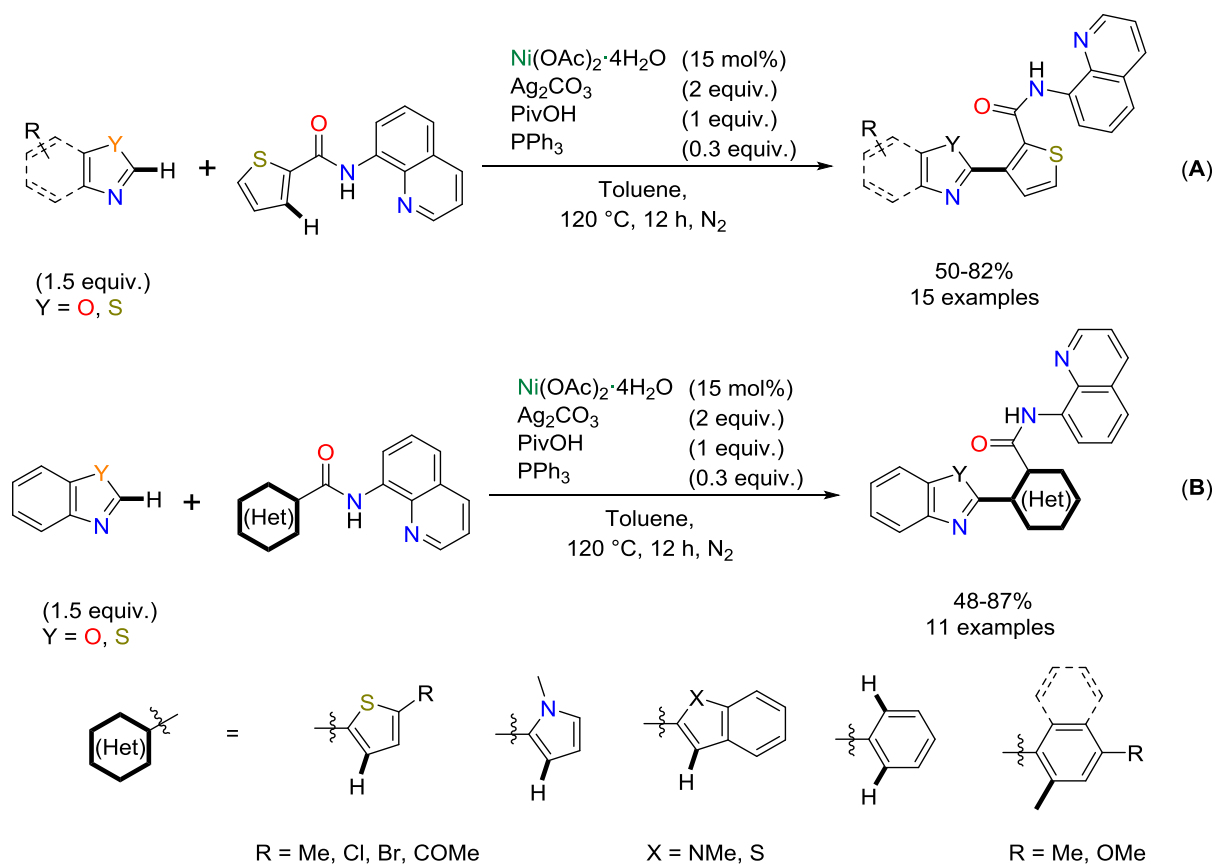
Using the similar catalyst systems, Ni^{II}Br₂/bipy (1:2 ratio, 10 mol%) or Ni^{II}Br₂/phen (1:2 ratio, 5 mol%), in the presence of an inorganic base, aryl and alkenyl boronic acids could also be used as coupling partners, when heated in DMAc to 120 °C under air. The choice of the base to match the catalyst/ligand pair proved crucial: Ni^{II}Br₂/bipy needed K₃PO₄ to couple benzoxazoles in moderate to good yields (7 examples, 50-76% yield; Scheme 76, **A**) and 5-aryl-1,3,4-oxadiazoles in low to good yields (9 examples, 32-84% yield; Scheme 76, **A**); whereas Ni^{II}Br₂/phen required the employment of NaO*t*-Bu to transform 5-aryloxazoles in moderate to good yields (13 examples, 43-77% yield; Scheme 76, **B**).



Scheme 76. Boronic acids as coupling partners for benzoxazoles, 5-aryl-1,2,3-oxathiazoles (A) and 5-aryl-oxazoles (B). Nickel/dinitrogen ligand system's reactivity controlled by the choice of base.

1.2.2.B. X = Hydrogen (-H)

Finally, the holy grail of oxidative cross-coupling was observed by You and collaborators. Employing 8-aminoquinoline as a directing group,²⁶¹ they established a series of oxidative dehydrogenative couplings in the presence of $\text{Ni}^{\text{II}}(\text{OAc})_2 \cdot 4\text{H}_2\text{O}$ (15 mol%) as a catalyst and Ag_2CO_3 , pivalic acid and PPh_3 as additives (Scheme 77).



Scheme 77. First example of nickel-catalyzed oxidative C–H/C–H azole-aryl cross coupling.

Thus, *N*-(quinolin-8-yl)thiophene-2-carboxamide could be successfully coupled with benzothiazoles (3 examples, 64-78% yield), thiazoles (6 examples, 50-82% yield), benzoxazoles (2 examples, 53 and 58% yield; Scheme 77, **A**) and other nitrogen heterocycles (i. e.: purine, caffeine; 4 examples, 50-74% yield; C–H functionalization not always at C(2)). The same directing group could be placed in other aromatic substrates, constructing thienyl, benzothienyl, indolyl and pyrrolyl, as well as phenyl and 1-naphthyl bis-aryls with benzothiazole (7 examples, 49-87% yield) and benzoxazole (4 examples, 48-74% yield; Scheme 77, **B**).

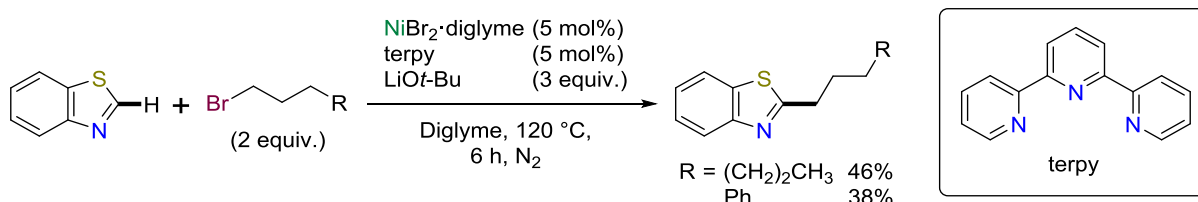
1.3. C(2)–H/C_{sp³}–X

Despite years of mastering biaryl system construction that seem universal in successful drugs (see Schemes 61-63 and 73) a new paradigm has been growing since the late 2000's of "escaping the flatland" that focuses on improvement of drugs by adding more complex saturated molecules.^{262,263} In this context adding aliphatic groups to azoles is of great synthetic interest.

1.3.1. Electrophilic coupling partners

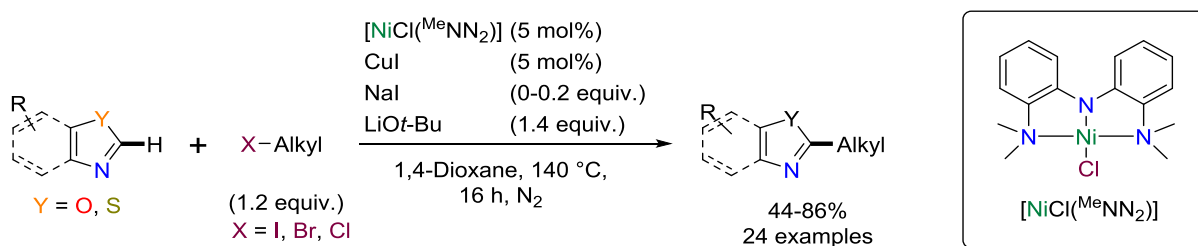
1.3.1.A. X = Halogen (-Br, -I)

In 2010, two reports described the first examples of Ni-catalyzed C–H alkylation of azoles.^{264,265} In the first case, nickel catalysis proved essential to the successful alkylation of benzothiazole with alkyl bromides. Indeed $[\{\text{Pd}^{\text{II}}\text{Cl}(\eta^3\text{-C}_3\text{H}_5)\}_2]/\text{P}(n\text{-Bu})_3$ (1:8 ratio, 3.75 mol%) that had proven successful for oxazole substrates, could not efficiently achieve this reaction. The use of $\text{Ni}^{\text{II}}\text{Br}_2$ -diglyme/terpy (terpyridine, 1:1 ratio, 5 mol%) and LiOt-Bu in diglyme in contrast succeeded in attaching a *n*-hexyl or a 3-phenylpropyl group to benzothiazole from the corresponding alkyl bromides, albeit in moderate yields (38-46% yields, Scheme 78).²⁶⁴



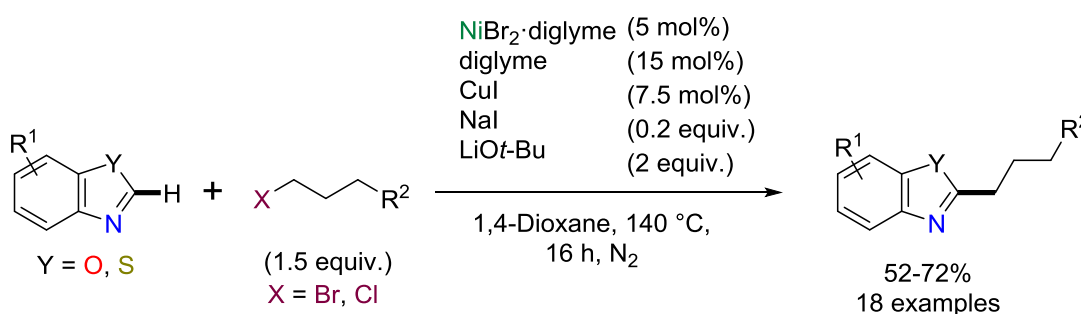
Scheme 78. Alkylation of benzothiazole with bromoalkanes. Nickel catalysis can transform substrates palladium fails at.

The second example explored the efficiency of a *N,N,N* pincer complex, $[\text{Ni}^{\text{II}}\text{Cl}(\text{MeNN}_2)]$, for alkylating azoles (Scheme 79).²⁶⁵ Combining the latter (5 mol%) with CuI as a cocatalyst (5 mol%) and LiOt-Bu as base, benzoxazole could be coupled with numerous haloalkanes (13 examples, 44-86% yield), including bromides and chlorides when NaI was present as an additive. Other azoles were also found to undergo functionalization under these conditions: 5-aryloxazoles (4 examples, 74-86% yield), benzothiazoles (3 examples, 72-78% yields) and thiazoles (4 examples, 60-85% yield). Of note, however, the authors did not report a control experiment in the absence of the copper salt, which raises a question regarding the true nature of the catalyst.



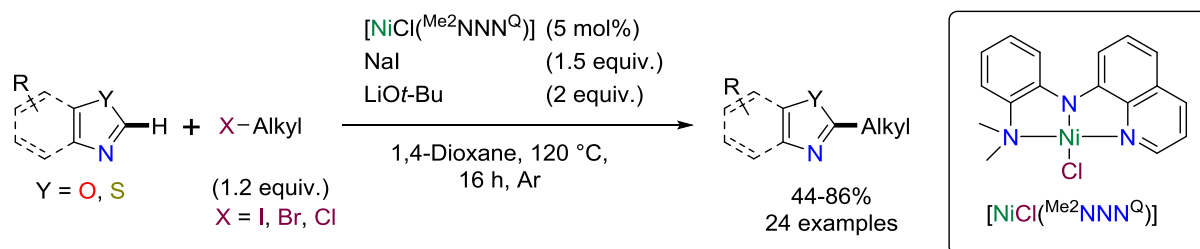
Scheme 79. Direct azole alkylation with haloalkanes catalyzed by a pincer complex of nickel(II) and CuI.

Shortly after, Ackermann, Punji and Song²⁶⁶ divulged another alkylating system comprised of $\text{Ni}^{\text{II}}\text{Br}_2$ -diglyme (5 mol%), CuI (5 mol%) as a cocatalyst, LiOt-Bu as a base, NaI as a halide exchange additive and, curiously, additional diglyme (15 mol%). Heating these in 1,4-dioxane generated a series of functionalized benzoxazoles (15 examples, 52-72% yield) and benzothiazoles (3 examples, 52-55% yield, Scheme 80) with alkyl chlorides and bromides. Regrettably, once more, no control experiment in the absence of the copper salt was described.



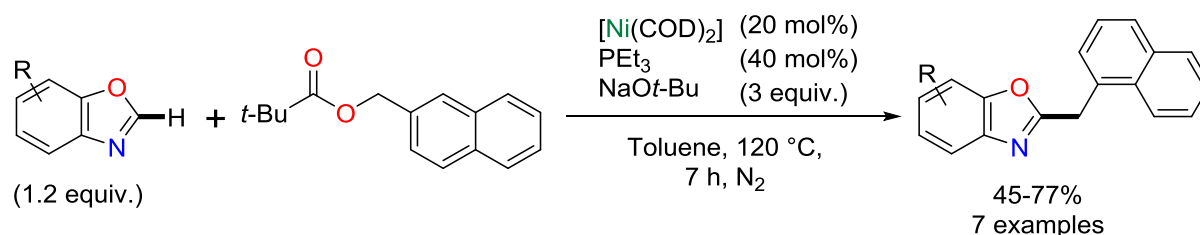
Scheme 80. Simple Ni-catalyzed benzo-azole C–H alkylation.

Devoting further time to this transformation, Punji later reprised this subject and removed the need for a cocatalyst by employing the *N,N,N* pincer complex $[\text{Ni}^{\text{II}}\text{Cl}(\text{Me}_2\text{NNN}^{\text{O}})]$ (5 mol%), under otherwise similar conditions (Scheme 80).²⁶⁷ This resulted in a broad scope of alkylated benzothiazoles (16 examples, 40-88% yields) and 5-aryloxazoles (5 examples, 40-70% yield).

Scheme 81. Copper-free azole alkylation by a *N,N,N*-nickel(II) pincer complex.

I.3.1.B. X = Carbonyl (-COOR)

2-Naphthylmethyl pivalate was also shown to act as a fitting coupling partner to access benzoxazole-naphthylmethanes.²⁶⁸ Thus, using $[\text{Ni}^0(\text{COD})_2]/\text{PEt}_3$ (1:2 ratio, 20 mol%) and NaOt-Bu, a small array of benzoxazoles could be coupled with 2-naphthylmethyl pivalate in moderate to good yields (7 examples, 45-77% yield, Scheme 81).

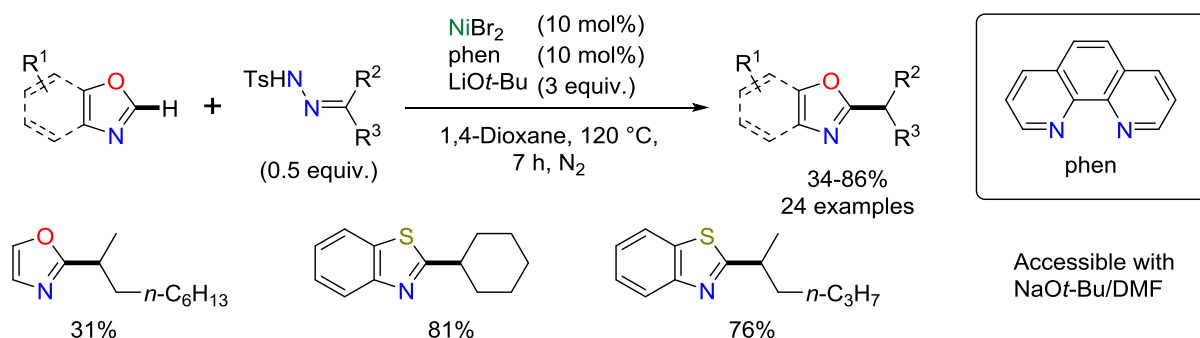


Scheme 82. Benzoxazole direct functionalization with 2-naphthylmethyl pivalate.

I.3.2. Nucleophilic coupling partners

I.3.2.A. X = Hydrazone (=N-NHR)

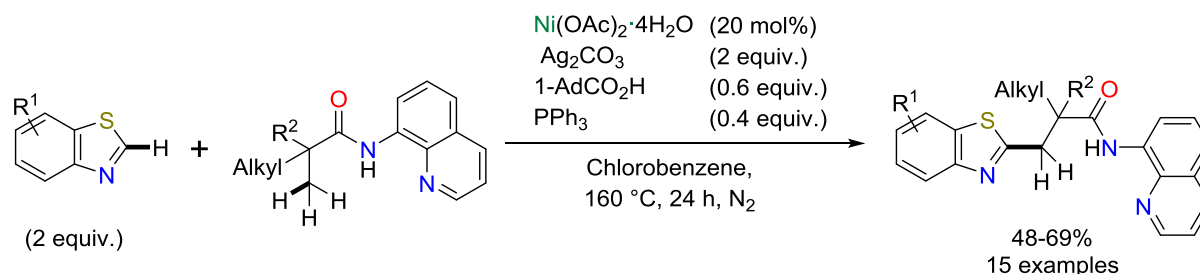
Moving away from electrophiles as reagents, secondary alkyl hydrazones²⁶⁹ were also found to be viable for constructing C(2)–C_{sp3} bonds. The $\text{Ni}^{\text{II}}\text{Br}_2/\text{phen}$ pair (1:1, 10 mol%) in the presence of LiOt-Bu was successful at constructing secondary alkyl azoles from hydrazones and a series of benzoxazoles (13 examples, 34-86% yield) and 5-aryloxazoles (11 examples, 40-76% yield) in moderate to good yields (Scheme 82). One example, using the hydrazone of octanal, successfully makes use of a primary hydrazone (50%). Benzothiazole and oxazole could also be coupled to hydrazones under slightly modified conditions (NaOt-Bu and DMF, Scheme 82, bottom).



Scheme 83. Alkyl hydrazones expand the scope of reagents suitable for nickel-catalyzed C_{sp^2} – C_{sp^3} bond formation.

I.3.2.B. X = Hydrogen (-H)

Once more (see Scheme 77), You and coworkers delved on the C–H/C–H oxidative cross-coupling of azoles, this time to construct azole-alkylmethanes.²⁷⁰ A catalytic system similar to the one used for the C–H/C–H arylation was reported: $Ni^{II}(\text{OAc})_2 \cdot 4\text{H}_2\text{O}$ (5 mol%) and Ag_2CO_3 in the presence of PPh_3 and 1-adamantanecarboxylic acid (1-AdCO₂H). With this system in chlorobenzene heated to 160 °C, aliphatic β -methyl *N*-(quinolin-8-yl)-carboxamides could be successfully coupled with benzothiazoles in moderate to good yields (15 examples, 45-69% yield, Scheme 84).



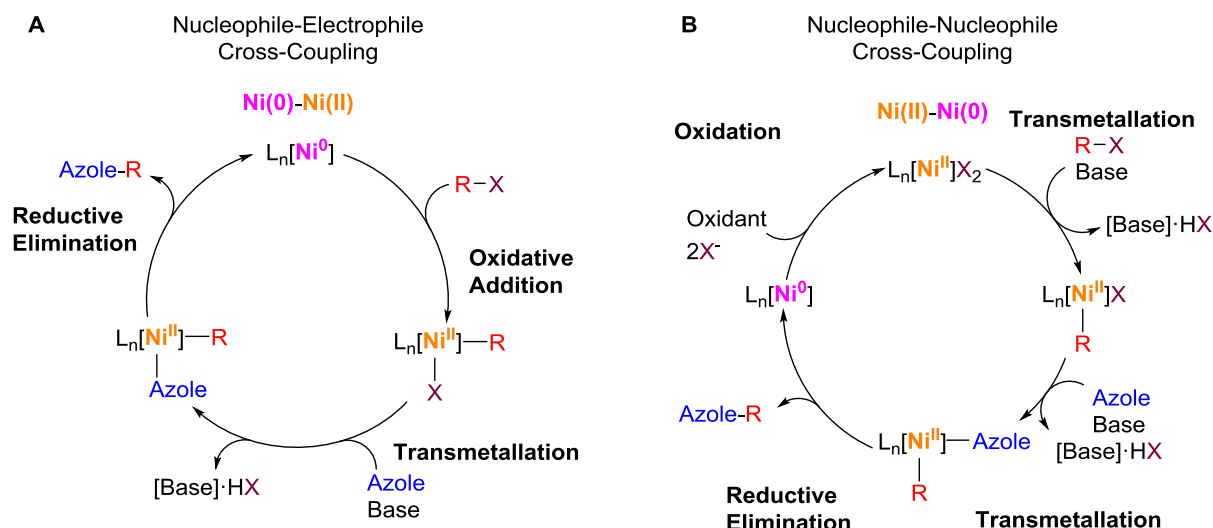
Scheme 84. Benzothiazole alkylation via C–H/C–H oxidative coupling catalyzed by nickel.

I.4. Mechanistic considerations

I.4.1. Catalytic cycles

Despite growth in the methodologies reported for the C–H functionalization of azoles, there is a noticeable lack of detailed studies of the mechanisms by which these reactions occur. Proposals for the operative mechanisms are at times made with no support other than mass and charge balance and intuitiveness, while others undertake some experiments to better understand one or another step of the reaction, but the focus of these experiments remains rather limited. The two most invoked mechanistic manifolds implicate either $\text{Ni}(0)/\text{Ni}(\text{II})$ ^{94,234,236–}

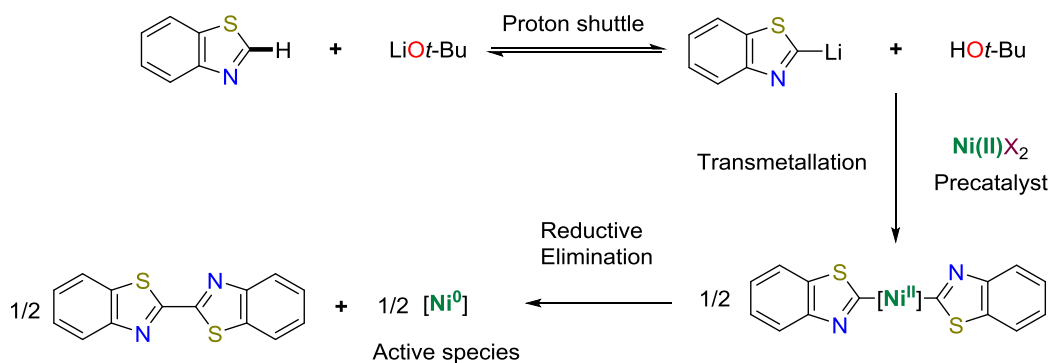
^{239,248,249} or Ni(II)/Ni(0)^{252,253,259,260} based mechanisms (Scheme 85). In particular, reactions between a nucleophile/electrophile pair (C–H/C–X couplings) are proposed to go through the former, while couplings between two nucleophiles go through the latter. It should be noted that, in decarbonylative reactions where extrusion of CO₂ takes place, the initial reagent is often an electrophile that is proposed to eliminate CO₂ and in situ generate a nucleophilic M–C that then interacts with the catalyst.^{252,253}



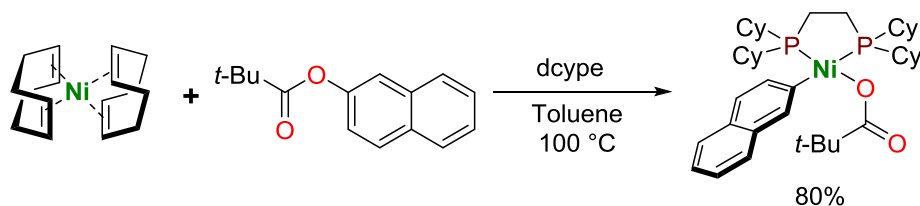
Scheme 85. Main proposed mechanistic manifolds: Ni(0)/Ni(II) (A) and Ni(II)/Ni(0) (B).

The popularity of these postulates is most likely their easy rational, inspired by historically well-known electron-pair transfers, based on second and third row transition metals such as nickel's 4*d* counterpart, palladium.

Mechanisms where a Ni(0) species is proposed to be the operative catalyst (Scheme 85, A) can either involve a direct source of Ni(0) – overwhelmingly [Ni⁰(COD)₂] – or, the in situ reduction of the Ni(II) precatalyst to the desired Ni(0) catalyst. To this effect, a chemical reductant such as Zn can be purposefully added – as observed for other Ni-catalyzed cross-couplings⁸⁴ – or the reduction can occur via oxidation of the reagents. This is supported by the common observation of oxidized subproducts, commonly substrate dimers.^{236,237,239,252} In particular, Itami and coworkers did a series of control experiments in the absence of the electrophilic coupling partner to try to elucidate the generation of the active species for their Ni^{II}(OAc)₂/bipy catalyst system for azole/haloaryl coupling (see Scheme 57, A).²³⁹ These experiments revealed that the formation of the dimerization product of that substrate (2,2'-bisbenzothiazole) in good yield (74% yield vs. Ni) in the sole presence of both the catalyst system and the base (Scheme 86). From these experiments it follows that a reduced nickel species (postulated to be a Ni(0) species) is in situ generated and this would be compatible with a classical Ni(0)/Ni(II) catalytic cycle.

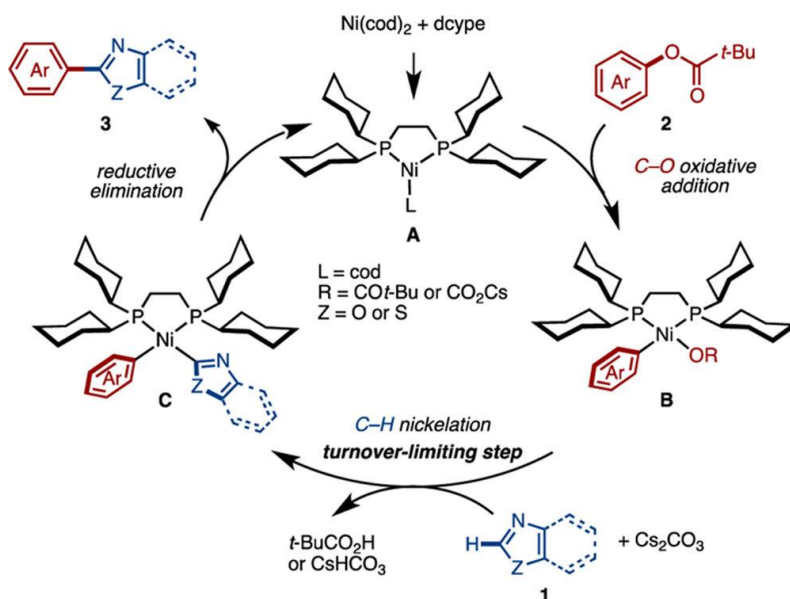
Scheme 86. Proposed catalyst generation by Ni(II)/Ni(0) by substrate dimerization.²³⁹

For the coupling of benzoxazole with 1-naphthyl *t*-butanoate catalyzed by $[\text{Ni}^0(\text{COD})_2]/\text{dcype}$ (see Scheme 69), Itami's group isolated a $[\text{Ni}^{\text{II}}(\text{naphthyl})(\text{OCO}t\text{-Bu})(\text{dcype})]$ oxidative addition intermediate (Scheme 87) that allowed them to carry on more detailed mechanistic studies.²⁷¹ Attempts to generate analogous complexes based on other phosphine ligands (PCy_3 , 1,2-bis(diphenylphosphino)ethane) showed the crucial role of this specific ligand in generating this intermediate.²⁷²



Scheme 87. Oxidative addition of 1-naphthyl pivalate to Ni(0) in the presence of dcype.

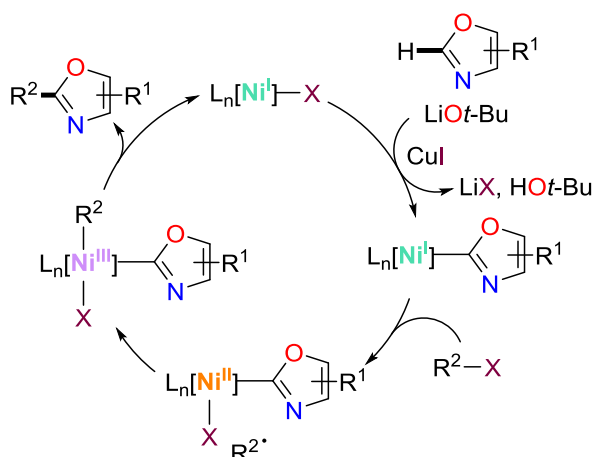
They further showed that this intermediate reacted with a stoichiometric amount of benzothiazole in the absence of a base to give the naphthyl-benzoxazole coupling product; the addition of base was found nonetheless to increase the yield. Importantly, this intermediate only behaved as an efficient catalyst in the presence of COD as an additive, most probably to stabilize the resting state of the catalyst. Finally, the determination of the rate orders of the reaction together with KIE measures demonstrated that the azole C–H bond breaking is the rate limiting step of the reaction. These combined investigations allowed them to propose the most comprehensive reaction mechanism for nickel-catalyzed azole C–H bond functionalization to date (Scheme 88).



Scheme 88. Reaction mechanism for C–H/C–O cross-coupling of azoles with aryl esters. Adapted from ref²⁷¹.

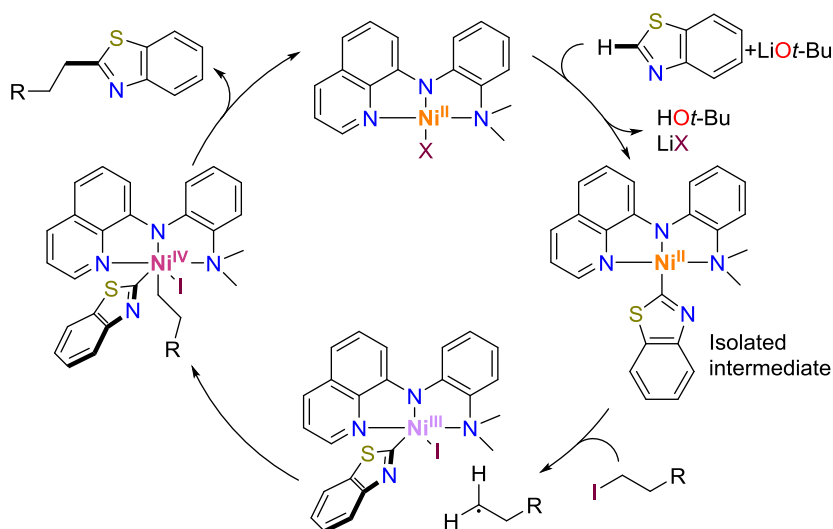
Reversely, Ni(II)/Ni(0) manifolds proposed generally for nucleophile-nucleophile cross-coupling can make use of widely available Ni(II) precursors but require oxidation of the Ni(0) species generated after the reductive elimination of the product (Scheme 85, **B**). This is achieved by the use of air or O₂ or addition of oxidant additives (air, O₂, CuF₂, Ag₂CO₃, AgOTf, BQ). Thus, the sensitivity to O₂ can be seen as distinguishing feature of the reactions filed under each of these manifolds.

However, there are proposals that escape the electron-pair manifolds and consider elemental steps involving odd-electron species. One example can be found in Ackermann and coworkers' proposal of a Ni(I)/Ni(II)/Ni(III) mechanism (Scheme 89) for their azole alkylation reaction (see Scheme 80).²⁶⁶ Although they offer no explanation for the generation of the active Ni(I) catalyst, they performed a series of radical clock experiments consistent with the involvement of an odd-electron manifold.



Scheme 89. Proposed Ni(I)/Ni(II)/Ni(III) pathway for the nickel-catalyzed direct alkylations of azoles.²⁶⁶

In contrast, Punji's group proposed a Ni(II)/Ni(III)/Ni(IV) mechanism for their *N,N,N*-Ni^{II}-catalyzed azole alkylation (see Scheme 81).²⁶⁷ Uniquely, they undertook a detailed mechanistic study based on the isolation of a rare Ni(II)-benzothiazolyl intermediate.²⁷³ Radical clock experiments and DFT calculations corroborated the involvement of radical species and the intermediacy of a Ni(III) complex, although unfortunately no experimental confirmation was provided for the intermediacy of a high-valent nickel species (Scheme 90).



Scheme 90. Catalytic cycle proposed for benzothiazole alkylation developed from the isolation of a Ni(II)-benzothiazolyl intermediate.

Lastly, You and collaborators proposed a Ni(I)/Ni(III) mechanism for their C–H/C–H alkylation (see Scheme 77) based on their observation of a possible Ni(III) intermediate by MALDI-TOF-MES.²⁶⁷ They proposed access to this Ni(III) state by the initial oxidation of Ni^I(OAc)₂ by Ag₂CO₃ to Ni^{III}X₃ (X = OAc or OPiv) which is proposed to be the active species. Oddly, their spin trapping experiments are inconsistent with a mechanism where the operative catalyst is a radical species, and no studies were carried out on the mechanism of their reaction.

I.4.2. Breaking the C–H bond

All the reactions presented above require the use of a base (*t*-butoxide, carbonate, phosphate) suggesting that none of these reactions do take place via “true C–H bond activation” (i.e. by oxidative addition).²⁷⁴ Interestingly however there is no clear trend between the strength of the base, azole acidity and yield (Figure 39). Some couplings work best with weaker carbonate bases that should be inefficient at deprotonating azoles. Likewise in some cases benzothiazole or benzoxazole cannot be converted, indicating that more electronic

effects other than acidity are at play. One remarkable trend is the need for a lithium alkoxide base for halogen electrophilic coupling partners whereas most carbon electrophiles prefer weaker carbonate or phosphate bases. Another trend is the prevalence of a high influence of the cation in all these reactions.

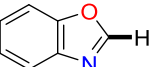
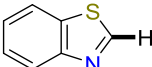
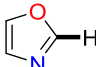
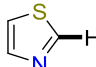
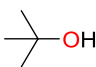
							H_3PO_4	H_2CO_3
$pK_a =$	24.4	27.0	27.1	29.0		24.4	2.2 7.2 12.3	6.4 10.3

Figure 39. First (C(2) position) pK_a values for azoles (DMSO, 25°C²⁷⁵ or theoretical value)²⁷⁶ and the conjugate acids of bases commonly used.^{149,277}

It is noteworthy that a few deuterium isotope labeling studies have focused on this step.^{239,261,265,273} In their study of azole coupling with haloarenes Itami and coworkers notably showed (see Scheme 58, **A**) that an equilibrium which involved the azole substrate and the alkoxide took place.²³⁹ Adding *t*-BuOD and interrupting the reaction led to the isolation of benzothiazole with a 58/42 H/D ratio. The observed H/D scrambling allowed them to propose that a chemical equilibrium between the azole and the lithiated azole would act as a proton shuttle (Scheme 86) and would allow a controlled release of a thermally unstable lithiated benzothiazole.

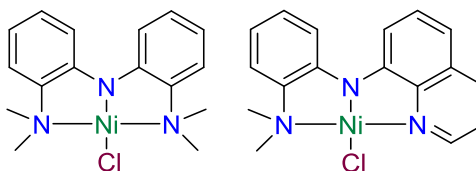
1.4.3. Heterogeneous vs. homogeneous catalysis

The harsh reaction conditions often necessary (sealed tubes, $T > 100\text{ }^\circ\text{C}$, systems under pressure) make all the more difficult to understand, not only the operation of the catalysts, but even their nature. Thus, the question is raised whether these are homogenous or heterogeneous catalysts.²⁷⁸

Researchers using well-defined complexes have paid some attention to this problem and a couple of examples exist in exploring this mechanistic feature. For instance, nickel-pincer complexes used for the alkylation of azoles (see Scheme 79 and Scheme 80) were subjected to, reaction mixture analyses, mercury drop poisoning and filtration experiments (Table 7).^{265,267} While Hu observed (by ^1H NMR analysis of the reaction mixture) the presence of free ligand, which suggested decoordination, Punji reported not observing free ligand by GC analysis of the reaction mixture. Filtration tests led to a diminished yield in the former's system, but had minimal effect in the latter's. Finally, both systems were investigated by the Hg drop poisoning test. Once again the yield of Hu's catalyst system was strongly reduced whereas Punji's system was not affected which points to two very different mechanisms operating

despite the similar starting structures of the (pre)catalysts: one acting as a homogeneous catalyst, the other acting as a precatalyst that in situ would generate the active catalyst in the form of metal particles. It is important however to stress that no controls for the Hg poisoning test were reported although this test is known for giving false positive results.^{††}

Table 7. Homogeneous or heterogeneous catalysis: the case of two *N,N,N*-nickel pincer complexes.



Tests	Observations	
Reaction mixture	Free ligand	Complex
Filtration test	Yield loss	Yield unaffected
Hg poisoning test	Yield loss	Yield unaffected
Conclusion	Heterogeneous	Homogeneous

1.5. Overview

Analysis of the literature show a few trends: nickel precursors are largely comprised of $[\text{Ni}^0(\text{COD})_2]$ or $\text{Ni}(\text{II})$ salts mixed in situ with ligands. These ligands have been overwhelmingly off-the-shelf nitrogen (bipy, phen, etc) or phosphine (dcype, dppf, dcypt) chelating ligands. It is surprising to observe a lack of NHC ligands, given their widespread presence in Ni-catalyzed C–H bond functionalization^{11,12,279} and the thermal robustness associated with M–NHC complexes, especially in light of the harsh reaction conditions commonly employed here (pressure, $T > 100\text{ }^\circ\text{C}$). High sensitivity to the base and its counter-cation is observed but poorly understood. A number of diverse coupling partners has been shown to successfully work: from halogens to diverse phenol derivatives and carbonyl electrophiles. Nucleophiles (boranes, silanes) were also demonstrated as viable partners, and even the challenging C–H/C–H dehydrogenative oxidative cross-coupling is accessible. These methodologies have

^{††} The Hg poisoning test is one of the most commonly employed experiments used to determine if a metal catalyst acts as a homogenous or heterogeneous catalyst.²⁷⁸ This is based on Hg^0 forming amalgams with other $\text{M}(0)$ metals (namely group 10 metals), which would cause a loss of catalyst concentration in the reaction media and thus a loss of yield. However, a requirement for this test to be valid is that that Hg^0 does not also react with molecular complexes, which can also lead to a loss of yield (false positive).³⁵⁷ Although, Hg^0 is often inert towards molecular metallic species it is advisable to run control experiments to test this behavior for each specific system.

been used in selected examples of complex molecules showing their validity beyond model substrates.

However, there is a very limited understanding of the mechanisms governing these reactions, the reaction conditions are often very harsh and the catalysts often show low activities and thus require high catalyst loadings. Furthermore, there is little diversity on the ligand scaffolds utilized in these reactions. The very frequent use of in situ generated catalysts make the understanding of the reactions all the more challenging.

The domain has therefore two main challenges: increasing catalyst activity and using milder reaction conditions. These challenges are opportunities for the increased development of well-defined complexes in these reactions. They indeed afford a better control of the catalyst properties that should allow more efficient generation of the catalyst species, and thus lower catalyst charges and milder reaction conditions. In addition, the precise structural control of the (pre)catalysts should allow much more structural diversity than pnictogen chelating ligands, which may afford novel reactivity. But, perhaps the most important bottleneck to either of these issues is the lack of clear understanding of the mechanisms these reactions operate by. Fundamental studies involving well-defined intermediates have shown to be crucial to map out the elemental steps taking place. It would therefore be very useful if high performing well-defined complexes were developed as they provide a better starting platform for a systematic study than a complex mixture, from which even the initial steps are complex to parse out.

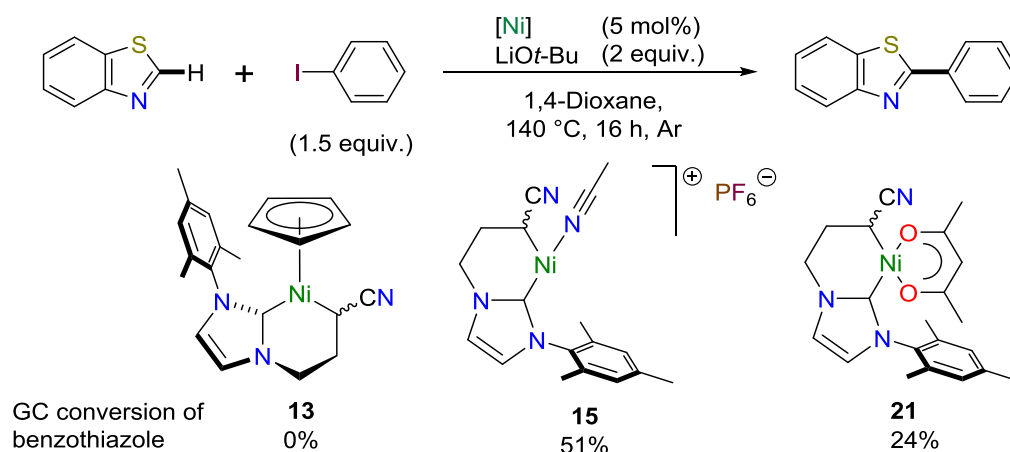
These opportunities are a good fit for the new cationic $C_{\text{NHC}}, C_{\text{alkyl}}$ -chelating nickel(II) complexes described in Chapter 2. The C,C chelates mimic the chelating ligands often used but bring a different electronic and steric environment. Notably, they are equipped with a NHC ligand that may potentially stabilize the catalysts under the harsh reaction conditions often required for azole direct coupling thus possibly allowing for higher turnover numbers. In addition, the structural variation of the nickelacycles can afford an understanding on the parameters governing the reaction works and thus give some clues how to improve catalyst performance.

II. Results and discussion

II.1. Benzothiazole C_{sp^2} cross-coupling

We initially focused our attention on the coupling of benzothiazole with iodobenzene. We took the conditions laid out by Itami's group – $Ni^{II}(\text{OAc})_2/\text{bipy}$ (1:1 ratio, 10 mol%) in 1,4-dioxane at 140 °C in the presence of LiOt-Bu , see Scheme 58, **A**. We applied some minor

modifications (lower catalyst loading – 5 mol%, use of excess of iodobenzene)^{‡‡} to test a series of our complexes bearing the developed $C_{\text{NHC}}, C_{\text{alkyl}}$ -nickelacyclic motif (**13**, **15**, $[\text{Ni}^{\text{II}}(\text{acac})\{\text{Mes-NHC}-(\text{CH}_2)_2\text{CH}(\text{CN})\}]$ (**21**), Scheme 91). The obtained results showed the inactivity of electron-rich half-sandwich complex **13**. In contrast, the unsaturated complexes **15** and **21** allowed 51 and 24% conversion of benzothiazole, respectively. The importance of an easily accessible coordination sphere was highlighted with the tripling of performance of **15** vs. **21**; thereby validating our strategy of Cp removal (see Chapter 2).

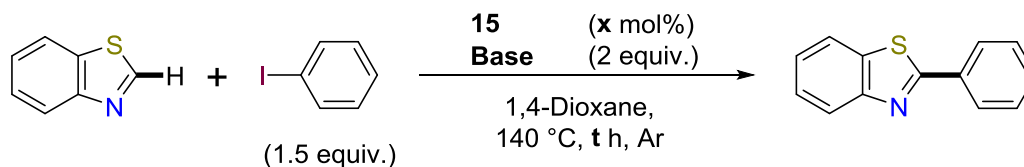


Scheme 91. Precatalyst screening for benzothiazole direct functionalization with iodobenzene. GC conversion values (%) are the average of at least two runs.

Adopting the best performing complex **15**, selected reaction parameters were varied (Table 8) from the benchmark conditions (entry **1**). First, lowering the reaction temperature to 90 °C led to no conversion (entry **2**). Increasing the number of equivalents (3 equiv.) of iodobenzene did not alter the conversion (entry **3**), indicating that a competing dehalogenation reaction is not limiting the reaction. The effect of catalyst charge was then studied (entries **4-6**). Lowering the catalyst charge to 3 mol% (entry **4**) halved the conversion. In contrast, doubling to 10 mol% did not provide significantly better conversion (entry **5**), and further increasing it to 15 mol% proved highly detrimental to the conversion (entry **6**), possibly by favoring competing reactions. Increasing the reaction time to 18 h (entry **7**) proved beneficial achieving 69% conversion. Next, a series of bases was screened (entries **8-15**). The obtained results clearly show the importance of LiOt-Bu as the sole fitting base for this reaction, as no coupling was observed for any other base studied. Changing the alkali cation (entries **8** and **9**) led to no conversion, demonstrating the importance of lithium as a counter-cation.

^{‡‡} Iodobenzene was used in excess to avoid competing dehalogenation reaction.²⁸⁸

Table 8. Optimization of the reaction conditions of benzothiazole direct functionalization with iodobenzene.



Entry	T (h)	Base	x (mol%)	Conversion (%) ^{a, b}
1	16	LiO <i>t</i> -Bu	5	51
2^c	16	LiO <i>t</i> -Bu	5	0
3^d	16	LiO <i>t</i> -Bu	5	51
4	16	LiO <i>t</i> -Bu	3	26
5	16	LiO <i>t</i> -Bu	10	56
6	16	LiO <i>t</i> -Bu	15	15
7	18	LiO <i>t</i> -Bu	5	69
8	18	NaO <i>t</i> -Bu ^e	5	0
9	18	KO <i>t</i> -Bu ^e	5	0
10	18	Cs ₂ CO ₃	5	0
11	18	K ₃ PO ₄ ^f	5	0
12	18	KOAc ^f	5	0
13	18	NaOH	5	11 ^g
14	18	LiOH	5	0
15	18	NEt ₃	5	0
16	36	LiO <i>t</i> -Bu	5	78

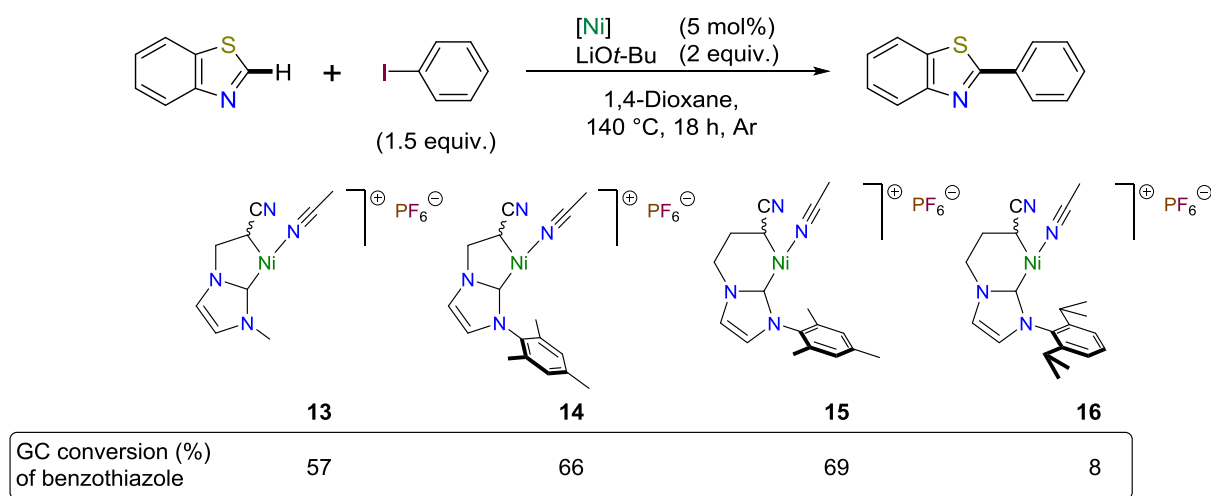
^a Average value of at least two runs. ^b GC conversion (%) of benzothiazole. ^c Reaction ran at T = 90 °C. ^d 3 equiv. of iodobenzene. ^e Purified by sublimation before use. ^f Activated by heating to 150 °C and cooling under Ar. ^g No conversion to coupling product.

Weaker inorganic bases (entries **10-12**) and hydroxides (entries **13-14**) also gave no conversion, even when bearing the lithium cation (entry **13**). Organic base NEt₃ (entry **14**) was also ineffective. Finally, allowing the reaction to proceed until 36 h (entry **16**) allowed to increase the conversion to 78%.

With these optimized conditions in hand (Table 8, entry **7**)^{§§} we compared the activities of the different cationic C_{NHC}, C_{alkyl}-nickelacycles **13-16** in this reaction (Scheme 92). Both five-

^{§§} For practical reasons, a reaction time of 18 h was chosen instead of the optimal 36 h.

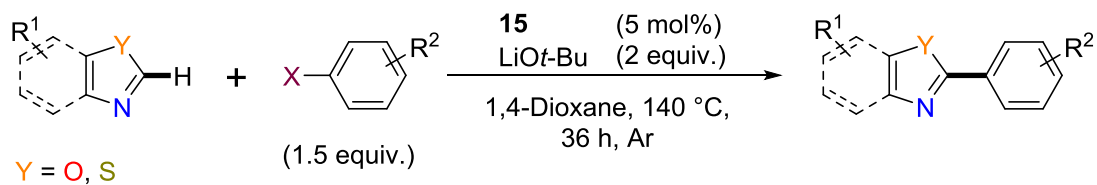
membered metallacycles **13** and **14**, showed moderate to good conversions (57 and 66%), with the *N*-mesityl substituted **14** being the better of the two. Interestingly, comparison with the benchmark **15** shows essentially no effect of the metallacycle size on conversion. Finally, the bulkier **16** shows a very poor 8% conversion. While steric bulk might contribute to this disappointing result, such a large difference from **15** is striking and might instead suggest catalyst deactivation by ligand degradation as the reason for such a poor conversion.²⁸⁰ In summary, the metallacycle size seems to have little influence on the reaction but *N*-mesityl substituted NHCs give the highest conversions.



Scheme 92. Screening of $[\text{Ni}^{\text{II}}\{\text{R-NHC}-(\text{CH}_2)_n\text{CH}(\text{CN})\}(\text{NCMe})]\text{PF}_6$ complexes **13-16** for the direct coupling of benzothiazole and iodobenzene. GC conversion (%) values are the average of at least two runs.

We thus reprised **15** and the optimized conditions (Table 8, entry **16**) and studied the scope of heteroarylation of different haloarenes and N,chalcogen-azoles (Table 9). A difference in substrate conversion (78%) and isolated product yield (43%) can be seen in the coupling of benzothiazole and iodobenzene (entry **1**). This suggests that competing reactions take place during the reaction. No conversion was observed when using chlorobenzene or 4-bromotoluene (entries **2** and **4**). The addition of alkali metal iodides (NaI, KI) to the coupling with 4-bromotoluene, for in situ formation of the iodoarene,²⁸¹ did not lead to substrate conversion (entry **5**). The electronic effect of different substituents in the *p*-position of iodobenzene was then studied (entries **3**, **6-9**).

Table 9. Azole and haloarene scope. Conversion of benzothiazole measured by GC. Yields are isolated yields.



Entry	Azole	Aryl halide	X	Conversion (%) ^{a, b}	Yield (%) ^{a, b}
1			I	78	43
2			Cl	0	-
3			I	56	47
4			Br	0	-
5 ^d			Br	0	-
6				35	25
7				68	58
8				49	45
9				-	14
10				-	13
11				-	0
12				-	n. d. ^e
13				-	n. d. ^e
14				-	17
15				-	11
16				-	0

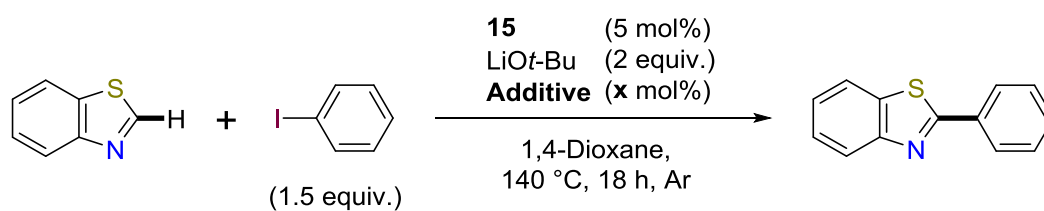
^a Average value of a minimum of two runs. ^b GC conversion of benzothiazole. ^c Isolated yield. ^d Reactions ran in the presence of NaI or KI (1 equiv.) ^e n. d. – Not determined.

Mild electron-donating –Me substituent (entry **3**) gave a moderate conversion and isolated yield (47%). The stronger electron-donating –OMe group (entry **6**) was much less reactive, giving low 35% conversion and 25% isolated yield. Electron-withdrawing –CF₃ (entry **7**) gave the best result with a moderate 58% isolated yield. However, –CN (entry **8**) gave a yield similar to iodobenzene (45% isolated yield), and –Cl (entry **9**) gave a poor 14% isolated yield. It should be noted that these last two examples might be “non-innocent”: the cationic C_{NHC}, C_{alkyl}-nickelacycles **13-16** have shown a great affinity to nitrile groups which might compete with the reactive iodide; and these complexes have shown some intolerance to chlorinated molecules (entry **2** and see Chapter 2). Also, only the iodide position was reactive forming exclusively the 2-(4-chlorobenzene)benzothiazole product. We then assessed if *o*-substituted iodoarenes could be coupled (entries **10** and **11**). A poor isolated yield (13%) was obtained when using a *o*-Me substituent (entry **10**), and no coupling product was observed when an *o*-Ph group was introduced (entry **11**). We then studied the scope of azoles in this reaction (entries **12-16**). Arylation of simple thiazole (entry **12**) and oxazole (entry **13**) were unselective and gave complex mixtures of coupling products. Blocking the C(4) and/or C(5) position of these azoles (entries **14** and **15**) gave the desired coupling products in low isolated yields (17-11%). Surprisingly, benzoxazole (entry **16**) showed no reactivity in these reaction conditions.

Disappointingly this catalyst system has proven to be neither very active, with isolated yields being moderate at best, nor broadly applicable, with only benzothiazole and a limited set of iodoarenes being moderately coupled. Oddly, although benzothiazole is often a more challenging substrate to couple than benzoxazole, it was the most reactive here.

A series of mechanistic tests was carried out as a way to overcome the limitations of the present catalytic system (Table 10). Coligand acetylacetonate (acac, entry **1**) was added to test the importance of keeping open coordination positions or inversely of facilitating the stabilization of the catalyst resting state after it was formed, and was found to fully quench the reaction. Interestingly, this contrasts with what is observed in the early catalyst screening (see Scheme 91) where **21** was still somewhat active in the reaction. This leaves open whether the acac anion deactivated the in situ generated active species or, if the presence of K⁺ in the mixture interferes with the reaction, given the high sensitivity to the base's counter-cation observed earlier (see Table 8). Furthermore, hypothesizing that the catalyst's solubility could be an issue, MeCN was added, but resulted in no improvement was observed (entry **2**). Finally, the radical initiator azaisobutyronitrile (AIBN) was added, revealing the system's sensitivity to radicals by reducing the conversion (entry **3**). This radical initiator could however not trigger the reaction in the absence of nickel complex **15** (entry **4**).

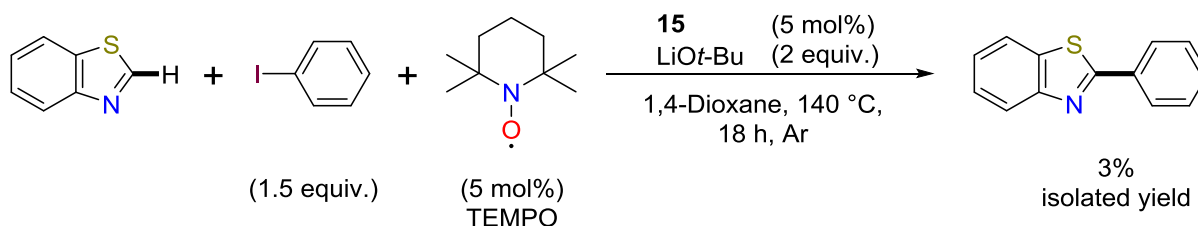
Table 10. Effect of additives in the coupling of benzothiazole and iodobenzene.



Entry	Additive	x (mol%)	Conversion (%) ^{a, b}
1	K(acac)	5	0
2	MeCN	10	56
3	AIBN	5	36
4	AIBN	5	0 ^c

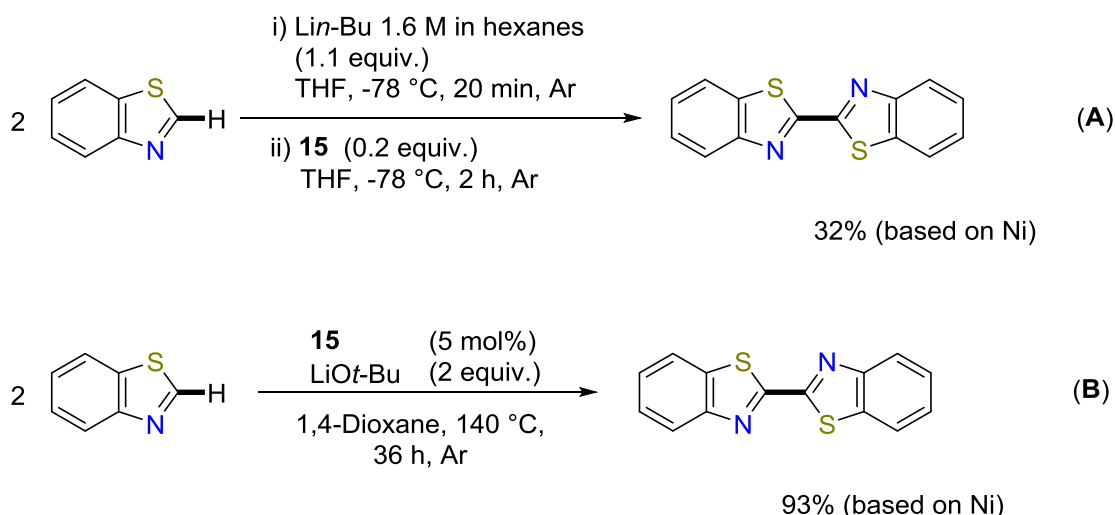
^a Values are an average of at least two runs. ^b GC conversion (%) of benzothiazole. ^c No **15** used.

Developing on this sensitivity to radicals, we then ran a radical trap experiment using the free radical 2,2,6,6-tetramethylpiperidin-1-yl)oxyl (TEMPO). Even with catalytic amounts (5 mol%) of the latter, the reaction was fully quenched (Scheme 92). This reinforced the hypothesis of the involvement of radical species in the reaction mechanism, put forward above (see Table 10).

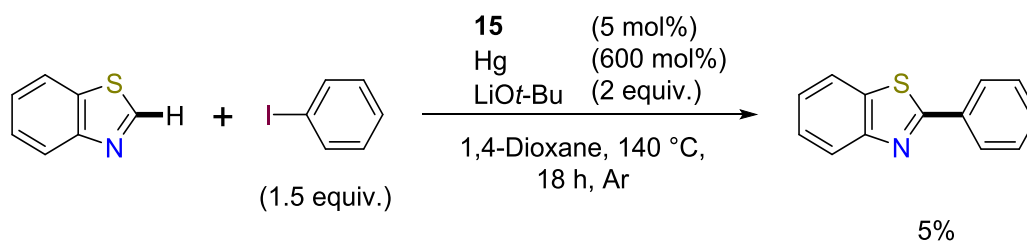


Scheme 93. Radical trap experiment using TEMPO.

Furthermore, detailed analyses of the reaction mixture identified the systematic formation of a small amount (< 5% yield) of 2,2'-bisbenzothiazole as a byproduct. The formation of this product suggested the initial reduction of the Ni(II) precursor to a Ni(0) species akin to what was postulated by Itami et al.²³⁹ (see Scheme 86). To test this hypothesis we carried out a control experiment using a substoichiometric amount of nickel complex with freshly prepared lithiated benzothiazole. The formation of 2,2'-bisbenzothiazole was observed in 32% yield vs. Ni (Scheme 94, **A**). To confirm whether this mechanism would be operable under our reaction conditions we then ran a control experiment in the absence of iodobenzene (Scheme 94, **B**). The dimer, 2,2'-bisbenzothiazole, was obtained as a product in 93% yield based on Ni. Despite the high efficiency in consuming nickel, the reaction does not proceed to consume all the benzothiazole. This is consistent with the dimerization taking place at the start of the reaction, possibly acting as a catalyst activation step.

Scheme 94. Dimer formation by **15** (A) and control experiment in the absence of iodobenzene (B).

To obtain further insight into the mechanism, we sought to determine the nature of the reduced nickel species generated from benzothiazole dimerization; as a molecular low-valent Ni species or, as metallic particles. For that purpose, we conducted a Hg poisoning experiment. Thus, carrying out the coupling of benzothiazole with iodobenzene in the presence of 120 equiv. of Hg (relative to nickel) led to the formation of 2,2'-bisbenzothiazole in the same proportions as in a typical catalytic run (Scheme 95). However, almost complete inhibition of the heterocoupling was observed thus suggesting that a process catalysed by nickel particles could follow the initial reduction of the nickel(II) precatalyst.^{***}



Scheme 95. Mercury drop poisoning test.

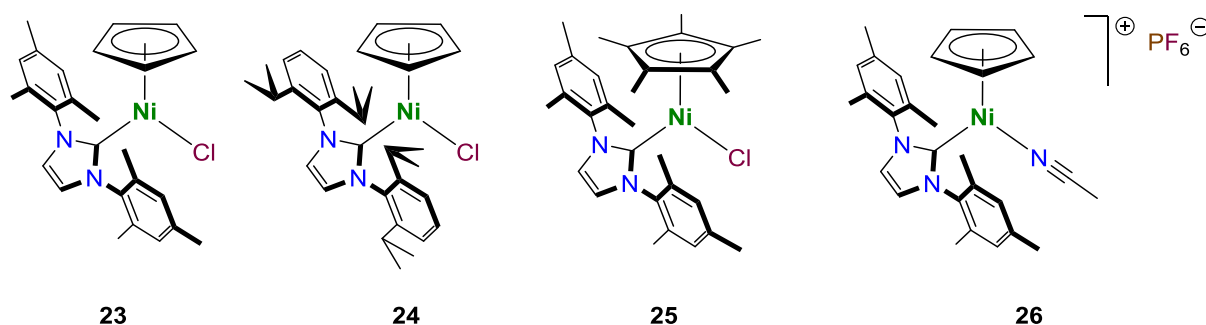
These results paint a complex mixture at play in this catalytic reaction. If it seems that the reaction starts by sacrificial substrate dimerization to generate a reduced Ni(0) species, this species' role is unclear. The Hg poisoning test is wholly consistent with the generation of

^{***} We present no control experiment to account for the possible reaction between a putative Ni(0) molecular species with Hg(0) (see page 139, footnote †† for a discussion of this problematic) in lieu of an amalgam formation as we were only made aware of this possibility during the preparation of this manuscript.

a Ni(0) species, likely heterogeneous metal particles, but this fails to explain the high sensitivity to the presence of free radicals. Albeit purely speculative, this suggests that the Ni(0) species would not be the active catalyst but that it might undergo disproportionation reactions²⁷ to generate the true catalyst species as a radical species.

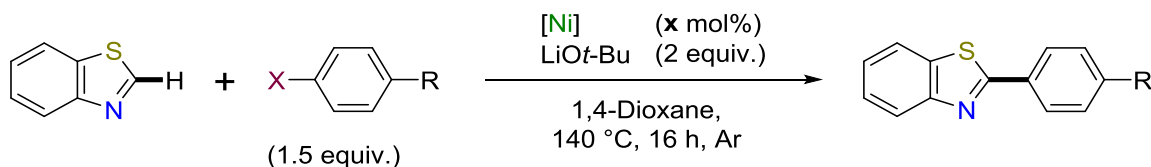
II.2. Benzothiazole C_{sp}³ cross-coupling

In parallel to the study of the C_{NHC}, C_{alkyl}-nickelacycles' activity for the direct arylation of azoles, we also tested a set of acyclic half-sandwich Ni(II)-NHC complexes [Ni(Cp[†])L(NHC)]⁽⁺⁾, which had previously been successful in the C–H arylation of ketones.⁸⁶ Thus we tested the complexes [NiCl(Cp)(NHC-Mes₂)] (**23**),¹⁴⁷ [NiCl(Cp)(NHC-DIPP₂)] (**24**),¹²⁶ [NiCl(Cp^{*})(NHC-Mes₂)] (**25**) (Cp^{*} = η⁵-C₅Me₅ = 1,2,3,4,5-pentamethylcyclopentadienyl)¹²³ and [Ni(Cp)(NHC-Mes₂)(NCMe)]PF₆ (**26**) (Scheme 96),¹²⁴ for the coupling of benzothiazole with iodobenzene or 4-bromotoluene under similar conditions, but, to our disappointment, all complexes proved totally inactive in the direct arylation of benzothiazole (Table 11).



Scheme 96. Selected half-sandwich Ni(II)-NHC [Ni(Cp[†])L(NHC)]⁽⁺⁾.

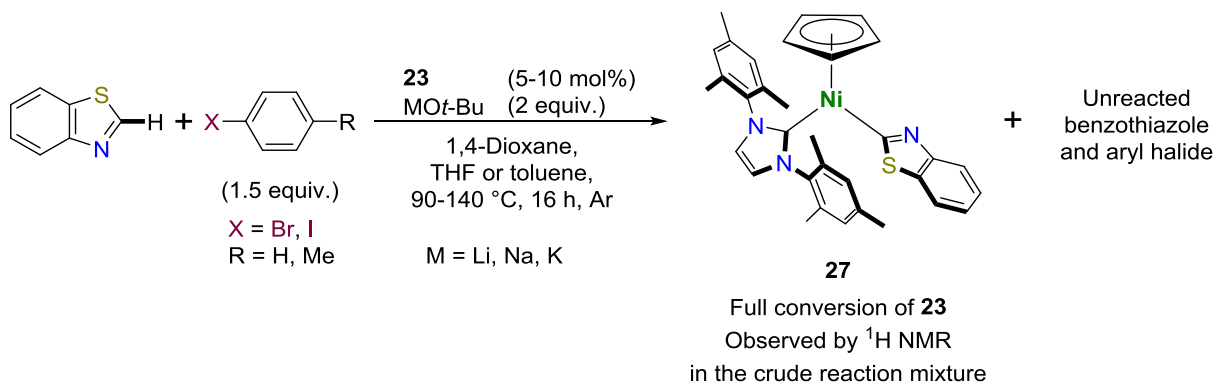
Intrigued by the incapacity of the [Ni(Cp[†])L(NHC)]⁽⁺⁾ complexes to catalyze these direct couplings, we attempted to establish the fate of the latter under the reaction conditions. To our surprise, the ¹H NMR spectra of the reaction media (after removal of the insoluble and volatiles) of reactions run with **23** (5 or 10 mol%) under various conditions of solvent (THF, toluene or 1,4-dioxane), base (LiO*t*-Bu, NaO*t*-Bu, KO*t*-Bu) and temperature (from 90 to 140 °C) systematically indicated the presence of unreacted benzothiazole and 4-bromotoluene or iodobenzene as well as the full and clean conversion of **23** to a novel [Ni^{II}L(Cp)(NHC-Mes₂)] complex **27** bearing a C(2)-metallated benzothiazolyl (btz) group (Scheme 97), the identity of which was confirmed by an independent synthesis (*vide infra*).

Table 11. Attempted coupling of benzothiazole with aryl halides in the presence of $[\text{NiCp}^+\text{L}(\text{NHC})]^{(+)}$ complexes.

Entry	Complex	x (mol%)	X	R	Conversion (%) ^a
1	23	5	Br	Me	0 ^b
2	23	10	Br	Me	0 ^b
3	23	5	I	H	0
4	23	10	I	H	0
5	24	5	I	H	0 ^c
6	25	5	I	H	0 ^c
7	25	10	I	H	13
8	26	5	I	H	0

^a GC analysis of benzothiazole, value is the average of two runs. ^b T = 120 °C. ^c LiOt-Bu (1.5 equiv.)

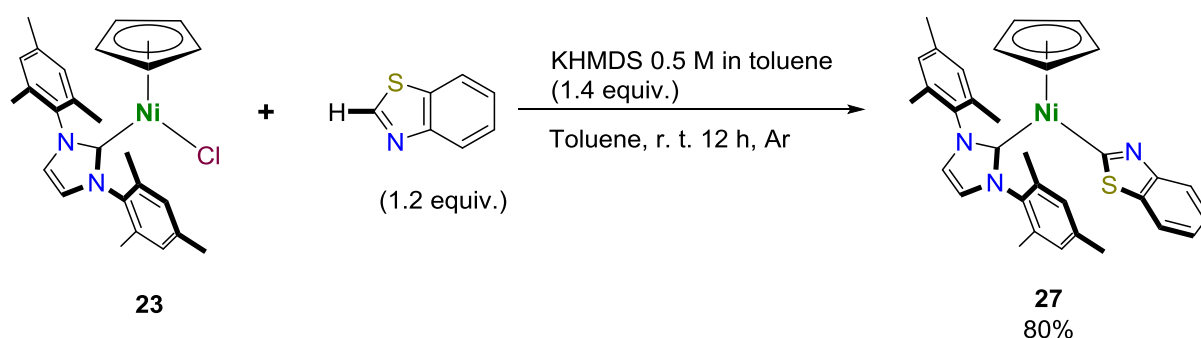
The latter was indeed characterized by typical signals of the NHC-Mes₂ and Cp ligands, but which were shifted compared to those of **23**, as well as by two apparent triplets centred at 7.11 and 6.97 ppm, which integrate for one proton each relative to the Cp and NHC-Mes₂ signals and correspond to the H(5) and H(6) protons of a benzothiazolyl unit. However, the signals of the H(4) and H(7) overlapped with those of unreacted benzothiazole and were not unambiguously observed.



Scheme 97. Benzothiazolyl trapping under catalytic conditions.

Interestingly, although C(2)-benzoxazolyl or benzothiazolyl complexes are often proposed as intermediates in C–H/C–X couplings between heteroarenes and aryl, alkenyl or alkyl electrophiles,^{237,239,248,249,271,273,282–284} they remain very rare. We are indeed aware of only four related *P,C,N*-Pd^{285–287} and *N,N,N*-Ni²⁷³ pincer species, which have been isolated with a benzothiazolyl ligand and demonstrated to be intermediates in similar couplings. Thus, although it obviously constitutes a potential energy well, complex **27** is an interesting example of azolyl trapping in such (attempted) direct coupling.

To confirm the identity of **27**, complex **23** was treated with a small excess of benzothiazole (1.2 equiv.) in the presence of KHMDS as a base in toluene at room temperature (Scheme 98). The resulting complex was isolated in 80% yield as an air-stable green-brown powder after work-up. Full characterization by ¹H and ¹³C {¹H} NMR, HRMS spectroscopies and CHN microanalyses confirmed the expected formulation. Thus, for instance, the ¹H NMR spectrum of **27** no longer displays the H(2) proton of benzothiazole, but displays the H(5) and H(6) protons as two apparent triplets at 7.12 and 6.98 ppm, as seen in the spectra of the catalytic attempts (vide supra), and the H(4) and H(7) protons as two doublets at 7.58 and 7.51 ppm. The Cp and NHC-Mes₂ protons are found at typical values for Ni^{II}Cp(NHC) compounds.^{86,124,135,147,288–290} Regarding the ¹³C {¹H} NMR spectrum, the C(2) carbon of the benzothiazolyl moiety is observed at 176.0 ppm, which is significantly downfield when compared to the corresponding carbon of benzothiazole (153.8 ppm),²⁹¹ and thus confirms its metallation.²⁷³ In addition, it is worth mentioning that the C_{NHC} signal of **27** is downfield shifted (177.9 ppm) when compared to that of **23** (165.9 ppm),¹⁴⁷ which likely indicates a decrease in the Lewis acid character of the nickel centre caused by an increase in the σ -donor ability of the ancillary ligand,^{71,292–294} similarly to what is observed with the phenyl and methyl derivatives: [Ni^{II}(Ph)(Cp)(NHC-Mes₂)] (181.2 ppm)⁸⁶ and [Ni^{II}(Me)(Cp)(NHC-Mes₂)] (187.4 ppm).¹⁴⁷



Scheme 98. Synthesis of half-sandwich Ni(II)-NHC benzothiazolyl complex **27**.

A single crystal X-ray diffraction study of complex **27** corroborated the NMR data and confirmed the molecule's structure (Figure 40). Key bond distances and bond angles are listed

in Figure 40 and selected crystallographic data and data collection parameters can be found in the Experimental section. Complex **27** crystallizes in the orthorhombic chiral space group $P2_12_12_1$. The Ni–C(1) distance [C(1) = the carbene carbon atom] and Ni–C(2) distances are respectively 1.873(2) and 1.875(2) Å, which falls slightly below the range observed for related [Ni(L)(Cp)(NHC-Mes)₂] complexes bearing a third C-bound ligand, such as [Ni(Ph)(Cp)(NHC-Mes₂)] (Ni–C(1): 1.875(2), Ni–C(2): 1.908(2) Å)⁸⁶ and [Ni(Cp)(NHC-Mes₂)(NHC-Me₂)]BF₄ (Ni–C(1): 1.899(3), Ni–C(2): 1.906(3) Å).¹²⁵ Similarly, the C(1)–Ni–C(2) angle of 94.26(10)° also falls slightly below the range observed for [Ni(Ph)(Cp)(NHC-Mes₂)] (95.35(9)°)⁸⁶ and [Ni(Cp)(NHC-Mes₂)(NHC-Me₂)]BF₄ (96.91(11)°).¹²⁵ This might indicate a slightly smaller steric pressure exerted by the benzothiazolyl ligand compared to a phenyl or NHC-Me₂ ligand. Of note, the Ni–C(2) distance is also significantly shorter than that observed in the only other fully characterized Ni–C(2)-benzothiazolyl complex (1.936(8) Å), that was just reported.²⁷³ Finally, when one considers the plane formed by the Cp centroid, C(1), and C(2), the nickel atom is essentially in a planar environment as is typically observed in similar two-legged piano-stool NiCp(NHC) complexes.^{86,124,135,147,288–290}

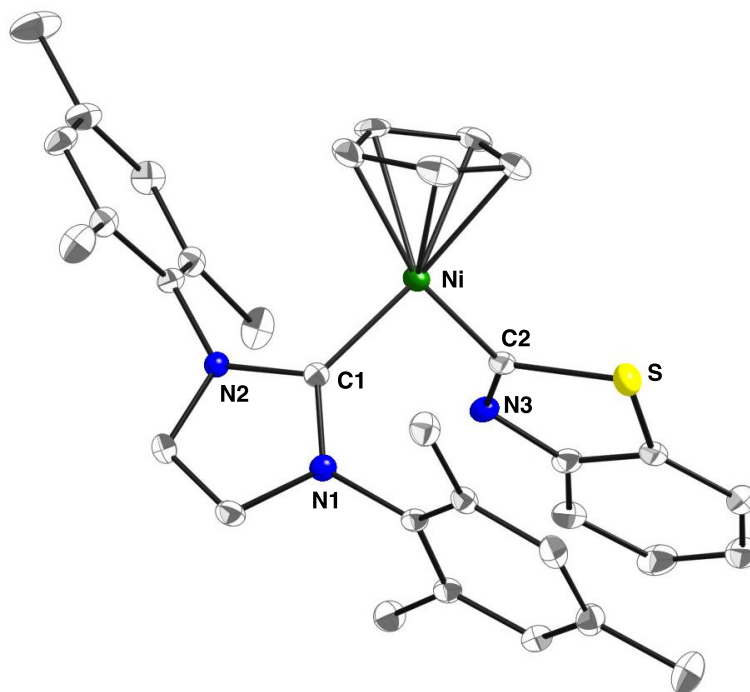
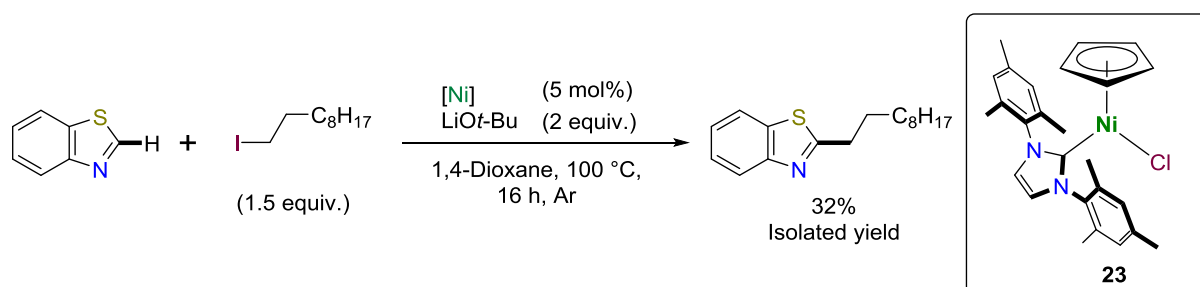


Figure 40. Molecular structure of **27** showing all non-H atoms. Ellipsoids are shown at the 50% probability level and key atoms are labelled. Selected bond distances (Å) and angles (°) with esd's in parentheses: Ni–C(1), 1.873(2); Ni–C(2), 1.875(2); Ni–Cp_{cent}, 1.774; Ni–Cp_{av},^b 2.140; C(1)–Ni–C(2), 94.26(10); C(1)–Ni–Cp_{cent}, 135.3; C(2)–Ni–Cp_{cent}, 130.4; Ni–(C(1)–Cp=C(2)), 0.037. ^a Cp_{cent} = centroid of the Cp group. ^b Average Ni–C distance to the Cp ring.

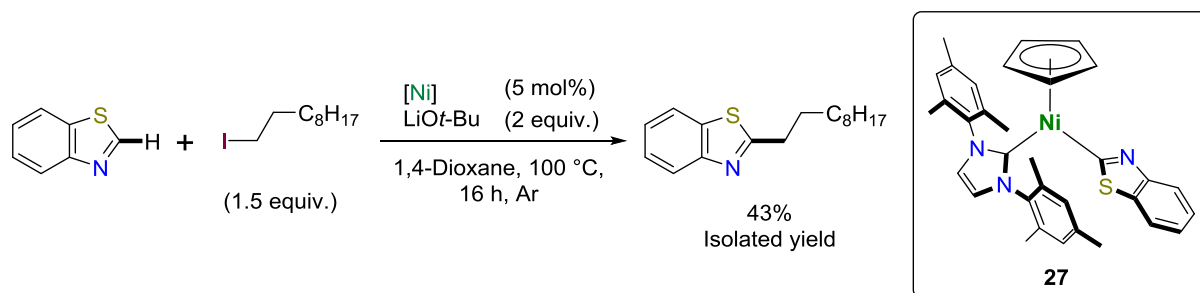
The thermal stability in solution of complex **27** is remarkable when the harsh reaction conditions (pressure, 140 °C, 36 h) under which it was first formed are considered. This stability can be related to that observed for bis-NHC $[\text{Ni}^{\text{II}}(\text{Cp})(\text{NHC}^1)(\text{NHC}^2)]^+$ complexes¹³⁰ and the nickelacycles **9-12**. Furthermore the inertness of this intermediate is again in line with the hypothesis that a labile coordination position is required in these half-sandwich platforms to be reactive.

At this time we became aware of a report detailing mechanistic studies by Punji's group²⁷³ on a square planar Ni-benzothiazolyl complex isolated as a reaction intermediate in the catalytic alkylation of azoles (see Scheme 90). We thus decided to test whether complex **23** would react as a catalyst for azole alkylation despite being inert in arylation reactions. Using the same reaction conditions developed by Punji (benzothiazole (0.5 mmol), iodoalkane (1.5 equiv.), complex (5 mol%), LiOt-Bu (2 equiv.) in 1,4-dioxane (1 cm³) heated to 100 °C for 16 h; see Scheme 80)²⁶⁷ we were delighted to see that the coupling of benzothiazole with 1-iododecane took place in low yield (Scheme 98). The difference in reactivity was to us very surprising given the inertness of complex **23** in benzothiazole arylation. However, it has been highlighted that the mechanism at play (namely odd- or even-electron based) can be determined by the coupling partner (vide supra, I.4. Mechanistic considerations).²⁹⁵



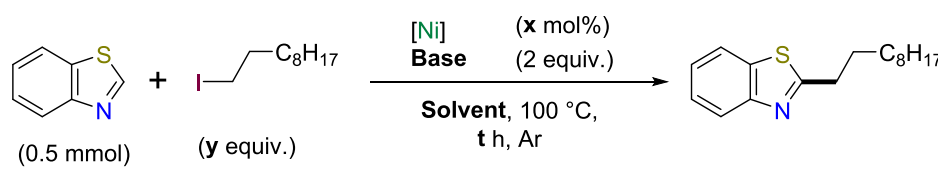
Scheme 99. First Ni-NHC alkylation of benzothiazole.

Excited by this result, but wary that our observed putative intermediate **27** would in fact be inert in the reaction, we decided to test it in the alkylation reaction. To our delight it proved to be even more efficient than complex **23** (Scheme 100). Furthermore, a control experiment in the absence of any nickel complex gave no yield, as observed by GC, allowing us to affirm that indeed the nickel-NHC complexes are needed for the reaction to take place.

Scheme 100. Alkylation of benzothiazole catalyzed by **27**.

With a potentially interesting reaction at hand we decided to begin optimizing the reaction parameters (Table 12). From the initial reaction conditions (entry **1**) we began by reducing the excess of iodoalkane (entry **2**), which led to a large drop of the yield (-24%). We then screened a series of inorganic bases (entries **3-8**). Varying the counter-cation from Li⁺ (entry **1**) to Na⁺ (entry **3**) or K⁺ (entry **4**) led to no product formation, as for the benzothiazole arylation reaction (vide supra), but showed a high conversion of benzothiazole. ¹H NMR analysis of the crude reaction mixtures reveals, in addition to peaks attributable to unreacted chemicals, small amounts of mixtures in the aromatic region and large indistinguishable peaks in the aliphatic region. We then tried common alternative bases, such as Cs₂CO₃ (entry **5**) and K₃PO₄ (entry **6**) both of which failed to give the coupling product, but also showed only minor benzothiazole substrate conversion. Given the importance that Li⁺ has shown, we then sought to use other Li bases such as Li₂CO₃ (entry **7**) and LiOH (entry **8**), but these two were also ineffective. Then we looked to see whether the acyclic ether DME (entry **9**) or the hydrocarbon toluene (entry **10**) could also be suitable for this reaction, but they resulted only in poor yields (<20%). At this point, we revisited the the remaining Ni^{II}CpNHC complexes **24-26** inactive in benzothiazole arylation (entries **11-13**). The higher steric bulk of **24** (entry **11**) led to a marked halving of the yield, but gratifyingly Cp* substituted **25** (entry **12**) gave the best yield up to this point (53%), finally the cationic complex **26** behaved poorly with a 26% yield (entry **13**). Using complex **25** and halving the catalytic charge (entry **14**) led to a loss of yield, while at the same time increasing the catalytic charge to 7.5 mol% (entry **15**) also failed to improve the reaction yield. At this point we revisited the issue of iodoalkane excess and used 2 equiv. of 1-iododecane (entry **16**) but the yield remained the same (entry **12**). Lastly, we increased the reaction temperature to 120 °C (entry **17**) to obtain our best yield of 60%.

Table 12. Optimization of the reaction parameters for the coupling of benzothiazole with 1-iododecane.



Entry	y (equiv.)	Base	Solvent	[Ni]	x (mol%)	Conv. (%) ^{a, b}	Yield (%) ^{a, c}
1	1.5	LiO <i>t</i> -Bu	1,4-Dioxane	23	5.0	81	43
2	1.2	LiO <i>t</i> -Bu	1,4-Dioxane	23	5.0	71	19
3	1.5	NaO <i>t</i> -Bu ^d	1,4-Dioxane	23	5.0	94	3
4	1.5	KO <i>t</i> -Bu ^d	1,4-Dioxane	23	5.0	91	0
5	1.5	Cs ₂ CO ₃ ^e	1,4-Dioxane	23	5.0	14	0
6	1.5	K ₃ PO ₄ ^e	1,4-Dioxane	23	5.0	32	0
7	1.5	Li ₂ CO ₃ ^e	1,4-Dioxane	23	5.0	14	0
8	1.5	LiOH ^e	1,4-Dioxane	23	5.0	0	0
9	1.5	LiO <i>t</i> -Bu	DME	23	5.0	50	16
10	1.5	LiO <i>t</i> -Bu	Toluene	23	5.0	33	6
11	1.5	LiO <i>t</i> -Bu	1,4-Dioxane	24	5.0	65	23
12	1.5	LiO <i>t</i> -Bu	1,4-Dioxane	25	5.0	82	53
13	1.5	LiO <i>t</i> -Bu	1,4-Dioxane	26	5.0	92	26
14	1.5	LiO <i>t</i> -Bu	1,4-Dioxane	25	2.5	76	33
15	1.5	LiO <i>t</i> -Bu	1,4-Dioxane	25	7.5	90	49
16	2.0	LiO <i>t</i> -Bu	1,4-Dioxane	25	5.0	>95	54
17 ^f	1.5	LiO <i>t</i> -Bu	1,4-Dioxane	25	5.0	>95	60

^a Values are the average of at least two runs. ^b Determined by GC analysis of benzothiazole.

^c Determined by GC analysis of 2-decylbenzothiazole. ^d Purified by sublimation prior to use. ^e Kept in an oven set to 115 °C overnight before use. ^f Reaction ran at 120 °C.

From this optimization study some remarks can be made. As commonly observed in azole C–H functionalization reactions the choice of base is crucial and, more often than not, this choice is LiO*t*-Bu. To our surprise, the other alkoxide bases (NaO*t*-Bu and KO*t*-Bu) also gave considerable conversion of the benzothiazole substrate without producing the desired 2-decylbenzothiazole coupling product. This strongly suggests that competing reactions are taking place by virtue of the alkoxide and might explain the discrepancy between substrate conversion and product yield.

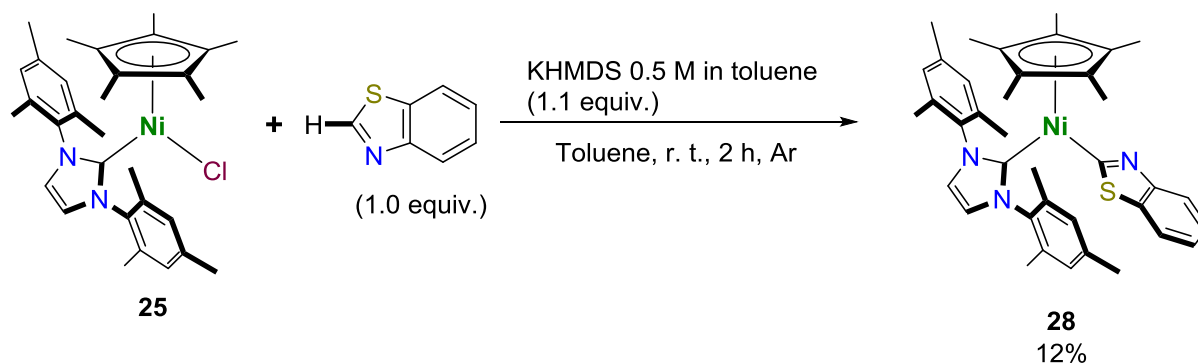
Observing that both the benzothiazolyl complex **27** and the Cp* complex **25** both outperformed complex **23**, we remarked the apparent importance of enriching the electron-

density at the Ni(II) center to improve performance. This can be firstly related by each complex's C_{NHC} chemical shift (**23**: 165.9 ppm,¹⁴⁷ **25**: 177.1 ppm,²⁹⁶ **27**: 177.9 ppm) but this value does not always accurately reflect a complex's electronic properties.²⁹⁰ To better understand this relationship between metal electron-density and catalytic performance we decided to undertake electrochemical studies on selected complexes.

To this end, the complex $[\text{Ni}^{\text{II}}(\text{btz})(\text{Cp}^*)(\text{NHC-Mes}_2)]$ (btz = 2-benzothiazolyl) (**28**) was synthesized (Scheme 101). Dissolving **25** and benzothiazole in toluene followed by addition of a slight excess of a 0.5 M solution of KHMDS toluene, gave an olive brown mixture that upon filtration over activated neutral Al_2O_3 and solvent removal yielded an olive solid. The solid was characterized by ^1H and ^{13}C $\{^1\text{H}\}$ NMR (benzene- d_6), which show shifts similar to those of **25**. An immediate difference from parent chloride complex **25** is that the NHC ligand's heterocyclic protons and the mesityl groups' *m*-H and *o*-Me substituents signals are once again equivalent, indicating that the restricted rotation imposed by the Cl ligand²⁹⁶ does not occur with the btz ligand. Besides that these same signals of the NHC ligand are all found at their usual chemical shift positions and deserve no further comment. The presence of a btz unit is confirmed by the appearance of four signals (d:d:t:t) integrating in a 1:1:1:1 ratio from the btz unit, in the same region (7-8 ppm) as is observed for complex **27**. In ^{13}C $\{^1\text{H}\}$ NMR the Cp^* ligand displays only minor shifts (< 1 ppm) when compared to complex **25**.²⁹⁶ The most notable NMR spectroscopic features of **28** are the chemical shifts of C_{NHC} ($\delta = 180.5$ ppm) and C_{btz} ($\delta = 187.1$ ppm). The shift in the C_{NHC} signal from **25** \rightarrow **28** (< 5 ppm) is markedly smaller than the shift observed for **23** \rightarrow **27** (> 10 ppm). On the other hand, the C_{btz} signal is more deshielded in **28**, with a difference of about 10 ppm between the two btz complexes **27** (176.0 ppm) and **28** (187.1 ppm). This large deshielding places C_{btz} of **28** closer to the other known Ni-btz complexes,^{273,†††} whereas **27** seems closer to the related Pd-btz complexes.^{285–287,‡‡‡} Undoubtedly the Cp^* ligand plays a determining role in this electronic difference, and it has a definite impact enriching the electron density in the btz-C(2).

††† In their communication the authors did not assign the ^{13}C signals of these complexes, but comparison between the data of the parent Ni–X (Cl, Br, AcO) complexes²⁶⁷ and the different Ni–btz complexes described shows one new quaternary C center between (190.1–194.5 ppm, CDCl_3)²⁷³ that we tentatively assign to the metallated C(2) position of the benzothiazolyl ligand.

‡‡‡ See note above.

Scheme 101. Synthesis of $[\text{Ni}^{\text{II}}(\text{btz})(\text{Cp}^*)(\text{NHC-Mes}_2)]$ **28**.

Given their likely role as reaction intermediates in this nickel-catalyzed benzothiazole coupling with iodoalkanes, complexes **27** and **28** were studied by cyclic voltammetry (CV). A report by Crabtree and coworkers divulged the study of a series of Cp-Ni(II)-NHC complexes with varying NHC ligands.²⁹⁷ One notable feature of all those complexes was a first oxidation event attributed to the oxidation of the nickel center to Ni(III). In this report complex **23** was studied and its potential for Ni(II)/Ni(III) oxidation determined as $E = 0.72 \text{ V vs. Fc/Fc}^+$.^{§§§}

For complex **27**, a first oxidation event is observed at $E = 0.06 \text{ V vs. Fc/Fc}^+$, and assigned as a Ni(II)/Ni(III) oxidation (Figure 41). This large difference ($> 0.5 \text{ V}$) in oxidation potential translates the increase in electron density at the metal center. The well-defined oxidation wave contrasts with the reverse reduction Ni(III)/Ni(II) that is not observed under these conditions, in contrast to **23**.²⁹⁷ At lower potentials a reduction event is observed at $-1.55 \text{ V vs. Fc/Fc}^+$ and attributed to a Ni(II)/Ni(I) reduction. This peak is also largely shifted (this time to a more negative potential) when compared to **23**.²⁹⁷

§§§ This potential was reportedly measured at a scan rate of 100 mV s^{-1} . Given the scan rate dependence exhibited by complexes **27** and **28** we report the redox potentials as measured at this same scan rate.

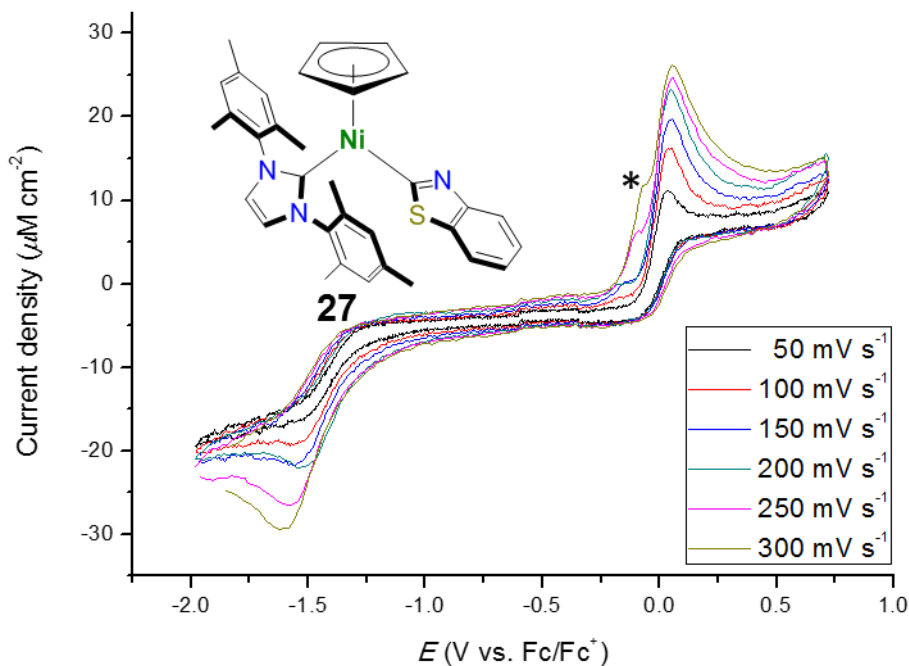


Figure 41. Cyclic voltammogram of complex **27**: 1 mM in a 0.1 M *n*-BuNPF₆ solution in MeCN, using a glassy carbon working electrode, a platinum wire counter electrode and an Ag/AgCl, KCl 3 M reference electrode. Scan rates were varied at 50, 100, 150, 200, 250 and 300 mV s⁻¹. Referenced to a Fc 2 mM external standard $E = 0.48$ vs. Ag/AgCl, KCl 3 M. The shoulder denoted with an asterisk (*) seen at 250 and 300 mV s⁻¹ scan rates was irreproducible in replicate experiments.

Complex **28** displays an oxidation peak at $E = -0.44$ V vs. Fc/Fc⁺ (Figure 42). This value is not only much lower than the observed for complex **23**,²⁹⁷ it shows a large shift even compared to benzothiazolyl complex **27**, in agreement with the more electron-rich character of Cp*. Noteworthy, the current density values obtained when studying complex **28** are about an order of magnitude smaller than those obtained for complex **27**. Once again the reverse reduction Ni(III)/Ni(II) is imperceptible. The CV at lower potentials also shows lower current density values and the Ni(II)/Ni(I) one-electron reduction is observed by too poorly defined to attribute a definite value, but would appear to be found between -1.4 and 1.2 V vs. Fc/Fc⁺. This makes the Ni(II)/Ni(I) reduction in **28** slightly less negative than what was observed for **27**, despite the more facile Ni(II)/(Ni(III)) oxidation. Albeit, this unintuitive result, the Cp* ligand has been described as having an ‘electronic buffer effect’,²⁹⁸ which might mean that neither of these redox processes are ‘purely metal-centered’ in complex **28**.

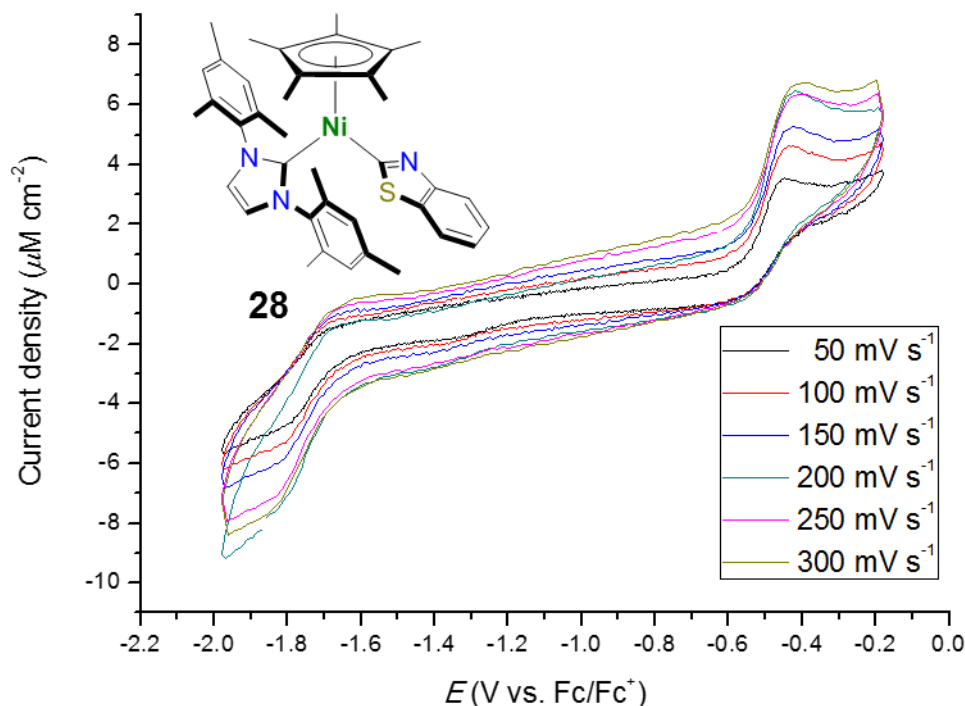


Figure 42. Cyclic voltammogram of complex **28**: 1 mM in a 0.1 M *n*-BuNPF₆ solution in MeCN, using a glassy carbon working electrode, a platinum wire counter electrode and an Ag/AgCl, KCl 3 M reference electrode. Scan rates were varied at 50, 100, 150, 200, 250 and 300 mV s⁻¹. Referenced to 2 mM Fc external standard E = 0.48 vs. Ag/AgCl, KCl 3 M.

Working under the hypothesis that **27** and **28** are indeed intermediates of this coupling between benzothiazole and 1-iododecane (see Scheme 100) it seems that catalyst performance can be correlated with the facility with which these complexes undergo one-electron oxidations. Hence a one-electron oxidation to a Ni(III)-btz species can be proposed as the next elemental step in the reaction.

This is a marked difference from mechanistic manifold apparently at play for the arylation of benzothiazole, in which a reduction to Ni(0) apparently takes place as a first catalyst activation step. Indeed, when generating an half-sandwich Ni(II)-NHC-btz intermediate, this complex's coordination sphere becomes saturated and cannot easily bind a second benzothiazolyl unit to undergo reductive elimination and generate the required Ni(0) species. However, in the case of alkylation reactions using iodoalkanes, the I–C_{sp3} bond can break in a homolytic manner, by photochemical cleavage²⁹⁹ or by an iodine atom transfer reaction,²⁹⁵ to generate a highly reactive primary radical species, C_{sp3}•.**** These radical

**** Iodoalkanes more readily generate radical species than iodoarenes, and the resulting alkyl radicals are more reactive than phenyl radicals as, like carbocation and carboanions, radicals are stabilized by

species can now interact with the Ni(II)-btz species and by either a one-electron chemical oxidation – Ni(II)/Ni(III) or, a radical oxidative addition³⁰⁰ – Ni(II) + I[•]/C_{sp³}[•] → Ni(III)–I/C_{sp³} – generating a Ni(III) species with a different coordination preference. Alternatively, if the Ni(II)-btz species is involved in the iodine atom transfer reaction, a Ni(III)–I complex can be generated and react with the alkyl radical. This would explain the relationship between ease of one-electron oxidation and catalytic activity as dictating the ease with which this Ni(III) species is formed.

On this basis we envisioned if it would be possible to further enrich the electron density of the metal, but using a different NHC ligand. Taking note of the adverse effect that modifying the steric environment of the NHC *N*-substituents might have on the catalytic activity (Table 12), we chose to test if increasing the NHC donor character by modification of the NHC backbone would be beneficial. As such we targeted the doubly backbone methylated ^{4,5}Me₂NHC-Mes₂,³⁰¹ reported to be more electron-donating than NHC-Mes₂ (Table 13) and having shown superior performance than NHC-Mes₂ in other Ni-catalyzed systems.^{302,303}

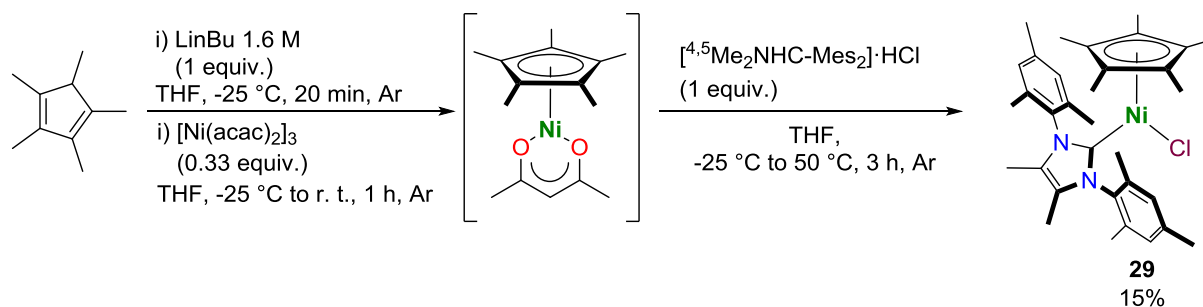
Table 13. Comparison between the electron-donating strength of NHC-Mes₂ and ^{4,5}Me₂NHC-Mes₂.

	TEP (cm ⁻¹) ⁵⁷		δC _{NHC} (ppm) ³⁰⁴	pK _a value ^{a,136}
	[RhCl(CO) ₂ (NHC)]	[IrCl(CO) ₂ (NHC)]		
NHC-Mes ₂	2049.6	2049.6	177.2	19.40 ± 0.12
^{4,5} Me ₂ NHC-Mes ₂	2046.9	2046.7	180.1	23.79 ± 0.15

^a Of the corresponding imidazolium salt in DMSO at 25 °C.

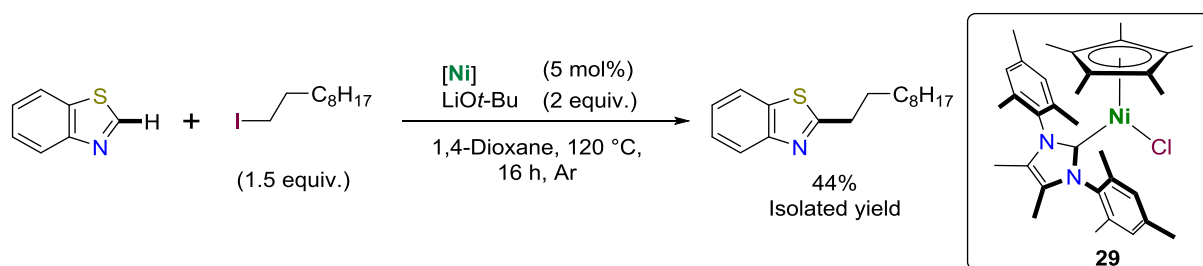
As such, we synthesized the new complex [Ni^{II}Cl(Cp^{*})(^{4,5}Me₂NHC-Mes₂)] **29** (Scheme 102), following the same methodology developed by our group for accessing Ni^{II}(Cp^{*})(NHC) complexes.¹²³ At -25 °C 1,2,3,4,5-pentamethylcyclopentadiene was deprotonated and the resulting lithium salt added to a slurry of [Ni^{II}(acac)₂]₃ to give the non-isolated intermediate [Ni^{II}(acac)(Cp^{*})], that can then react with the imidazolium salt [^{4,5}Me₂NHC-Mes₂]⁺·Cl⁻ to give the desired complex **29** in a poor yield (15%).

resonance.²⁹⁹ Experimental bond enthalpy (in kcal mol⁻¹, respective uncertainties in parenthesis) of organoiodines I–Me = 57.6(04), I–Et = 56.9(0.7), I–(*i*-Pr) = 57(1), I–(*t*-Bu) = 55.6(0.9) < I–(Ph) = 67(2).³⁵⁸

Scheme 102. Synthesis of backbone modified Cp* complex **29**.

Analysis of the ¹H NMR spectra of this complex gives a spectrum similar to that of complex **25**, with the signals of both the *o*-Me and *m*-H groups being inequivalent, by virtue of restricted rotation about the *N*-mesityl bond on the NMR time scale at r. t. The NHC backbone Me groups appear as a singlet at 1.42 ppm. The ¹³C {¹H} NMR spectra likewise shows a doubling of the Mes groups' *o*-Me and *m*-H signals, a new signal at 9.2 ppm corresponding to NHC backbone Me groups. Of note in the ¹³C {¹H} NMR spectra of **29** the mesityl *m*-C, *o*-Me *o*-C are also inequivalent, the new backbone Me groups can be found as a single peak at 9.2 ppm, and the C_{NHC} peak is found at 173.1 ppm. Although this peak is found at upfield shift when compared to **25**, contrary to what would be expected for a more electron-donating NHC ligand, this inconsistency between ranked donating power (see Chapter 1) and chemical shift in half-sandwich Ni(II)-NHC complexes has been observed before.²⁹⁰

We then tested complex **29** in the alkylation of benzothiazole by 1-iododecane (Scheme 103). The reaction proceeded to give a moderate isolated yield of 44% of 2-decylbenzothiazole, which does not significantly improve from that obtained with complex **25** (44% isolated yield).

Scheme 103. Catalytic alkylation of benzothiazole by 1-iododecane using complex **29**.

II.3. Conclusions

In conclusion, we have shown that the new cationic $C_{\text{NHC}}C_{\text{alkyl}}$ -chelate Ni(II) complexes act as catalysts in the C–H functionalization of benzothiazole with iodoarenes. They showed low reactivity and scope of the reaction, but are the first example of a C,C-Ni chelate system as a catalyst in this reaction. More importantly, these complexes were active where half-sandwich nickel(II)-NHC catalysts, known in a series of other cross-coupling reactions were totally unreactive. We attribute this to the combined benefits from having both a chelating structure and very labile ligands, which mimics highly active pnictogen chelates active in this reaction.

Experiments to unveil the mechanistic steps of the reaction suggest that the complexes act as precatalysts that experience in situ reduction to a Ni(0) species, by azole dimerization. This species seems however not to be the active catalyst as after it is apparently formed, the catalyst system displays a high sensitivity to even catalytic amounts of a radical trapping agent. It is noteworthy that, Hg poisoning experiments suggest that this Ni(0) species is actually a form of metallic particles and not a discreet molecular entity. This suggests that the Ni(0) species would not be the active catalyst but that it might undergo disproportionation reactions to generate the true catalyst species as a radical species.

Serendipitous discovery of a CpNi(NHC)-benzothiazolyl complex formed as a reactional dead-end in the arylation reaction led to the study of the complementary alkylation reaction. The complex proved effective in the alkylation of benzothiazole with 1-iododecane and this reactivity could be exploited by known $[\text{NiClCp}^+(\text{NHC})]$ type complexes. A direct correlation between the facility of the Ni-benzothiazolyl intermediate complexes to undergo a one-electron oxidation, and their performance as catalysts was established with recourse to electrochemical measurements.

The ease of one electron oxidation of the intermediate complexes and the propensity of iodoalkanes to generate reactive primary radical species both point to a mechanistic manifold involving odd-electron count intermediates, and most probably involving a Ni(III) species.

Experimental section

Experimental section

I. Generalities.....	168
I.1. Materials.....	168
I.2. Methods.....	169
II. Synthetic procedures	171
II.1. Imidazolium salts	171
II.1.2. Compound 2 : [Mes-NHC-(CH ₂)CH ₂ CN]·HBr	171
II.1.2. Compound 3 : [Mes-NHC-(CH ₂) ₂ CH ₂ CN]·HCl	172
II.1.3. Compound 4 : [DIPP-NHC-(CH ₂) ₂ CH ₂ CN]·HCl.....	172
II.2. Nickel(II) complexes	173
II.2.1. Compound 5 : [Ni ^{II} I(Cp)(Me-NHC-(CH ₂)CH ₂ CN)].....	173
II.2.2. Compound 6 : [Ni ^{II} Br(Cp)(Mes-NHC-(CH ₂)CH ₂ CN)]	173
II.2.3. Compound 8 : [Ni ^{II} Cl(Cp)(DIPP-NHC-(CH ₂) ₂ CH ₂ CN)]	174
II.2.4. Compound 9 : [Ni ^{II} (Cp){Me-NHC-(CH ₂)CH(CN)}]	174
II.2.5. Compound 10 : [Ni ^{II} (Cp){Mes-NHC-(CH ₂)CH(CN)}].....	175
II.2.5. Compound 11 : [Ni ^{II} (Cp){Mes-NHC-(CH ₂) ₂ CH(CN)}]	175
II.2.6. Compound 12 : [Ni ^{II} (Cp){DIPP-NHC-(CH ₂) ₂ CH(CN)}].....	176
II.2.7. Compound 13 : [Ni ^{II} {Me-NHC-(CH ₂)CH(CN)}(MeCN)]PF ₆	176
II.2.8. Compound 14 : [Ni ^{II} {Mes-NHC-(CH ₂)CH(CN)}(MeCN)]PF ₆	177
II.2.9. Compound 15 : [Ni ^{II} {Mes-NHC-(CH ₂) ₂ CH(CN)}(MeCN)]PF ₆	178
II.2.10. Compound 16 : [Ni ^{II} {DIPP-NHC-(CH ₂) ₂ CH(CN)}(MeCN)]PF ₆	178
II.2.11. Compound 17 : [Ni ^{II} {Mes-NHC-(CH ₂) ₂ CH(CN)}(PPh ₃)]PF ₆	179
II.2.12. Compound 18 : [Ni ^{II} {Mes-NHC-(CH ₂) ₂ CH(CN)}(PMe ₃)]PF ₆	180
II.2.13. Compound 19 : [Ni ^{II} (μ ² -OH){Mes-NHC-(CH ₂) ₂ CH(CN)}]PF ₆	180
II.2.14. Compound 22 : [Ni ^{II} {Mes-NHC-(CH ₂) ₂ CH(CN)}(bipy)]PF ₆	180
II.2.15. Compound 27 : [Ni ^{II} (btz)(Cp)(NHC-Mes ₂)]	181
II.2.16. Compound 28 : [Ni ^{II} (btz)(Cp*)(NHC-Mes ₂)].....	181
II.2.17. Compound 29 : [Ni ^{II} Cl(Cp*)(^{4,5} Me ₂ NHC-Mes ₂)].....	182
III. Catalytic reactions.....	183
III.1. Benzothiazole arylation	183
III.2. Benzothiazole alkylation	183
III.3. NMR data of the azole coupling products.....	184

IV. Crystal data and refinement data.....	187
IV.1. Hexaacetone-nickel(II) hexafluorophosphate $[\text{Ni}^{\text{II}}(\text{NCMe})_6](\text{PF}_6)_2$	187
IV.2. Complexes 9 and 10	189
IV.3. Complexes 19 and 27	190
V. Computational methods.....	191

Experimental section

I. Generalities

I.1. Materials

Solvents and chemicals were purchased from, Acros Organics, Alfa-Aesar, Fischer Scientific, Fluorochem, Prolabo, Sigma-Aldrich/Merk, Strem, TCI Chemicals or VWR without further purification unless otherwise stated. Argon gas was purchased from Air Products. Celite, silica gel (43-60 μm or 60-200 μm mesh) and aluminum oxide 90 active neutral (activity stage I, 63-200 μm mesh) were pre-dried by heating in an oven at 115 °C, under air, for a minimum of 16 h before use. All reactions were carried out under magnetic stirring using a Teflon coated magnetic stir bar previously dried in an oven at 115 °C, under air, before use. The identity and purity of known compounds were determined by ^1H and/or ^{13}C $\{^1\text{H}\}$ NMR spectroscopy in relationship to their described spectra. Known compounds: mesitylisonitrile,²¹⁰ 2,5-bisphenyl-oxazole,²⁴⁴ 2,4,6-trimethylphenyl-1-imidazole, 1-(2,6-di-*i*-propylphenyl)-1-imidazole, 3-propylnitrile-1-imidazole,³⁰⁵ bis(2,4,6-trimethyl-*N*-phenylbisethaneimine),³⁰⁶ 1,3-bis-(2,4,6-trimethylphenyl)-imidazolium chloride,³⁰⁷ 1,3-bis-(2,4,6-trimethylphenyl)-bis-4,5-methylimidazolium chloride,³⁰⁸ nickel(II) bis-acetylacetonate³⁰⁹, hexaminonickel(II) chloride, nickelocene,¹²⁶ **1**,¹²⁸ **7**,¹²⁷ **21**,¹³¹ **23**,³¹⁰ **24**,²⁸⁸ **25**,¹²³ and **26**¹²⁴ were obtained following the reported procedures.

The purifications described below follow the methods described in Perrin and Armarego's "Purification of Laboratory Chemicals".³¹¹ Solvents were refluxed with appropriate drying agents under a flow of argon gas for a minimum of 10 h on their first batch and routinely for 1 h before collection and use. Drying agents as follows: THF, DME, Et₂O – Na/benzophenone (deep blue/purple red color was used as an indicator for the absence of oxygen and moisture); 1,4-dioxane, toluene – Na; *n*-pentane, *n*-hexane, acetonitrile – CaH₂. Small volumes (< 10 cm³) of each of the above were occasionally dried over 3 Å molecular sieves (activated by drying under vacuum at T > 150 °C for a minimum of 3 h and then cooling off under an argon flow)³¹² and degassed by three freeze-pump-thaw cycles. Liquid azoles: thiazole, 4,5-dimethylthiazole, benzothiazole, oxazole and benzoxazole as well as haloarenes: iodobenzene, 2-iodotoluene, 2-iodobiphenyl were obtained from suppliers and distilled over CaH₂ and were considered pure by ^1H NMR spectroscopy. They were then bubbled with argon or degassed by freeze-pump-thaw and stored under an argon atmosphere. 1-Iodododecane was dissolved in Et₂O, washed

with a saturated $\text{Na}_2\text{S}_2\text{O}_3$ (aq.) solution, the aqueous phase extracted with Et_2O thrice, dried over anhydrous MgSO_4 , filtered, evaporated and distilled over CaH_2 under vacuum at temperature ≤ 135 °C, to give the product as a colorless liquid. They were then bubbled with argon or degassed by freeze-pump-thaw and stored under and argon atmosphere, kept from light and over a drop of mercury.

I.2. Methods

All reactions involving organometallic compounds were carried out using Schlenk techniques or in a glovebox using argon as working gas, unless otherwise noted.³¹³ Synthesis using heating by microwave irradiation heating were conducted in a Biotage Microwave Initiator running at a frequency of 2.3 GHz in 2-5 mL vials, equipped with a Teflon coated magnetic stir bar and sealed with a crimp.

IR spectra were recorded on a FT-IR PerkinElmer Spectrum Two spectrometer equipped with a diamond ATR.

Solution NMR spectra were recorded at 298 K on Bruker Ultra Shield 300, Bruker Spectrospin 400, or Bruker Avance III HD 500 spectrometers operating at 300.13, 400.14, or 500.14 MHz for ^1H , at 75.47, 100.61, or 125.77 MHz for ^{13}C $\{^1\text{H}\}$ and, at 161.97 MHz for ^{31}P $\{^1\text{H}\}$. Variable temperature NMR experiments were carried out by Dr. Bruno Vincent at the Service of RMN, Institute of Chemistry of Université de Strasbourg on a Bruker Avance III - 600 MHz spectrometer operating at 600.13 MHz for ^1H and at 242.92 MHz for ^{31}P $\{^1\text{H}\}$. Chemical shifts (δ) and coupling constants (J) are expressed in ppm and Hz, respectively. The chemical shifts are referenced to the residual deuterated, ^{13}C solvent peaks or to an external reference of 85% H_3PO_4 in $\text{H}_2\text{O} = 0$ ppm.^{314,315}

X-ray diffraction studies were performed by Dr. Lydia Karmazin and Corinne Bailly at Service de radiocristallographie of Fédération de Chimie "Le Bel" FR2010. Diffraction data were collected at 173(2) K on a Bruker APEX II DUO Kappa CCD area detector diffractometer equipped with an Oxford Cryosystem liquid N_2 device using $\text{Mo-K}\alpha$ radiation ($\lambda = 0.71073$ Å). The crystal-detector distance was 38 mm. The cell parameters were determined (APEX2 software) from reflections taken from three sets of twelve frames, each at ten second exposure. The structure was solved using direct methods with SHELXS-97 and refined against F^2 for all reflections using SHELXL-97 software.^{316,317} A semi-empirical absorption correction was applied using SADABS in APEX II.³¹⁸ All non-hydrogen atoms were refined with anisotropic displacement parameters, using weighted full-matrix least-squares on F^2 . Hydrogen atoms

were included at calculated positions and treated as riding atoms using SHELXL default parameters.

Elemental analyses were performed by the Service d'Analyses, de Mesures Physiques et de Spectroscopie Optique, UMR CNRS 7177, Institut de Chimie, Université de Strasbourg.

High resolution mass spectra were recorded on a Bruker micrOTOF-Q mass spectrometer by the Service the Spectrométrie de Masse, UMR CNRS 7177, Université de Strasbourg or by Dr. Jean-Marc Strub at Laboratoire de Spectrométrie de Masse Bio-Organique, Institut Pluridisciplinaire Hubert Curien, UMR7178.

GC analyses were carried out by injection of 1 mm³ to an inlet at 250 °C, on splitless mode. Eluent had a set flow of 2.5 cm³ min⁻¹. Temperature ramp: i) isotherm 50 °C for 5 min. ii) heat to 150 °C at 10 °C min⁻¹ iii) isotherm at 150 °C for 5 min. iv) heat to 240 °C at a rate of 20 °C min⁻¹ v) isotherm at 240 °C for 5 min.

Retention times: *n*-Dodecane – 10.7 min; Benzothiazole – 10.9 min, 1-Iododecane – 14.0 min, 2-Decylbenzothiazole – 24.3 min.

Quantification was performed by tracing calibration curves for: benzothiazole, and 2-decylbenzothiazole. Calibration curves were performed by preparing five solutions of varying concentrations of analyte and a known, fixed concentration of internal standard *n*-dodecane (132 μM) and plotting the ratio of analyte and standard area by the ration of analyte and standard area. Samples were diluted as necessary to obtain values within these curves.

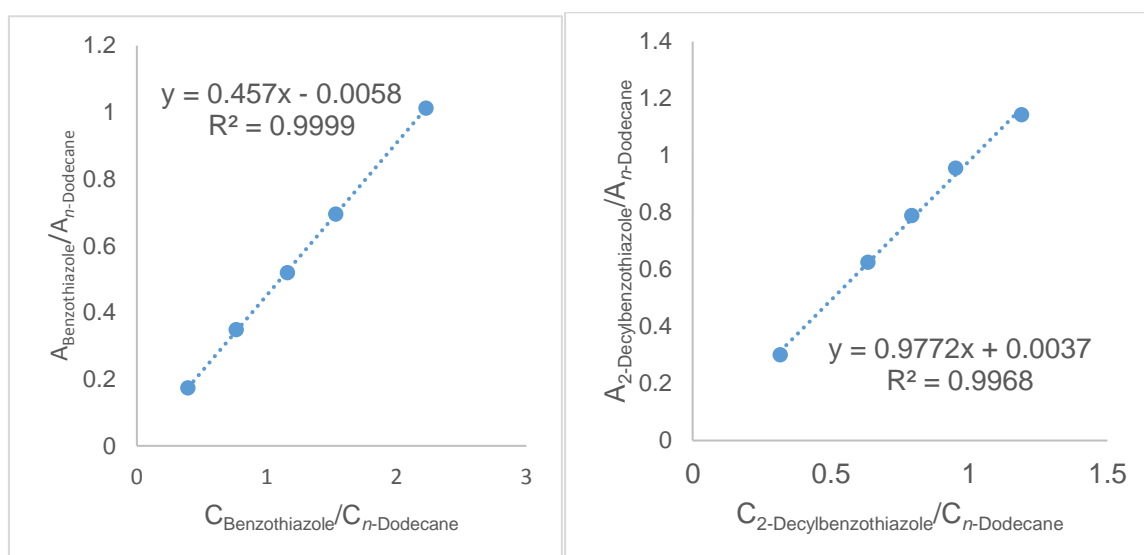


Figure 43. GC calibration curve for benzothiazole and 2-decylbenzothiazole. All solutions are in ethyl acetate. *n*-Dodecane was used as internal standard with a fixed concentration of 132 μM. Concentrations of Benzothiazole: 52, 101, 153, 202 and 294 μM. Concentrations of 2-Decylbenzothiazole: 41, 82, 103, 124 and 155 μM. Intensity values of 250 and 50 were taken as maximum and minimum cutoff points.

GC sample preparation: the reaction mixture was cooled to r. t., stirring stopped and an aliquot (15 mm³) filtered over a Celite (1.5 × 0.5 cm)-cotton plug, diluted with an *n*-dodecane 130 μM solution in ethyl acetate (5 cm³). From this solution an aliquot (1 cm³) was further diluted ($V_{\text{total}} = 6 \text{ cm}^3$) and then analyzed by GC. If necessary, the more concentrated solution was also analyzed to quantify the more dilute analytes.

Electrochemical measurements: Cyclic voltammetry (CV) experiments using complexes **15**, **21**, **22**, **27** and **28** (1 mM) were first performed using a Voltalab 50 potentiostat/galvanostat (Radiometer Analytical MDE15 polarographic stand, PST050 analytical voltammetry and CTV101 speed control unit) controlled by the Voltmaster 4 electrochemical software. A conventional three-electrode cell (10 cm³) was employed in our experiments with a glassy carbon disk ($s = 0.07 \text{ cm}^2$) set into a Teflon rotating tube as a working electrode, a Pt wire as a counter electrode, and a KCl (3 M)/Ag/AgCl reference electrode (+210 mV vs. NHE).³¹⁹ Prior to each measurement, the surface of the glassy carbon electrode was carefully polished with 0.3 μm aluminum oxide suspension (Escil) on a silicon carbide abrasive sheet of grit 800/2400. Thereafter, the glassy carbon electrode was copiously washed with water and dried with paper towel and argon gas. The electrode was installed into the voltammetry cell along with a platinum wire counter electrode and the reference. The solutions containing ca. 1 mM of the titled complexes were vigorously stirred and purged with O₂-free (Sigma Oxiclear cartridge) argon for 15 minutes before the voltammetry experiment was initiated, and maintained under an argon atmosphere during the measurement procedure. The voltammograms were recorded at room temperature (23(1) °C) in MeCN with 100 mM tetra-*n*-butylammonium hexafluorophosphate as supporting and inert electrolyte.³¹⁹ For the CV measurements, the voltage sweep rate was varied from 50 to 300 mV s⁻¹ and several cyclic voltammograms were recorded from +0.5 V to -2.2 V. Peak potentials were measured at a scan rate of 200 mV s⁻¹ unless otherwise indicated.

II. Synthetic procedures

II.1. Imidazolium salts

II.1.2. Compound 2: [Mes-NHC-(CH₂)CH₂CN]·HBr

1-(2,4,6-trimethylphenyl)-3-propyl nitrile-imidazolium bromide¹⁴⁵

1-(2,4,6-Trimethylphenyl)-imidazole (5.01 mmol, 0.934 g) and 3-bromopropionitrile (20.0 mmol, 2.68 g, 1.66 cm³) were refluxed for two days in ethyl acetate (150 cm³). The resulting white suspension (in an orange solution) was cooled to r. t., and the precipitate was collected by filtration, rinsed with ethyl acetate until the washings were colorless, and air-dried to afford the title compound as motherpearl flakes or as a light whiteish powder (285 mg, 0.890 mmol, 18%). Anal. Calcd for C₁₅H₁₈N₃Br: C, 56.26; H, 5.67; N, 13.12. Found: C, 56.14; H, 5.59; N, 13.08. ¹H NMR (CDCl₃, 300.13 MHz): δ 10.23 (t, ⁴J n. r., 1H, NCHN), 8.40 (t, ³J n. r., 1H, NCH), 7.19 (t, ³J = 1.8, 1H, NCH), 7.01 (s, 2H, *m*-H), 5.18 (t, ³J = 6.3, 2H, NCH₂), 3.49 (t, ³J = 6.3, 2H, CH₂CN), 2.35 (s, 3H, *p*-Me), 2.08 (s, 6H, *o*-Me). ¹³C {¹H} NMR (CDCl₃, 75.47 MHz): δ 141.8 (*p*-C_{Ar}), 138.2 (NCHN), 134.4 (*o*-C_{Ar}), 130.6 (*ipso*-C_{Ar}), 130.1 (*m*-C_{Ar}), 124.2 (NCH), 123.4 (NCH), 116.8 (CN), 46.1 (NCH₂), 21.2 (*p*-Me), 20.7 (CH₂CN), 17.8 (*o*-Me).

II.1.2. Compound 3: [Mes-NHC-(CH₂)₂CH₂CN]·HCl

1-(2,4,6-trimethylphenyl)-3-propylnitrile-imidazolium chloride¹²⁷

Thermal: 2,4,6-Trimethylphenyl-1-imidazole (21.7 mmol, 4.04 g), 4-chlorobutyronitrile (24.0 mmol, 2.48 g, 2.3 cm³, 1.1 equiv.) and 1,4-dioxane (50 cm³) were heated to 155 °C for 16 h. The reaction mixture was then cooled to r. t., and ethyl acetate (50 cm³) was added to precipitate a tan paste, that was then stirred for 1 h. A white powder precipitated; the solution was filtered off and the powder washed again with ethyl acetate (5 × 50 cm³) until the washings came out colorless. The white powder was then dried under vacuum at r. t. to give the title compound (2.70 g, 9.41 mmol, 43%).

Microwave irradiation: 2,4,6-Trimethylphenyl-1-imidazole (7.03 mmol, 1.31 g), 4-chlorobutyronitrile (7.30 mmol, 0.760 g, 0.70 cm³, 1 equiv.) and THF (3 cm³) were added to a 2-5 mL vial, sealed with a crimp and heated under microwave irradiation to 180 °C for 1 h. The reaction mixture was then cooled to r. t., the solvent removed under vacuum. The resulting oily residue was extracted with CH₂Cl₂ (2 cm³) and triturated with *n*-pentane until a beige solid precipitated that was then washed with ethyl acetate (1 × 50 cm³ overnight, and 2 × 30 cm³ for 1 h) and dried under vacuum to yield the title compound (1.56 g, 5.39 mmol, 77%).

II.1.3. Compound 4: [DIPP-NHC-(CH₂)₂CH₂CN]·HCl

1-(2,6-Diisopropylphenyl)-3-butylnitrile-imidazolium chloride

1-(2,6-Diisopropylphenyl)-1-imidazole (7.88 mmol, 1.80 g) and 4-chlorobutyronitrile (7.88 mmol, 745 mm³) and THF (3 cm³) were added to a 2-5 mL vial, sealed with a crimp and heated under microwave irradiation to 180 °C for 1 h. The reaction mixture was then cooled to

r. t., the solvent removed under vacuum. The resulting oily residue was extracted with CH_2Cl_2 (2 cm^3) and triturated with *n*-pentane until a beige solid precipitated that was then washed with ethyl acetate ($1 \times 50 \text{ cm}^3$ overnight, and $2 \times 30 \text{ cm}^3$ for 1 h) and dried under vacuum to yield the title compound. (1.46 g, 4.42 mmol, 56%). Anal. Calcd for $\text{C}_{19}\text{H}_{26}\text{N}_3$: C, 68.76; H, 7.90; N, 12.66. Found: C, 68.73; H, 7.94; N, 12.52. HR-MS (ESI): *m/z* calcd for $\text{C}_{19}\text{H}_{26}\text{N}_3$ 296.2121, found 296.2128. ^1H NMR (CDCl_3 , 300.13 MHz): δ 10.65 (t, 4J n. r., 1H, NCHN), 8.44 (t, 3J n. r., 1H, NCH), 7.55 (t, $^3J = 1.8$, 1H, *p*-Ar), 7.31 (d, $^3J = 8.1$, 2H, *m*-H_{Ar}), 7.20 (t, $^3J = 1.8$, 1H, NCH), 5.04 (t, $^3J = 6.9$, 2H, *CHMe*₂), 2.78 (t, $^3J = 6.9$, 2H, CH_2CN), 2.51 (quint., $^3J = 6.9$, 2H, CH_2), 2.31 (sept., $^3J = 6.9$, 2H, *CHMe*₂), 1.22 (d, $^3J = 6.9$, 6H, *CHMe*₂), 1.16 (d, $^3J = 6.9$, 6H, *CHMe*₂). ^{13}C $\{^1\text{H}\}$ NMR (CDCl_3 , 75.47 MHz): δ 145.5 (*o*-C_{Ar}), 139.0 (NCHN), 132.0 (*p*-C_{Ar}), 130.3 (*ipso*-C_{Ar}), 124.4 (NCH), 123.8 (NCH), 118.9 (CN), 48.9 (NCH₂), 28.8 (*CHMe*₂), 26.7 (CH_2), 24.5 (*CHMe*₂), 14.4 (CH_2CN).

II.2. Nickel(II) complexes

II.2.1. Compound 5: $[\text{Ni}^{\text{II}}(\text{Cp})(\text{Me-NHC}-(\text{CH}_2)\text{CH}_2\text{CN})]$

Complex **5** was prepared by a modified literature procedure.¹²⁸ Nickelocene (6.83 mmol, 1.29 g, 1.1 equiv.) and **1** (6.01 mmol, 1.58 g) were refluxed in toluene (80 cm^3) for 2 days. The mixture progressively turned from dark green to black. The reaction mixture was cooled to r. t. the solvent evaporated. The residue was then extracted with THF and loaded onto a SiO_2 (43-60 μm , $6 \times \varnothing 3 \text{ cm}$) pad that was then eluted with THF and the second dark red fraction recovered. This fraction was then concentrated to circa 10 cm^3 and layered with *n*-hexane (1:6 ratio) and cooled to $-28 \text{ }^\circ\text{C}$ overnight to precipitate a dark red solid. The supernatant was filtered off and the solid washed with dry *n*-hexane ($3 \times 10 \text{ cm}^3$) and dried under vacuum to give the title compound as a dark red powder (1.11 g, 2.88 mmol, 48%).

II.2.2. Compound 6: $[\text{Ni}^{\text{II}}\text{Br}(\text{Cp})(\text{Mes-NHC}-(\text{CH}_2)\text{CH}_2\text{CN})]$

Nickelocene (4.60 mmol, 868 g, 1.5 equiv.) and **2** (3.06 mmol, 981 mg) were refluxed in THF (30 cm^3) for 4 days. The mixture progressively turned from dark green to cherry red. After 4 days the reaction mixture was cooled to r. t. and filtered over a degassed Celite pad ($4 \times \varnothing 3 \text{ cm}$) that was then washed with THF until the washings were colorless. The solvent was then evaporated and the residue washed with dry *n*-pentane until the washings came out colorless. The resulting solid was then dried overnight to afford the title compound as a pink

powder (802 mg, 1.81 mmol, 59% yield). Anal. Calcd for $C_{20}H_{22}N_3NiBr$: C, 54.22; H, 5.01; N, 9.49. Found: C, 54.48; H, 4.97; N, 9.10. 1H NMR ($CDCl_3$, 300.13 MHz): δ 7.37 (d, $^3J = 1.5$, 1H, NCH), 7.09 (s, 2H, *m*-H), 6.92 (d, $^3J = 1.5$, 1H, NCH), 5.30 (t, $^3J = 6.0$, 2H, NCH₂), 4.80 (s, 5H, C₅H₅), 3.44 (t, $^3J = 6.0$, 2H, CH₂CN), 2.43 (s, 3H, *p*-Me), 2.13 (s br., 6H, *o*-Me). ^{13}C { 1H } NMR ($CDCl_3$, 75.47 MHz): δ 166.8 (C_{NHC}), 139.5, 136.6 and 136.0 (*o*-, *ipso*- and *p*-C_{Ar}), 129.4 (*m*-C_{Ar}), 124.6 (NCH), 123.2 (NCH), 117.7 (CN), 92.2 (C₅H₅), 48.0 (NCH₂), 21.3 (*p*-Me), 20.4 (CH₂CN), 18.7 (*o*-Me). IR [ATR]: $\nu(C_{sp^2-H})$ 3164 (w), 3131 (m), 3098 (w); $\nu(C_{sp^3-H})$ 2952 (w), 2910 (m), 2855 (w); $\nu(C\equiv N)$ 2253 (w).

II.2.3. Compound 8: [Ni^{II}Cl(Cp)(DIPP-NHC-(CH₂)₂CH₂CN)]

Nickelocene (6.81 mmol, 1.29 g, 1.5 equiv.) and **4** (4.54 mmol, 1.51 g) were refluxed in THF (45 cm³) for 19 h. The mixture progressively turned from dark green to purple-red. The reaction mixture was cooled to r. t., diluted in THF (40 cm³) and filtered over a Celite pad (4 × Ø3 cm) that was then rinsed with THF until the washings were colorless. The solvent was then evaporated and the residue washed with dry *n*-pentane until the washings came out colorless. The pink powder was then dissolved in toluene, and filtered through a SiO₂ pad (43-60 μm, 4 × Ø3 cm) that was rinsed with toluene until the washings were colorless. The resulting dark pink solution was then evaporated and the resulting solid dried overnight under vacuum at 60 °C to afford the title compound as a pink powder (1.12 g, 2.47 mmol, 54%). Anal. calcd for $C_{24}H_{30}N_3NiCl$: C, 63.40; H, 6.65; N, 9.24. Found: C, 63.43; H, 6.61; N, 9.24. 1H NMR ($CDCl_3$, 300.13 MHz): δ 7.57 (t, $^3J = 7.7$, 1H, *p*-H), 7.40 (d, $^3J = 7.7$, 2H, *m*-H), 7.21 (d, $^3J = 2.0$, 1H, NCH), 6.96 (d, $^3J = 2.0$, 1H, NCH), 5.20 (t, $^3J = 6.8$, 2H, NCH₂), 4.69 (s, 5H, C₅H₅), 2.60 (m, 6H, CH₂CH₂CN and CHMe₂), 1.37 (d, $^3J = 6.6$, 6H, CHMe₂), 1.05 (d, $^3J = 6.6$, 6H, CHMe₂). ^{13}C { 1H } NMR ($CDCl_3$, 75.47 MHz): δ 165.7 (C_{NHC}), 146.8 (*o*-C_{Ar}), 136.4 (*ipso*-C_{Ar}), 130.5 (*p*-C_{Ar}), 125.8 (NCH), 124.3 (*m*-C_{Ar}), 122.1 (NCH), 119.1 (CN), 91.9 (C₅H₅), 50.7 (NCH₂), 28.4 (CHMe₂), 27.0 (CH₂), 26.4 (CHMe₂), 22.8 (CHMe₂), 15.1 (C α -CN). IR [ATR]: $\nu(C_{sp^2-H})$ 3122 (w); $\nu(C_{sp^3-H})$ 2961 (m), 2926 (m), 2865 (m); $\nu(C\equiv N)$ 2245 (w).

II.2.4. Compound 9: [Ni^{II}(Cp){Me-NHC-(CH₂)CH(CN)}]

Complex **9** was prepared by a modified literature procedure.¹²⁸ A 0.5 M solution of KHMDS in toluene (1.20 mmol, 2.4 cm³, 1 equiv.) was added dropwise to a dark pink solution of **5** (1.18 mmol, 524 mg) suspended in toluene (11 cm³) at r. t. The mixture gradually became a dark olive thick suspension as the addition progressed. The reaction mixture was stirred for

1 h and was filtered through a Celite pad (4 × Ø3 cm) that was rinsed with toluene until the washings were colorless (note: the dark brown degradation products on the top of the Celite pad rendered the filtration slow). The collected dark olive solution was then evaporated, and the residue was extracted with toluene and applied onto an alumina column (7 × Ø3 cm) that was eluted with toluene to give a light blue fraction, and with THF to recover a dark green solution. The dark green solution was then evaporated under vacuum, and the residue was washed with *n*-pentane (3 × 3 cm³) and dried under vacuum overnight, to afford the title compound as a green powder (121 mg, 0.334 mmol, 28%).

II.2.5. Compound 10: [Ni^{II}(Cp){Mes-NHC-(CH₂)CH(CN)}]

A 0.5 M solution of KHMDS in toluene (1.20 mmol, 2.4 mL) was added dropwise to a dark pink solution of **6** (1.18 mmol, 524 mg) suspended in toluene (11 cm³) at r. t. The resulting dark olive mixture was stirred for 1 h and was filtered through a Celite pad (4 × Ø3 cm) that was rinsed with toluene until the washings were colorless (note: the dark brown degradation products on the top of the Celite pad rendered the filtration slow). The collected dark olive solution was then evaporated, and the residue was extracted with toluene and applied onto an alumina column (7 × Ø5 cm) that was eluted with toluene to give a light blue fraction, and with THF to recover a dark green solution. The dark green solution was then evaporated under vacuum, and the residue was washed with *n*-pentane (3 × 3 cm³) and dried under vacuum overnight, to afford the title compound as a green powder (121 mg, 0.334 mmol, 28%). Anal. calcd for C₂₀H₂₁N₃Ni: C, 66.34; H, 5.85; N, 11.61. Found: C, 66.20; H, 5.89; N, 11.26. ¹H NMR (CDCl₃, 300.13 MHz): δ 6.99 (s, 1H, *m*-H), 6.97 (s, 1H, *m*-H), 6.96 (d, ³J = 2.0, 1H, NCH), 6.62 (d, ³J = 2.0, 1H, NCH), 4.77 (s, 5H, C₅H₅), 3.89 (m, 2H, NCH₂), 2.75 (dd, ³J = 7.8, ³J = 6.0, 1H, CHCN), 2.35 (s, 3H, *p*-Me), 2.08 (s, 3H, *o*-Me), 2.01 (s, 3H, *o*-Me). ¹³C {¹H} NMR (CDCl₃, 75.47 MHz): δ 175.9 (C_{NHC}), 139.4, 136.4, 136.1 and 135.5 (*p*-, *ipso*-, *o*-C_{Ar}), 131.5 (CN), 129.1 (*m*-C_{Ar}), 128.9 (*m*-C_{Ar}), 122.1 (NCH), 117.7 (NCH), 90.0 (C₅H₅), 54.2 (NCH₂), 21.3 (*p*-Me), 18.0 (*o*-Me), 17.8 (*o*-Me), -11.0 (C_{alkyl}). IR [ATR]: ν(C_{sp2}-H) 3153 (w), 3127 (m); ν(C_{sp3}-H) 2952 (w), 2919 (m), 2856 (w); ν(C≡N) 2185 (s).

II.2.5. Compound 11: [Ni^{II}(Cp){Mes-NHC-(CH₂)₂CH(CN)}]

Complex **11** was prepared by a modified literature procedure.¹²⁸ A 0.5 M solution of KHMDS in toluene (2.89 mmol, 5.78 cm³) was added dropwise to a dark pink solution of **7** (2.89 mmol, 1.19 g) suspended in toluene (24 cm³) at r. t. The resulting dark olive mixture was stirred for

2 h and was filtered through a Celite pad (4 × Ø3 cm) that was rinsed with toluene until the washings were colorless (note: the dark brown degradation products on the top of the Celite pad rendered the filtration slow). The collected dark green solution was then evaporated under vacuum, and the residue was washed with *n*-pentane (3 × 10 cm³) and dried under vacuum overnight to afford the title compound as a dark green powder (715 mg, 1.90 mmol, 66%).

II.2.6. Compound 12: [Ni^{II}(Cp){DIPP-NHC-(CH₂)₂CH(CN)}]

A 0.5 M solution of KHMDS in toluene (2.50 mmol, 5 cm³) was added dropwise to a dark pink solution of **8** (2.47 mmol, 1.12 g) in toluene (20 cm³) at r. t. The resulting dark green mixture was stirred for 1 h and was filtered through a Celite pad (4 × Ø3 cm) that was rinsed with toluene until the washings were colorless (note: the dark brown degradation products on the top of the Celite pad rendered the filtration slow). The collected dark green solution was then evaporated under vacuum, and the residue was washed with *n*-pentane (3 × 10 cm³) and dried under vacuum for 3 h to afford the title compound as a green powder (665 mg, 1.59 mmol, 64%). Anal. calcd for C₂₄H₂₉N₃Ni: C, 68.93; H, 6.99; N, 10.05. Found: C, 69.19; H, 7.01; N, 10.02. ¹H NMR (CDCl₃, 300.13 MHz): δ 7.49 (t, ³J = 7.8, 1H, *p*-H), 7.34 (dd, ³J = 7.8, ⁴J = 1.4, 1H, *m*-H), 7.27 (dd, ³J = 7.8, ⁴J = 1.4, 1H, *m*-H), 7.05 (d, ³J = 2.1, 1H, NCH), 6.73 (d, ³J = 2.1, 1H, NCH), 4.67 (s, 5H, C₅H₅), 4.01 (m, 1H, NCH₂), 3.84 (m, 1H, NCH₂), 2.78 (sept, ³J = 6.9, 1H, CHMe₂), 2.44 (sept, ³J = 6.9, 1H, CHMe₂), 2.15 (t, ³J = 6.6, 1H, CHCN), 1.68 (m, 1H, CH₂), 1.51 (d, ³J = 6.9, 3H, CHMe₂), 1.43 (m, 1H, CH₂), 1.34 (d, ³J = 6.9, 3H, CHMe₂), 1.07 (d, ³J = 6.9, 3H, CHMe₂), 1.02 (d, ³J = 6.9, 3H, CHMe₂). ¹³C {¹H} NMR (CDCl₃, 75.47 MHz): δ 172.6 (C_{NHC}), 146.9 and 145.8 (*o*-C_{Ar}), 137.2 (*ipso*-C_{Ar}), 132.5 (CN), 130.1 (*p*-C_{Ar}), 124.2 (NCH), 123.8 and 123.7 (*m*-C_{Ar}), 121.6 (NCH), 91.2 (C₅H₅), 50.3 (NCH₂), 30.2 (CH₂), 28.7 and 28.3 (CHMe₂), 25.9 and 25.7 (CHMe₂), 22.7 and 22.7 (CHMe₂), -25.1 (C_{alkyl}). IR [ATR]: ν(C_{sp²}-H) 3140 (w); ν(C_{sp³}-H) 2951 (m), 2924 (w), 2862 (w); ν(C≡N) 2179 (m).

II.2.7. Compound 13: [Ni^{II}{Me-NHC-(CH₂)CH(CN)}(MeCN)]PF₆

Aqueous HCl (37%) diluted in acetonitrile to 1.0 M (1.06 mmol, 1.06 cm³, 1 equiv.) was added dropwise to an equimolar amount of a dark green suspension of **9** (1.07 mmol, 277 mg) and KPF₆ (1.06 mmol, 196 mg) in acetonitrile (16 cm³) at 0 °C. The reaction mixture rapidly turned ochre yellow and was stirred for 10 min at 0 °C before being warmed to r. t. and filtered on a Celite pad (4 × Ø3 cm), which was subsequently rinsed with acetonitrile until the washings were colorless. Volatiles were evaporated under vacuum, and the resulting solid was washed with pentane (3 × 3 cm³), and dried overnight under vacuum at r. t. to afford the title compound

as a dark yellow solid (380 mg, 1.00 mmol, 95%). Anal. calcd for C₉H₁₁F₆N₄NiP: C, 28.53; H, 2.93; N, 14.79. Found: C, 28.78; H, 3.00; N, 12.99. Repeated attempts to obtain correct elemental analyses gave low nitrogen values. HR-MS (ESI): m/z [M]⁺ calcd for C₉H₁₁N₄Ni 233.0332, found 233.0328. ¹H NMR (CD₃CN, 400.14 MHz): δ 7.07 (d, ³J = 2.0, 1H, NCH), 6.90 (d, ³J = 2.0, 1H, NCH), 3.86 (dd, ²J = 12.8, ³J = 7.6, 1H, NCH₂), 3.62 (s, 3H, NMe), 3.55 (dd, ²J = 12.8, ³J = 2.8, 1H, NCH₂), 2.59 (m, 1H, CHCN), 1.96 (s, 3H, free CH₃CN). ¹H NMR (C₅D₅N, 300.13 MHz): δ 7.19 (s, 1H, NCH), 6.94 (s, 1H, NCH), 3.81 (m, 2H, NCH₂), 2.49 (s, 3H, NMe), 2.42 (br., 1H, CHCN), 1.83 (s, 3H, CH₃CN). ¹³C {¹H} NMR (CD₃CN, 100.61 MHz): δ 156.6 (br., C_{NHC}), 126.2 and 119.1 (NCH), 52.4 (NCH₂), 37.7 (NMe), 7.1 (br., C_{alkyl}). ¹³C {¹H} NMR (C₅D₅N, 125.77 MHz): δ 161.0 (C_{NHC}), 128.8 and 128.4 (CH₃CN and CHCN), 126.3 and 119.1 (NCH), 52.8 (NCH₂), 35.4 (NMe), 8.9 (br. C_{alkyl}), 1.8 (CH₃CN). IR [ATR]: ν(C_{sp²-H}) 3174 (w), 3149 (w); ν(C_{sp³-H}) 2951 (w); ν(C≡N) 2239 (m); ν(P-F) 823 (s).

II.2.8. Compound 14: [Ni^{II}{Mes-NHC-(CH₂)CH(CN)}(MeCN)]PF₆

Aqueous HCl (37%) diluted in acetonitrile to 1.0 M (0.130 mmol, 0.13 cm³, 1 equiv.) was added dropwise to an equimolar amount of a dark green suspension of **10** (0.133 mmol, 48 mg) and KPF₆ (0.125 mmol, 23 mg, 0.95 equiv.) in acetonitrile (2 cm³) at 0 °C. The reaction mixture rapidly turned ochre yellow and was stirred for 10 min at 0 °C, before being warmed to r. t. and filtered on a Celite pad (4 × Ø3 cm) that was rinsed with acetonitrile until the washings were colorless. Volatiles were evaporated under vacuum, and the resulting solid was washed with *n*-pentane (3 × 2 cm³), and dried overnight under vacuum at r. t. to afford the title compound as a dark yellow solid (52 mg, 0.108 mmol, 86%). Anal. calcd for C₁₇H₁₉F₆N₄NiP: C, 42.27; H, 3.97; N, 11.60. Found: C, 41.68; H, 4.07; N, 11.30. HR-MS (ESI): m/z [M]⁺ calcd for C₁₇H₁₉N₄Ni 337.0958, found 337.0985. ¹H NMR (CD₃CN, 500.15 MHz): δ 7.32 (s, 1H, NCH), 7.07 (s, 1H, *m*-H), 7.02 (s, 1H, *m*-H), 6.89 (d, 1H, NCH), 3.96 (dd, ²J = 12.5, ³J = 7.5, 1H, NCH₂), 3.67 (m, 1H, NCH₂), 2.65 (m, 1H, CHCN), 2.29 (s, 3H, *p*-Me), 2.20 (br. s, 3H, *o*-Me), 2.06 (s, 3H, *o*-Me), 1.97 (s, 3H, free CH₃CN). ¹H NMR (C₅D₅N, 300.13 MHz): δ 7.58 (d, ³J = n. d., 1H, NCH), 7.01 (d, ³J = 1.8, 1H, NCH), 6.59 (s, 1H, *m*-H), 6.31 (s, 1H, *m*-H), 4.15 (dd, ²J = 12.6, ³J = 7.5, 1H, NCH₂), 3.92 (dd, ²J = 12.6, ³J = 3.0, 1H, NCH₂), 2.29 (dd, ³J = 7.5, ³J = 3.0, 1H, CHCN), 2.21 (s, 3H, *o*-Me), 2.06 (s, 3H, *p*-Me), 1.86 (s, 6H, *o*-Me and free CH₃CN). ¹³C {¹H} NMR (CD₃CN, 125.77 MHz): δ 158.6 (br., C_{NHC}), 140.6 136.5, 136.2, 135.8 (*ipso*-, *p*-, *o*-C_{Ar}), 130.0 and 129.8 (*m*-C_{Ar}), 125.5 and 120.4 (NCH), 53.1 (NCH₂), 21.0 (*p*-Me), 17.9 and 17.6 (*o*-Me), 7.8 (C_{alkyl}). ¹³C {¹H} NMR (C₅D₅N, 125.77 MHz): δ 162.8 (C_{NHC}), 139.7, 135.2, 134.7, 134.3 (*ipso*-, *p*-, *o*-C_{Ar}), 129.8 (*m*-C_{Ar}), 126.6 (CHCN), 125.7 and 120.4 (NCH), 117.9 (free CH₃CN), 53.2 (NCH₂),

20.9 (*p*-Me), 18.1 and 17.9 (*o*-Me), 9.7 (C_{alkyl}), 1.4 (free CH_3CN). IR [ATR]: $\nu(\text{C}_{\text{sp}^2\text{-H}}$) 3169 (w), 3144 (w); $\nu(\text{C}_{\text{sp}^3\text{-H}}$) 2941 (w), 2924 (w), 2864 (w); $\nu(\text{C}\equiv\text{N})$ 2243 (m); $\nu(\text{P-F})$ 829 (s).

II.2.9. Compound 15: $[\text{Ni}^{\text{II}}\{\text{Mes-NHC}-(\text{CH}_2)_2\text{CH}(\text{CN})\}(\text{MeCN})]\text{PF}_6$

Complex **15** was prepared by a modified literature procedure.¹³¹ Aqueous HCl (37%) diluted in acetonitrile to 1.0 M (1.30 mmol, 1.30 cm^3 , 1 equiv.) was added dropwise to an equimolar amount of a dark green suspension of **11** (1.30 mmol, 536 mg) and KPF_6 (1.30 mmol, 239 mg) in acetonitrile (10 cm^3) at 0 °C. The reaction mixture rapidly turned ocher yellow and was stirred for 10 min at 0 °C, before being warmed to r. t. and filtered on a Celite pad (4 × Ø3 cm) that was rinsed with acetonitrile until the washings were colorless. Volatiles were evaporated under vacuum, and the resulting solid was washed with *n*-pentane (3 × 10 cm^3) and dried overnight under vacuum at 50 °C to afford the title compound as a dark yellow solid (627 mg, 1.26 mmol, 97%). Anal. calcd for $\text{C}_{18}\text{H}_{21}\text{F}_6\text{N}_4\text{NiP}$: C, 43.50; H, 4.26; N, 11.27. Found: C, 43.49; H, 4.31; N, 10.82. HR-MS (ESI): m/z $[\text{M}]^+$ calcd for $\text{C}_{18}\text{H}_{21}\text{N}_4\text{Ni}$ 351.1114, found 351.1126. ^1H NMR (CD_3CN , 500.14 MHz): δ 7.32 (s, 1H, NCH), 7.30 (br., 1H, *m*-H), 7.07 (s, 1H, *m*-H), 7.04 (s, 1H, NCH), 4.13 and 4.03 (2 m, 2 × 1H, NCH_2), 2.57 (s, 3H, *o*-Me), 2.42 (br. s, 4H, *p*-Me and CHCN), 2.03 (s, 3H, *o*-Me), 1.96 (s, 3H, free CH_3CN), 1.67 (br., 1H, NCH_2CH_2), 1.05 (br., 1H, NCH_2CH_2). ^1H NMR ($\text{C}_5\text{D}_5\text{N}$, 300.13 MHz): δ 7.58 (d, $^3J = \text{n. d.}$, 1H, NCH), 7.1 (d, $^3J = 1.8$, 1H, NCH), 6.89 (s, 1H, *m*-H), 6.41 (s, 1H, *m*-H), 4.41 (m, 1H, NCH_2), 4.30 (m, 1H, NCH_2), 2.81 (s, 3H, *o*-Me), 2.20 (s, 3H, *p*-Me), 2.01 (dd, 1H, $^3J = 8.1$, $^3J = 6.9$, CHCN), 1.86 (s, 3H, free CH_3CN), 1.82 (m, 1H, CH_2), 1.46 (s, 3H, *o*-Me), 1.29 (m, 1H, CH_2). ^{13}C $\{^1\text{H}\}$ NMR (CD_3CN , 125.77 MHz): δ 155.4 (br., C_{NHC}); 140.4, 136.5, 136.2, 135.7 (*ipso*-, *p*-, *o*- C_{Ar}), 130.4 and 130.1 (*m*- C_{Ar}), 125.5 and 123.7 (NCH), 50.5 (NCH_2), 29.2 (CH_2), 21.1 (*p*-Me), 19.1 and 18.3 (*o*-Me), -2.0 (br., C_{alkyl}). ^{13}C $\{^1\text{H}\}$ NMR ($\text{C}_5\text{D}_5\text{N}$, 125.77 MHz): δ 161.9 (C_{NHC}), 139.6, 134.4, (*ipso*-, *p*- or *o*- C_{Ar}), 130.5 and 130.0 (*m*- C_{Ar}), 128.1 (CHCN), 125.0 (NCH), 118.0 (free CH_3CN), 50.9 (NCH_2), 30.3 (CH_2), 21.1 (*p*-Me), 19.8 and 18.4 (*o*-Me), 1.5 (free CH_3CN), 0.9 (C_{alkyl}). IR [ATR]: $\nu(\text{C}_{\text{sp}^2\text{-H}}$) 3174 (w), 3146 (w); $\nu(\text{C}_{\text{sp}^3\text{-H}}$) 2943 (w), 2922 (w), 2862 (w); $\nu(\text{C}\equiv\text{N})$ 2236 (m); $\nu(\text{P-F})$ 829 (s).

II.2.10. Compound 16: $[\text{Ni}^{\text{II}}\{\text{DIPP-NHC}-(\text{CH}_2)_2\text{CH}(\text{CN})\}(\text{MeCN})]\text{PF}_6$

Aqueous HCl (37%) diluted in acetonitrile to 1.0 M (0.430 mmol, 0.43 m^3 , 1 equiv.) was added dropwise to an equimolar amount of a dark green suspension of **12** (0.495 mmol, 207 mg) and KPF_6 (0.429 mmol, 79 mg) in acetonitrile (4 cm^3) at 0 °C. The reaction mixture rapidly turned ocher yellow and was stirred for 10 min at 0 °C, before being warmed to r. t. and filtered on a

Celite pad (4 × Ø3 cm) that was rinsed with acetonitrile until the washings were colorless. Volatiles were evaporated under vacuum, and the resulting solid was washed with *n*-pentane (3 × 3 cm³), and dried overnight under vacuum at r. t. to afford the title compound as a dark yellow solid (200 mg, 0.371 mmol, 86%). Anal. calcd for C₂₁H₂₇F₆N₄NiP: C, 46.78; H, 5.05; N, 10.39. Found: C, 46.72; H, 5.33; N, 10.19. HR-MS (ESI): *m/z* [M]⁺ calcd for C₂₁H₂₇N₄Ni 393.1584, found 393.1604. ¹H NMR (CD₃CN, 400.14 MHz): δ 7.50 (d, ³*J* = 5.4, 1H, *m*-H), 7.50 (d, ³*J* = 4.0, 1H, *m*-H), 7.35 (dd, ³*J* = 5.4, ³*J* = 4.0, 1H, *p*-H), 7.32 (d, ³*J* = 1.4, 1H, NCH), 7.11 (d, ³*J* = 1.4, 1H, NCH), 4.09 (m, 2H, NCH₂), 3.42 (sept, 1H, CHMe₂), 2.50 (sept, ³*J* = 6.8, 1H, CHMe₂), 2.28 (t, ³*J* = 6.4, 1H, CHCN), 1.96 (s, 3H, free CH₃CN), 1.89 (d, ³*J* = 6.8, 3H, CHMe₂), 1.75 (m, 1H, CH₂), 1.24 (d, ³*J* = 6.8, 3H, CHMe₂), 1.16 (d, ³*J* = 6.8, 3H, CHMe₂), 1.15 (m, 1H, CH₂), 1.13 (d, ³*J* = 6.8, 3H, CHMe₂). ¹H NMR (C₅D₅N, 300.13 MHz): δ 7.62 (d, ³*J* = 1.4, 1H, NCH), 7.53 (m, 2H, *m*-H), 7.45 (d, ³*J* = 1.4, 1H, NCH), 6.97 (dd, ³*J* = 6.6, ³*J* = n. d., 1H, *p*-H), 4.54 (m, 2H, NCH₂ and CHMe₂), 4.40 (m, 1H, NCH₂), 2.08 (d, ³*J* = 6.6, 3H, CHMe₂), 2.00 (m, 2H, CHMe₂ and CHCN), 1.85 (s, 3H, free CH₃CN), 1.30 (m, 2H, CH₂), 1.04 (d, ³*J* = 6.6, 3H, CHMe₂), 0.98 (d, ³*J* = 6.6, 3H, CHMe₂), 0.38 (d, ³*J* = 6.8, 3H, CHMe₂). ¹³C {¹H} NMR (CD₃CN, 100.61 MHz): δ 153.8 (br., C_{NHC}), 146.9 and 146.2 (*o*-C_{Ar}), 136.4 (*ipso*-C_{Ar}), 131.4 (*m*-C_{Ar}), 126.9 (NCH), 125.4 and 125.2 (*p*- and *m*-C_{Ar}), 123.6 (NCH), 49.8 (NCH₂), 29.7 and 29.1 (CHMe₂), 28.1 (CH₂), 25.3, 25.1, 24.4 and 23.5 (CHMe₂), -2.7 (br., C_{alkyl}). ¹³C {¹H} NMR (C₅D₅N, 125.77 MHz): δ 161.8 (C_{NHC}), 146.3 and 145.9 (*o*-C_{Ar}), 131.0 (*m*-C_{Ar}), 127.9 (CHCN), 127.2 (NCH), 125.2 (*p*- or *m*-C_{Ar}), 123.1 (NCH), 118.0 (free CH₃CN), 50.9 (NCH₂), 30.3 (CHMe₂), 28.4 (CH₂), 26.7, 25.6, 24.0 and 22.6 (CHMe₂), 1.4 (free CH₃CN), 0.8 (C_{alkyl}). IR [ATR]: ν(C_{sp²}-H) 3179 (w), 3164 (w); ν(C_{sp³}-H) 2966 (m), 2922 (m), 2867 (m); ν(C≡N) 2233 (m); ν(P-F) 834 (s).

II.2.11. Compound 17: [Ni^{II}{Mes-NHC-(CH₂)₂CH(CN)}(PPh₃)]PF₆

Complex **15** (0.296 mmol, 147 mg) and PPh₃ (0.297 mmol, 78 mg, 1 equiv.) were stirred in acetonitrile (4.5 cm³) for 30 min at r. t., filtered over a Celite pad (4 × Ø3 cm). The solvent was evaporated and the residue washed with *n*-pentane (3 × 3 cm³) and dried overnight under vacuum at r. t. to yield the title compound as an orange powder (176 mg, 0.256 mmol, 85%). ¹H NMR (CD₃CN, 400.13 MHz): δ 7.47-7.37 (m, 15H, PPh₃), 7.34 (s, 1H, NCH), 7.28 (s, 1H, *m*-H), 7.10 (s, 1H, NCH), 7.03 (s, 1H, *m*-H), 4.13 (t, ³*J* = 6.0, 2H, NCH₂), 2.60 (s, 3H, *o*-Me), 2.34 (s, 3H, *p*-Me), 2.00 (s, 3H, *o*-Me) 1.24 (br., 1H, CH₂). ³¹P {¹H} NMR (CD₃CN, 161.97 MHz): δ -5.23 (v. br., PPh₃), -144.36 (sept, ¹*J*_{P-F} = 712.67, PF₆⁻).

II.2.12. Compound **18**: $[\text{Ni}^{\text{II}}\{\text{Mes-NHC}-(\text{CH}_2)_2\text{CH}(\text{CN})\}(\text{PMe}_3)]\text{PF}_6$

A 0.5 M solution of PMe_3 in *n*-pentane (0.200 mmol, 0.40 cm³, 1 equiv.) was dropwise added to a yellow solution of **15** (0.203 mmol, 101 mg) in acetonitrile (3 cm³) and stirred at r. t. for 15 min. As the addition progressed the color of the solution turned from dark yellow to a blood-orange. The solvent was then evaporated and the residue washed with *n*-pentane (3 × 3 cm³) and dried overnight under vacuum at r. t. to yield the title compound as an orange powder (0.197 mmol, 99 mg, 97%). ¹H NMR (CD₃CN, 400.13 MHz): δ 7.31 (d, ³J = 4.0, NCH), 7.156 (s, 1H, *m*-H), 7.12 (s, 1H, NCH), 7.04 (s, 1H, *m*-H), 4.22-4.10 (m, 2H, NCH₂), 2.53 (s, 3H, *o*-Me), 2.34 (s, 3H, *p*-Me), 2.11 (s, 3H, *o*-Me), 1.5 (br, 1H, CH₂), 1.27 (br., 9H, PMe_3). ³¹P {¹H} NMR (CD₃CN, 161.97 MHz): δ -12.01 (v. br., PMe_3), -144.62 (sept, ¹J_{P-F} = 706.19, PF_6^-). IR [ATR]: ν(C_{sp²}-H) 3147; ν(C_{sp³}-H) 2919 (m); ν(C≡N) 2213 (m); ν(P-F) 828 (s).

II.2.13. Compound **19**: $[\text{Ni}^{\text{II}}(\mu^2\text{-OH})\{\text{Mes-NHC}-(\text{CH}_2)_2\text{CH}(\text{CN})\}]\text{PF}_6$

Complex **15** (0.207 mmol, 103 mg) and KO*t*-Bu (0.205 mmol, 23 mg, 1 equiv.) were suspended in CH₂Cl₂ (3 cm³). The resulting dark yellow suspension was stirred for 25 min at r. t. and then filtered on a Celite pad (4 × Ø3 cm) that was rinsed with CH₂Cl₂ until the washings were colourless. The collected dark yellow solution was then evaporated to dryness and the resulting solid was washed with pentane (3 × 3 cm³). Recrystallization from CH₂Cl₂ (2 cm³) and *n*-hexane (8 cm³) at -28 °C for 1 night then afforded a brown precipitate that was washed with *n*-pentane (3 × 3 cm³) and dried under vacuum to give a brown powder (49 mg, 0.075 mmol, 73%). **19-RS and 19-SR**: ¹H NMR (CDCl₃, 400.14 MHz): δ 7.15 (s, 1H, *m*-H), 6.91 (s, 1H, *m*-H), 6.82 (d, ³J = 1.6, 1H, NCH), 6.52 (d, ³J = 1.6, 1H, NCH), 3.91-3.75 (m, 2H, NCH₂), 2.76 (s, 3H, *p*-Me), 2.33 (s, 3H, *o*-Me), 1.96 (s, 3H, *o*-Me), 1.69 (m, 1H, NCH₂CH₂), 0.99 (m, 1H, NCH₂CH₂), 0.12 (dd, ³J = 5.6, ³J = 6.0, 1H, CHCN), -5.34 (s, 1H, OH). **19-RR and 19-SS**: ¹H NMR (CDCl₃, 400.14 MHz): δ 7.30 (s, 1H, *m*-H), 6.86 (s, 1H, *m*-H), 6.80 (d, ³J = 2.0, 1H, NCH), 6.54 (d, ³J = 2.0, 1H, NCH), 3.91-3.75 (m, 2H, NCH₂), 2.87 (s, 3H, *p*-Me), 2.36 (s, 3H, *o*-Me), 1.96 (s, 3H, *o*-Me), 1.17 (m, 2H, NCH₂CH₂), -0.14 (t, ³J = 5.0, 1H, CHCN), -5.60 (s, 1H, OH). **19**: IR [ATR]: ν(O-H) 3627 (m), ν(C_{sp²}-H) 3160 (w), 3126 (w), 3093 (w); ν(C_{sp³}-H) 2970 (w), 2950 (w), 2913 (m), 2857 (w); ν(C≡N) 2190 (m).

II.2.14. Compound **22**: $[\text{Ni}^{\text{II}}\{\text{Mes-NHC}-(\text{CH}_2)_2\text{CH}(\text{CN})\}(\text{bipy})]\text{PF}_6$

Complex **15** (0.052 mmol, 26 mg) and bipy (0.058 mmol, 9 mg) were dissolved in acetonitrile (1 cm³) and stirred at r. t. for 5 min. The mixture immediately turned orange. The residue was

evaporated, and washed with Et₂O (3 × 5 cm³), *n*-pentane (3 × 5 cm³) and dried under vacuum overnight at r. t. to yield the title compound as an orange powder (27 mg, 0.044 mmol, 85%). ¹H NMR (CD₃CN, 300.13 MHz): δ = 8.10-8.02 (m, 4H, bipy), 7.93-7.87 (m, 2H, bipy), 7.41 (s, 1H, *m*-H_{Mes} or NCH), 7.31 (s, 1H, *m*-H_{Mes} or NCH), 6.62 (s, 1H, *m*-H_{Mes} or NCH), 6.55 (s, 1H, *m*-H_{Mes} or NCH) 4.43-4.39 (m, 1H, NCH₂), 4.31-4.21 (m, 1H, NCH₂), 2.62 (s, 3H, *o*-Me), 2.51 (br., 1H, CHCN), 2.32 (s, 1H, CH₂), 2.20 (s, 3H, *p*-Me), 2.02 (s, 3H, *o*-Me), 1.73 (d, ³J = n. d., CH₂). IR [ATR]: ν(C_{sp2}-H) 3174 (w), 3464 (w), 3091 (w); ν(C_{sp3}-H) 2957 (m), 2921 (m), 2857 (m); ν(C≡N) 2193 (m); ν(P-F) 829 (s).

II.2.15. Compound 27: [Ni^{II}(btz)(Cp)(NHC-Mes₂)]

A 0.5 M solution of KHMDS in toluene (0.600 mmol, 1.2 cm³) was added to a solution of **24** (0.431 mmol, 200 mg) and benzothiazole (0.514 mmol, 56 mm³) in toluene (12 cm³) at r. t., resulting in an immediate change of color from red to green. After 12 h, the reaction medium was filtered through a Celite pad (4 × Ø3 cm) and concentrated in vacuo to give a brownish powder that was washed with *n*-pentane (3 × 10 cm³). Re-dissolution of this solid in toluene (10 cm³) and THF (0.5 cm³) and filtration through neutral alumina with toluene and toluene/THF (20:1) as successive eluents then afforded a green solution that was evaporated to dryness to give the title compound as a green-brown powder (193 mg, 0.343 mmol, 80%). Anal. Calcd for C₃₃H₃₃N₃NiS: C, 70.48; H, 5.91; N, 7.47. Found: C, 70.55; H, 5.98; N, 7.80. HR-MS (ESI): *m/z* [M+H]⁺ calcd for C₃₃H₃₄N₃NiS 562.1821, found 562.1789. ¹H NMR (CDCl₃, 300.13 MHz): δ 7.58 (d, ³J = 8.1, 1H, btz), 7.51 (d, ³J = 7.8, 1H, btz), 7.12 (m, 1 H, btz), 6.98 (m, 1H, btz), 6.91 (s, 2H, NCH), 6.89 (s, 4H, *m*-H_{Mes}), 4.83 (s, 5H, C₅H₅), 2.38 (s, 3H, *p*-Me), 2.10 (s, 6H, *o*-Me). ¹³C {¹H} NMR (CDCl₃, 75.47 MHz): δ 177.9 (C_{NHC}), 176.0 (C_{btz}), 155.1 (C_{3a_{btz}}), 140.6 (C_{7a_{btz}}), 138.8 (*p*-C_{Mes}), 136.8 (*ipso*-C_{Mes}), 135.6 (*o*-C_{Mes}), 129.1 (*m*-C_{Mes}), 123.5 (NCH), 122.8, 120.4, 119.5 and 118.6 -C(3,4,5,6)_{btz}, 91.4 (C₅H₅), 21.3 (*p*-Me), 18.5 (*o*-Me).

II.2.16. Compound 28: [Ni^{II}(btz)(Cp*)(NHC-Mes₂)]

A 0.5 M solution of KHMDS in toluene (0.500 mmol, 90 mm³, 1.1 equiv.) was added to a solution of **25** (0.442 mmol, 236 mg) and benzothiazole (0.442 mmol, 59.7 mg, 47.5 mm³, 1 equiv.) in toluene (12 cm³) at r. t., resulting in an immediate change of color from red to olive. After 2 h, volatiles were evaporated, *n*-pentane (10 cm³) was added and evaporated, the brown residue extracted in toluene and loaded atop an alumina pad (4 × Ø3 cm) that was rinsed with dry toluene, to elute a yellow fraction, followed by a mixture of toluene/THF (20/1) to recover a second olive fraction that was then evaporated and dried under vacuum at r. t. to give the title

compound as an olive solid (34 mg, 0.054 mmol, 12%). ^1H NMR (C_6D_6 , 300.13 MHz): δ 7.92 (d, $^3J = 7.8$, 1H, H7_{btz}), 7.76 (d, $^3J = 7.5$, 1H, H4_{btz}), 7.12 (td, $^3J = 7.2$, $^4J = 1.2$, 1 H, H6_{btz}), 7.02 (td, $^3J = 7.2$, $^4J = 1.2$, 1H, H5_{btz}), 6.16 (s, 4H, $m\text{-H}_{\text{Mes}}$), 6.00 (s, 2H, $m\text{-H}_{\text{Mes}}$), 2.23 (s, 6H, $p\text{-Me}$), 2.09 (s, 12H, $o\text{-Me}$), 1.43 (s, 15H, C_5H_5). ^{13}C $\{^1\text{H}\}$ NMR (C_6D_6 , 125.78 MHz): δ 187.1 (C_{NHC}), 176.0 (C_{NHC}), 156.8 (C7_{btz}), 141.0 (C3_{btz}), 138.2 ($p\text{-C}_{\text{Mes}}$), 137.9 ($o\text{-C}_{\text{Mes}}$), 136.8 ($ipso\text{-C}_{\text{Mes}}$), 129.3 ($m\text{-C}_{\text{Mes}}$), 123.9 (NCH), 120.6 (C4_{btz}), 120.0 (C7_{btz}), 119.4 (C5_{btz}), 111.9 (C6_{btz}), 101.3 (C_5Me_5), 21.2 ($p\text{-Me}$), 19.1 ($o\text{-Me}$), 19.1 (C_5Me_5).

II.2.17. Compound 29: $[\text{Ni}^{\text{II}}\text{Cl}(\text{Cp}^*)(^{4,5}\text{Me}_2\text{NHC-Mes}_2)]$

1,2,3,4,5-Pentamethylcyclopentadiene (1.66 mmol, 226 mg, 266 mm^3) was dissolved in THF (2 cm^3) and the resulting colorless solution cooled to $-25\text{ }^\circ\text{C}$. A 1.5 M *Li**n*-Bu solution in hexanes (1.70 mmol, 1.0 cm^3 , 1 equiv.) was added dropwise added and stirred for 20 min at $-25\text{ }^\circ\text{C}$. A thick white/pink slurry formed. This slurry was then added to a green slurry of $[\text{Ni}(\text{acac})_2]_3$ (0.559 mmol, 431 mg, 0.33 equiv.) in THF (5 cm^3) also at $-25\text{ }^\circ\text{C}$. The cooling bath was then removed, and the mixture warmed to r. t. and the mixture stirred for 1 h. The reaction mixture progressively turns rust/brick red colored. The mixture was then cooled again to $-25\text{ }^\circ\text{C}$ and a suspension of 1,3-bis-(2,4,6-trimethylphenyl)-4,5-bis-methyl-imidazolium chloride (1.66 mmol, 611 mg, 1 equiv.) in THF (5 cm^3), also at $-25\text{ }^\circ\text{C}$, was added to the slurry. The resulting mixture was stirred at $-25\text{ }^\circ\text{C}$ for 30 min and then warmed to r. t. for 30 min and heated to $50\text{ }^\circ\text{C}$ for 30 min during which the mixture turned purple. After cooling the medium to r. t., the solvent was evaporated and the residue extracted with toluene and filtered over a Celite pad (4 \times \varnothing 3 cm) that was rinsed with toluene until the washings came out colorless. The purple filtrate was then concentrated under vacuum, and *n*-pentane (6 \times 10 cm^3) was added to precipitate a pink solid. The solution was filtered off and the solid washed with *n*-pentane (3 \times 10 cm^3). The solid was then extracted with *n*-hexane and filtered over a Celite pad (4 \times \varnothing 3 cm) that was rinsed with dry *n*-hexane until the washings came out colorless. The pink filtrate was then evaporated and dried under vacuum for 3 h at r. t. to give the title compound as a pink powder (144 mg, 0.256 mmol, 15%). HR-MS (ESI): m/z $[\text{M}]^+$ calcd for $\text{C}_{33}\text{H}_{43}\text{ClN}_2\text{Ni}$ 560.2468, found 560.2454. ^1H NMR (C_6D_6 , 500.18 MHz): δ 7.00 (s, 2H, $m\text{-H}$), 6.83 (s, 2H, $m\text{-H}$), 2.77 (s, 6H, $o\text{-Me}$), 2.22 (s, 6H, $p\text{-Me}$), 1.74 (s, 6H, $o\text{-Me}$), 1.42 (s, 6H, NCMe), 1.26 (s, 15H, C_5Me_5). ^1H NMR (C_6D_6 , 125.78 MHz): δ 173.1 (C_{NHC}), 139.2 ($o\text{-C}$), 138.2 ($o\text{-C}$), 136.3 ($ipso\text{-C}$), 135.3 ($p\text{-C}$), 130.5, 129.3 ($m\text{-C}$), 127.3 (NCMe), 101.9 (C_5Me_5), 21.1 ($o\text{-Me}$), 20.7 ($o\text{-Me}$), 18.6 ($p\text{-Me}$), 9.9 (C_5Me_5), 6.2 (NCMe). IR [ATR]: $\nu(\text{C}_{\text{sp}^3\text{-H}}$) 2948 (s), 2919 (vs), 2853 (s).

III. Catalytic reactions

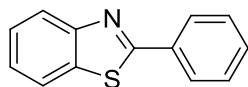
III.1. Benzothiazole arylation

Typical procedure: an oven dried Schlenk tube equipped with a magnetic stir bar was charged with **15** (0.020 mmol, 10 mg, 5 mol%), LiO*t*-Bu (0.737 mmol, 59 mg, 2 equiv.), benzothiazole (0.369 mmol, 50 mg, 40 mm³) and iodobenzene (0.536 mmol, 112 mg, 60 mm³, 1.5 equiv.) and 1,4-dioxane (3 cm³), and sealed. The Schlenk tube was then introduced into an oil bath that was heated up to a temperature of 140 °C. After 36 h, the reaction medium was cooled to room temperature, and the volatiles were evaporated under high vacuum. The resulting brown residue was extracted with diethyl ether and filtered over a silica pad (43-60 μm, 2.5 × Ø1 cm). The collected filtrate was then concentrated under vacuum, and loaded onto a silica column (Merck Silica Gel 60 - mesh size 43-60 μm; 28 × Ø3.5 cm) pre-wet with petroleum ether (bp. 40-70 °C). Elution with a petroleum ether/ethyl acetate mixture (benzothiazole derivatives: 98/2; other azoles: 90/10) afforded the coupling product.

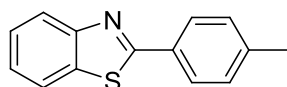
III.2. Benzothiazole alkylation

Typical procedure: an oven dried Schlenk tube (5 cm³) with a Teflon lined screw cap was charged with **25** (0.024 mmol, 13 mg, 5 mol%), and white powder LiO*t*-Bu (1.049 mmol, 84 mg, 2 equiv.). The solids were degassed and put under an Ar flow. Colorless liquids benzothiazole (0.502 mmol, 67.9 mg, 54.7 mm³) and 1-iododecane (0.750 mmol, 201.1 mg, 160 mm³, 1.5 equiv.) were added followed by 1,4-dioxane (1 cm³) and the system closed. The reaction mixture was stirred for 30 seconds at r. t. and then heated in an oil bath pre-heated to 120 °C. After 16 h the reaction mixture was cooled to r. t., quenched with water (5 cm³), diluted with HCl 2 M (aq.) (1 cm³). It was then extracted with ethyl acetate (3 × 15 cm³), dried over anhydrous MgSO₄, filtered and evaporated. The crude was extracted in a toluene/*n*-hexane mixture and loaded onto a silica gel column (43-60 μm; 4 × Ø5 cm) column packed in *n*-hexane. The column was slowly eluted (NOTE: the solvent level above the column must remain less than 1 cm in height or the weight of the solvent will be enough to mix the fractions) and the first fraction, collected and evaporated. The resulting dark yellow oil was then extracted in toluene and reloaded onto a silica gel column (60-200 μm; 6 × Ø2 cm) and eluted with pure toluene to recover the third fraction, that was then concentrated, evaporated and dried under vacuum to give 2-decylbenzothiazole as a yellow oil (61 mg, 0.221 mmol, 44%).

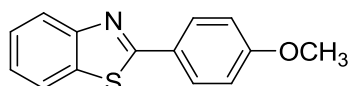
III.3. NMR data of the azole coupling products

2-Phenylbenzo[d]thiazole³²⁰

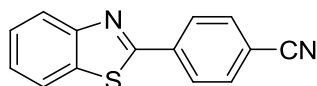
¹H NMR (CDCl₃, 300 MHz): δ 8.12-8.07 (m, 3H), 7.92 (d, ³J = 7.8, 1H), 7.53-7.47 (m, 4H) 7.39 (ddd, ³J = 8.1, ³J = 7.2, ⁴J = 1.2, 1 H). ¹³C {¹H} NMR (CDCl₃, 75 MHz): δ 168.2 (NCS), 154.3 (NCCH), 135.2, 133.8, 131.1, 129.1 (C₆H₅), 127.7 (C₆H₅), 126.4, 125.3, 123.4, 121.7.

2-(*p*-Tolyl)benzo[d]thiazole³²¹

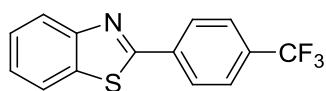
¹H NMR (CDCl₃, 300 MHz): δ 8.06 (d, ³J = 8.1, 1H, C₆H₄NS), 7.99 (d, ³J = 8.1, 2H, C₆H₄Me), 7.89 (d, ³J = 8.1, C₆H₄NS), 7.49 (ddd, ³J = 8.1, ³J = 7.2, ⁴J = 1.5, 1H, C₆H₄NS), 7.37 (ddd, ³J = 8.1, ³J = 7.2, ⁴J = 1.2, 1H, C₆H₄NS), 7.30 (d, ³J = 8.1, 2H, C₆H₄Me), 2.43 (s, 3H, CH₃). ¹³C {¹H} NMR (CDCl₃, 75 MHz): δ 168.4 (NCS), 154.3 (NCCH), 141.6, 135.1, 131.1, 129.9, 127.7, 126.4, 125.2, 123.2, 121.7, 21.7 (CH₃).

2-(4-Methoxyphenyl)benzo[d]thiazole³²⁰

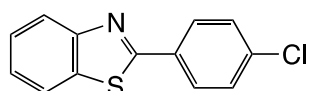
¹H NMR (CDCl₃, 500 MHz): δ 8.05 (d, ³J = 9.0, 2H, C₆H₄OMe), 8.04 (m, 1H, C₆H₄NS), 7.88 (ddd, ³J = 8.3, ⁴J n. d., ⁵J n. d., 1 H, C₆H₄NS), 7.47 (ddd, ³J = 8.3, ³J = 7.0, ⁴J = 1.3, 1H, C₆H₄NS), 7.36 (ddd, ³J = 8.3, ³J = 7.0, ⁴J = 1.0, 1H, C₆H₄NS), 7.01 (d, ³J = 9.0, 2H, C₆H₄OMe), 3.89 (s, 3H, OCH₃). ¹³C NMR (CDCl₃, 125 MHz): δ 168.1 (NCS), 162.1 (COMe), 154.2 (NCCH), 134.9, 129.3 (C₆H₄OMe), 126.5, 126.4, 125.0, 122.9, 121.7, 114.5 (C₆H₄OMe), 55.6 (OCH₃).

2-(4-Cyanophenyl)benzo[d]thiazole³²²

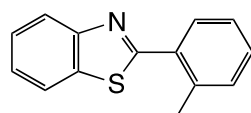
¹H NMR (CDCl₃, 500 MHz): δ 8.18 (d, ³J = 8.0, 2H, C₆H₄CN), 8.10 (d, ³J = 8.5, 1H, C₆H₄NS), 7.93 (d, ³J = 8.5, 1H, C₆H₄NS), 7.77 (d, ³J = 8.0, 2H, C₆H₄CN), 7.54 (dd, ³J = 8.5, ³J n.r., 1 H, C₆H₄NS), 7.45 (dd, ³J = 8.5, ³J n.r., 1H, C₆H₄NS). ¹³C {¹H} NMR (CDCl₃, 125 MHz): δ 165.4 (NCS), 154.1 (NCCH), 137.6, 135.4, 132.9 (C₆H₄CN), 128.0 (C₆H₄CN), 127.0, 126.2, 123.9, 121.9, 118.4 (CN), 114.2 (CCN).

2-(4-Trifluoromethylphenyl)benzo[d]thiazole²³⁷

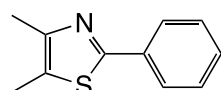
¹H NMR (CDCl₃, 300 MHz): δ 8.21 (d, ³J = 8.1, 2H, C₆H₄CF₃), 8.11 (d, ³J = 8.1, 1H, C₆H₄NS), 7.93 (ddd, ³J = 8.1, ⁴J n.r., ⁵J n.r., 1H, C₆H₄NS), 7.75 (d, ³J = 8.1, 2H, C₆H₄CF₃), 7.53 (ddd, ³J = 8.1, ³J = 7.2, ⁴J = 1.2, 1H, C₆H₄NS), 7.43 (ddd, ³J = 8.1, ³J = 7.2, ⁴J = 1.2, 1H, C₆H₄NS). ¹³C {¹H} NMR (CDCl₃, 75 MHz): δ 166.2 (NCS), 154.2 (NCCH), 137.0, 135.4, 132.6 (q, ²J_{C,F} = 32.6, CCF₃), 127.9 (C₆H₄CF₃), 126.8, 126.2 (q, ³J_{C,F} = 3.6, C₆H₄CF₃) 124.0 (q, ¹J_{C,F} = 270.8, CF₃), 123.8, 121.9.

2-(4-Chlorophenyl)benzo[d]thiazole³²³

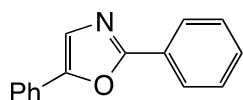
¹H NMR (CDCl₃, 400 MHz): δ 8.07 (ddd, ³J = 8.0, ⁴J n. r., ⁵J n. r., 1H, C₆H₄NS), 8.03 (d, ³J = 8.6, 2H, C₆H₄Cl), 7.90 (ddd, ³J = 8.0, ⁴J n. r., ⁵J n. r., 1H, C₆H₄NS), 7.50 (ddd, ³J = 8.0, ³J = 7.2, ⁴J = 0.8, 1H, C₆H₄NS), 7.46 (d, ³J = 8.6, 2H, C₆H₄Cl), 7.41 (ddd, ³J = 8.0, ³J = 7.2, ⁴J = 0.8, 1H, C₆H₄NS). ¹³C {¹H} NMR (CDCl₃, 75 MHz): δ 166.7 (NCS), 154.2 (NCCH), 137.2, 135.2, 132.3, 129.4 (C₆H₄Cl), 128.8 (C₆H₄Cl), 126.6, 125.6, 123.4, 121.8.

2-(o-Tolyl)benzo[d]thiazole²³⁷

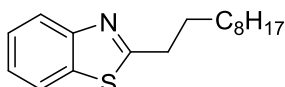
¹H NMR (CDCl₃, 500 MHz): δ 8.14 (d, ³J = 8.0, 1H), 7.94 (d, ³J = 8.0, 1H), 7.79 (dd, ³J = 8.0, ⁴J = 1.0, 1H), 7.53 (ddd, ³J = 8.5, ³J = 7.5, ⁴J = 1.0, 1H), 7.44-7.31 (m, 4H), 2.69 (s, 3H, CH₃). ¹³C {¹H} NMR (CDCl₃, 125 MHz): δ 168.1 (NCS), 153.9 (NCCH), 137.3, 135.7, 133.2, 131.6, 130.6, 130.1, 126.2, 126.2, 125.2, 123.5, 121.4, 21.5 (CH₃).

2-Phenyl-4,5-dimethylthiazole²³⁹

¹H NMR (CDCl₃, 500 MHz): δ 7.86 (d, ³J = 7.0, 2H, C₆H₅), 7.41-7.36 (m, 3H, C₆H₅), 2.39 (s, 3H, CH₃), 2.39 (s, 3H, CH₃). ¹³C {¹H} NMR (CDCl₃, 125 MHz): δ 163.5 (NCS), 149.4 (NCCH₃), 134.1, 129.5 (C₆H₅), 128.9 (C₆H₅), 126.7, 126.2 (C₆H₅), 14.5 (NCCH₃), 11.6 (SCCH₃).

2,5-Diphenyloxazole³²⁴

¹H NMR (CDCl₃, 500 MHz): δ 8.12 (dd, ³J = 8.0, ⁴J = 2.0, 2H, C₆H₅), 7.73 (dd, ³J = 8.5, ⁴J = 1.5, 2H, C₆H₅), 7.51-7.43 (m, 6H, C₆H₅ and NCH), 7.34 (ddd, 1H, ³J = 7.5, C₆H₅). ¹³C {¹H} NMR (CDCl₃, 125 MHz): δ 161.2 (NCO), 151.4 (OCPh), 130.4, 129.0, 128.9, 128.5, 128.1, 127.6, 126.4, 124.3, 123.6.

2-Decylbenzothiazole²⁶⁷

¹H NMR(CDCl₃, 400.13 MHz): δ = 7.97 (dq, ⁴J = 0.4, ³J = 8.4, 1H), 7.83 (dq, ⁴J = 0.8, J = 8.0, 1H), 7.44 (td, J = 1.2 Hz, J = 7.2, 1H), 7.36 (td, J =, 1H), 3.108 (t, ³J = 7.6 Hz, 1H), 1.88 (quint, ³J = 7.6, 2H), 1.48-1.40 (m, 2H), 1.38-1.26 (m, H), 0.88 (t, ³J = 6.4, 3H). ¹³C {¹H} NMR (CDCl₃, 125.78 MHz): δ = 172.6 (NCS), 153.4, 135.3, 126.0, 124.7, 122.6, 121.6, 34.5 (btz-CH₂), 32.0, 29.9, 29.7, 29.6, 29.4, 29.3, 22.8, 14.2. HR-MS (ESI): *m/z* [M+H]⁺ calcd. for C₁₇H₂₆NS, 276.1786 found.276.1793.

IV. Crystal data and refinement data

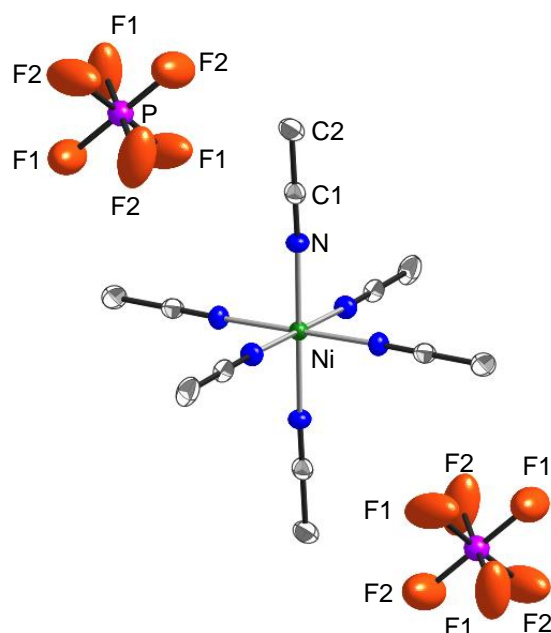
IV.1. Hexaacetone-nickel(II) hexafluorophosphate $[\text{Ni}^{\text{II}}(\text{NCMe})_6](\text{PF}_6)_2$ 

Figure 44. Molecular structure of $[\text{Ni}^{\text{II}}(\text{NCMe})_6](\text{PF}_6)_2$ showing all non-H atoms. Ellipsoids are shown at the 50% probability level, and independent atoms are labelled. Selected distances (\AA) and angles ($^\circ$) with esds. in parenthesis: Ni–N, 2.060(3); N–C1, 1.142(5); C1–C2, 1.451(5); P–F1 = 1.587(4); P–F2 = 1.554(4); Ni–N–C1, 174.3(3); N–C1–C2, 179.6(4); N–Ni–N', 88.31(12); N–Ni–N'', 91.69(12); N'–Ni–N'', 88.31(12); N–Ni–N = N'–Ni–N' = N''–Ni–N'' = 180.0; F1–P–F1 = 91.6(4); F1–P–F2 = 85.7(3), 86.4(3) or 176.6(4); F2–P–F2 = 96.2(3).

Table 14. X-ray crystallographic data and data collection parameters for complex $[\text{Ni}^{\text{II}}(\text{NCMe})_6](\text{PF}_6)_2$.

Complex	$[\text{Ni}^{\text{II}}(\text{NCMe})_6](\text{PF}_6)_2$
Empirical formula	$\text{C}_{12}\text{H}_{18}\text{N}_6\text{Ni}\cdot 2(\text{F}_6\text{P})$
Formula weight	594.97
Crystal system	Trigonal
Space group	$R\bar{3}$
Temperature (K)	173(2)
a (Å)	11.094(5)
b (Å)	11.094(5)
c (Å)	16.660(5)
α (°)	90
β (°)	90
γ (°)	120
V (Å ³)	1775.7(17)
Z	3
$D_{\text{calculated}}$ (Mg m ⁻³)	1.669
Absorption coefficient (mm ⁻¹)	1.060
Crystal form, color	Prism, purple
Crystal size (mm)	0.35 × 0.30 × 0.25
h, k, l_{max}	14, 15, 23
$T_{\text{min}}, T_{\text{max}}$	0.601, 0.746
Reflections collected	5187
Independent reflections, R_{int}	1137, 0.0382
Reflections with $I > 2\sigma(I)$	928
$R [F^2 > 2\sigma(F^2)]$	0.0690
$wR(F^2)$	0.2222
GOF on F^2	1.041

IV.2. Complexes **9** and **10**Table 15. X-ray crystallographic data and data collection parameters for complexes **9** and **10**.

Complex	9	10
Empirical formula	C ₁₂ H ₁₃ N ₃ Ni	C ₂₀ H ₂₁ N ₃ Ni
Formula weight	257.96	362.11
Crystal system	Monoclinic	Triclinic
Space group	<i>P2₁/c</i>	<i>P</i> $\bar{1}$
Temperature (K)	173(2)	173(2)
<i>a</i> (Å)	8.4784(2)	9.3425(10)
<i>b</i> (Å)	17.3913(5)	13.7491(15)
<i>c</i> (Å)	8.5806(2)	14.2032(15)
α (°)	90	80.591(6)
β (°)	118.362(1)	86.833(7)
γ (°)	90	82.101(7)
<i>V</i> (Å ³)	1113.34(5)	1781.8(3)
<i>Z</i>	4	4
<i>D</i> _{calculated} (Mg m ⁻³)	1.539	1.350
Absorption coefficient (mm ⁻¹)	1.716	1.592
Crystal form, color	Prism, green	Needle, green
Crystal size (mm)	0.32 × 0.20 × 0.14	0.25 × 0.10 × 0.06
<i>h</i> , <i>k</i> , <i>l</i> _{max}	12, 17, 11	11, 16, 16
<i>T</i> _{min} , <i>T</i> _{max}	0.670, 0.747	0.617, 0.753
Reflections collected	16574	27037
Independent reflections, <i>R</i> _{int}	4192, 0.0196	6205, 0.0760
Reflections with <i>I</i> > 2σ(<i>I</i>)	3557	4232
<i>R</i> [<i>F</i> ² > 2σ(<i>F</i> ²)]	0.0260	0.0883
<i>wR</i> (<i>F</i> ²)	0.0648	0.2721
GOF on <i>F</i> ²	1.050	1.066

IV.3. Complexes **19** and **27**Table 16. X-ray crystallographic data and data collection parameters for complexes **19** and **27**.

Complex	19	27
Empirical formula	C ₃₂ H ₃₈ N ₆ Ni ₂ O ₂ ·(CH ₂ Cl ₂)	C ₃₃ H ₃₃ N ₃ NiS
Formula weight	825.95	562.39
Crystal system	Monoclinic	Orthorhombic
Space group	<i>P2₁/c</i>	<i>P2₁2₁2₁</i>
Temperature (K)	173(2)	173(2)
<i>a</i> (Å)	10.4595(5)	7.6555(4)
<i>b</i> (Å)	15.1175(10)	9.7436 (5)
<i>c</i> (Å)	15.4486(7)	37.6422(19)
α (°)	90	90
β (°)	127.088(3)	90
γ (°)	90	90
<i>V</i> (Å ³)	1948.61	2807.8(2)
<i>Z</i>	2	4
<i>D</i> _{calculated} (Mg m ⁻³)	1.408	1.330
Absorption coefficient (mm ⁻¹)	1.278	0.792
Crystal form, color	Block, orange	Prism, brown
Crystal size (mm)	0.28 × 0.20 × 0.16	0.40 × 0.16 × 0.06
<i>h</i> , <i>k</i> , <i>l</i> _{max}	13, 18, 20	4, 12, 49
<i>T</i> _{min} , <i>T</i> _{max}	0.716, 0.822	0.742, 0.954
Reflections collected	16201	11624
Independent reflections, <i>R</i> _{int}	4462, 0.0721	5624, 0.0204
Reflections with <i>I</i> > 2σ(<i>I</i>)	2931	5008
<i>R</i> [<i>F</i> ² > 2σ(<i>F</i> ²)]	0.0629	0.0350
<i>wR</i> (<i>F</i> ²)	0.1990	0.0685
GOF on <i>F</i> ²	1.096	1.047

V. Computational methods

The calculations were performed by Dr. Luis F. Veiros at Centro de Química Estrutural (CQE) using the Gaussian 09 software package and the PBE0 functional, without symmetry constraints. This functional uses a hybrid generalized gradient approximation (GGA), including a 25% mixture of Hartree-Fock exchange³²⁵ with the DFT³²⁶ exchange–correlation, given by the Perdew, Burke and Ernzerhof functional (PBE).^{327–329} The basis set used for geometry optimizations (b1) consisted of the Stuttgart/Dresden ECP (SDD) basis set^{330–332} augmented with a f-polarization function³³³ to describe the electrons of Ni, and a standard 6-31G(d,p) basis set^{334–340} for all other atoms. The transition state optimization was performed with the Synchronous Transit-Guided Quasi-Newton (STQN) method developed by Schlegel et al.,^{341,342} following extensive search of the potential energy surface. Frequency calculations were performed to confirm the nature of the stationary points, yielding one imaginary frequency for the transition state and none for the minima. The transition state was further confirmed by following its vibrational mode downhill on both sides and obtaining the minima presented on the energy profile. The electronic energies (Eb1) obtained at the PBE0/b1 level of theory were converted to free energy at 298.15 K and 1 atm (Gb1) by using zero point energy and thermal energy corrections based on structural and vibration frequency data calculated at the same level. Single point energy calculations were performed on the geometries obtained at the PBE0/b1 level using the M06 functional, and a 6-311++G(d,p) basis set.^{334–340,343,344} The M06 functional is a hybrid meta-GGA functional developed by Truhlar and Zhao,³⁴⁵ and it was shown to perform very well for the kinetics of transition metal molecules, providing a good description of weak and long range interactions.^{346,347} Solvent effects (MeCN) were accounted for in the M06/6-311++G(d,p)//PBE0/b1 calculations by means of the Polarizable Continuum Model (PCM) initially devised by Tomasi and coworkers^{348–350} with radii and non-electrostatic terms of the SMD solvation model, developed by Truhlar and co-workers.³⁵¹ The free energy values presented (Gb2soln) were derived from the electronic energy values obtained at the M06/6-311++G(d,p)//PBE0/b1 level, including solvent effects (Eb2soln), according to the following expression: $G_{b2soln} = E_{b2soln} + G_{b1} - E_{b1}$. The calculated frequencies for the CN stretch in all species were corrected with a scale factor of 0.932 resulting from the comparison of the calculated and experimental CN frequency values observed for **11**. The presented calculated frequency spectra were drawn using the Chemcraft program³⁵² and a Lorentzian line broadening of 30% at peak half-width to account.

General conclusions

General conclusions

In Chapter 1, an overview of the development of Ni-NHC systems as catalysts was presented, highlighting the technological and scientific importance of each half and their sum. An overview of the most recent (2015-2018) examples of Ni-NHC catalytic systems applied to C–C bond formation by C–H bond functionalization reactions revealed a focus on their utility in formal 1,2-addition reactions to unsaturated C=C/C≡C bonds along with a surprising paucity of cross-coupling reactions. Furthermore, ill-defined $[\text{Ni}^0(\text{COD})_2]/(\text{pro})\text{ligand}$ mixtures comprise the majority of the catalytic systems studied, with most reports being dedicated to developing new reactions and synthetic methodologies. The few reports that develop detailed mechanistic studies on these reactions highlight the non-innocent role that the near-omnipresent 1,5-cyclooctadiene ligand can play.

In Chapter 2, a robust methodology for the multi-step synthesis of a family of cationic 14 valence electron $\kappa^2\text{-C}_{\text{NHC}, \text{C}_{\text{alkyl}}}\text{-Ni(II)}$ complexes of the general formula $[\text{Ni}^{\text{II}}\{\text{R-NHC}-(\text{CH}_2)_n\text{CH}(\text{CN})\}(\text{MeCN})]\text{PF}_6$ was described. The initial step of this methodology generates cyclometallated $\kappa^2\text{-C}_{\text{NHC}, \text{C}_{\text{alkyl}}}\text{-Ni(II)}$ half-sandwich complexes by base-assisted intramolecular C–H bond activation of half-sandwich Ni(II)-NHC complexes bearing a *N*-alkylnitrile arm. In a second step, the cyclopentadienyl ligand of the former 18-electron complexes is removed by acidolysis with HCl to yield the title cationic complexes.

The initial supposition, that the complexes of this family were square-planar 16-electron Ni(II) complexes bearing two MeCN ligands, was rectified by a combined experimental (NMR and IR spectroscopies and elemental analysis) and computational (DFT calculations) study. This complex family was found to be accurately described as T-shaped 14-electron Ni(II) complexes in the solid state, which make them rare examples of such electronically and coordinatively unsaturated Ni(II) species. These complexes showed a peculiar solubility only amenable to dissolution in pyridine and nitriles (notably, MeCN), in which they displayed a dynamic exchange behavior with the solvent. Substitution of the MeCN ligand with phosphine ligands (PPh₃, PMe₃) gave complexes that displayed a similar dynamic behavior with the solvent in solution. Multinuclear (¹H, ¹³C, ³¹P) NMR spectroscopic studies on these species provided insights to this dynamic behavior. From these studies, we propose that competing solvent/ligand equilibria, mediated by a *cis/trans* isomerization of the monodentate ligand, by means of an in-plane migration in solution, explain the dynamic behavior observed by NMR spectroscopy.

In Chapter 3, nickel-catalyzed 1-chalcogen-azole C(2)–H cross-coupling reactions were reviewed. The literature showed a preference for C_{sp2}–C_{sp2} bond construction with few

examples of either $C_{sp^2}-C_{sp}$ or $C_{sp^2}-C_{sp^3}$ bond construction. Chelating N,N or P,P pnictogen ligands were the overwhelming majority and most nickel sources resorted to simple Ni(II) salts or to $[Ni^0(COD)_2]$. Like other nickel-catalyzed C–H bond functionalization reactions, these often require harsh reaction conditions (sealed reactors, $> 100\text{ }^\circ\text{C}$) and high catalyst loadings (5-30 mol%).

The cationic $\kappa^2-C_{NHC}, C_{alkyl}-Ni(II)$ complexes synthesized in Chapter 2 were successfully applied to the coupling of benzothiazole with haloarenes, making them the first example of a κ^2-C,C -chelated precatalyst in Ni-catalyzed azole C(2)–H bond functionalization. In contrast, acyclic half-sandwich or neutral nickelacyclic Ni(II)-NHC complexes bearing either a cyclopentadienyl or an acetylacetonate ligand were found not to catalyze this coupling reaction. We attribute this to the combination of both the metallacyclic scaffold and the labile MeCN ligand. Despite this initial success, they were only moderately active and their reaction scope was limited, both in terms of azole (benzothiazole) and haloarene (neutral or electron-poor sterically unencumbered iodoarenes) partners. Mechanistic studies on this reaction suggest that the complexes utilized first undergo a reduction to a Ni(0) species, by dimerization of the substrate, and to yield a particular Ni(0) species that most probably reacts by single-electron transfers.

The poor performance of the acyclic half-sandwich Ni(II)-NHC complexes in the benzothiazole arylation reaction could be explained by generation of an inert Ni(II)-benzothiazolyl species, which was observed in the reaction mixture. This species could be independently synthesized and isolated and is one of the rare examples of a M–azolyl species, often postulated to intermediate azole functionalization reactions. Surprisingly this complex displayed was found to be active in catalyzing the alkylation of benzothiazole with 1-iododecane. This difference in reactivity can be related to the different manner in which $C_{sp^2}-I$ (heterolytic) and $C_{sp^3}-I$ (homolytic) bonds are broken. The Ni(II)-benzothiazolyl is formally saturated which prevents it both from directly to breaking the $C_{sp^2}-I$ bond via oxidative addition, and to generate a Ni(0) species by the coordination of another benzothiazolyl unit needed for reductive elimination. On the other hand, a radical species formed from the scission of the $C_{sp^3}-I$ bond (I^\bullet or $C_{10}H_{21}^\bullet$) can react with the Ni(II)-benzothiazolyl species to give a one-electron oxidized Ni(III) species that is now unsaturated. A facile one-electron oxidation of Ni(II)-benzothiazolyl complexes to Ni(III) ($-0.44 E_{p,a}$ 0.06 V vs. Fc/Fc⁺) was observed by cyclic voltammetry and supports this hypothesis. These results suggest this reaction to take place using an odd-electron manifold involving a Ni(III) intermediate.

References

References

- (1) *R&D Magazine*. September 2005, p 20.
- (2) Nobelprize.org. All Nobel Laureates in Chemistry https://www.nobelprize.org/nobel_prizes/chemistry/laureates/ (accessed Aug 9, 2018).
- (3) Company, E. I. du P. de N. and. Mechanical Engineering at DuPont circa 1950 E. I. du Pont de Nemours and Company <https://www.youtube.com/watch?v=N83jwRtkr5k> (accessed Aug 11, 2018).
- (4) IUPAC Compendium of Chemical Terminology, E. version. IUPAC Goldbook - catalyst <http://goldbook.iupac.org/C00876.html> (accessed Aug 3, 2018).
- (5) In *Supercritical Fluids and Organometallic Compounds From Recovery of Trace Metals to Synthesis of Nanostructured Materials, Volume 1*; Erkey, C., Ed.; Elsevier B.V., 2011; pp 161–209.
- (6) *Applied Homogeneous Catalysis with Organometallic Compounds*, 3rd ed.; Cornils, B., Herrmann, W. A., Beller, M., Paciello, R., Eds.; Wiley-VCH Verlag GmbH & Co. KGaA: Weinheim, 2017.
- (7) Anastas, P.; Warner, J. *Green Chemistry: Theory and Practice*; Oxford University Press, Inc., 2000.
- (8) Rare Earth Elements—Critical Resources for High Technology | U.S. Geological Survey Fact Sheet 087-02 <https://pubs.usgs.gov/fs/2002/fs087-02/> (accessed Jul 31, 2018).
- (9) Housecroft, C. E.; Sharpe, A. G. *Inorganic Chemistry*, 4th ed.; Pearson Education Limited: Barcelona, 2012.
- (10) Trost, B. M. Palladium - the metal of the 21st Century explained in IPMI acceptance speech. <https://www.youtube.com/watch?v=6MNIKyb0Zbl> (accessed Jul 31, 2018).
- (11) Tasker, S. Z.; Standley, E. A.; Jamison, T. F. *Nature* **2014**, 509 (7500), 299–309.
- (12) Ananikov, V. P. *ACS Catal.* **2015**, 5 (3), 1964–1971.
- (13) Nobelprize.org. The Nobel Prize in Chemistry 1912 http://www.nobelprize.org/nobel_prizes/chemistry/laureates/1912/.
- (14) Sabatier, P.; Senderens, J.-B. *C. R. Acad. Sci. Paris* **1897**, 124, 1358–1360.
- (15) Thauer, R. K.; Diekert, G.; Schönheit, P. *Trends Biochem. Sci.* **1980**, 5 (11), 304–306.
- (16) Kumar, S.; Trivedi, A. V. *Int. J. Curr. Microbiol. Appl. Sci.* **2016**, 5 (3), 719–727.
- (17) Keim, W. *Angew. Chem., Int. Ed. Eng.* **1990**, 29 (3), 235–244.
- (18) Han, F.-S. *Chem. Soc. Rev.* **2013**, 42 (12), 5270.
- (19) Higuchi, Y.; Yagi, T.; Yasuoka, N. *Structure* **1997**, 5 (12), 1671–1680.
- (20) Mitchell, M. B.; Wallbank, P. J. *Tetrahedron Lett.* **1991**, 32 (20), 2273–2276.
- (21) Indolese, A. F. *Tetrahedron Lett.* **1997**, 38 (20), 3513–3516.

References

- (22) Q3D Elemental Impurities - Guidance for Industry <https://www.fda.gov/downloads/drugs/guidances/ucm371025.pdf> (accessed Jul 31, 2018).
- (23) *GUIDELINE ON THE SPECIFICATION LIMITS FOR RESIDUES OF METAL CATALYSTS*; London, 2007.
- (24) Pearson, R. G. *J. Am. Chem. Soc.* **1963**, *85* (22), 3533–3539.
- (25) Tellis, J. C.; Primer, D. N.; Molander, G. A. *Science* **2014**, *345* (6195), 433–436.
- (26) Zuo, Z.; Ahneman, D. T.; Chu, L.; Terrett, J. A.; Doyle, A. G.; MacMillan, D. W. C. *Science* **2014**, *345* (6195), 437–440.
- (27) Mohadjer Beromi, M.; Nova, A.; Balcells, D.; Brasacchio, A. M.; Brudvig, G. W.; Guard, L. M.; Hazari, N.; Vinyard, D. J. *J. Am. Chem. Soc.* **2017**, *139* (2), 922–936.
- (28) Balcells, D.; Nova, A. *ACS Catal.* **2018**, *8* (4), 3499–3515.
- (29) Van Vleck, J. H. *Phys. Rev.* **1932**, *41* (2), 208–215.
- (30) Crabtree, R. H. *The Organometallic Chemistry of the Transition Metals*; John Wiley & Sons, Inc., 2005.
- (31) Griffith, J. S.; Orgel, L. E. *Q. Rev. Chem. Soc.* **1957**, *11* (4), 381.
- (32) In *Applied Homogeneous Catalysis*; Behr, A., Neubert, P., Eds.; Wiley-VCH Verlag GmbH & Co. KGaA; p 79.
- (33) *Metal-catalysis in Industrial Organic Processes*; Chiusoli, G. P., Maitlis, P. M., Eds.; Royal Society of Chemistry: Cambridge, 2007.
- (34) Wanzlick, H.-W.; Schönherr, H.-J. *Angew. Chem., Int. Ed. Eng.* **1968**, *7* (2), 141–142.
- (35) Öfele, K. *J. Organomet. Chem.* **1968**, *12* (3), P42–P43.
- (36) Arduengo, A. J.; Harlow, R. L.; Kline, M. *J. Am. Chem. Soc.* **1991**, *113* (1), 361–363.
- (37) Igau, A.; Grutzmacher, H.; Baceiredo, A.; Bertrand, G. *J. Am. Chem. Soc.* **1988**, *110* (19), 6463–6466.
- (38) Herrmann, W. A.; Elison, M.; Fischer, J.; Köcher, C.; Artus, G. R. J. *Angew. Chem. Int. Ed.* **1995**, *34* (21), 2371–2374.
- (39) Herrmann, W. A.; Broßmer, C.; Öfele, K.; Beller, M.; Fischer, H. *J. Organomet. Chem.* **1995**, *491* (1–2), 2–5.
- (40) Scholl, M.; Ding, S.; Lee, C. W.; Grubbs, R. H. *Org. Lett.* **1999**, *1* (6), 953–956.
- (41) Scholl, M.; Trnka, T. M.; Morgan, J. P.; Grubbs, R. H. *Tetrahedron Lett.* **1999**, *40* (12), 2247–2250.
- (42) 2014, N. M. A. The Nobel Prize in Chemistry 2005 http://www.nobelprize.org/nobel_prizes/chemistry/laureates/2005/ (accessed Jul 30, 2018).
- (43) Royo, B.; Peris, E. *Eur. J. Inorg. Chem.* **2012**, (9), 1309–1318.

References

- (44) Peris, E. *Chem. Rev.* **2018**, *118* (19), 9988–10031.
- (45) Riener, K.; Haslinger, S.; Raba, A.; Högerl, M. P.; Cokoja, M.; Herrmann, W. A.; Kühn, F. E. *Chem. Rev.* **2014**, *114* (10), 5215–5272.
- (46) Kubiak, C. P.; Simón-Manso, E. In *Comprehensive Organometallic Chemistry III*; Elsevier, 2007; Vol. 9, pp 1–26.
- (47) Díez-González, S.; Marion, N.; Nolan, S. P. *Chem. Rev.* **2009**, *109* (8), 3612–3676.
- (48) Hopkinson, M. N.; Richter, C.; Schedler, M.; Glorius, F. *Nature* **2014**, *510* (7506), 485–496.
- (49) Fukui, K.; Yonezawa, T.; Shingu, H. *J. Chem. Phys.* **1952**, *20* (4), 722–725.
- (50) Wanzlick, H.-W.; Schikora, E. *Chem. Ber.* **1961**, *94* (9), 2389–2393.
- (51) Wanzlick, H.-W.; Schikora, E. *Angew. Chem.* **1960**, *72* (14), 494–494.
- (52) Fischer, E. O.; Maasböl, A. *Angew. Chem., Int. Ed. Eng.* **1964**, *3* (8), 580–581.
- (53) Schrock, R. R. *J. Am. Chem. Soc.* **1974**, *96* (21), 6796–6797.
- (54) Crabtree, R. H. In *The Organometallic Chemistry of the Transition Metals*; John Wiley & Sons, Inc.: Hoboken, NJ, USA, 2005; pp 309–341.
- (55) Parr, R. G.; Yang, W. *Density-functional theory of atoms and molecules*, 1st ed.; Breslow, R., Goodenough, J. B., Eds.; Oxford University Press, Inc.: New York, 1989.
- (56) Nemcsok, D.; Wichmann, K.; Frenking, G. *Organometallics* **2004**, *23* (15), 3640–3646.
- (57) Nelson, D. J.; Nolan, S. P. *Chem. Soc. Rev.* **2013**, *42* (16), 6723–6753.
- (58) Nolan, S. P.; Nelson, D. J.; Gómez-Suárez, A. *Chem. Commun.* **2017**, *42* (16), 6723.
- (59) Huynh, H. V. *Chem. Rev.* **2018**, *118* (19), 9457–9492.
- (60) Falivene, L.; Poater, A.; Cavallo, L. In *N-Heterocyclic Carbenes*; Wiley-VCH Verlag GmbH & Co. KGaA: Weinheim, Germany, 2014; pp 25–38.
- (61) Alder, R. W.; Allen, P. R.; Williams, S. J. *J. Chem. Soc., Chem. Commun.* **1995**, (12), 1267.
- (62) Kovač, B.; Ljubić, I.; Kivimäki, A.; Coreno, M.; Novak, I. *Phys. Chem. Chem. Phys.* **2015**, *17* (16), 10656–10667.
- (63) Maji, B.; Breugst, M.; Mayr, H. *Angew. Chem. Int. Ed.* **2011**, *50* (30), 6915–6919.
- (64) Leuthäuser, S.; Schwarz, D.; Plenio, H. *Chem. Eur. J.* **2007**, *13* (25), 7195–7203.
- (65) Lever, A. B. P. *Inorg. Chem.* **1990**, *29* (6), 1271–1285.
- (66) Lever, A. B. P. *Inorg. Chem.* **1991**, *30* (9), 1980–1985.
- (67) Tolman, C. A. *J. Am. Chem. Soc.* **1970**, *92* (10), 2953–2956.
- (68) Lappert, M. F.; Pye, P. L. *J. Chem. Soc., Dalt. Trans.* **1977**, (21), 2172.
- (69) Chianese, A.; Li, X.; Janzen, M.; Faller, J.; Crabtree, R. *Organometallics* **2003**, *22* (8), 1663–1667.
- (70) Huynh, H. V.; Han, Y.; Jothibasur, R.; Yang, J. A. *Organometallics* **2009**, *28* (18), 5395–

References

- 5404.
- (71) Teng, Q.; Huynh, H. V. *Dalton Trans.* **2017**, 46 (3), 614–627.
- (72) Back, O.; Henry-Ellinger, M.; Martin, C. D.; Martin, D.; Bertrand, G. *Angew. Chem. Int. Ed.* **2013**, 52 (10), 2939–2943.
- (73) Liske, A.; Verlinden, K.; Buhl, H.; Schaper, K.; Ganter, C. *Organometallics* **2013**, 32 (19), 5269–5272.
- (74) Verlinden, K.; Buhl, H.; Frank, W.; Ganter, C. *Eur. J. Inorg. Chem.* **2015**, 2015 (14), 2416–2425.
- (75) Buhl, H.; Verlinden, K.; Ganter, C.; Novaković, S. B.; Bogdanović, G. A. *Eur. J. Inorg. Chem.* **2016**, 2016 (21), 3389–3395.
- (76) Hillier, A. C.; Sommer, W. J.; Yong, B. S.; Petersen, J. L.; Cavallo, L.; Nolan, S. P. *Organometallics* **2003**, 22 (21), 4322–4326.
- (77) Poater, A.; Ragone, F.; Mariz, R.; Dorta, R.; Cavallo, L. *Chem. Eur. J.* **2010**, 16 (48), 14348–14353.
- (78) Owen, M. R.; Luscombe, C.; Lai; Godbert, S.; Crookes, D. L.; Emiabata-Smith, D. *Org. Proc. Res. Dev.* **2001**, 5 (3), 308–323.
- (79) Murray, P. M.; Tyler, S. N. G.; Moseley, J. D. *Org. Proc. Res. Dev.* **2013**, 17 (1), 40–46.
- (80) Khazipov, O. V.; Shevchenko, M. A.; Chernenko, A. Y.; Astakhov, A. V.; Pasyukov, D. V.; Eremin, D. B.; Zubavichus, Y. V.; Khrustalev, V. N.; Chernyshev, V. M.; Ananikov, V. P. *Organometallics* **2018**, 37 (9), 1483–1492.
- (81) Chernyshev, V. M.; Khazipov, O. V.; Shevchenko, M. A.; Chernenko, A. Y.; Astakhov, A. V.; Eremin, D. B.; Pasyukov, D. V.; Kashin, A. S.; Ananikov, V. P. *Chem. Sci.* **2018**, 9 (25), 5564–5577.
- (82) Astakhov, A. V.; Khazipov, O. V.; Degtyareva, E. S.; Khrustalev, V. N.; Chernyshev, V. M.; Ananikov, V. P. *Organometallics* **2015**, 34 (24), 5759–5766.
- (83) Ritleng, V.; Henrion, M.; Chetcuti, M. J. *ACS Catal.* **2016**, 6 (2), 890–906.
- (84) Henrion, M.; Ritleng, V.; Chetcuti, M. J. *ACS Catal.* **2015**, 5 (2), 1283–1302.
- (85) Prakasham, A. P.; Ghosh, P. *Inorg. Chim. Acta* **2015**, 431, 61–100.
- (86) Henrion, M.; Chetcuti, M. J.; Ritleng, V. *Chem. Commun.* **2014**, 50 (35), 4624–4627.
- (87) Henrion, M.; de P. Cardoso, B.; César, V.; Chetcuti, M. J.; Ritleng, V. *Organometallics* **2017**, 36 (6), 1113–1121.
- (88) Ishikawa, M.; Ohshita, J.; Ito, Y. *Organometallics* **1986**, 5 (7), 1518–1519.
- (89) Ogoshi, S.; Ueta, M.; Oka, M.; Kurosawa, H. *Chem. Commun.* **2004**, 1 (23), 2732.
- (90) Clement, N. D.; Cavell, K. J. *Angew. Chem. Int. Ed.* **2004**, 43 (29), 3845–3847.
- (91) Matsubara, K.; Ueno, K.; Koga, Y.; Hara, K. *J. Org. Chem.* **2007**, 72 (14), 5069–5076.
- (92) Sonogashira, K.; Tohda, Y.; Hagihara, N. *Tetrahedron Lett.* **1975**, 16 (50), 4467–4470.

References

- (93) Wang, Z.; Zheng, T.; Sun, H.; Li, X.; Fuhr, O.; Fenske, D. *New J. Chem.* **2018**, *42* (14), 11465–11470.
- (94) Yin, Y.; Yue, X.; Zhong, Q.; Jiang, H.; Bai, R.; Lan, Y.; Zhang, H. *Adv. Synth. Catal.* **2018**, *360* (8), 1639–1643.
- (95) Yang, K.; Wang, P.; Zhang, C.; Kadi, A. A.; Fun, H.-K.; Zhang, Y.; Lu, H. *European J. Org. Chem.* **2014**, *2014* (34), 7586–7589.
- (96) Strieth-Kalthoff, F.; Longstreet, A. R.; Weber, J. M.; Jamison, T. F. *ChemCatChem* **2018**, *10* (13), 2873–2877.
- (97) Hazari, N.; Melvin, P. R.; Beromi, M. M. *Nat. Rev. Chem.* **2017**, *1* (3), 0025.
- (98) Heck, R. F.; Nolley, J. P. *J. Org. Chem.* **1972**, *37* (14), 2320–2322.
- (99) Itami, K.; Tanaka, S.; Sunahara, K.; Tatsuta, G.; Mori, A. *Asian J. Org. Chem.* **2015**, *4* (5), 477–481.
- (100) Oertel, A. M.; Ritleng, V.; Busiah, A.; Veiros, L. F.; Chetcuti, M. J. *Organometallics* **2011**, *30* (23), 6495–6498.
- (101) Lavallo, V.; Canac, Y.; Präsang, C.; Donnadieu, B.; Bertrand, G. *Angew. Chem. Int. Ed.* **2005**, *44* (35), 5705–5709.
- (102) Chatani, N. In *Top Organomet Chem*; 2015; Vol. 48, pp 19–46.
- (103) Castro, L. C. M.; Chatani, N. *Chem. Lett.* **2015**, *44* (4), 410–421.
- (104) Misal Castro, L. C.; Obata, A.; Aihara, Y.; Chatani, N. *Chem. Eur. J.* **2016**, *22* (4), 1362–1367.
- (105) Nett, A. J.; Zhao, W.; Zimmerman, P. M.; Montgomery, J. *J. Am. Chem. Soc.* **2015**, *137* (24), 7636–7639.
- (106) Wu, J.; Faller, J. W.; Hazari, N.; Schmeier, T. J. *Organometallics* **2012**, *31* (3), 806–809.
- (107) Nett, A. J.; Montgomery, J.; Zimmerman, P. M. *ACS Catal.* **2017**, *7* (10), 7352–7362.
- (108) Wang, H.; Lu, G.; Sormunen, G. J.; Malik, H. A.; Liu, P.; Montgomery, J. *J. Am. Chem. Soc.* **2017**, *139* (27), 9317–9324.
- (109) Nett, A. J.; Cañellas, S.; Higuchi, Y.; Robo, M. T.; Kochkodan, J. M.; Haynes, M. T.; Kampf, J. W.; Montgomery, J. *ACS Catal.* **2018**, *8* (7), 6606–6611.
- (110) Wang, H.; Negretti, S.; Knauff, A. R.; Montgomery, J. *Org. Lett.* **2015**, *17* (6), 1493–1496.
- (111) Vijaykumar, G.; Jose, A.; Vardhanapu, P. K.; P, S.; Mandal, S. K. *Organometallics* **2017**, *36* (24), 4753–4758.
- (112) Aldeco-Perez, E.; Rosenthal, A. J.; Donnadieu, B.; Parameswaran, P.; Frenking, G.; Bertrand, G. *Science* **2009**, *326* (5952), 556–559.
- (113) Schramm, Y.; Takeuchi, M.; Semba, K.; Nakao, Y.; Hartwig, J. F. *J. Am. Chem. Soc.* **2015**, *137* (38), 12215–12218.

References

- (114) Nakanowatari, S.; Müller, T.; Oliveira, J. C. A.; Ackermann, L. *Angew. Chem. Int. Ed.* **2017**, *56* (50), 15891–15895.
- (115) Okumura, S.; Komine, T.; Shigeki, E.; Semba, K.; Nakao, Y. *Angew. Chem. Int. Ed.* **2018**, *57* (4), 929–932.
- (116) Power, M. B.; Barron, A. R.; Bott, S. G.; Atwood, J. L. *J. Am. Chem. Soc.* **1990**, *112* (9), 3446–3451.
- (117) Maruoka, K.; Itoh, T.; Sakurai, M.; Nonoshita, K.; Yamamoto, H. *J. Am. Chem. Soc.* **1988**, *110* (11), 3588–3597.
- (118) Lee, W.-C.; Chen, C.-H.; Liu, C.-Y.; Yu, M.-S.; Lin, Y.-H.; Ong, T.-G. *Chem. Commun.* **2015**, *51* (96), 17104–17107.
- (119) Ghosh, A.; Walker, J. A.; Ellern, A.; Stanley, L. M. *ACS Catal.* **2016**, *6* (4), 2673–2680.
- (120) Michael, A. *J. für Prakt. Chemie* **1887**, *35* (1), 349–356.
- (121) In *March's Advanced Organic Chemistry*; John Wiley & Sons, Inc.: Hoboken, NJ, USA, 2006; pp 999–1250.
- (122) Rao, M. N.; Haridas, M.; Gangwar, M. K.; Rajakannu, P.; Kalita, A. C.; Ghosh, P. *Eur. J. Inorg. Chem.* **2015**, *2015* (9), 1604–1615.
- (123) Ritleng, V.; Barth, C.; Brenner, E.; Milosevic, S.; Chetcuti, M. J. *Organometallics* **2008**, *27* (16), 4223–4228.
- (124) Ritleng, V.; Oertel, A. M.; Chetcuti, M. J. *Dalton Trans.* **2010**, *39* (35), 8153–8160.
- (125) Oertel, A. M.; Ritleng, V.; Burr, L.; Chetcuti, M. J. *Organometallics* **2011**, *30* (24), 6685–6691.
- (126) Ritleng, V.; Brenner, E.; Chetcuti, M. J. *J. Chem. Educ.* **2008**, *85* (12), 1646–1648.
- (127) Oertel, A. M.; Ritleng, V.; Chetcuti, M. J.; Veiros, L. F. *J. Am. Chem. Soc.* **2010**, *132* (39), 13588–13589.
- (128) Oertel, A. M.; Freudenreich, J.; Gein, J.; Ritleng, V.; Veiros, L. F.; Chetcuti, M. J. *Organometallics* **2011**, *30* (12), 3400–3411.
- (129) Oertel, A. M.; Ritleng, V.; Busiah, A.; Veiros, L. F.; Chetcuti, M. J. *Organometallics* **2011**, *30* (23), 6495–6498.
- (130) Oertel, A. M.; Ritleng, V.; Chetcuti, M. J. *Organometallics* **2012**, *31* (7), 2829–2840.
- (131) Henrion, M.; Oertel, A. M.; Ritleng, V.; Chetcuti, M. J. *Chem. Commun.* **2013**, *49* (57), 6424–6426.
- (132) Rocquin, M.; Ritleng, V.; Barroso, S.; Martins, A. M.; Chetcuti, M. J. *J. Organomet. Chem.* **2016**, *808*, 57–62.
- (133) Cardoso, B. de P.; Bernard-Schaaf, J.-M.; Shahane, S.; Veiros, L. F.; Chetcuti, M. J.; Ritleng, V. *Dalton Trans.* **2018**, *47* (5), 1535–1547.
- (134) Bheeter, L. P.; Henrion, M.; Brelot, L.; Darcel, C.; Chetcuti, M. J.; Sortais, J. B.; Ritleng,

References

- V. *Adv. Synth. Catal.* **2012**, *354* (14–15), 2619–2624.
- (135) Bheeter, L. P.; Henrion, M.; Chetcuti, M. J.; Darcel, C.; Ritleng, V.; Sortais, J.-B. *Catal. Sci. Technol.* **2013**, *3* (12), 3111–3116.
- (136) Dunn, M. H.; Konstandaras, N.; Cole, M. L.; Harper, J. B. *J. Org. Chem.* **2017**, *82* (14), 7324–7331.
- (137) Matthews, W. S.; Bares, J. E.; Bartmess, J. E.; Cornforth, F. J.; Drucker, G. E.; McCallum, R. J.; McCollum, G. J.; Vanier, N. R.; Bordwell, F. G.; Margolin, Z. *J. Am. Chem. Soc.* **1975**, *97* (24), 7006–7014.
- (138) Henrion, M. *Synthèses et applications en catalyse homogène de complexes nickel(II)-carbène N-hétérocyclique*, Thèse de doctorat, Université de Strasbourg, 2014.
- (139) Benhamou, L.; Chardon, E.; Lavigne, G.; Bellemin-Lapponnaz, S.; César, V. *Chem. Rev.* **2011**, *111* (4), 2705–2733.
- (140) Zhao, D.; Fei, Z.; Scopelliti, R.; Dyson, P. J. *Inorg. Chem.* **2004**, *43* (6), 2197–2205.
- (141) Pitula, S.; Mudring, A.-V. *Phys. Chem. Chem. Phys.* **2010**, *12* (26), 7056–7063.
- (142) Varma, R. S.; Namboodiri, V. V. *Pure Appl. Chem.* **2001**, *73* (8), 1309–1313.
- (143) Oertel, A.; Ritleng, V.; Chetcuti, M. *Synthesis* **2009**, *2009* (10), 1647–1650.
- (144) Zhang, J.; Xie, X.; Li, L.; Wu, X.; Ma, C. *Heterocycles* **2016**, *92* (7), 1171–1185.
- (145) Huynh, H. V.; Wu, J. *J. Organomet. Chem.* **2009**, *694* (3), 323–331.
- (146) von Hofmann, A. W. *Ann. Chem. Pharm.* **1851**, *78* (3), 253–286.
- (147) Abernethy, C. D.; Cowley, A. H.; Jones, R. A. *J. Organomet. Chem.* **2000**, *596* (1–2), 3–5.
- (148) Buchowicz, W.; Wojtczak, W.; Pietrzykowski, A.; Lupa, A.; Jerzykiewicz, L. B.; Makal, A.; Woźniak, K. *Eur. J. Inorg. Chem.* **2010**, (4), 648–656.
- (149) Olmstead, W. N.; Margolin, Z.; Bordwell, F. G. *J. Org. Chem.* **1980**, *45* (16), 3295–3299.
- (150) Fraser, R. R.; Mansour, T. S.; Savard, S. *J. Org. Chem.* **1985**, *50* (17), 3232–3234.
- (151) Begun, G. M.; Rutenberg, A. C. *Inorg. Chem.* **1967**, *6* (12), 2212–2216.
- (152) Spingler, B.; Schnidrig, S.; Todorova, T.; Wild, F. *CrystEngComm* **2012**, *14* (3), 751–757.
- (153) Jandl, C.; Pöthig, A. *Chem. Commun.* **2017**, *53* (13), 2098–2101.
- (154) Jandl, C.; Stegbauer, S.; Pöthig, A. *Acta Crystallogr. Sect. C Struct. Chem.* **2016**, *72* (7), 509–513.
- (155) Andrews, M. A.; Knobler, C. B.; Kaesz, H. D. *J. Am. Chem. Soc.* **1979**, *101* (24), 7260–7264.
- (156) Cotton, F. A.; Kühn, F. E. *J. Am. Chem. Soc.* **1996**, *118* (24), 5826–5827.
- (157) Lorber, C.; Choukroun, R.; Vendier, L. *Organometallics* **2008**, *27* (19), 5017–5024.
- (158) Joensen, H. A. N.; Hansson, G. K.; Kozlova, S. G.; Gushchin, A. L.; Sotofte, I.; Ooi, B.-

References

- L. *Inorg. Chem.* **2010**, *49* (4), 1720–1727.
- (159) Davenport, T. C.; Tilley, T. D. *Angew. Chem. Int. Ed.* **2011**, *50* (51), 12205–12208.
- (160) Cotton, F. A.; Haefner, S. C.; Sattelberger, A. P. *Inorg. Chim. Acta* **1997**, *266* (1), 55–63.
- (161) Hoffman, D. M.; Lee, S. *Inorg. Chem.* **1992**, *31* (13), 2675–2676.
- (162) Garcia Alonso, F. J.; Garcia Sanz, M.; Riera, V.; Anillo Abril, A.; Tiripicchio, A.; Ugozzoli, F. *Organometallics* **1992**, *11* (2), 801–808.
- (163) Eglin, J. L.; Marie Hines, E.; Valente, E. J.; Zubkowski, J. D. *Inorg. Chim. Acta* **1995**, *229* (1–2), 113–119.
- (164) Cotton, F. A.; Daniels, L. M.; Murillo, C. A.; Wang, X. *Polyhedron* **1998**, *17* (17), 2781–2793.
- (165) Evans, W. J.; Greci, M. A.; Ziller, J. W. *Chem. Commun.* **1998**, (21), 2367–2368.
- (166) Tikhonova, I. .; Dolgushin, F. .; Yanovsky, A. .; Starikova, Z. .; Petrovskii, P. .; Furin, G. .; Shur, V. . *J. Organomet. Chem.* **2000**, *613* (1), 60–67.
- (167) Beckwith, J. D.; Tschinkl, M.; Picot, A.; Tsunoda, M.; Bachman, R.; Gabbaï, F. P. *Organometallics* **2001**, *20* (14), 3169–3174.
- (168) Lin, P.; Clegg, W.; Harrington, R. W.; Henderson, R. A. *Dalton Trans.* **2005**, (14), 2349.
- (169) Takao, T.; Kawashima, T.; Matsubara, K.; Suzuki, H. *Organometallics* **2005**, *24* (14), 3371–3374.
- (170) Al-Mandhary, M. R. A.; Fitchett, C. M.; Steel, P. J. *Aust. J. Chem.* **2006**, *59* (5), 307.
- (171) Walther, D.; Schönberg, H.; Dinjus, E.; Sieler, J. *J. Organomet. Chem.* **1987**, *334* (3), 377–388.
- (172) Stolley, R. M.; Duong, H. A.; Thomas, D. R.; Louie, J. *J. Am. Chem. Soc.* **2012**, *134* (36), 15154–15162.
- (173) Shoshani, M. M.; Beck, R.; Wang, X.; McLaughlin, M. J.; Johnson, S. A. *Inorg. Chem.* **2018**, *57* (5), 2438–2446.
- (174) Bassi, I. W.; Benedicenti, C.; Calcaterra, M.; Intrito, R.; Rucci, G.; Santini, C. *J. Organomet. Chem.* **1978**, *144* (2), 225–237.
- (175) Garcia, J. J.; Jones, W. D. *Organometallics* **2000**, *19* (26), 5544–5545.
- (176) García, J. J.; Arévalo, A.; Brunkan, N. M.; Jones, W. D. *Organometallics* **2004**, *23* (16), 3997–4002.
- (177) Ateşin, T. A.; Li, T.; Lachaize, S.; Brennessel, W. W.; García, J. J.; Jones, W. D. *J. Am. Chem. Soc.* **2007**, *129* (24), 7562–7569.
- (178) Ohashi, M.; Ikawa, M.; Ogoshi, S. *Organometallics* **2011**, *30* (10), 2765–2774.
- (179) Ge, S.; Hartwig, J. F. *J. Am. Chem. Soc.* **2011**, *133* (41), 16330–16333.
- (180) Thomas, S.; Tiekink, E. R. T.; Young, C. G. *Organometallics* **1996**, *15* (10), 2428–2430.

References

- (181) Thomas, S.; Young, C. G.; Tiekink, E. R. T. *Organometallics* **1998**, *17* (2), 182–189.
- (182) Wright, T. C.; Wilkinson, G.; Motevalli, M.; Hursthouse, M. B. *J. Chem. Soc., Dalton Trans.* **1986**, (9), 2017–2019.
- (183) Anderson, S. J.; Wells, F. J.; Wilkinson, G.; Hussain, B.; Hursthouse, M. B. *Polyhedron* **1988**, *7* (24), 2615–2626.
- (184) Barrera, J.; Sabat, M.; Harman, W. D. *J. Am. Chem. Soc.* **1991**, *113* (21), 8178–8180.
- (185) Barrera, J.; Sabat, M.; Harman, W. D. *Organometallics* **1993**, *12* (11), 4381–4390.
- (186) Rouschias, G.; Wilkinson, G. *J. Chem. Soc. A* **1968**, *0*, 489–496.
- (187) Endres, H. In *Comprehensive Coordination Chemistry, Vol. 2*; Wilkinson, G., Gillard, R. D., McCleverty, J. A., Eds.; Pergamon: Oxford, 1987; p 261.
- (188) Evans, D. F. *J. Chem. Soc.* **1959**, 2003–2005.
- (189) Holland, P. L.; Cundari, T. R.; Perez, L. L.; Eckert, N. A.; Lachicotte, R. J. *J. Am. Chem. Soc.* **2002**, *124* (48), 14416–14424.
- (190) Hartmann, N. J.; Wu, G.; Hayton, T. W. *Angew. Chem. Int. Ed.* **2015**, *54* (49), 14956–14959.
- (191) Hope, H.; Olmstead, M. M.; Murray, B. D.; Power, P. P. *J. Am. Chem. Soc.* **1985**, *107* (3), 712–713.
- (192) Ortuño, M. A.; Conejero, S.; Lledós, A. *Beilstein J. Org. Chem.* **2013**, *9* (li), 1352–1382.
- (193) Bell, S. A.; Lancaster, J. C.; McWhinnie, W. R. *Inorg. Nucl. Chem. Lett.* **1971**, *7* (5), 405–407.
- (194) Bauer, H.; Nagel, U.; Beck, W. *J. Organomet. Chem.* **1985**, *290* (2), 219–229.
- (195) Beck, W.; Schlöter, K. *Z. Naturforsch.* **1978**, *33b* (11), 1214–1222.
- (196) Beck, W.; Suenkel, K. *Chem. Rev.* **1988**, *88* (7), 1405–1421.
- (197) Tamaki, T.; Nagata, M.; Ohashi, M.; Ogoshi, S. *Chem. Eur. J.* **2009**, *15* (39), 10083–10091.
- (198) Laskowski, C. A.; Hillhouse, G. L. *J. Am. Chem. Soc.* **2008**, *130* (42), 13846–13847.
- (199) Lipschutz, M. I.; Tilley, T. D. *Chem. Commun.* **2012**, *48* (57), 7146.
- (200) Pelties, S.; Wolf, R. *Organometallics* **2016**, *35* (16), 2722–2727.
- (201) Saper, N. I.; Hartwig, J. F. *J. Am. Chem. Soc.* **2017**, *139* (48), 17667–17676.
- (202) Tamaki, T.; Ohashi, M.; Ogoshi, S. *Chem. Lett.* **2011**, *40* (3), 248–249.
- (203) Hoshimoto, Y.; Ohata, T.; Ohashi, M.; Ogoshi, S. *Chem. Eur. J.* **2014**, *20* (14), 4105–4110.
- (204) Laskowski, C. A.; Morello, G. R.; Saouma, C. T.; Cundari, T. R.; Hillhouse, G. L. *Chem. Sci.* **2013**, *4* (1), 170–174.
- (205) Bunce, R. A.; Herron, D. M.; Ackerman, M. L. *J. Org. Chem.* **2000**, *65* (10), 2847–2850.
- (206) Kühn, O. *Phosphorus-31 NMR Spectroscopy*; Kühn, O., Ed.; Springer Berlin Heidelberg:

References

- Berlin, Heidelberg, 2009.
- (207) Tolman, C. A. *Chem. Rev.* **1977**, *77* (3), 313–348.
- (208) Tolman, C. A. *J. Am. Chem. Soc.* **1970**, *92* (10), 2956–2965.
- (209) Guo, Y.; Zhang, X.; Wang, L.; Sun, H.; Li, X. Z. *Anorg. Allg. Chem.* **2015**, *641* (3–4), 669–672.
- (210) Bardsley, K.; Hagigeorgiou, M.; Lengyel, I.; Cesare, V. *Synth. Commun.* **2013**, *43* (12), 1727–1733.
- (211) Dible, B. R.; Sigman, M. S.; Arif, A. M. *Inorg. Chem.* **2005**, *44* (11), 3774–3776.
- (212) Dible, B. R.; Sigman, M. S. *J. Am. Chem. Soc.* **2003**, *125* (4), 872–873.
- (213) Li, Y.; Jiang, L.; Wang, L.; Gao, H.; Zhu, F.; Wu, Q. *Appl. Organomet. Chem.* **2006**, *20* (3), 181–186.
- (214) Cornella, J.; Gómez-Bengoa, E.; Martin, R. *J. Am. Chem. Soc.* **2013**, *135* (5), 1997–2009.
- (215) Ölscher, F.; Göttker-Schnetmann, I.; Monteil, V.; Mecking, S. *J. Am. Chem. Soc.* **2015**, *137* (46), 14819–14828.
- (216) Lopez, G.; Garcia, G.; Sanchez, G.; Garcia, J.; Ruiz, J.; Hermoso, J. A.; Vegas, A.; Martinez-Ripoll, M. *Inorg. Chem.* **1992**, *31* (8), 1518–1523.
- (217) Ghilardi, C. A.; Innocenti, P.; Midollini, S.; Orlandini, A. *J. Chem. Soc., Dalton Trans.* **1988**, (4), 1063–1066.
- (218) Carmona, E.; Marin, J. M.; Palma, P.; Paneque, M.; Poveda, M. L. *Inorg. Chem.* **1989**, *28* (10), 1895–1900.
- (219) Morales-Becerril, I.; Flores-Álamo, M.; Tlahuext-Aca, A.; Arévalo, A.; García, J. J. *Organometallics* **2014**, *33* (23), 6796–6802.
- (220) Mooibroek, T. J.; Wenker, E. C. M.; Smit, W.; Mutikainen, I.; Lutz, M.; Bouwman, E. *Inorg. Chem.* **2013**, *52* (14), 8190–8201.
- (221) Lee, K.; Donahue, C. M.; Daly, S. R. *Dalton Trans.* **2017**, *46* (29), 9394–9406.
- (222) Yao, S.; Bill, E.; Milsman, C.; Wieghardt, K.; Driess, M. *Angew. Chem. Int. Ed.* **2008**, *47* (37), 7110–7113.
- (223) Reinhard, G.; Soltek, R.; Huttner, G.; Barth, A.; Walter, O.; Zsolnai, L. *Chem. Ber.* **1996**, *129* (1), 97–108.
- (224) Gilroy, J. B.; Patrick, B. O.; McDonald, R.; Hicks, R. G. *Inorg. Chem.* **2008**, *47* (4), 1287–1294.
- (225) Pickel, M.; Casper, T.; Rahm, A.; Dambouwy, C.; Chen, P. *Helv. Chim. Acta* **2002**, *85* (12), 4337–4352.
- (226) Camasso, N. M.; Sanford, M. S. *Science* **2015**, *347* (6227), 1218–1220.
- (227) Chong, E.; Kampf, J. W.; Ariafard, A.; Canty, A. J.; Sanford, M. S. *J. Am. Chem. Soc.*

References

- 2017**, 139 (17), 6058–6061.
- (228) Camasso, N. M.; Canty, A. J.; Ariafard, A.; Sanford, M. S. *Organometallics* **2017**, 36 (22), 4382–4393.
- (229) Bour, J. R.; Camasso, N. M.; Meucci, E. A.; Kampf, J. W.; Canty, A. J.; Sanford, M. S. *J. Am. Chem. Soc.* **2016**, 138 (49), 16105–16111.
- (230) Meucci, E. A.; Camasso, N. M.; Sanford, M. S. *Organometallics* **2017**, 36 (2), 247–250.
- (231) Cámpora, J.; Gutiérrez, E.; Monge, A.; Palma, P.; Poveda, M.; Ruíz, C.; Carmona, E. *Organometallics* **1994**, 13 (5), 1728–1745.
- (232) Klein, A.; Kaiser, A.; Sarkar, B.; Wanner, M.; Fiedler, J. *Eur. J. Inorg. Chem.* **2007**, 2007 (7), 965–976.
- (233) Eicher, T.; Hauptmann, S. *The Chemistry of Heterocycles*; 2nd, Ed.; John Wiley & Sons, 2003.
- (234) Matsuyama, N.; Hirano, K.; Satoh, T.; Miura, M. *Org. Lett.* **2009**, 11 (18), 4156–4159.
- (235) Patel, U. N.; Punji, B. *Asian J. Org. Chem.* **2018**, 7 (7), 1390–1395.
- (236) Matsuyama, N.; Kitahara, M.; Hirano, K.; Satoh, T.; Miura, M. *Org. Lett.* **2010**, 12 (10), 2358–2361.
- (237) Hachiya, H.; Hirano, K.; Satoh, T.; Miura, M. *Org. Lett.* **2009**, 11 (8), 1737–1740.
- (238) Canivet, J.; Yamaguchi, J.; Ban, I.; Itami, K. *Org. Lett.* **2009**, 11 (8), 1733–1736.
- (239) Yamamoto, T.; Muto, K.; Komiyama, M.; Canivet, J.; Yamaguchi, J.; Itami, K. *Chem. Eur. J.* **2011**, 17 (36), 10113–10122.
- (240) Yin, Y.; Yue, X.; Zhong, Q.; Jiang, H.; Bai, R.; Lan, Y.; Zhang, H. *Adv. Synth. Catal.* **2018**, 360 (8), 1639–1643.
- (241) Becker, M. A.; Schumacher, H. R.; Wortmann, R. L.; MacDonald, P. A.; Eustace, D.; Palo, W. A.; Streit, J.; Joseph-Ridge, N. *N. Engl. J. Med.* **2005**, 353 (23), 2450–2461.
- (242) Okamoto, K.; Eger, B. T.; Nishino, T.; Kondo, S.; Pai, E. F.; Nishino, T. *J. Biol. Chem.* **2003**, 278 (3), 1848–1855.
- (243) Razavi, H.; Palaninathan, S. K.; Powers, E. T.; Wiseman, R. L.; Purkey, H. E.; Mohamedmohaideen, N. N.; Deechongkit, S.; Chiang, K. P.; Dendle, M. T. A.; Sacchettini, J. C.; Kelly, J. W. *Angew. Chem. Int. Ed.* **2003**, 42 (24), 2758–2761.
- (244) Besselièvre, F.; Mahuteau-Betzer, F.; Grierson, D. S.; Piguel, S. *J. Org. Chem.* **2008**, 73 (8), 3278–3280.
- (245) Giddens, A. C.; Boshoff, H. I. M.; Franzblau, S. G.; Barry, C. E.; Copp, B. R. *Tetrahedron Lett.* **2005**, 46 (43), 7355–7357.
- (246) Domínguez, X. A.; de la Fuente, G.; González, A. G.; Reina, M.; Timón, I. *Heterocycles* **1988**, 27 (1), 35–38.
- (247) Muto, K.; Yamaguchi, J.; Itami, K. *J. Am. Chem. Soc.* **2012**, 134 (1), 169–172.

References

- (248) Amaike, K.; Muto, K.; Yamaguchi, J.; Itami, K. *J. Am. Chem. Soc.* **2012**, *134* (33), 13573–13576.
- (249) Muto, K.; Hatakeyama, T.; Yamaguchi, J.; Itami, K. *Chem. Sci.* **2015**, *6* (12), 6792–6798.
- (250) Meng, L.; Kamada, Y.; Muto, K.; Yamaguchi, J.; Itami, K. *Angew. Chem. Int. Ed.* **2013**, *52* (38), 10048–10051.
- (251) Steinberg, D. F.; Turk, M. C.; Kalyani, D. *Tetrahedron* **2017**, *73* (16), 2196–2209.
- (252) Crawford, J. M.; Shelton, K. E.; Reeves, E. K.; Sadarananda, B. K.; Kalyani, D. *Org. Chem. Front.* **2015**, *2* (6), 726–729.
- (253) Yang, K.; Zhang, C.; Wang, P.; Zhang, Y.; Ge, H. *Chem. Eur. J.* **2014**, *20* (24), 7241–7244.
- (254) Coqueron, P.-Y.; Didier, C.; Ciufolini, M. A. *Angew. Chem. Int. Ed.* **2003**, *42* (12), 1411–1414.
- (255) Muir, J. C. *Synthesis* **1998**, *1998* (S1), 613–618.
- (256) Wipf, P.; Venkatraman, S. *J. Org. Chem.* **1996**, *61* (19), 6517–6522.
- (257) Nagatsu, A.; Kajitani, H.; Sakakibara, J. *Tetrahedron Lett.* **1995**, *36* (23), 4097–4100.
- (258) Hanson, M. G.; Olson, N. M.; Yi, Z.; Wilson, G.; Kalyani, D. *Org. Lett.* **2017**, *19* (16), 4271–4274.
- (259) Hachiya, H.; Hirano, K.; Satoh, T.; Miura, M. *Angew. Chem. Int. Ed.* **2010**, *49* (12), 2202–2205.
- (260) Hachiya, H.; Hirano, K.; Satoh, T.; Miura, M. *ChemCatChem* **2010**, *2* (11), 1403–1406.
- (261) Cheng, Y.; Wu, Y.; Tan, G.; You, J. *Angew. Chem. Int. Ed.* **2016**, *55* (40), 12275–12279.
- (262) Lovering, F.; Bikker, J.; Humblet, C. *J. Med. Chem.* **2009**, *52* (21), 6752–6756.
- (263) Blakemore, D. C.; Castro, L.; Churcher, I.; Rees, D. C.; Thomas, A. W.; Wilson, D. M.; Wood, A. *Nat. Chem.* **2018**, *10* (4), 383–394.
- (264) Yao, T.; Hirano, K.; Satoh, T.; Miura, M. *Chem. Eur. J.* **2010**, *16* (41), 12307–12311.
- (265) Vechorkin, O.; Proust, V.; Hu, X. *Angew. Chem. Int. Ed.* **2010**, *49* (17), 3061–3064.
- (266) Ackermann, L.; Punji, B.; Song, W. *Adv. Synth. Catal.* **2011**, *353* (18), 3325–3329.
- (267) Patel, U. N.; Pandey, D. K.; Gonnade, R. G.; Punji, B. *Organometallics* **2016**, *35* (11), 1785–1793.
- (268) Xiao, J.; Chen, T.; Han, L.-B. *Org. Lett.* **2015**, *17* (4), 812–815.
- (269) Yao, T.; Hirano, K.; Satoh, T.; Miura, M. *Angew. Chem. Int. Ed.* **2012**, *51* (3), 775–779.
- (270) Tan, G.; Zhang, L.; Liao, X.; Shi, Y.; Wu, Y.; Yang, Y.; You, J. *Org. Lett.* **2017**, *19* (18), 4830–4833.
- (271) Muto, K.; Yamaguchi, J.; Lei, A.; Itami, K. *J. Am. Chem. Soc.* **2013**, *135* (44), 16384–16387.
- (272) Clevenger, A. L.; Stolley, R. M.; Staudaher, N. D.; Al, N.; Rheingold, A. L.; Vanderlinden,

References

- R. T.; Louie, J. *Organometallics* **2018**, *37* (19), 3259–3268.
- (273) Patel, U. N.; Jain, S.; Pandey, D. K.; Gonnade, R. G.; Vanka, K.; Punji, B. *Organometallics* **2018**, *37* (6), 1017–1025.
- (274) Shilov, A. E.; Shul, G. B. *Chem. Rev.* **1997**, *97* (94), 2879–2932.
- (275) Bordwell, F. G. *Acc. Chem. Res.* **1988**, *21* (12), 456–463.
- (276) Shen, K.; Fu, Y.; Li, J.-N.; Liu, L.; Guo, Q.-X. *Tetrahedron* **2007**, *63* (7), 1568–1576.
- (277) *CRC Handbook of Chemistry and Physics, 84th Edition*, 84th ed.; Lide, D. R., Ed.; CRC Press, 2003.
- (278) Crabtree, R. H. *Chem. Rev.* **2012**, *112* (3), 1536–1554.
- (279) Cai, X.; Xie, B. *Arkivoc* **2015**, *2015* (1), 184–211.
- (280) Crabtree, R. H. *Chem. Rev.* **2015**, *115* (1), 127–150.
- (281) Finkelstein, H. *Ber. Dtsch. Chem. Ges.* **1910**, *43* (2), 1528–1532.
- (282) Yamaguchi, J.; Muto, K.; Itami, K. *European J. Org. Chem.* **2013**, *2013* (1), 19–30.
- (283) Xu, H.; Muto, K.; Yamaguchi, J.; Zhao, C.; Itami, K.; Musaev, D. G. *J. Am. Chem. Soc.* **2014**, *136* (42), 14834–14844.
- (284) Kruckenberg, A.; Wadepohl, H.; Gade, L. H. *Organometallics* **2013**, *32* (18), 5153–5170.
- (285) Khake, S. M.; Soni, V.; Gonnade, R. G.; Punji, B. *Dalton Trans.* **2014**, *43* (42), 16084–16096.
- (286) Khake, S. M.; Jagtap, R. A.; Dangat, Y. B.; Gonnade, R. G.; Vanka, K.; Punji, B. *Organometallics* **2016**, *35* (6), 875–886.
- (287) Wang, C.; Li, Y.; Lu, B.; Hao, X.-Q.; Gong, J.-F.; Song, M.-P. *Polyhedron* **2018**, *143*, 184–192.
- (288) Kelly, R. A.; Scott, N. M.; Díez-González, S.; Stevens, E. D.; Nolan, S. P. *Organometallics* **2005**, *24* (14), 3442–3447.
- (289) Malyshev, D. A.; Scott, N. M.; Marion, N.; Stevens, E. D.; Ananikov, V. P.; Beletskaya, I. P.; Nolan, S. P. *Organometallics* **2006**, *25* (19), 4462–4470.
- (290) Banach, Ł.; Guńka, P. A.; Górska, D.; Podlewska, M.; Zachara, J.; Buchowicz, W. *Eur. J. Inorg. Chem.* **2015**, *2015* (34), 5677–5686.
- (291) Itoh, T.; Mase, T. *Org. Lett.* **2007**, *9* (18), 3687–3689.
- (292) Herrmann, W. A.; Runte, O.; Artus, G. *J. Organomet. Chem.* **1995**, *501* (1–2), C1–C4.
- (293) Baker, M. V.; Barnard, P. J.; Brayshaw, S. K.; Hickey, J. L.; Skelton, B. W.; White, A. H. *Dalton Trans.* **2005**, *8* (1), 37.
- (294) Chernyshova, E. S.; Goddard, R.; Pörschke, K.-R. *Organometallics* **2007**, *26* (13), 3236–3251.
- (295) Omer, H. M.; Liu, P. *J. Am. Chem. Soc.* **2017**, *139* (29), 9909–9920.
- (296) Ritleng, V.; Barth, C.; Brenner, E.; Milosevic, S.; Chetcuti, M. J. *Organometallics* **2008**,

References

- 27 (16), 4223–4228.
- (297) Luca, O. R.; Thompson, B. A.; Takase, M. K.; Crabtree, R. H. *J. Organomet. Chem.* **2013**, 730, 79–83.
- (298) Peñas-Defrutos, M. N.; Bartolomé, C.; Espinet, P. *Organometallics* **2018**, 37 (20), 3533–3542.
- (299) March, J.; Smith, M. B. In *March's Advanced Organic Chemistry*; John Wiley & Sons, Inc.: Hoboken, NJ, USA, 2006; pp 234–298.
- (300) Crabtree, R. H. In *The Organometallic Chemistry of the Transition Metals*; John Wiley & Sons, Inc.: Hoboken, NJ, USA, 2005; pp 159–182.
- (301) Urban, S.; Tursky, M.; Fröhlich, R.; Glorius, F. *Dalton Trans.* **2009**, (35), 6934.
- (302) Morioka, T.; Nishizawa, A.; Furukawa, T.; Tobisu, M.; Chatani, N. *J. Am. Chem. Soc.* **2017**, 139 (4), 1416–1419.
- (303) Yi, Y.-Q.-Q.; Yang, W.-C.; Zhai, D.-D.; Zhang, X.-Y.; Li, S.-Q.; Guan, B.-T.; Senanayake, C. H. *Chem. Commun.* **2016**, 52 (72), 10894–10897.
- (304) Han, Y.; Huynh, H. V.; Tan, G. K. *Organometallics* **2007**, 26 (25), 6447–6452.
- (305) Macaev, F.; Gavrilov, K.; Muntyanu, V.; Styngach, E.; Vlad, L.; Bets, L.; Pogrebnoi, S.; Barba, A. *Chem. Nat. Compd.* **2007**, 43 (2), 114–116.
- (306) Arduengo, A. J.; Krafczyk, R.; Schmutzler, R.; Craig, H. A.; Goerlich, J. R.; Marshall, W. J.; Unverzagt, M. *Tetrahedron* **1999**, 55 (51), 14523–14534.
- (307) Kyan, R.; Sato, K.; Mase, N.; Watanabe, N.; Narumi, T. *Org. Lett.* **2017**, 19 (10), 2750–2753.
- (308) Hirano, K.; Urban, S.; Wang, C.; Glorius, F. *Org. Lett.* **2009**, 11 (4), 1019–1022.
- (309) In *Inorganic Syntheses*; Rauchfuss, T. B., Ed.; John Wiley & Sons, Inc., 2010; pp 109–128.
- (310) Cooke, J.; Lightbody, O. C. *J. Chem. Educ.* **2011**, 88 (1), 88–91.
- (311) Perrin, D. D.; Armarego, W. L. F. *Purification of Laboratory Chemicals*, 4th ed.; Butterworth-Heinemann: Woburn, MA, 2000.
- (312) Williams, D. B. G.; Lawton, M. J. *Org. Chem.* **2010**, 75 (24), 8351–8354.
- (313) Shriver, D. F. *The Manipulation of Air-sensitive Compounds*, Reprint.; Robert E. Krieger Publishing Company, Inc.: New York, USA, 1982.
- (314) Fulmer, G. R.; Miller, A. J. M.; Sherden, N. H.; Gottlieb, H. E.; Nudelman, A.; Stoltz, B. M.; Bercaw, J. E.; Goldberg, K. I. *Organometallics* **2010**, 29 (9), 2176–2179.
- (315) *The Merck Index: An Encyclopedia of Chemicals, Drugs, and Biologicals*, 14th ed.; O'Neil, M. J., Heckelman, P. E., Koch, C. B., Roman, K. J., Eds.; Merck & Co., Inc.: Whitehouse Station, 2006.
- (316) Sheldrick, G. M. *Acta Crystallogr. Sect. A Found. Crystallogr.* **2008**, 64 (1), 112–122.

References

- (317) Sheldrick, G. M. *SHELXS97 and SHELXL97. Program for Crystal Structure Solution and Refinement*, University of Göttingen: Göttingen 1997.
- (318) Sheldrick, G. M. *SADABS, Program for Empirical Absorption Correction*, University of Göttingen: Göttingen 1996.
- (319) Sawyer, D. T.; Sobkowiak, A.; Roberts, J. *Electrochemistry for Chemists*, 2nd ed.; John Wiley & Sons, Inc., 1995.
- (320) Billeau, S.; Chatel, F.; Robin, M.; Faure, R.; Galy, J.-P. *Magn. Reson. Chem.* **2006**, *44* (1), 102–105.
- (321) Huang, J.; Chan, J.; Chen, Y.; Borths, C. J.; Baucom, K. D.; Larsen, R. D.; Faul, M. M. *J. Am. Chem. Soc.* **2010**, *132* (11), 3674–3675.
- (322) Inamoto, K.; Hasegawa, C.; Kawasaki, J.; Hiroya, K.; Doi, T. *Adv. Synth. Catal.* **2010**, *352* (14–15), 2643–2655.
- (323) Chakraborti, A. K.; Rudrawar, S.; Kaur, G.; Sharma, L. *Synlett* **2004**, (9), 1533–1536.
- (324) Do, H.; Daugulis, O. *J. Am. Chem. Soc.* **2007**, *129* (41), 12404–12405.
- (325) Wiberg, K. B. *J. Comput. Chem.* **1986**, *7* (3), 379–379.
- (326) Frisch, M. J.; Trucks, G. W.; Schlegel, H. B.; Scuseria, G. E.; Robb, M. A.; Cheeseman, J. R.; Scalmani, G.; Barone, V.; Mennucci, B.; Petersson, G. A.; Nakatsuji, H.; Caricato, M.; Li, X.; Hratchian, H. P.; Izmaylov, A. F.; Bloino, J.; Zheng, G.; Sonnenberg, J. L.; Hada, M.; Ehara, M.; Toyota, K.; Fukuda, R.; Hasegawa, J.; Ishida, M.; Nakajima, T.; Honda, Y.; Kitao, O.; Nakai, H.; Vreven, T.; Montgomery, J. A., Jr.; Peralta, J. E.; Ogliaro, F.; Bearpark, M.; Heyd, J. J.; Brothers, E.; Kudin, K. N.; Staroverov, V. N.; Kobayashi, R.; Normand, J.; Raghavachari, K.; Rendell, A.; Burant, J. C.; Iyengar, S. S.; Tomasi, J.; Cossi, M.; Rega, N.; Millam, N. J.; Klene, M.; Knox, J. E.; Cross, J. B.; Bakken, V.; Adamo, C.; Jaramillo, J.; Gomperts, R.; Stratmann, R. E.; Yazyev, O.; Austin, A. J.; Cammi, R.; Pomelli, C.; Ochterski, J. W.; Martin, R. L.; Morokuma, K.; Zakrzewski, V. G.; Voth, G. A.; Salvador, P.; Dannenberg, J. J.; Dapprich, S.; Daniels, A. D.; Farkas, Ö.; Foresman, J. B.; Ortiz, J. V.; Cioslowski, J.; Fox, D. J. *Gaussian 09, Revision D.01*, Gaussian, Inc.: Wallingford CT 2009.
- (327) Perdew, J. P. *Phys. Rev. B* **1986**, *33* (12), 8822–8824.
- (328) Perdew, J. P.; Burke, K.; Ernzerhof, M. *Phys. Rev. Lett.* **1997**, *78* (7), 1396–1396.
- (329) Perdew, J. P.; Burke, K.; Ernzerhof, M. *Phys. Rev. Lett.* **1996**, *77* (18), 3865–3868.
- (330) Häussermann, U.; Dolg, M.; Stoll, H.; Preuss, H.; Schwerdtfeger, P.; Pitzer, R. M. *Mol. Phys.* **1993**, *78* (5), 1211–1224.
- (331) Leininger, T.; Nicklass, A.; Stoll, H.; Dolg, M.; Schwerdtfeger, P. *J. Chem. Phys.* **1996**, *105* (3), 1052–1059.
- (332) Küchle, W.; Dolg, M.; Stoll, H.; Preuss, H. *J. Chem. Phys.* **1994**, *100* (10), 7535–7542.

References

- (333) Ehlers, A. W.; Böhme, M.; Dapprich, S.; Gobbi, A.; Höllwarth, A.; Jonas, V.; Köhler, K. F.; Stegmann, R.; Veldkamp, A.; Frenking, G. *Chem. Phys. Lett.* **1993**, *208* (1–2), 111–114.
- (334) Hay, P. J.; Wadt, W. R. *J. Chem. Phys.* **1985**, *82* (1), 270–283.
- (335) Wachters, A. J. H. *J. Chem. Phys.* **1970**, *52* (3), 1033–1036.
- (336) Krishnan, R.; Binkley, J. S.; Seeger, R.; Pople, J. A. *J. Chem. Phys.* **1980**, *72* (1), 650–654.
- (337) McLean, A. D.; Chandler, G. S. *J. Chem. Phys.* **1980**, *72* (10), 5639–5648.
- (338) Raghavachari, K.; Trucks, G. W. *J. Chem. Phys.* **1989**, *91* (2), 1062–1065.
- (339) Binning, R. C.; Curtiss, L. A. *J. Comput. Chem.* **1990**, *11* (10), 1206–1216.
- (340) McGrath, M. P.; Radom, L. *J. Chem. Phys.* **1991**, *94* (1), 511–516.
- (341) Peng, C.; Bernhard Schlegel, H. *Isr. J. Chem.* **1993**, *33* (4), 449–454.
- (342) Peng, C.; Ayala, P. Y.; Schlegel, H. B.; Frisch, M. J. *J. Comput. Chem.* **1996**, *17* (1), 49–56.
- (343) Clark, T.; Chandrasekhar, J.; Spitznagel, G. W.; Schleyer, P. V. R. *J. Comput. Chem.* **1983**, *4* (3), 294–301.
- (344) Frisch, M. J.; Pople, J. A.; Binkley, J. S. *J. Chem. Phys.* **1984**, *80* (7), 3265–3269.
- (345) Zhao, Y.; Truhlar, D. G. *Theor. Chem. Acc.* **2008**, *120* (1–3), 215–241.
- (346) Zhao, Y.; Truhlar, D. G. *Chem. Phys. Lett.* **2011**, *502* (1–3), 1–13.
- (347) Zhao, Y.; Truhlar, D. G. *Acc. Chem. Res.* **2008**, *41* (2), 157–167.
- (348) Cancès, E.; Mennucci, B.; Tomasi, J. *J. Chem. Phys.* **1997**, *107* (8), 3032–3041.
- (349) Tomasi, J.; Mennucci, B.; Cammi, R. *Chem. Rev.* **2005**, *105* (8), 2999–3093.
- (350) Cossi, M.; Barone, V. *J. Chem. Phys.* **1998**, *109* (15), 6246–6254.
- (351) Marenich, A. V.; Cramer, C. J.; Truhlar, D. G. *J. Phys. Chem. B* **2009**, *113* (18), 6378–6396.
- (352) Zhurko, G. A. *Chemcraft*, 2013
- (353) Egorova, K. S.; Ananikov, V. P. *Angew. Chem. Int. Ed.* **2016**, *55* (40), 12150–12162.
- (354) Egorova, K. S.; Ananikov, V. P. *Organometallics* **2017**, *36* (21), 4071–4090.
- (355) Horváth, A. *Synthesis* **1994**, *1994* (1), 102–106.
- (356) Salman, A. W.; Haque, R. A.; Budagumpi, S.; Zetty Zulikha, H. *Polyhedron* **2013**, *49* (1), 200–206.
- (357) Gorunova, O. N.; Novitskiy, I. M.; Grishin, Y. K.; Gloriov, I. P.; Roznyatovsky, V. A.; Khrustalev, V. N.; Kochetkov, K. A.; Dunina, V. V. *Organometallics* **2018**, *37* (17), 2842–2858.
- (358) Blanksby, S. J.; Ellison, G. B. *Acc. Chem. Res.* **2003**, *36* (4), 255–263.

Annex

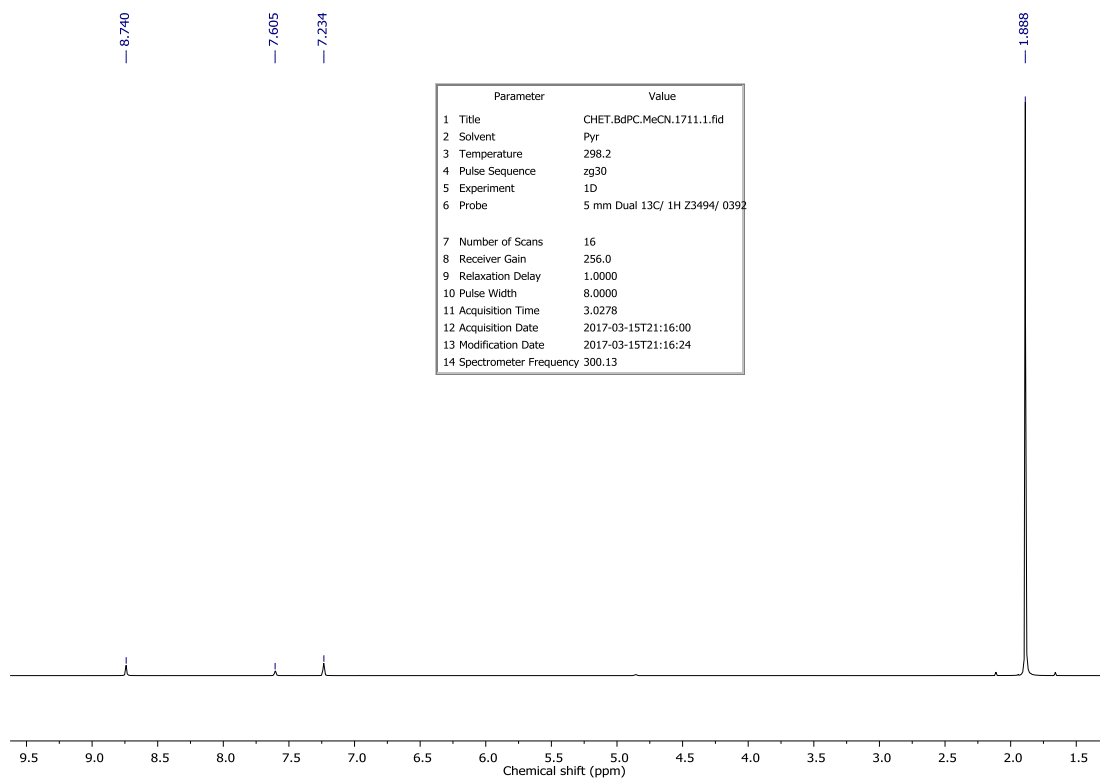


Figure S1. ^1H NMR spectra of acetonitrile in pyridine- d_5 .

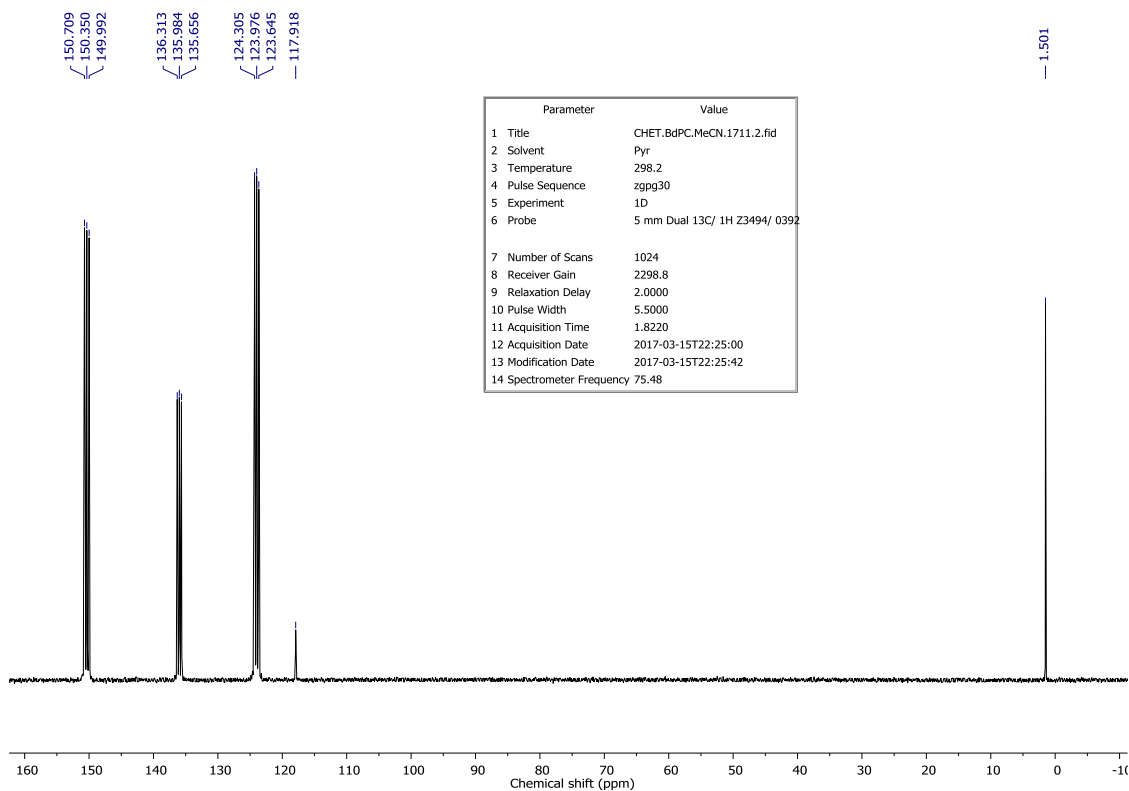


Figure S2. ^{13}C $\{^1\text{H}\}$ NMR of acetonitrile in pyridine- d_5 .

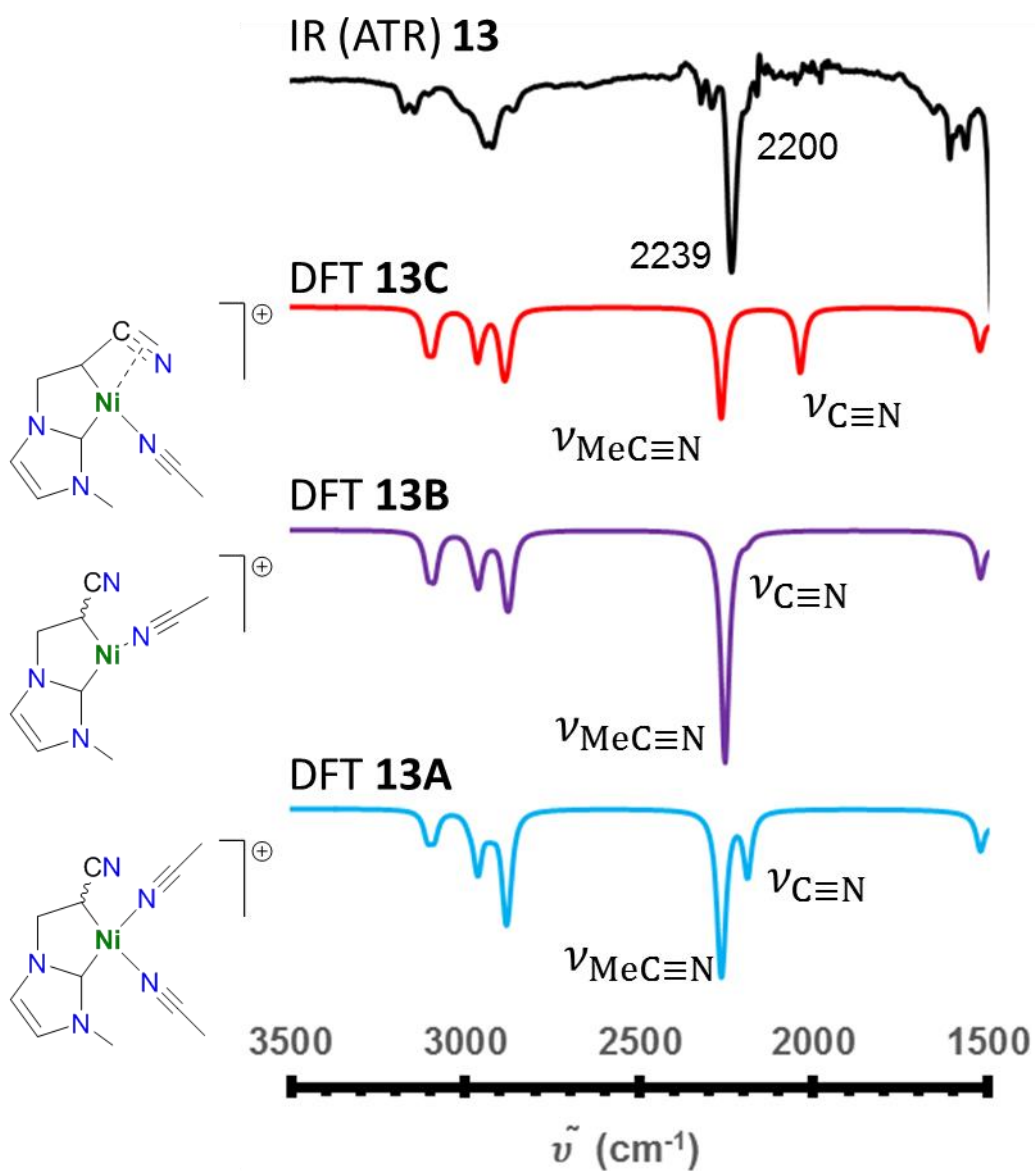


Figure S3. Detail of experimental IR (ATR) spectra of **13** (black), DFT calculated vibrational frequencies of **13A** (blue), **13B** (purple) and **13C** (red).

Publications

[1] B. de P. Cardoso, J.-M. Bernard-Schaaf, S. Shahane, L. F. Veiros, M. J. Chetcuti, V. Ritleng
“Displacement of η^5 -cyclopentadienyl ligands from half-sandwich C,C-(NHC-cyanoalkyl)-nickel(II) metallacycles: further insight into the structure of the resulting Cp-free nickelacycles and a catalytic activity study”
Dalton Trans. **2018**, 47 (5), 1535-1547. DOI: [10.1039/C7DT04560C](https://doi.org/10.1039/C7DT04560C)

[2] M. Henrion, B. de P. Cardoso, V. César, M. J. Chetcuti, V. Ritleng
“Nickel(II) complexes of highly σ -donating cyclic (alkyl)(amino)- and malonate-carbenes: syntheses and catalytic studies”
Organometallics **2017**, 36 (6), 1113-1121. DOI: [10.1021/acs.organomet.6b00906](https://doi.org/10.1021/acs.organomet.6b00906)

Oral communications

[1] B. de P. Cardoso*, S. Shahane, J.-M. Bernard-Schaaf, M. J. Chetcuti, V. Ritleng
“Insight to the structure of cationic C_{NHC}, C_{alkyl} -nickelacycles and study as azole C–H functionalization catalysts”
9th Barrande-Vltava French-Czech Chemistry Meeting (Barrande-Vltava 2018), August 2018, Strasbourg, France.

[2] B. de P. Cardoso, L. F. Veiros, M. J. Chetcuti, V. Ritleng
“Structure et activité catalytique de nickelacycles cationiques C_{NHC}, C_{Alkyle} pour la fonctionnalisation de liaisons C–H”
GECOM-CONCOORD 2018, Longeville-sur-Mer, 21-25 May 2018.

[2] B. de P. Cardoso, M. Henrion, V. César, M. J. Chetcuti, V. Ritleng
“Synthesis and applications of nickel complexes of highly σ -donating N-heterocyclic carbenes”
Journée des Doctorants de l’Ecole Doctorale des Sciences Chimiques, Strasbourg, 10 November 2017.

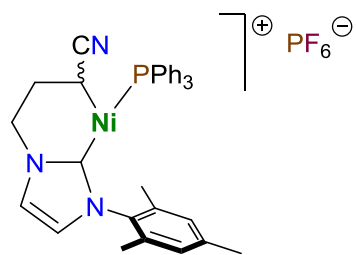
[3] B. de P. Cardoso, M. Henrion, V. César, M. J. Chetcuti, V. Ritleng
“*Synthesis and applications of nickel complexes of highly σ -donating N-heterocyclic carbenes*”
3rd International Green Catalysis Symposium, Rennes, 23 March 2017

[4] V. Ritleng, B. de P. Cardoso, S. Shahane, M. Henrion, M. J. Chetcuti
“*Facile displacement of η^5 -cyclopentadienyl ligands from 18-electron half-sandwich alkyl,NHC–nickel complexes: original routes to 16- or rare 14-electron nickel(II) complexes*”
27th International Conference on Organometallic Chemistry (ICOMC), Melbourne (Australie),
19 July 2016.

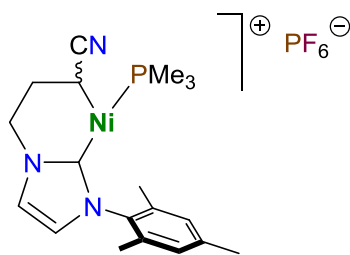
Poster communications

[1] Bernardo de P. Cardoso*, Luis F. Veiros, Michael J. Chetcuti, Vincent Ritleng
“*Insight to the structure of Cationic C_{NHC}, C_{alkyl} -nickelacycles and study as Azole C–H functionalization Catalysts*” XXVIII International Conference on Organometallic Chemistry (ICOMC2018), July 2018, Florence, Italy.

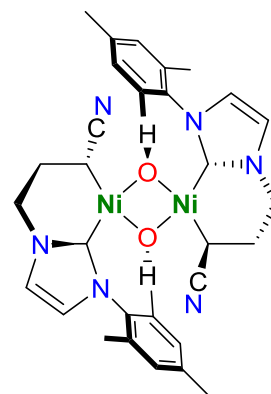
Chart 2. Structures of numbered compounds 17-29.



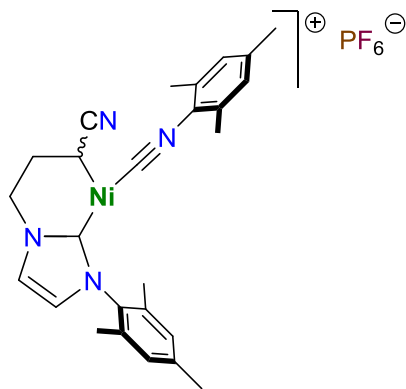
17



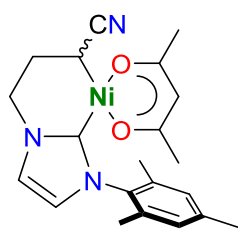
18



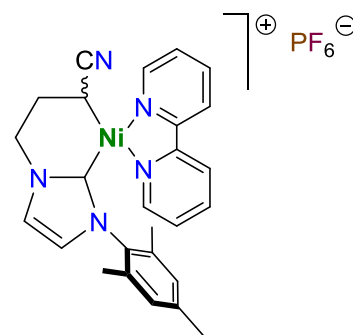
19



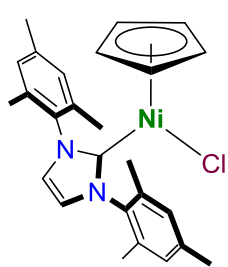
20



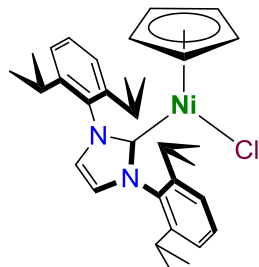
21



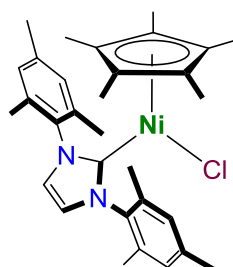
22



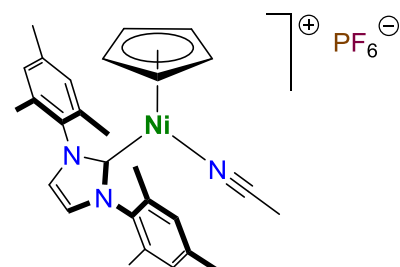
23



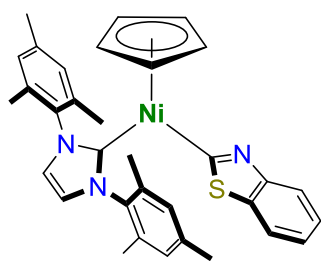
24



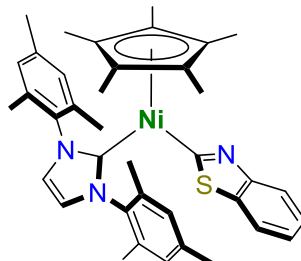
25



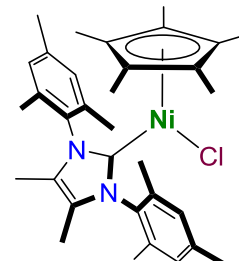
26



27



28



29

Structure de nickelacycles cationiques C_{NHC}, C_{alkyle} et activité pour la fonctionnalisation catalytique de liaisons C–H d'azoles

Résumé

Cette thèse développe l'étude des complexes de nickel(II) porteurs de ligands carbènes *N*-hétérocycliques (NHC) selon deux axes: la synthèse et la caractérisation de complexes nickelacycliques avec un ligand chélatant carbone-carbone (C_{NHC}, C_{alkyl}); et leur activité catalytique dans la construction des liaisons carbone-carbone ($C_{sp^2}-C_{sp^2}/C_{sp^3}$) des 1-chalcogènes-azoles par fonctionnalisation des liaisons carbone-hydrogène (C–H). Une série de produits d'addition d'acétonitrile métallacycliques $C_{NHC}, C_{alkyl}-Ni(II)$ cationiques a été synthétisée par élimination d'un ligand cyclopentadiényle des nickelacycles demi-sandwich à 18 électrons de valence parents. Il a été déterminé que les complexes cationiques existaient en tant qu'espèce Ni(II) à 14 électrons de valence en forme de T, insaturée de manière coordonnée et électronique, à l'état solide. L'application de ces nouveaux complexes au couplage croisé du benzothiazole avec les iodoarènes s'est avérée une stratégie efficace dans la formation des liaisons $C_{sp^2}-C_{sp^2}$, par la combinaison d'un échafaudage métallacyclique stabilisant avec des ligands labiles. La découverte d'une espèce demi-sandwich Ni(II)-(NHC)-(benzothiazolylo) inactif dans l'arylation du benzothiazole, mais actif dans le couplage du benzothiazole avec les iodoalcanes, constitue le premier exemple de construction des liaisons $C_{sp^2}-C_{sp^3}$ du benzothiazole avec un catalyseur Ni(II)-NHC.

Mots-clés: nickel, carbène *N*-hétérocyclique, fonctionnalisation C–H, azole, couplage-croisé

Abstract

This thesis develops the study of nickel(II) complexes bearing *N*-heterocyclic carbene ligands (NHC) in two axes: the synthesis and characterization of nickelacyclic complexes with a carbon-carbon chelating ligand (C_{NHC}, C_{alkyl}); and their catalytic activity in the construction of carbon-carbon bonds ($C_{sp^2}-C_{sp^2}/C_{sp^3}$) of 1-chalcogene-azoles by carbon-hydrogen (C–H) bond functionalization. A series of cationic $C_{NHC}, C_{alkyl}-Ni(II)$ metallacyclic acetonitrile adducts was synthesized by the removal of a cyclopentadienyl ligand from parent 18 valence electron half-sandwich nickelacycles. The cationic complexes were determined to exist as rare coordinatively and electronically unsaturated T-shaped 14 valence electron Ni(II) species, in the solid state. Application of these new complexes to the cross-coupling of benzothiazole with iodoarenes proved to be a successful strategy in $C_{sp^2}-C_{sp^2}$ bond formation, by the combination of a stabilizing metallacyclic scaffold with labile ligands. The discovery of a half-sandwich Ni(II)-(NHC)-(benzothiazolylo) species, inactive in the arylation of benzothiazole, but active for the cross-coupling of benzothiazole with iodoalkanes shows the first example of benzothiazole $C_{sp^2}-C_{sp^3}$ bond construction with a Ni(II)-NHC catalyst.

Keywords: nickel, *N*-heterocyclic carbene, C–H functionalization, azole, cross-coupling